UNIVERSITÀ DI PARMA

UNIVERSITA' DEGLI STUDI DI PARMA

DOTTORATO DI RICERCA IN
"*Scienze Chimiche*"

CICLO XXXIV

COMBINING LIGNIN WITH METALS FOR AGROCHEMICAL APPLICATIONS

Coordinatore:

Chiar.ma Prof. Bacchi Alessia

Tutore:

Chiar.mo Prof. Pelagatti Paolo

Dottorando: Gazzurelli Cristina

Anni Accademici 2018/2019 – 2020/2021

A tutte quelle persone insostituibili

che hanno fatto parte della mia vita in questi meravigliosi anni.

"Colgo dei particolari in loro,
dei dettagli che mi colpiscono
e di cui poi sento la mancanza,
a volte per sempre.
Non puoi rimpiazzare nessuno,
perché ognuno porta con sé
dettagli magnifici e unici"

(from the movie, "Before Sunset")

To all those special people

who have been part of my life in these wonderful years.

"I catch some details in them,
details that affect me
and which I then miss, sometimes forever.
You can never replace anyone,
because everyone
is made of such beautiful specific details"

(from the movie, "Before Sun

Table of contents:

Chapter 1: Lignin, a Powerful and Natural Resource

Wood is often associated to cellulose for its extraction in the production of paper. This polysaccharide is the most abundant biopolymer in nature. Its structure consists of glucose monomers linked by β-1,4 glycosidic bonds to form linear chains arranged parallel to each other by means of hydrogen bonds[1]. Cellulose constitutes the cell wall in plants, and it is organized on three levels: elementary fibrils, microfibrils and macrofibrils oriented in the fiber axis[2].

Cellulose represents about 45% of the dry wood weight, but it is not the only constituent of wood. Together with hemicellulose, that constitutes about 25% in dried wood, a very important role in plants is played by lignin (30% of dried matter)[3]. This natural aromatic polymer surrounds cellulose microfibrils and hemicellulose (figure 1.1) and confers to plants mechanical support and protection against pests and disease[2,4,5].

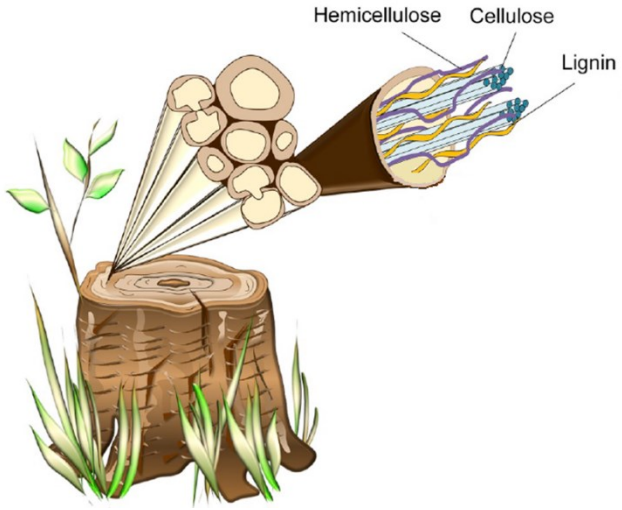

Figure 1.1. Schematic representation of the distribution of cellulose, hemicellulose, and lignin in wood. The picture is part of a figure reported in the review A field of dreams: Lignin valorization into chemicals, materials, fuels, and health-care products, Biotechnology Advances 37 (2019) 107360[4].

Huge quantities of technical lignins ($2x10^{11}$ t/year worldwide) are obtained mainly from paper mills or bio-ethanol industries. Nowadays, 40% of this polymer is burnt to meet energy needs of the industrial process, the remaining 60%, therefore, exceeds the energy demand of biorefinery and can be considered a potentially useful material[6,7]. Thanks to its interesting properties and with a view

of circular economy, the research on this polymer has been increasing year by year, as reported in figure 1.2.
It is precisely on this material that this thesis focuses on.

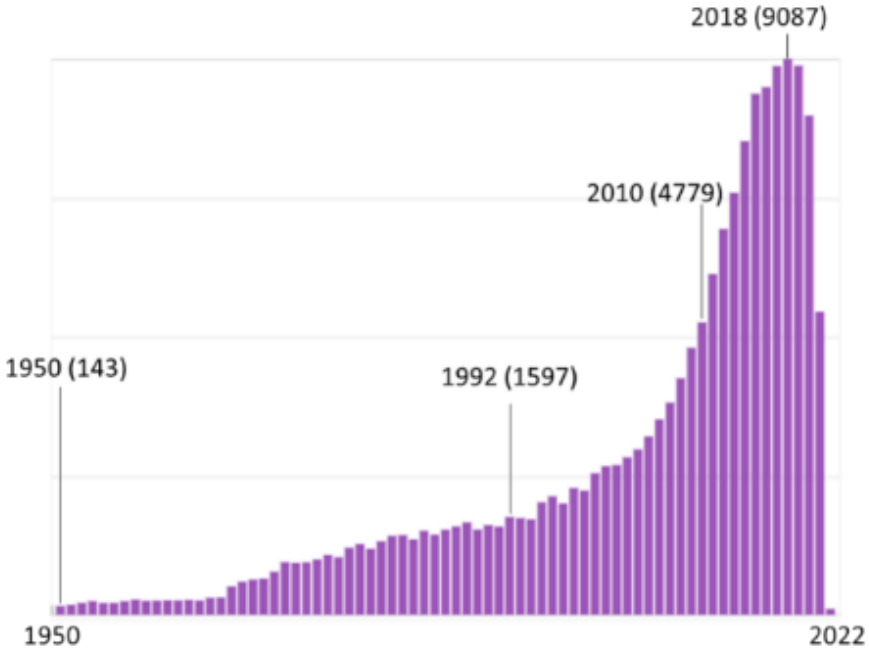

Figure 1.2. Publications about "lignin applications" from 1950 to 2022, in brackets the total number of papers per year. Source: SciFinder[n].

Lignin: what it is.

Lignin has a complex 3D structure characterized by three different phenyl propanoic units called *p*-hydroxyphenyl (H), guaiacyl (G) and syringyl (S) deriving respectively from the three monolignols: p-coumaryl alcohol, coniferyl alcohol and sinapyl alcohol, as reported in Figure 1.3[8,9].

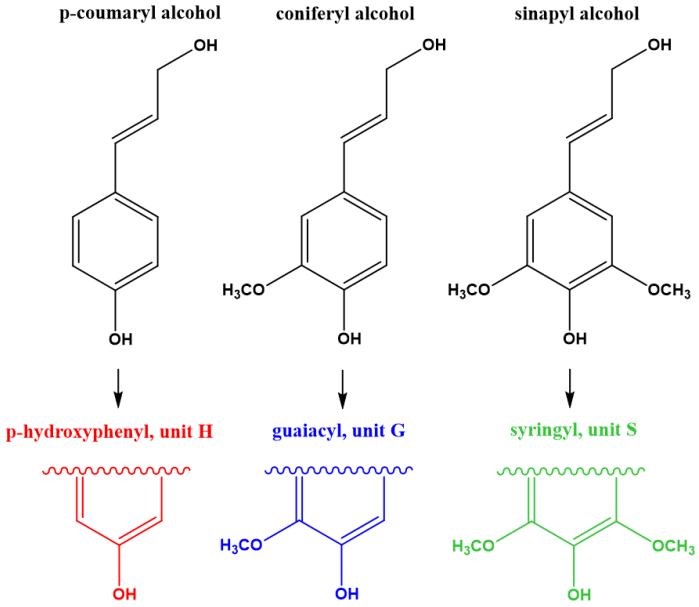

Figure 1.3. Representation of the three monolignols and their related phenyl propanoic units that build the structure of lignin.

These three monolignols combine by means of a peroxidase-mediated dehydrogenation to form both C-O and C-C linkages, shown in figure 1.4[9,10].
The ratio of these three monolignols in lignin is strictly related both to the plant from which lignin is derived and to the extraction method used, causing a high level of heterogeneity in the structure of different lignins[9–11]. Because of this, the structure in figure 1.5 is only a "representative model" of the structure of the polymer.

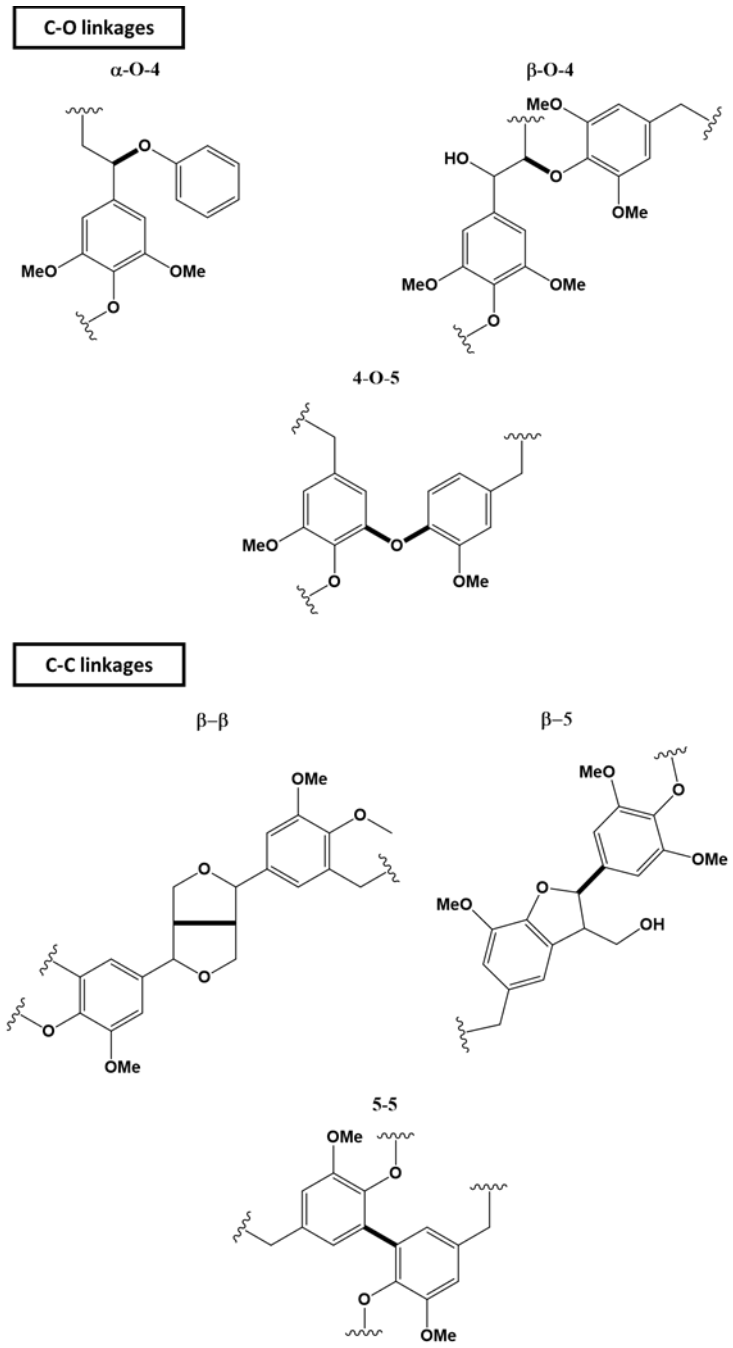

Figure 1.4. Linkages between monolignols.

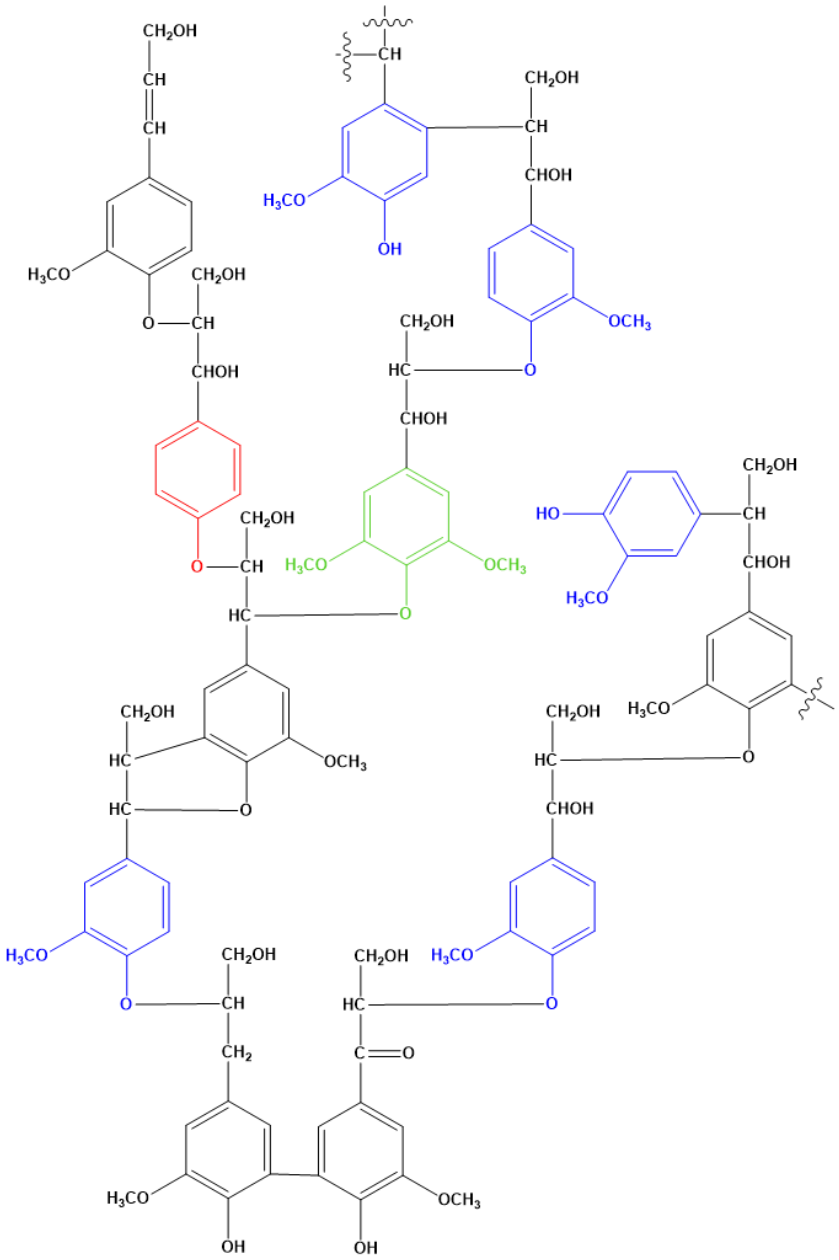

Figure 1.5. General model of lignin structure.

A first classification according to the type of plant is made between hardwood lignin, softwood lignin and the lignin of grasses. Hardwood lignin, deriving from angiosperms, contains coniferyl and sinapyl alcohols in almost equal proportions, while softwood lignin, deriving from gymnosperms (conifers), presents as major unit in the coniferyl one. The lignin of grasses is, instead, characterized by all the three units (coniferyl, sinapyl and p-coumaryl alcohols)[3,9]. This reflects also in the type of interunit linkages. While the ether bond β-O-4 is always the most abundant constituting about 50-80% of all interunit bonds, the prevalence of the monolignols with ortho-methoxy groups in the structure will lead to a reduction of the 5-5 and the β-5 carbon-carbon linkages[4]. Thus, hardwood lignin will contain these bonds to a lesser extent than softwood lignin.
A different monolignols ratio will also lead to a different amount of functional groups that affects the reactivity of the different lignins. Table 1.1 compares the content of the functional groups for softwood and hardwood lignin.

Table 1.1. Amount of main functional groups in softwood and hardwood lignin[12]

Functional groups	**Native lignin (per 100 C_6C_3 units)**	
	Softwood lignin	**Hardwood lignin**
Phenolic hydroxyl	20-30	10-20
Aliphatic hydroxyl	115-120	110-115
Methoxyl	90-95	140-160
Carbonyl	20	15

Concerning the extraction methods used, the main types of lignins are: kraft lignin, soda lignin, lignosulfonates, organosolv lignin, steam-exploded lignin and enzymatic hydrolysed lignin[9,11,13,14].

Kraft lignin is obtained from kraft delignification process. Wood is cooked in aqueous solution of NaOH/Na_2S (white liquor) between 155-175°C in such a way to separate cellulose as a solid from the fluid part (black liquor). During this treatment, hydroxide and hydrosulfide anions break the aromatic ether bonds giving a material with a reduced molecular mass compared to the native lignin. We can distinguish three phases in the dissolution step: the extraction phase, the bulk delignification phase, and the residual delignification. The treatment lasts several hours, and then the black liquor is precipitated with an acid solution. In the precipitation process, the pH is lowered through two successive steps which

first involve the use of carbon dioxide (pH=9/10) and then of sulfuric acid (up to pH=1/2).[15] The drying step allows to obtain lignin as a brown powder.
Kraft lignin is water-insoluble, while it dissolves in strong basic aqueous solutions and in some organic solvents, including acetone, pyridine, and ethylene glycol. Its highly condensed structure is mainly characterized by β-O-4, β-5, and β-β linkages[16,17]. For what concern the composition, kraft lignin has a percentage of sulphur between 1 and 3 wt% and the ash content is approximately 1-2.5 wt%[11,13].

Soda lignin is derived from soda pulping process, mainly used for non-wood fibers, like surgarcane bagasse, straw, flax etc. This process is conducted at about 160°C with aqueous solution of sodium hydroxide and anthraquinone as catalyst. This reagent helps to dissolve lignin and to reduce carbohydrates degradation. With similar conditions of the kraft process, soda pulping process has also the same main steps: the breaking of lignin-carbohydrate bonds, the subsequent depolymerization and lignin precipitation. Differently from kraft lignin it doesn't contain sulphur. The percentage of nitrogen is 0.2-1.0% and the ash content is between 0.7 and 2.3%. The percentage of carbohydrates is between 1.5-3.0%[14].

Lignosulfonate is obtained by sulfite pulping. This process consists of using different sulfite salts and very different range of pH and temperature to obtain a chemically modified lignin with sulfonate groups.
In the acid sulfite process, for example, lignin is extracted at 125-145°C using as reactive agents SO_2/HSO_3^- and setting the pH of the system at 1-2. Higher temperatures (150-175°C) are used both in the bisulfite and neutral sulfite processes. The first one exploits HSO_3^- ions as reactive agent with a pH between 3-5, while the second one maintains a neutral pH with both HSO_3^- and SO_3^{2-} species as reactive agents. Completely different is the alkaline sulfite/ anthraquinone procedure which works in basic environment at 50-175°C. In this case the reactive agent is Na_2SO_3.
This delignification method causes the hydrolysis of the ether bonds with consequently sulfonation by the sulfite ions. The final lignin presents a higher molecular mass than kraft lignin and a higher sulfur content, too (4-7wt%)[14]. The ash content is between 4.0 and 8.0%[14]. Lignosulfonate usually has a higher solubility in water than non-sulfonated lignin.

Organosolv lignin is obtained at high temperature and high pressure, using different solvent mixtures. The most common solvents are alcohols as ethanol and methanol in a mixture with water, but also acetic acid, formic acid and phenol

are used among the other. Thanks to its low viscosity, the organic solvent, as delignification agent, penetrates the wood chips, dissolving lignin. This sulfur-free lignin (less than 1wt% of sulfur[14]) is isolated by acid precipitation.
Among the advantage of this process, compared to the Kraft one, there is the production of a more homogeneous lignin structure. Despite this, the use of corrosive solvents limits its breakthrough on industrial scale as well as the problem of solvent recovery. The composition of organosolv lignin consists of a carbohydrates content between 1.0-3.0% and an ash content of about 1.7 %[14].

Steam-exploded lignin is a partially hydrolysed lignin obtained by means of a very hard treatment, sometimes in presence of alkaline environment or with hot alkali peroxide[18]. Wood is subjected to high pressure and high temperature, between 180-200°C, and subsequently a sudden decompression is applied. The obtained lignin is water-insoluble with a reduced molecular mass. The hard condition of the treatment leads to the breaking of β-O-aryl ether linkages and to an increasing in the phenolic content. Furthermore, by oxidation of ether and hydroxyl groups an increase in the carbonyl groups is also observed[18].
Combined with enzymatic hydrolysis this process leads to carbohydrates which can be subsequently used for fermentation processes.

Enzymatic hydrolysed lignin is obtained by the action of enzymes as cellulases, hemicellulases and laccases and micro-organisms[18]. To make the biomass more accessible to the enzymes, some chemical and physical pre-treatments are used before the enzymatic degradation. Among others, milling, treatments with dilute acid or steam, ammonia fiber explosion and alkaline or organosolv processes[18].
This type of lignin presents high chemical reactivity thanks to the high number of active functional groups[19]. The main advantage of enzymatic hydrolysis is the absence of toxic and corrosive by-products. However, the obtained lignin contains impurities also after the purification step and it presents a high-water retention ability limiting its use as fuel[14].

Characterization.

The high heterogeneity of its structure makes the characterization of this polymer a challenge in all respects. Such structural differences, also, reflect on the most trivial properties like the possibility to find both water-soluble lignins and completely water insoluble ones.
However Nuclear Magnetic Resonance is a very powerful technique to analyse the structural differences of each type of lignin by ^{31}P-NMR, ^{13}C-NMR, and HSQC[16,17] (see paragraph Nuclear Magnetic Resonance).
In this paragraph an overview of the main lignin characterization techniques is presented. So, the combination of all the complementary characterization techniques does not furnish in the absolute structural description but give us a picture of the type of lignin.
The following list of the characterization techniques was inspired by Chapter 4 and Chapter 5 of the book "Methods in Lignin Chemistry"[20].

Ultraviolet spectrophotometry

Looking at its aromatic structure, the ultraviolet spectrophotometry is one of the main characterization techniques for this polymer. In particular, the interesting region is from 200 nm to 380 nm in which three bands can be distinguished. Softwood lignin presents the maximum absorption at 280 nm with an absorptivity value 18 – 21 l g^{-1} cm^{-1}, a shoulder at 230 nm and a sharp peak between 200-210 nm. Hardwood lignin is, instead, characterized by a band with lower absorbance values (absorptivity around 12 – 14 l g^{-1} cm^{-1}) and at shorter wavelengths (268-277 nm). Sometimes, we can also appreciate differences in absorbance between kraft lignin and lignosulfonate, because of the presence of more conjugated groups in the first one, whereas the maximum is always set at 280 nm.
The great advantage of this technique is the easy way for preparing samples and for carrying out measurements, offering both qualitative and quantitative analyses. From the study of lignin solutions is, in fact, possible, not only to distinguish between softwood and hardwood lignin, but also to determine its concentration. By means of derivative ultraviolet spectrophotometry is possible to identify lignin in complex organic mixtures. This technique, very useful for

industries, is based on the derivative of absorption spectra (derivative of the absorbance against wavelength) to highlight more structural details then the usual measurement, thus offering a real fingerprint for lignin. Studying lignin model compounds is also possible to obtain an estimate of the functional groups content in the polymer. Through ultraviolet difference spectroscopy, for example, is possible to deduce the concentration of phenol groups. This technique consists of registering adsorption spectra of a sample, before and after a specific treatment, as, for example, ionization[21–23], or reduction with $NaBH_4$, to gain the difference spectra.

Infrared spectroscopy

An important contribution to the analysis of lignin functional groups is given by infrared spectroscopy in the mid infrared region (4000-500 cm^{-1}). Due to the complex structure of the polymer, the spectrum cannot be easily interpreted, but some bands can be unequivocally assigned. This is the case, for example, of the stretching modes of: OH groups (region: 3412-3460 cm^{-1}), C-H of methylene and methyl groups (3000-2842 cm^{-1}), carbonyl groups of both esters and not conjugated ketone and aldehyde (1738-1709 cm^{-1}), of carboxylic acids (about 1700) as well as aryl ketones (1655-1675 cm^{-1}). Particularly useful, also to face a semi-quantitative analysis of H, G and S units present in lignin, are the vibrations of the aromatic skeleton around 1510 cm^{-1}. After normalization and correction of the baseline of the spectra, the latter are used as internal standard to calculate all the relative intensities of the other absorption bands. Based on the observation that a different ratio between H, G and S units leads to different intensity of the bands rather than to their position, infrared spectroscopy can be used for lignin classification, too.

Pyrolysis-GC/MS

A useful technique both for the recognition of different types of lignin and for an investigation of the polymer in lignocellulosic materials is pyrolysis, because it gives characteristic fragmentations of the polymer.

The most usual instrumental setting for pyrolysis is pyrolysis associated with gas chromatography coupled to mass spectrometry for molecular recognition.
Normalization of peak areas, use of internal standard, in addition to different instrumental setting lead to the possibility of performing both qualitative and quantitative analysis according to phenyl propanoic unit ratios. The evaluation of the pyrolytic system reproducibility and the comparison between pyrograms takes place through similarity index. It is a percentage value obtained from the formula reported below which considers areas and retention time peaks of the two pyrograms in comparison. For a right calculation the two analyses must be conducted in the same conditions and in the same laboratory. A value of 95% is a good result for an identical material across replicated pyrolysis-GC tests. Such a technique is also useful to determine the kind of lignin in an unknown sample comparing its pyrogram with the one of a known sample.

$$\text{Similarity Index (SI)}\ \% = 100 - \frac{\sum_{n=1}^{k}(RRT_n^a \text{ x } Ar_n^a - RRT_n^b \text{x } Ar_n^b)}{\sum_{n=1}^{k}(RRT_n^a \text{x } Ar_n^a) + \sum_{n=1}^{k}(RRT_n^b \text{ x } Ar_n^b)} \text{ x } 100$$

With $\mathrm{RTT_n^a}$ and $\mathrm{RTT_n^b}$ relative retention times of the nth peak in pyrogram a, and b respectively, and $\mathrm{Ar_n^a}$, $\mathrm{Ar_n^b}$ normalized peak area of the nth peak in pyrogram a and b respectively.

Nuclear Magnetic Resonance

When we talk about organic molecules, it is impossible not to think to NMR spectroscopy as technique for structural investigation. ^{1}H-NMR and ^{31}P{^{1}H}-NMR are used after proper derivatization. In the case of protonic NMR, derivatization is used too simplify the spectra and to avoid exchange phenomena; this can be done functionalizing both aromatic and aliphatic OH groups through acetylation. In the case of ^{31}P-NMR, a phosphitylation is executed on the same groups, taking advantage from the higher sensitivity of phosphorous with respect to carbon. By ^{31}P-NMR spectroscopy is possible to quantify and to distinguish OH functional groups in the polymer obtaining information on the different units. In particular, we can recognize the different hydroxyl groups using cyclohexanol (144-146 ppm) as internal standard. The spectroscopic windows of interest are: 150-145 ppm for aliphatic OH, 144-140 ppm for syringyl OH groups, while guaiacyl OHs are placed

in the interval 140-138 ppm, finally the p-hydroxyphenyl groups fall between 138-136 ppm. The region of OH groups from carboxylic acids is, instead, between 135-133 ppm.
Acetylation is conducted reacting lignin with acetic anhydride in pyridine at room temperature for at least 12 hours. As phosphitylation reagent, 2-chloro-4,4,5,5-tetramethyl-1,2,3-dioxyphospholane, TMDP, is used, in a mixture of deuterated chloroform and pyridine, and with an appropriate internal standard for quantitative analysis.
Despite its low isotopic abundance, also $^{13}C\{^{1}H\}$-NMR is a very important technique for the study of this polymer. In a ^{13}C spectrum we can distinguish three regions: from 200 to 165 ppm, where the carbonylic carbons signals are found, between 165 and 100 ppm, where the aromatic and olefinic carbons are found and between 100 and 10 ppm, where the aliphatic carbons are found. Quantitative analysis is also possible. ^{13}C-NMR is used by Obst and Landucci, for example, to determine the methoxy groups content, in several species of wood[20,24].
Thanks to DEPT (Distortionless Enhancement by Polarization Transfer) it is possible to obtain clearer information about primary, secondary and tertiary carbons, since this technique allows to remove overlapping of some signals. Very important are also bidimensional spectra as, for example, ^{13}C-^{1}H 2-D HSQC (Heteronuclear Single Quantum Coherence), which give a contribution both for quantitative and qualitative analysis.
NMR spectroscopy is then a powerful method to understand lignin with a lot of different experiments possible.

Gel Permeation Chromatography

When we talk about polymers, a key feature is the distribution of molecular weight which in turn affects their properties. The main technique for this kind of investigation is GPC (Gel Permeation Chromatography) or SEC (Size Exclusion Chromatography), based on the different separation of polymer fractions thanks to their size by means of a three-dimensional porous material. The separation will depend on the dimension of pores of the stationary phase. Polymer molecules too large to enter the pores will elute quickly through the column, while smaller molecules will interact with the stationary phase eluting at longer times. Several

instrumental settings can be tuned and the best analysis conditions must be defined for the type of lignin in use. Both organic solvents and aqueous solutions (for example of NaOH) are used as eluent, according, also, to the stationary phase available. The mobile phase effects on the polymeric structure, such as ionization of functional groups, or the ionic force, are aspects to consider, because they affect the retention of the polymer molecules. With the necessary precautions this technique allows to obtain accurate information about the number-average molecular weight, M_n, the weight average molecular weight, M_w and polydispersity index, PD, (M_w/M_n) of different kinds of lignin.

Thermal analyses

Less explanatory from a point of view of the structure investigation, but really important for a complete characterization, are thermal analyses, and, in particular, thermo gravimetric analysis, TGA, differential scanning calorimetry, DSC, and differential thermal analysis, DTA. From the TGA profile, characterized by weight loss as function of temperature, it is possible to obtain information about lignin degradation temperatures, strictly related to its thermal resistance, as well as residual water content.
The differential thermal analysis and the differential scanning calorimetry give, instead, information about phase transitions and heat capacity. The first one measures the temperature difference between sample and reference as function of temperature, while in differential scanning calorimetry the necessary energy to maintain the sample at the same reference temperature is measured as a function of temperature. In the case of lignin, the phase transition of greater interest is the glass transition one. Strongly influenced by molecular weight, branches, and the presence of hydrogen bonds, the temperature range in which this transition is observed is really wide, according to lignin type.

Lignin analysis in wood

Some techniques are used for lignin analysis in wood, allowing, sometimes, to determine its concentration. It is the case of Raman spectroscopy, that exploits spectral region around 1600 cm^{-1} in which signals are due only to the stretching

vibrations of native lignin aromatic rings. Another band extremely important is at 1595 cm^{-1}, used to determine lignin concentration in lignocellulosic material as well as to study the orientation of the polymer in the woody tissue.
The analysis of sections of wood is possible thanks to ultraviolet, interference and electronic microscopy. While the latter provides only a visual characterization of the cell wall structure, unless proper treatments on lignin are conducted, ultraviolet and interference microscopy allow both a qualitative and quantitative investigation.

Properties and applications:

Looking at its structure (figure 1.5) several properties can be detected. It is thanks, for example, to its aromatic components if lignin provides mechanical support to plants, while the presence of polyphenolic species gives rise to antibacterial and antioxidant properties. Strictly related to the latter it is also the ability of lignin to prevent photo oxidation as well as to act as radicals scavenger. A very important feature deriving from its bio-nature is, also, biodegradability.

Biodegradability[4,5]

Despite its complex structure lignin degradation is conducted by several micro-organisms, as, for example, *Phanerochaete chrysosporium* and *Fusarium oxysporum*, among fungi and *Pseudomonas putida*, *Streptomyces coelicolor* and *Enterobacter lignolyticus* among bacteria.
The ligninolytic activity is due to two main oxidative enzymes, laccases and peroxidases. While laccases cleave only phenolic lignin units, peroxidases act on lignin both directly and creating radical mediators which penetrate lignin, initiating depolymerization. We can distinguish four different types among peroxidases, according to the catalytic reaction involved: manganese peroxidases (MnPs), lignin peroxidases (LiPs), versatile peroxidases (VPs) and dye-decolorizing peroxidases (DyPs). As described by the name, versatile proxidases (VPs) combine mechanism of both MnPs and LiPs. The latter attacks lignin via intermediate radicals, after activation by H_2O_2, while manganese peroxidases use Mn^{+3} ions to exert their action. Completely different is the action of DyPs. Suitable for a lot of substrates, they act at acid pH oxidizing aromatic lignin monomers and cleaving ether bonds.
So, thanks to these enzymes the degradation process starts. The first step is the ligninolysis in which the main lignin bonds, β-O-4, α-O-4, 5-5, β-β and β-5 are broken forming monolignin products such as guaiacol, phenol, vanillin, cresol and others.
The second step occurs with the participation of other enzymes such as acyl-CoA synthetases, acyl-CoA hydratases/lyases, decarboxylases and alcohol and aldehyde dehydrogenases. The large number of molecules obtained by the ligninolysis process is subsequently reduced by specific pathways leading to a restricted number of species. In particular, ligninolysis products deriving from G-type and H-type aromatic units are metabolized in protocatechuate and catechol.

The degradation of S-type lignin derivatives leads to gallate and 3-O-methylgallate.
The range of molecules derived from lignin, widens with the third step of degradation which involves the breaking of aromatic rings. Depending on the position in which such rings open (ortho, metha, para), among others, 5-carboxy-2-hydroxy-muconate semialdehyde, 3-carboxy cis-cis-muconate and 4-oxalomesaconate can be obtained. The last metabolites of lignin degradation process are pyruvate and oxaloacetate.

Antioxidant Power and Methods for its determination

The antioxidant activity of lignin is due to its polyphenolic structure. Mechanisms at the base of this property are not completely known yet, but the more convincing hypothesis is related to the polyphenolic structure of lignin as radical scavenger. From this point of view the antioxidant action of phenolic groups could occur both by transfer of hydrogen atom and by transfer of electrons with the formation of phenoxy radical cations which are then deprotonated to give phenoxy radicals[25].
Pan et al. conducted a study aimed to correlate lignin structure with, first, the extraction process conditions, and then with the antioxidant activity[26]. They revealed that harder process conditions, as, for example, higher temperatures and more catalyst, lead not only to a greater depolymerization, reflected in a narrower polydispersity, but also to an increasing in the antioxidant power. This trend is explained by the higher concentration of free phenolic hydroxyl groups that are generated due to the breaking of ether bonds.
Furthermore, the radical scavenging activity of the phenolic compounds depends not only by the ability to form phenoxy radicals but also by the stability of such species[26]. Studies conducted on lignin model compounds have, in fact, shown how the presence of methoxy groups in an ortho position stabilize the phenoxy radicals by resonance, hindering their propagation. Further delocalization is also provided by conjugated double bonds as shown in figure 1.6[26,27]. Less clear, however, is the role of aliphatic hydroxyl groups. Experiments conducted on model compounds, in fact, have revealed a positive effect of these groups on scavenging activity while in the real lignin they seem to have an inhibitory effect[28].
The same trend is also confirmed by Ugartondo et al. in which the antioxidant power of different type of lignin is evaluated, underlying how the activity decreases in the order: bagasse > steam explosion ≈ kraft > lignosulfonate[29]. Even

in this case, in fact, the greatest efficacy is manifested in the lignins obtained from extraction methods that lead to lower molecular weights and lower polydispersity, as well as a lower heterogeneity which is reflected in the carbohydrate content. These species, in fact, would reduce the antioxidant action of phenols by creating hydrogen bonds with their polar groups.
Crouvisier-Urion et al. investigated the antioxidant activity of lignin in lignin-chitosan film[30]. They showed how the antioxidant capacity of lignin is attributed to a surface activity and how an excessive amount of lignin leads to a decrease in antioxidant activity. This can be caused by some sort of clumping of the polymer molecules which could hide the active groups.

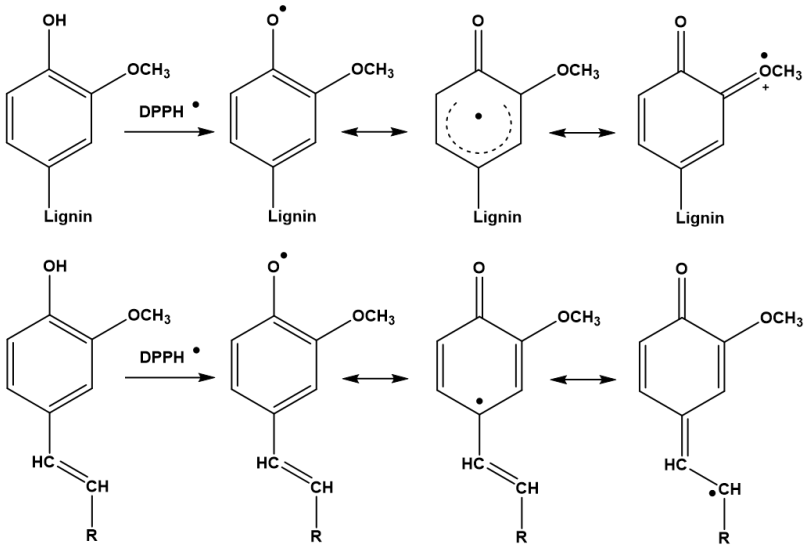

Figure 1.6. Stabilization of phenoxy radicals by means of methoxy groups and conjugated double bonds; DPPH = 2,2'-diphenyl-1-picrylhydrazyl[26,27].

Given the great importance of the antioxidant activity of lignin, a brief description of the main methods by which this property can be evaluated is reported. In most cases, these are colorimetric assays in which the change in the absorption band of the radical reagent by reaction with the analyte is spectrophotometrically monitored[31]. The evaluation of the radical scavenger properties of the analyte is obtained from the kinetic profiles of this reaction which must be carried out at different concentrations of the analyte[32].

Among tests based on this principle, the most popular are based on DPPH method (DPPH = 2,2-diphenyl-1-picrylhydrazyl), ABTS assay (ABTS = 2,2'-azino-bis-(3-ethylbenzothiazoline-6-sulfonic acid)), the FRAP (FRAP = Ferric Reducing Antioxidant Power) method and on the Folin-Ciocalteau test[25]. The first three methods are, often, associated to the TEAC assay (Trolox Equivalent Antioxidant Capacity) that use Trolox as standard. Trolox is an antioxidant molecule analogue to vitamin E, but soluble in water. In this case the result is expressed with Trolox Equivalents (TE), for example, as micromoleTE/100g or mgTE/100g of dry weight of the analyte[10,25,33]. As regards the Folin-Ciocalteau assay, this uses gallic acid as standard and the results are reported as milligrams of gallic acid equivalents (GAES) per gram of sample[33]. Sometimes, results are expressed as IC_{50} or EC_{50}, that is the antioxidant concentration necessary to decrease the concentration of the radical reagent by 50%[32].

More in detail, the DPPH method is based on the colour transition of the solution from violet (due to the radical species of DPPH) to pale yellow after the reaction with the analyte. Such reaction is monitored with the absorption band at about 520 nm. While the intensity of the adsorption band will be related to the analyte concentration, how quickly the band decreases will indicate the antioxidant power of the analyte[28,31,32,34,35].

ABTS decolorization assay exploits, instead, ABTS which by reaction with sodium persulfate is converted into a radical cation giving a blue solution with absorptions at 415, 645, 734 and 815 nm[28,36].

In the case of FRAP, the reduction of the Fe^{3+} tripyridyl triazine complex to its ferrous form is monitored under acidic conditions at 37°C, measuring the absorption band at 593nm[25,37].

The Folin-Ciocalteau assay, instead, is a colorimetric test which uses a mixture of phosphomolybdate and phosphotungstate[33,38]. In this case the estimation of the total phenolic content is based on the measurement of the absorbance at 750-765 nm after reaction of the sample with the Folin-Ciocalteau reagent[39].

Another test is the haemolysis of red blood cells mediated by the peroxyl radical initiator AAPH (AAPH = 2,2-azobis(2-amidinopropane)dihydrochloride). This biological assay evaluates the antioxidant activity of lignin according to how much it inhibits the destruction of erythrocytes [36].

Among the other tests that can be used to investigate the antioxidant activity of lignins, it is also worth mentioning the Superoxide Anion Radical ($O_2^{\cdot-}$) scavenging and Oxygen Uptake Inhibition (OUI) methods[25].
Obviously, these tests were not created to investigate the antioxidant power of lignins alone, therefore different experimental conditions are possible, such as variation of the solvent, temperature, and incubation time, as well as doses of reagents, depending on the matrix. In literature, many examples can be found in which the best experimental conditions are investigated for a given analyte. It is the case, for example, of S. Klein et al. who present three different methods for Folin-Ciocalteau assay on Kraft and Organosolv lignins[38]. Among the three methods, the best one uses DMSO as solvent, Na_2CO_3 as base for setting pH at about 10 and an incubation time of 30 minutes at 40°C. The absorption wavelength used is 740 nm.
Even when dealing with simpler antioxidants, some problems in determining the unreacted radical species must be considered. A. L. Dawidowicz et al., in fact, report a study on how some parameters can affect the determination of the concentration of unreacted $DPPH^{\cdot}$ radical species[32]. Among other, the type and volume of solvent used to dissolve the antioxidant must be mentioned. For this reason, when the antioxidant activity of lignins is evaluated, it is mandatory to taken into account several parameters and experimental conditions under which the experiments have been conducted. This can hamper a correlation within data collected by different approaches.

The relationship between antioxidant activity and lignin cytotoxicity has also been investigated, confirming that a higher antioxidant power leads to greater cytotoxicity. What makes the difference, however, is the concentration in which the two phenomena occur. An effective antioxidant power, in fact, occurs at much lower concentrations than those in which cytotoxicity would occur. Therefore lignin is a natural non-toxic antioxidant[25].

Applications

Thanks to its important properties, alternative industrial uses of lignin have already been developed and other potential applications in several fields are object of an intense research.
We can distinguish two different approaches to exploit lignin. The first one is based on the obtaining of lignin derived products, for example, by means of depolymerization, while the second one consists in preserving its molecular nature both as bulk and on the micro/nano scale[13].

The production of small high-added value molecules from lignin is mainly limited to the production of vanillin. Although most vanillin is still of petrochemical origin, procedures for obtaining this molecule from different types of lignins are being developed[9]. The main challenge in this regard is that the alkaline oxidative treatment at the basis of this transformation has a yield around 6-12%, according to the type of lignin and oxidation conditions; in any case far from the theoretical yield (25-30%)[9,13,40].
A recent surprising discovery comes from the possibility to exploit the biodegradability of lignin for the isolation of high value-added products[4]. The idea is to use enzymes and microbes for lignin conversion. This synthetic routes leads to important chemicals such as adipic acid, cis,cis-muconic acid and terephtalic acid and they have been developed up to pilot scale. Compared to the classical depolymerization based on thermal, chemical or physical treatments, this new strategy has important advantages, such as the milder conditions applied and the possibility to overcome low yields and the problems related to the selectivity of the catalytic system. Unfortunately, some drawbacks limit the application on industrial scale. The biochemical lignin transformation takes, in fact, a very long time and also the cultivation of fungi is far from being simple.
Thanks to the production of dimethyl sulfide (DMS) during the kraft pulping, it is also possible to obtain dimethyl sulfoxide (DMSO) with demethylation/oxidation reactions[9]. This method is considered an alternative to the petrochemical method usually used for the synthesis of this solvent.
From a completely different perspective, it is also possible to obtain active carbon with notable adsorption abilities[9]. In this case, in fact, kraft lignin is not depolymerized, but treated in two steps. First, it is pyrolyzed around 600°C-900°C yielding a non-porous material, and subsequently the activation step occurs in a physical or chemical way.

Lignin carbonization allows to produce carbon fibres, too[9]. However, this application has no actual response because lignin recovered by paper-mill streams doesn't have proper levels of purity and suitable physical properties to meet the required quality[9].

Among applications aimed to preserve the molecular nature of lignin, its use as additive finds a real industrial development in several fields[41]. Lignosulfonate, is, in fact, used in the production of building materials such as cement, brick, concrete and plasterboard as well as binder for the granulation of finely divided raw materials[13]. Other applications for this type of lignin are as dispersing agent and heavy metals sequestering agent[9]. In road construction, lignin is used as dust suppressant[9,13].

Its phenolic component allows to add lignin in the formulations of polymer blends, for example, as substitute for phenol in the phenol-formaldehyde resins, used as adhesive (up to 50%)[9,13]. Lignin is introduced also in polyolefins to prevent photo-oxidative degradation processes and to increase the biodegradability of the polymer[9]. Its protective action against UV radiation has been demonstrated to be greater than 30% when lignin is added as nanoparticles, while its antioxidant and radical scavenger activity is not affected by this factor[6]. Recently, lignin has also been used in epoxydic resins and polyurethane foams to improve their performance by reducing the weight loss at high temperatures, thus avoiding the release of dangerous components[41].

Thanks to its important mechanical properties, lignin is added as bulk or micro/nano particles as copolymeric component to improve strength, rigidity, hardness and tenacity of blended materials[6,42–44].

Lignin applications are very wide, ranging from emulsions stabilizer to component of drilling fluids in the petroleum industry[13]. The study of lignin as nano/micro carrier of drugs in the biomedical sector, furthermore, is in strong development[6].

Among potential applications of lignin there is its use as bio-surfactant[10]. Surfactants are used in several fields, such as agriculture, detergent industry and cosmetics with increasing demand. The development of greener surfactants can find a solution in the use of lignin, since the final products are featured by higher sustainability and biodegradability than those based on oils. Furthermore, lignin modification can open the way to the synthesis of new type of surfactants. Some examples come from the cationic biosurfactants derived from the functionalization of lignin with amines, or the anionic biosurfactants obtained by lignin sulfonation. Amphoteric surfactants can be obtained by introducing cationic groups, such as ammonium groups, and anionic groups, such as deprotonated

hydroxyls. Mainly studied for healthcare and cosmetics, non-ionic surfactants can also be obtained from diethanolamine-based lignin.

From lignin and vegetables fibres, a thermoplastic composite material, Arboform, was synthesized[9,13]. Very similar to plastic in appearance, but with usual wood properties, it is ideal for the fabrication of objects as car interior panels, rifle butts, furniture parts and so on[13]. The great innovation of this material is, above all, its high recyclability. In fact, it can be reprocessed several times without modifying its properties. Its production is nowadays limited because of the release and accumulation of sulfurate gases, reaching 5 tons per month in Germany[45].

Especially important is its antibacterial activity which is object of investigation in several fields[6,10,41]. An Australian company developed a based lignin formulation to control microbial populations in industrial hydraulic circuits, while in zootechnical field lignin is added to animal's feed as antibiotic substituent[41].

An intense study concerns the use of lignin in active packaging[10,11,30]. Added as an additive to other materials such as polyvinyl alcohol, latex, polylactic acid, chitosan and alginate, lignin has a triple action[10]: antibacterial activity, antioxidant, and UV blocker that allow to preserve food. Other studies are related to the medical field. The evaluation of its activity against pathogens is conducted also in tissues or in plastic-based products as, for example, lignin-based polyurethanes[10].

Its biocidal activity is extensively studied, also in agronomical field, both as bulk polymer and nanoparticles, in combination with metals too[46–48]. It is in this sector that my research focuses, and a broader description of its antibacterial activity for agronomic purposes is present in "Chapter 2".

Lignin materials used in this work

Lignin used in this study, provided by UPM-Kymmene Oyj and Green Innovation GmbH, is named BioPiva and it is a softwood lignin (*Pinus taeda*) obtained by Kraft process. Table 1.2 shows its composition and characteristics (UPM internal data). Lignins used in this work are identified as BioPiva100 and BioPiva395. NMR spectra for BioPiva395 are presented in supporting information (figures S1.1 and S1.2). The comparison between BioPiva100 and BioPiva395 is reported in the supporting information through IR (figure S1.3), GPC (figure S1.4), pyrolysis-GC/MS (figure S1.5), and SEM images (figure S1.6). These two lignins differ for the drying process that leads to differences in the dry matter content see table 1.2, in the molecular weight distribution (table 1.2, and figure S1.4), and in the lignin particle size that in both cases is less than 25 µm (BioPiva395 has a finer structure than BioPiva100, see SEM images in figure S1.6). The different values in the molecular weight distribution will be important for future characterization and discussion.

The functional groups distribution, calculated through NMR, reveals an excess of guaiacyl units, as expected in typical softwood lignin.

The antioxidant capacity was also evaluated by UPM-Kymmene using DPPH method with Trolox as reference. Results are expressed in grams of lignin necessary to reach the same antioxidant capacity of 1 g of Trolox.

Toxicity studies are provided by Green Innovation. With a LD_{50}>2000 mg/kg (LD_{50} = Lethal Dose, concentration at which 50% of the treated animals die after the administration of a single quantity of the substance), BioPiva can be classified as non-hazardous substance. *In vivo* tests conducted on pigs using high dosages did not show the insurgent of diseases or anomalous states, thus confirming that it doesn't have negative effects on animals[49].

Table 1.2. Characteristics of BioPiva used in this study.

Composition	
pH (10 % slurry)	2,5-4,5
Particle size, µm	< 25
Dry matter content	63% (BioPiva100) 95% (BioPiva395)
Ash, %	< 2
Sulphur, %	< 3
Carbohydrates, %	< 5
Cellulose, %	0
Purity, %	> 95
Mw, g/mol	4400 – 5000 (BioPiva100) 5950 – 6000 (BioPiva395)
Mn, g/mol	1200 – 1300 (BioPiva100) 1560 – 1565 (BioPiva395)
Functional groups (mmol/g)	
Aliphatic OH	1,8
Carboxylic acid	0,5
p-OH-phenyl	0,3
Guaiacyl	1,9
Syringyl	1,7
Phenolic OH	3,9
Total OH	6,1
Property	
Antioxidant capacity, DPPH method TEAC	18,2
Lethal Dose 50%, LD_{50} mg/Kg	>2000

The experimental details of the characterization techniques used in this thesis are collected in the dedicated chapter “Characterization techniques”.

Company partners:

UPM-Kymmene Oyj[50]

UPM-Kymmene Oyj is a Finnish forest industry company formed by the merger of Kymmene Corporation with Repola Oy and its subsidiary United Paper Mills Ltd in 1996. It has a griffin as logo (figure 1.7). The reasons behind this elegant logo, designed by Hugo Simberg in 1899, are probably because griffin is considered the guardian of the northern forests.

Figure 1.7. UPM logo.

With annual sales of around 8.6 billion euros and a sales network that spans all six continents, UPM has 18'000 employees distributed in 12 countries where its headquarters are located (Finland, Austria, China, Estonia, France, Germany, Malaysia, Poland, Russia, United Kingdom, Uruguay and United States).

UPM business areas can be divided in UPM Biorefining, UPM Energy, UPM Raflatac, UPM Specialty Papers, UPM Communication Papers and UPM Plywood. UPM Biorefining includes Pulp, Timber and Biofuels. A brief description of all these trades follows.
UPM Pulp uses high quality eucalyptus, birch, and softwood pastes for the obtaining of final products such as tissue, specialty papers, graphic papers board and packaging. UPM Timber provides the customer with high quality redwood and conifer sawn wood, while UPM Biofuels is the sector in which an alternative to fossil fuels is produced. Biofuels such as, for example, UPM BioVerno diesel and naphtha obtained from a residue of UPM's own pulp production, allow to reduce greenhouse gas emissions starting from sustainable raw materials. UPM Energy is the second largest provider of energy in Finland. To gain energy the three main sources are wood-based biomass (peat and coal) by means of thermal power

stations, the flexible and renewable hydropower and CO_2-free nuclear power. With thirteen paper mills in Finland, Germany, Great Britain, France, Austria, China, and United States the paper production remains the central aim of this company, managed by three UPM sectors: UPM Raflatac, UPM Specialty Papers and UPM Communication Papers. The first one is dedicated to the labelling materials production for a wide range of commercial products of other companies (food, beverage, and personal care). UPM Specialty Papers, strictly related to UPM Raflatac, produces several types of high-quality papers, always by environmentally sustainable processes. Some products are labelling papers, but also papers for print, and packaging. UPM Communication Papers is the world's leading producer of graphic papers intended for the advertising sector, publishing as well as for domestic and office uses.

UPM Plywood is UPM sector not only for constructions but also for vehicle flooring and LNG shipbuilding. Their flagship product is high-quality WISA plywood.

With a view towards innovation, UPM produces also innovative and sustainable composite materials (UPM Biocomposite). These products, useful in several sectors, combine the modularity of plastic with the strength and the sustainability of wood and they are characterized by at least 50% of recycled raw material. In recent years biorefinery of UPM expanded towards biochemical sector. UPM Biochemicals, in Germany, has the purpose to produce biomolecules starting from wood. Lignin-based fillers, for example, replace silica and carbon black in rubber offering some advantages such as a greater purity and lightness. Another field of application is the conversion in several industrial products of bio-based glycols, made by UPM. UPM Biomedicals is the sector aimed at medicine and, in particular, to the care of skin injury, in cell therapy as well as in tissue engineering applications. This is possible thanks to nanofibrillar cellulose-based hydrogels highly compatible with human cells and tissues, but absolutely free of material of animal origin.

With about 570'000 hectares of forests in Finland and United States and 255'000 hectares of plantations in Uruguay, UPM is also involved in the growth of both corporate and private forests. The eco-sustainability of products synthesized from wood is based on sustainable forest management, aimed at maintaining biodiversity and combating deforestation. To do this, UPM uses modern forest management methods that have already proven successful in Finland. Although the production of wood-based products has increased, in recent years the growth of forests in Finland has increased, giving a concrete signal of the commitment that this company makes to tackle environmental problems.

About this, on the UPM-Kymmene website, we can read:

"Our business is based on forests. This is a strong reason to ensure that forests grow for many generations to come. Forests must remain forests.
We have zero tolerance for deforestation and have strict processes in place to ensure that forests always grow more than they are used."[50]

During my PhD I spent about 7 months at the UPM NERC (North European Research Centre) in Lappeenranta, Finland, under the supervision of the Manager Business Development, Biochemicals Dr. Suvi Pietarinen.
During this period, the hybrid materials lignin@metals that I'm going to present, were characterized focusing on the lignin matrix to understand if the polymer underwent some modifications after the syntheses (Chapter 2). Lignin functionalization was also performed and in particular acetylation of lignin allowed to functionalize all the OH groups. Preliminary in vitro studies was also conducted on acetylated lignin to evaluate its antibacterial activity after the removal of aromatic and aliphatic OH groups.
Phosphorylation of lignin was also conducted with the aim to study in future works its adsorption and reducing properties towards Cr(VI) in water.

Green Innovation GmbH[51]

Green Innovation is an Austrian Company founded in 2015 with headquarters in Innsbruck. In figure 1.8, its logo.

Figure 1.8. Green Innovation logo

It operates in the zootechnical field, in particular to ensure sustainable breeding that places the welfare of the animals at the centre. About this, the flagship product is Oxilem TM, a product for animal husbandry obtained starting from BioPiva, the lignin I used in my PhD. Recently, their work has also expanded in the agronomic field with the development of new products based on polyphenols, and microorganisms thanks to the support of an advanced microbiology research. As its name suggests, the focus of the company is the development of new products not only for the "green sector" related to animal and agronomic field, but also with a green perspective based on sustainable and renewable sources.
To do this, Green Innovation invests heavily on research. With 20 research projects, and several collaborations spread throughout Europe, in 2020 sums that exceeded 20% of revenues.
The development of new products is coordinated by several collaborations including UPM-Kymmene (since 2015), Garant (GmbH, Austria) and Zoogamma (S.p.A, Italy), which follow all the steps of the process from the idea to the marketing of the finished product. Green Innovation is on international markets including Europe, Asia, Australia, Canada, Mexico and China.
The Green Innovation economy is always in strong development. In 2020 it had a turnover of more than 2'200'000 euros. This also denotes the new and renewed sentiment on the market for sustainable solutions that best enhance ideas and natural products.

Aim of the thesis

It is precisely from the great potential of this biopolymer and from the intention to enhance its use that the PhD project begins.
In particular, the research project focused on the possibility of obtaining new potential pesticides for the agrochemical field, combining lignin with the metal most commonly used for this purpose like copper and, to a lesser extent, iron. In fact, if on the one hand, recent studies show the potential of lignin as an antibacterial, on the other the agronomic sector is experiencing an increasingly urgent need to develop new pesticides that can respond to the problem of the accumulation of the metal in the soil.
From here, then, the intuition of exploiting the biocidal action of lignin to obtain new pesticides which, with a smaller amount of metal, can be more effective than the inorganic products currently on the market. In this regard, three hybrid materials lignin@brochantite, lignin@cuprite and lignin@goethite will be presented here. The synthetic procedures of these products have been optimized by taking into account the simplicity, eco-sustainability and scalability of operations with a view to possible future industrial developments. The characterization of these materials concerned both the inorganic part and lignin and allowed to understand if the polymer has undergone structural changes following the synthesis. Finally, the biocidal activity was evaluated against various pathogens through in vitro and in vivo tests.

Furthermore, two lignin functionalizations will be taken into consideration. Acetylation was conducted in order to evaluate the influence of phenolic groups on the antibacterial activity of lignin, while phosphorylation opens a new future chapter on the uses of lignin for the remediation of Cr (VI) polluted waters.

Finally, the study of the coordinative properties of lignin starting from lignin-inspired ligands will lead to the isolation of a new 1D coordination polymer in which an octahedral and a tetrahedral cobalt atoms are bridged by a ferulate dianion.

References:

1. Brown, R. M. Cellulose Structure and Biosynthesis: What is in Store for the 21st Century? *J. Polym. Sci. Part A Polym. Chem.* **42**, 487–495 (2003).

2. Salmén, L., Olsson, A. M., Stevanic, J. S., Simonovic, J. & Radotic, K. Structural organisation of the wood polymers in the wood fibre structure. *BioResources* **7**, 521–532 (2012).

3. Sjostrom, E. & Westermark, U. Chemical Composition of Wood and Pulps : Basic Constituent and Their Distribution. *Anal. Methods Wood Chem. Pulping, Papermak.* 1–19 (1999) doi:10.1007/978-3-662-03898-7_1.

4. Becker, J. & Wittmann, C. A field of dreams: Lignin valorization into chemicals, materials, fuels, and health-care products. *Biotechnol. Adv.* **37**, 107360 (2019).

5. Ten Have, R. & Teunissen, P. J. M. Oxidative mechanisms involved in lignin degradation by white-rot fungi. *Chem. Rev.* **101**, 3397–3413 (2001).

6. Beisl, S., Friedl, A. & Miltner, A. Lignin from micro- To nanosize: Applications. *Int. J. Mol. Sci.* **18**, (2017).

7. Lora, J. *Industrial Commercial Lignins: Sources, Properties and Applications. Monomers , Polymers and Composites from Renewable Resources*. (2008). doi:10.1016/b978-0-08-045316-3.00010-7.

8. Lundquist, K. & Parkås, J. Different types of phenolic units in lignins. *BioResources* **6**, 920–926 (2011).

9. Calvo-Flores, F. G. & Dobado, J. A. Lignin as renewable raw material. *ChemSusChem* **3**, 1227–1235 (2010).

10. Solihat, N. N. *et al.* Lignin as an Active Biomaterial: A Review. *J. Sylva Lestari* **9**, 1–22 (2021).

11. Mandlekar, N. *et al.* An Overview on the Use of Lignin and Its Derivatives in Fire Retardant Polymer Systems. in *Lignin - Trends and Applications* vol. 32 207–232 (2018).

12. Alén, R. Chapter1: Structure and chemical composition of wood. in *Forest*

Products Chemistry (Fapet Oy, 2000).

13. Tsvetkov, M. V. & Salganskii, E. A. Lignin: Applications and Ways of Utilization (Review). *Russ. J. Appl. Chem.* **91**, 1129–1136 (2018).

14. Vishtal, A. & Kraslawski, A. Challenges in industrial applications of technical lignins. *BioResources* **6**, 3547–3568 (2011).

15. Tomani, P. The lignoboost process. *Cellul. Chem. Technol.* **44**, 53–58 (2010).

16. Crestini, C., Lange, H., Sette, M. & Argyropoulos, D. S. On the structure of softwood kraft lignin. *Green Chem.* **19**, 4104–4121 (2017).

17. Giummarella, N., Lindén, P. A., Areskogh, D. & Lawoko, M. Fractional Profiling of Kraft Lignin Structure: Unravelling Insights on Lignin Reaction Mechanisms. *ACS Sustain. Chem. Eng.* **8**, 1112–1120 (2020).

18. Palonen, H. Role of lignin in the enzymatic hydrolysis of lignocellulose. *VTT Publ.* 3–80 (2004).

19. Jin, Y., Ruan, X., Cheng, X. & Lü, Q. Liquefaction of lignin by polyethyleneglycol and glycerol. *Bioresour. Technol.* **102**, 3581–3583 (2011).

20. Stephen Y. Lin, C. W. D. *Methods in Lignin Chemistry*. (Springer Series in Wood Science: Wood structure and enviroment, 1992).

21. Goldmann, W. M. *et al.* Determination of phenolic hydroxyl groups in technical lignins by ionization difference ultraviolet spectrophotometry (Δε-IDUS method). *Periodica Polytechnica Chemical Engineering* vol. 61 93–101 (2017).

22. Gärtner, A., Gellerstedt, G. & Tamminen, T. Determination of phenolic hydroxyl groups in residual lignin using a modified UV-method. *Nord. Pulp Pap. Res. J.* **14**, 163–170 (1999).

23. Goldschmid, O. Determination of Phenolic Hydroxyl Content of Lignin Preparations by Ultraviolet Spectrophotometry. *Anal. Chem.* **26**, 1421–1423 (1954).

24. Obst, J. & Landucci, L. Quantitative 13 C NMR of lignins–Methoxyl: aryl ratio. *Holzforschung* **40**, 87–92 (1986).

25. Espinoza-Acosta, J. L., Torres-Chávez, P. I., Ramírez-Wong, B., López-Saiz, C. M. & Montaño-Leyva, B. Antioxidant, antimicrobial, and antimutagenic properties of technical lignins and their applications. *BioResources* **11**, 5452–5481 (2016).

26. Pan, X., Kadla, J. F., Ehara, K., Gilkes, N. & Saddler, J. N. Organosolv ethanol lignin from hybrid poplar as a radical scavenger: Relationship between lignin structure, extraction conditions, and antioxidant activity. *J. Agric. Food Chem.* **54**, 5806–5813 (2006).

27. Barclay, L. R. C., Xi, F. & Norris, J. Q. Antioxidant properties of phenolic lignin model compounds. *J. Wood Chem. Technol.* **17**, 73–90 (1997).

28. Dizhbite, T., Telysheva, G., Jurkjane, V. & Viesturs, U. Characterization of the radical scavenging activity of lignins - Natural antioxidants. *Bioresour. Technol.* **95**, 309–317 (2004).

29. Ugartondo, V., Mitjans, M. & Vinardell, M. P. Comparative antioxidant and cytotoxic effects of lignins from different sources. *Bioresour. Technol.* **99**, 6683–6687 (2008).

30. Crouvisier-Urion, K. *et al.* Biobased Composite Films from Chitosan and Lignin: Antioxidant Activity Related to Structure and Moisture. *ACS Sustain. Chem. Eng.* **4**, 6371–6381 (2016).

31. Peyrat-Maillard, M. N., Bonnely, S. & Berset, C. Determination of the antioxidant activity of phenolic compounds by coulometric detection. *Talanta* **51**, 709–716 (2000).

32. Dawidowicz, A. L., Wianowska, D. & Olszowy, M. On practical problems in estimation of antioxidant activity of compounds by DPPH method (Problems in estimation of antioxidant activity). *Food Chem.* **131**, 1037–1043 (2012).

33. Dong, X. *et al.* Antimicrobial and antioxidant activities of lignin from residue of corn stover to ethanol production. *Ind. Crops Prod.* **34**, 1629–1634 (2011).

34. Sun, S. L., Wen, J. L., Ma, M. G., Sun, R. C. & Jones, G. L. Structural features and antioxidant activities of degraded lignins from steam exploded bamboo stem. *Ind. Crops Prod.* **56**, 128–136 (2014).

35. Sun, S. N., Cao, X. F., Xu, F., Jones, G. L. & Baird, M. Alkaline and organosolv lignins from furfural residue: Structural features and antioxidant activity. *BioResources* **9**, 772–785 (2014).

36. Cazacu, G., Capraru, M. & Popa, V. I. *Advances concerning lignin utilization in new materials*. *Advanced Structured Materials* vol. 18 (2013).

37. Ramchoun, M. *et al.* Investigation of antioxidant and antihemolytic properties of Thymus satureioides collected from Tafilalet Region, south-east of Morocco. *Asian Pac. J. Trop. Biomed.* **5**, 93–100 (2015).

38. Klein, S. E., Rumpf, J., Alzagameem, A., Rehahn, M. & Schulze, M. Antioxidant activity of unmodified kraft and organosolv lignins to be used as sustainable components for polyurethane coatings. *J. Coatings Technol. Res.* **16**, 1543–1552 (2019).

39. Faustino, H., Gil, N., Baptista, C. & Duarte, A. P. Antioxidant activity of lignin phenolic compounds extracted from kraft and sulphite black liquors. *Molecules* **15**, 9308–9322 (2010).

40. Zakzeski, J., Bruijnincx, P. C. A., Jongerius, A. L. & Weckhuysen, B. M. The catalytic valorization of lignin for the production of renewable chemicals. *Chem. Rev.* **110**, 3552–3599 (2010).

41. Lora, J. H. & Glasser, W. G. Recent industrial applications of lignin: A sustainable alternative to nonrenewable materials. *J. Polym. Environ.* **10**, 39–48 (2002).

42. Moreno, A., Morsali, M., Liu, J. & Sipponen, M. H. Access to tough and transparent nanocompositesviaPickering emulsion polymerization using biocatalytic hybrid lignin nanoparticles as functional surfactants. *Green Chem.* **23**, 3001–3014 (2021).

43. Liu, J. *et al.* Fully Biobased Photothermal Films and Coatings for Indoor Ultraviolet Radiation and Heat Management. *ACS Appl. Mater. Interfaces* **14**, 12693–12702 (2022).

44. Farooq, M., Zou, T., Riviere, G., Sipponen, M. H. & Österberg, M. Strong, Ductile, and Waterproof Cellulose Nanofibril Composite Films with Colloidal Lignin Particles. *Biomacromolecules* **20**, 693–704 (2019).

45. Helmut Nagele, Jiirgen Pfitzer, Edgar Nagele, Emilia R. Inone, Norbert

Eisenreich, W. E. and P. E. ARBOFORM® - A THERMOPLASTIC, PROCESSABLE MATERIAL FROM LIGNIN AND NATURAL FIBERS, Chapter 6-. in *Chemical Modification, Properties, and Usage of Lignin* 101–119 (2002). doi:10.1007/978-1-4615-0643-0_10.

46. Chandna, S., Thakur, N. S., Reddy, Y. N., Kaur, R. & Bhaumik, J. Engineering Lignin Stabilized Bimetallic Nanocomplexes: Structure, Mechanistic Elucidation, Antioxidant, and Antimicrobial Potential. *ACS Biomater. Sci. Eng.* **5**, 3212–3227 (2019).

47. Roopan, S. M. An overview of natural renewable bio-polymer lignin towards nano and biotechnological applications. *Int. J. Biol. Macromol.* **103**, 508–514 (2017).

48. Richter, A. P. *et al.* An environmentally benign antimicrobial nanoparticle based on a silver-infused lignin core. *Nat. Nanotechnol.* **10**, 817–823 (2015).

49. Maggiolino, A. *et al.* Dry-aged beef steaks: Effect of dietary supplementation with pinus taeda hydrolyzed lignin on sensory profile, colorimetric and oxidative stability. *Foods* **10**, 1080 (2021).

50. UPM-kymmene website. https://www.upm.com/.

51. Green Innovation website. https://www.greeninnovation.at/en/.

Chapter 2: Lignin@metal, Novel Hybrid Materials for agrochemical applications

The intense exploitation of soils for cultivation and the deforestation of huge areas to create space for new arable fields are just two of the main problems linked to the ever-increasing needs of a growing world population[1,2]. An issue of great concern is the diffusion of pathogens that can cause a substantial decrease in land productivity and even irreparably damage hectares and hectares of cultivated fields. This is not only reflected in disastrous economic damage for companies[3], but, also, in the inability to meet the demand for food, causing famines especially in the poorest countries[4].

Pesticides represent the most common way to manage pest control and the development of increasingly efficient and safe pesticides for human health and the environment has always been an important issue for science.

Several products are currently being studied as pesticides. Among these, some are based on organic molecules[5] and others are based on metals such as copper, iron, zinc and silver, whose antibacterial properties have long been known[6]. Always used as bulk through formulations with salt mixtures[7], a growing interest is currently aimed at transition metal nanoparticles, which, thanks to the higher surface area to volume ratio, have often a greater activity[8]. In these systems, the important biological functions of transition metals such as hydroxylation, redox activity, and electron transport[8,9] are combined with the advantages of nanoscale materials. With metal transition nanoparticles, in fact, the bactericidal activity is enhanced thanks to a greater control over the release of active ionic species[10] and to the ability to generate Reactive Oxygen Species (ROS). Nanoparticles are also considered to be able to participate in subcellular reactions and, if they are positively charged, they can alter the electron transport chain in bacteria[8].

However, the proven activity of nanoparticles must take into account their potential toxicity to human health[8]. Their action, which is exerted on bacteria through a series of mechanisms such as ROS production, gene regulation changes, cell wall penetration, membrane depolarization[10] and metabolite binding, can, in fact, also have side effects on human cells[8]. This is due to the similarity of the biomolecules (DNA, lipids, proteins) with the target systems of these new potential antibacterial[8]. The main problem for their effective use is that the concentration as an effective antimicrobial is sometimes greater than the concentration at which their toxicity is exerted (5-10 µg/mL in eukaryotic cells)[8]. Regarding this aspect, there are still few studies hampered also by the high

heterogeneity of information present in the literature on nanoparticulate systems[8].

Some studies show that lignin has antibacterial and antifungal properties, but there are still many aspects that need to be evaluated in order to exploit this by-product for biocidal applications. Because of its complexity and the high heterogeneity of its structure it is difficult to categorically establish the degree of its activity. Solihat et al. report the efficacy of different types of lignins against different pathogens belonging to the two main categories of Gram positive and Gram negative[11]. The greatest biocidal activity has been attributed to softwood organosolv lignin, while the lowest activity to the organosolv lignin deriving from grass[11]. An intermediate activity, on the other hand, has been recognized for softwood kraft lignin[11].

Other searches compare the antibacterial activity between modified and not modified lignin. Klein et al., for example, report on studies about the antibacterial activity of intact Kraft lignin and the corresponding demethylated lignin[12]. In particular, they tested different concentrations of kraft lignin, precipitated at different pH (from 2 to 5) evaluating the activity of demethylated lignin in polyurethane coating. These materials have a good activity against *S. aureus* while for all concentrations used, kraft lignin with the best biocidal activity is the one precipitated at pH=5. Alzagameem et al. describe the action of kraft lignin fractions with a different grade of purification[13]. They showed that the first fractions obtained in the purification process have a higher activity, strictly correlated to the number of OH groups present. Probably, further purification steps can lead to a lower content of active compounds in the lignin such as, mainly, the differently substituted polyphenols. The effect of lignin storage on antibacterial activity has also been evaluated. After 6 months, the polymer is more active. This could be explained by partial lignin degradation that makes the active species more available and imparts higher antibacterial and antioxidant activity to the materials[13].

A further observation concerns the positive influence of γ-rays on antimicrobial properties of lignin[14]. El-Nemr et al. synthetised polyvinyl alcohol/gelatine-lignin blends varying both the concentration of lignin and the gamma irradiation power. Antibacterial properties of these blends were then tested on Gram-positive and Gram-negative bacteria revealing that the action of lignin is higher when a more intense gamma irradiation is used to prepare blends. Gamma irradiation would

cause the formation of radical intermediates in the structure of the polymer leading to the hypothesis that, like the antioxidant activity, the antibacterial activity of lignin can also be exerted through radical mechanisms[13–15]. Gyawali et al. report, in fact, how the scavenging of free radicals attributable to phenols can inhibit the growth of unwanted microorganisms by reducing the redox potential of the growth medium[16].

The comparison between lignin and lignin modified by oxidation was also evaluated underlying how the antibacterial activity is generally reduced in the second case[17].

Tests carried out on different types of lignins against a wide range of pathogens highlight the great variability of the results that can be obtained, thus not allowing a clear rationalization of the activity. The antimicrobial action of lignin, in fact, depends not only on a series of experimental factors, including the type of pathogen, the medium used, strictly connected to the solubility of the tested sample, and, in general, to the operating conditions under which the tests are carried out, but also from the origin of the polymer, from the extraction method used and, ultimately, therefore, from its structure[11,16,17].

In most cases, for example, it has been noted that the inhibitory action of lignin has a greater effect on Gram positive rather than Gram negative[11,14]. The reason could lie in the fact that Gram positive, contrary to Gram negative bacteria, do not possess the secondary cell wall; they have a thicker peptidoglycan layer with which lignin would interact with consequent breakage of the structure of the inner cell membrane, thus causing the infiltration of cellular components until the death of the pathogen[13,14,18].

The origin of lignin and the extraction processes are closely related to its structure (Chapter 1). The importance of these aspects on its antibacterial activity is explained by the nature of the constituent phenolic compounds[19]. The main antibacterial action is attributable to polyphenolic compounds having a double bond on the C^{α} and C^{β} of the side chain and a methyl group on the C^{γ}, see figure 2.1[11,17,18,20,21]. Their action is based on the rupture of the cell membrane of the bacterium resulting in the release of cellular content, while other molecules deriving from lignin, such as cinnamaldehyde, deplete adenosine triphosphate by infiltration of the bacterium and decrease of the intracellular pH[14,17,18].

In light of these considerations, the study of the antimicrobial activity of lignin inspired molecules assumes fundamental importance for understanding the

pesticidal action of the entire polymer. Gyawali et al. showed a detailed description of functional groups that can affect the antimicrobial activity of model compounds. The main phenomena that seem to have a fundamental role in the biocide action are the electron delocalization and the electron withdrawing of the functional groups of the molecules[16]. In this regard, the position and number of both hydroxyl groups on the aromatic ring and double bonds on the side chain can greatly alter the antibacterial activity of a molecule. Such groups, in fact, promoting the electron delocalization, act as proton exchanger and reduce the gradient across the cytoplasmic membrane[14]. This, following the exhaustion of the ATP pool, leads to cell death[16]. The influence of the position of OH groups on efficacy as an antibacterial is mainly observed in oxygenated terpenes[15,22]. Their action is based on making the cell membrane permeable causing the loss of potassium ions. Griffin et al. highlight, in fact, how the presence and position of OH groups in oxygenated terpenes affect their diffusion across the membrane by creating hydrogen bonds and increasing their solubility[22]. It is for these reasons that hydrocarbon terpenes have a lower activity than oxygenated terpenes[16].
Comparing the activity of caffeic acid and *p*-coumaric acid, it is clear how the number of OH groups can influence the antimicrobial activity of molecules. In fact, caffeic acid differs from *p*-coumaric only by an extra hydroxyl group in the aromatic ring, but this seems to be enough to exert greater activity[16]. It has been observed that the presence of multiple OH groups has also a significant importance in benzaldehyde derivatives as they favour the interaction of these molecules with the sulfhydryl groups of proteins on the outer surface of the cells[16]. The presence of double bonds and, in particular, conjugated systems that increase the tendency of the OH groups to release proton and to act as proton exchanger also contributes to the delocalization of electrons[16]. In this way the pH gradient across the cytoplasmic membrane is reduced leading to cell death. The location and number of double bonds are also important. In fact, it has been shown that molecules having two double bonds instead of one have an increased antibacterial activity while the effect of the position of the double bond is described by the comparison between the antibacterial activity of isoeugenol and eugenol[16]. Surprisingly, the double bond on carbons beta and gamma in eugenol, make this molecule more active than isoeugenol despite the conjugated system of the last one.

Anyway, the correlation between structure and activity is less clear when it comes to isomers. Sometimes the different activity of two isomers seems to depend more on the type of bacterium than on the molecule tested[16].
Also, the presence of alkyl substituents and their dimension can have a positive effect on the antimicrobial activity stabilizing the formation of radical species[15].
The high antibacterial and antifungal activity of hydroxycinnamaldehyde derivatives is instead related to electronegativity increased by the presence of alkyl, alkenyl and hydroxyl groups[14,19]. The most electronegative molecule interferes in biological processes involving electron transfer and, by reacting with the vital nitrogen components (proteins and nucleic acids), inhibits the growth of microorganisms[15,16].
Even the presence of acetate groups could positively influence the antibacterial activity. The lipophilic fragments could in fact have an action in the destruction of the cell membrane by inhibiting the transport of electrons, acting on the translocation of proteins, on phosphorylation and on other enzymatic activities, thus leading the microorganism to death[15,16].
Although the mechanism by which lignin acts has not yet been clarified, the important studies on model compounds allow us to understand what lies at the basis of its antimicrobial activity. Figure 2.1 shows the model compounds previously cited.

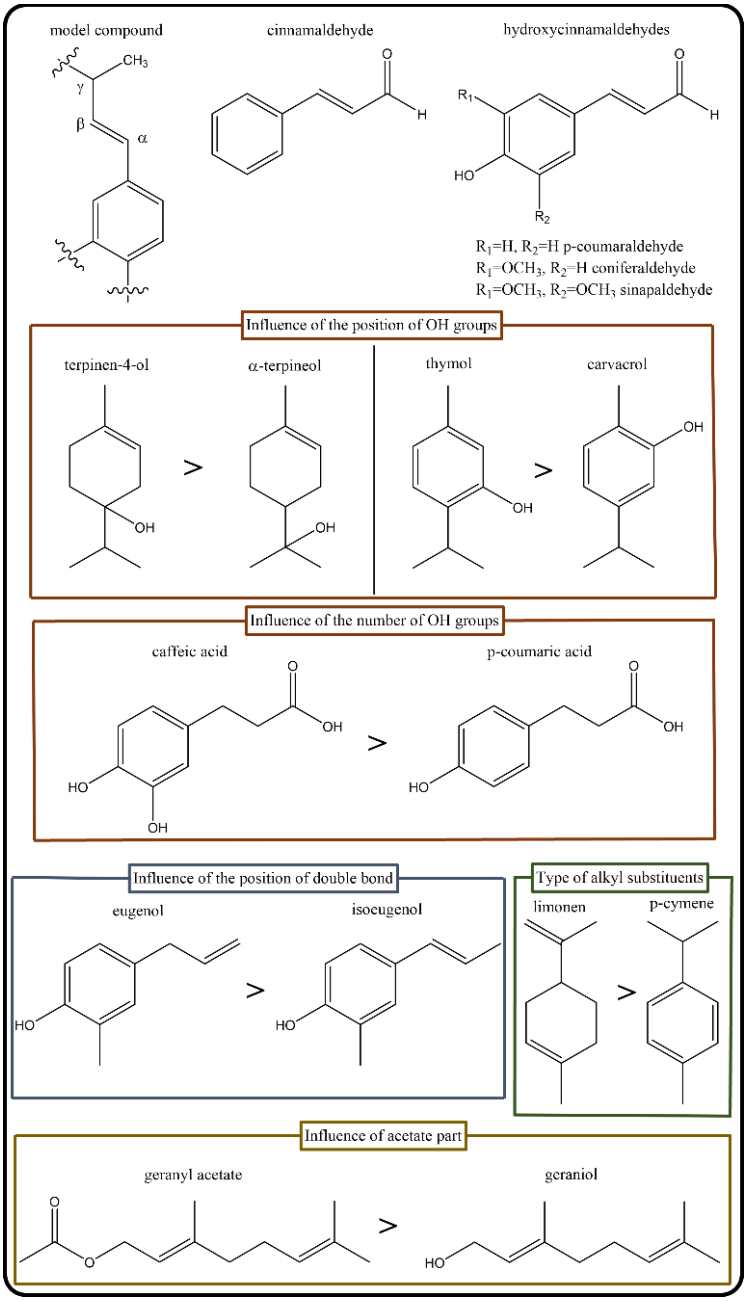

Figure 2.1 Lignin model compounds and their relative activity depending on functional groups.

On the other hand, the progenitor of pesticides is certainly copper. Its antibacterial properties were already known in the ancient Egypt in which this metal was used both to preserve water and food and for medical applications[23]. However, the first conscious use of copper dates back to the end of the 1800s as a pesticide for crops in the form of Bordeaux mixture[24]. Casually discovered in 1885 by Pierre-Marie Millardet, Bordeaux mixture is a blue colloidal suspension obtained mixing properly copper sulphate and calcium hydroxide. The latter added to fix the high solubility of the former which did not make the product suitable for foliar and fruits applications[7]. The insolubility in water of copper hydroxide formed and stabilized by the formation of calcium sulphate allowed the metal to be fixed, reducing its phytotoxicity while maintaining its activity against pathogens high[7].

Even today, copper remains one of the main systems for the protection of crops from fungi, bacteria and yeasts, and research has made progress in understanding the mechanism underlying its effectiveness, closely related to that of the other transition metals silver, zinc, and iron[8].

Although the antibacterial activity of copper depends on several factors, such as physical form of copper species, the oxidation state of the metal and the way of utilization[23], the mechanisms with which its biocidal activity manifests are the depolarization of the cell membrane and the generation of Reactive Oxygen Species (ROS)[10], both attributable to metal ions[8].

All microorganisms are characterized by an electrical potential difference between the inside and outside of the cell of about 100-200 eV[25]. Metal ions (Cu^{2+}, Cu^{+}, Ag^{+}), thanks to their positive charge, interact with negatively charged groups present on the cell membrane such as phosphate groups, amino groups and carboxyl groups reducing the potential difference until zero[8,10]. The increase in the permeability of the cell membrane and the plasmolysis of the cell are just some of the mechanisms that lead to the final rupture of the cell and the consequent death of the microorganism[8,10]. Warnes et al. demonstrated this mechanism using fluorescent probes properly attached on the cell membrane of *Escherichia coli* [25]. Bacteria in contact with copper-based surfaces, after a few minutes, lost fluorescence, indicating the rupture of the cell membrane. This did not happen with bacteria not exposed to any surface or put in contact with stainless steel surfaces. In conjunction with this process, the metal ions also have an action in the generation of reactive oxygen species (ROS) according to the

mechanism described by Fenton chemistry [8,10,25]. ROS are very reactive oxygen species produced during basic metabolism. Cellular stress conditions due, for example, to the action of metal nanoparticles can, however, increase the concentration of these species up to toxic levels. This occurs when oxygen acquires unwanted oxidation states and transforms into free radicals, superoxides and peroxides[8]. One of the key mechanisms is the Fenton reaction according to which hydroxyl radicals are formed by the reaction between hydrogen peroxide and the metal ion which is oxidated.

$$M^{n+} + H_2O_2 \rightarrow OH^- + OH^{\cdot} + M^{(n+1)+}$$

This mechanism can take place both inside and outside the cell, generating extracellular and intracellular ROS which cause the destruction of the cell membrane by lipid peroxidation following oxidative stress.
The high affinity of ROS for R-SH groups of amino acids such as cysteine can, furthermore, damage the function of specific enzymes as well as cause the rupture of disulfide bridges necessary to keep proteins folded. It has been shown that ROS are also responsible for DNA degradation, the destruction of which continues even after cell death[8,25]. It is not clear which mechanism predominates and in which conditions, but it is certain that there is always a concomitance of the two processes. Mitra et al. describe a process of “contact killing” for copper surfaces in contact with microorganisms which is based on the dissolution of copper ions causing the depolarization of the membrane. This leads to an initial loss of intracellular components, while ROS are responsible of their oxidative degradation until the genomic and plasmid degradation of DNA occur[10].
Another effect that seems to affect the bactericidal activity of metal ions is the change in the electronegativity of the cell membranes by interaction with negatively charged groups[8]. These groups are located in specific domains of the membrane, causing a high and localized stress at specific points. The antibacterial activity will also vary depending on the type of bacterium tested. Although copper is considered a pesticide with broad spectrum activity due to its ability to deactivate cellular enzymes by interaction with the hydroxyl, sulfhydryl, amino and carboxy groups of these systems[4], Slavin et al. show how, generally, Gram positive are also more resistant to the action of nanoparticles[8]. This is due to the presence of a thicker peptidoglycan layer than Gram negative[8].

Currently, copper remains the metal par excellence in the agricultural sector and copper-based compounds are the only pesticides that can be used in organic agriculture[4].

However, the problems associated with its intensive use are increasing. Among others, its accumulation in soils and the development of metal-resistant strains are the most urgent[4]. The accumulation in soils causes the death of the soil biota, plants phytotoxicity as well as extensive environmental pollution that can reach the underground aquifers[7]. In fact, copper penetrates downwards into the soil and the pH and the type of soil can be important factors in limiting or accentuating its spread[7]. Soils with higher pH, for example, would counteract the diffusion of copper as they would limit its dissolution. Sandy soils make copper penetrate more easily in depth unlike clayey soils or soils characterized by organic matter which would help to fix the metal. It has been found that about 30mg/kg of copper in the soil can cause toxicity in plants that can manifested on both leaves and fruits, making the product unmarketable[7]. Plants exposed to high copper concentrations exhibit chlorosis, darkening, necrotic spots, and leaf margin burns. In parallel to this, the development of copper resistant strains and the possibility of a horizontal transfer of the copper resistance gene that can occur between different genotypes of pathogenic bacteria are a further motivation to find valid alternatives to this metal[7]. Cameron et al. have shown, for example, that the Gram-negative bacteria *Pseudomonas syringae pv. actinidiae (Psa)* which exhibited resistance to copper were characterized by copR and copS genes[3].

It is for these reasons that today restrictions on the use of copper in agriculture are increasingly important. Currently the quantity of copper that can be used in Italy, Spain and France is 6 kg/ha/year while in Germany, Austria, and Switzerland it is even lower, at 3-4 kg/ha/year[7]. To limit the problems caused by its utilization there are also strategies concerning agricultural practice. Optimizing the use of copper does not mean, in fact, only reducing the quantity used, but also respecting the agricultural timing in the application of the product, preparing suitable formulations that release copper in a controlled way, for example, using copper species that are not too much soluble in water.

Alongside these solutions, research is focused on the finding of valid alternatives[3]. These include nanoparticle materials whose activity, based mainly on the release of ions, has been shown to be greater vs bulk[8].

Other alternatives may reside in organic molecules that exhibit antimicrobial properties. Cameron et al., for example, see chitosans, antimicrobial peptides and terpenes as valid alternatives against *Pseudomonas syringae pv. actinidiae*. The mechanism of action of terpenes, for example, lies in the alteration of the permeability of the membrane caused by interactions with its lipid fractions[3]. This inevitably leads to the leakage of intracellular material and to the cell death.
Composite copper materials with polymers can also be a way to optimize the distribution of the metal on the surfaces to be treated[10]. The use of polymer matrixes, in fact, could represent a double benefit. While these materials can be a larger reservoir of antimicrobial agent, on the other hand they can regulate its release, preventing the copper from being washed off the surfaces to which it is applied. However, a critical point of these materials will be the homogeneity of the metal distribution in the polymer[10]. The polymers used in combination with both nanoparticles and copper salts include, among others, polypropylene, polymethylmethacrylate, polyvinylmethylketone, polyvinylchloride. In the packaging and healthcare sectors, Cu-cellulose composite materials are also attracting great interest[10].

It is from these premises that the work presented here begins. Finding valid alternatives to the current copper-based pesticides on the market in order to reduce the copper accumulation in the soil is only one of our goals. The choice to use lignin, currently considered a waste from paper mills and bioethanol industries, also allow us to find solutions to encourage the circular economy. Using what should be thrown away not only allows to reduce disposal costs but has a much greater importance in terms of environmental sustainability. Most of lignin produced today is, in fact, burned to gain energy, producing CO_2, and preventing the exploitation of all potential properties of this interesting natural polymer (Chapter 1).
The starting idea was, therefore, to combine the antibacterial properties of copper with those of lignin. The possible combined effect of the two components will allow the use of a reduced metal content maintaining a biocidal efficacy comparable and, in some cases, greater, to that of the copper-based pesticides currently on the market.
In this regard, two copper-based hybrid materials, lignin@brochantite (see paragraph “Lignin@brochantite”) and lignin@cuprite (see paragraph

"Lignin@cuprite") were obtained. The name of "hybrid material" was decided mainly to distinguish them from composites in which a phase is dominant and continuous[26]. In our materials the use of hybrid term was to emphasize the presence of an organic and an inorganic part[27]. These two components constitute a mechanical mixture, thus not being able to consider the lignin as a continuous phase. The organic and inorganic parts, in fact, will constitute two completely distinct units and ideally separable in a mechanical way. The only requirements would be a huge lens and abundant patience!

A second metal of extreme importance for the agronomic sector is iron. Mainly used as fertilizer, especially as nanoparticles of iron oxide[6,28,29], it is currently studied as a potential anti-biocide due to its catalytic activity in Fenton reactions which play an important role in the generation of ROS responsible for the destruction of DNA[30]. A hybrid material based on iron(III), lignin@goethite, was then synthesized (see paragraph "Lignin@goethite").

In the context of environmental sustainability, a certain regard has also been given to synthetic procedures aimed at reducing consumption, using only reagents compatible with the agronomic field, up to moving, when possible, towards mechanochemical synthesis. One of the most critical points in mechanochemical synthesis is energy consumption, a parameter that must be taken into consideration when assessing the environmental impact of a given system[31]. In this regard Schneider et al. compare the efficiency in the Suzuki-Miyaura synthesis of mechanochemistry and microwave radiation, highlighting how mechanochemistry constitutes an advantage both from the point of view of yield and from the point of view of energy consumption[32]. Singh et al. instead, compare mechanochemistry with synthesis in solution for obtaining complexes by evaluating the energy usage, energy efficiency and the cost difference. According to their study, mechanochemistry appears to be energetically advantageous especially for large-scale synthesis[31].

Thus mechanochemistry opens a new way of making synthesis, faster, more suitable for a scale up synthesis and more eco-sustainable[33,34].

In vitro and *in vivo* tests were used to evaluate the effectiveness of each material presented here by making a comparison with the pesticides currently on the market.

Lignin@brochantite

Brochantite is the crystalline mineral phase of $Cu_4(SO_4)(OH)_6$, already used as antimicrobial copper compound for foliar diseases[7].
The hybrid material was synthesized by means of a heterogeneous reaction between lignin, $CuSO_4 \cdot 5H_2O$ and NaOH[35]. Subsequently the procedure was also optimized through mechanochemistry, in order to make it more suitable for industrial scale applications[36].
Brochantite phase within lignin matrix was characterized by means of XRPD. Materials with different percentages of copper (from 3% to 20%) were obtained and the complete upload of the metal was assessed by means ICP-AES analysis. A correlation between the copper concentrations and the morphology of brochantite crystals in the lignin matrix was also studied by means of TEM analysis, and the copper distribution evaluated by means of EDS mapping.
NMR, GPC and Py-GC/MS allowed to study the lignin in materials in order to understand if the synthetic procedure caused a modification in lignin structure. After a test to assert the stability of the material in aqueous environments with different pH, its activity was evaluated by both *in vitro* and *in vivo* tests. A correlation between crystals morphology and their activity was also conducted by *in vivo* trials.

Experimental Part:

The technical lignins employed without further purification were both Kraft lignins from Pinus taeda, provided by UPM-Kymmene Oyj and Green Innovation GmbH: BioPiva100 (M_w=4400-5000 g/mol, M_n= 1200-1300 g/mol) and BioPiva395 (M_w=5950-6000 g/mol, M_n= 1560-1565 g/mol). Their characteristics are presented in dedicated section in chapter 1, “Lignin materials used in this work”.
$CuSO_4 \cdot 5H_2O$ and NaOH were purchased from Sigma Aldrich and used without further purification.
pH was measured with a Crison pHmeter basic 20 equipped with an Ag/AgCl electrode.
Acetate and phosphate/phthalate buffers were purchased from Sigma Aldrich.

Mechanochemical syntheses were conducted through a planetary ball mill Retsch PM100.

Synthesis and characterization of materials:

Wet procedure

The reaction, conducted at room temperature, consisted in suspending lignin, BioPiva100, in distilled water (10mL). Under vigorous stirring a water solution of $CuSO_4 \cdot 5H_2O$ (5mL) containing the desired amount of the metal was added. The different lignin/$CuSO_4 \cdot 5H_2O$ mass ratio used are reported in Table 2.1 and labelled as lignin@brochantiteX%_W (X= 3, 6, 10, 15, 20 % Cu). The pH was settled at 7 with NaOH 1M added dropwise[35]. The molar ratio between copper salt and base was 0,5. The suspension became darker. The stirring after the addition of NaOH, was kept for 2 hours.
The brown solid was washed with water by filtration and, subsequently dried at 80°C overnight. A brown powder was obtained grinding the material for 2 min at 300 rpm. The experiments were performed at least twice.

Mechanochemical procedure

The materials synthesized with this procedure are identified as lignin@brochantiteX%_M (X= 3, 10, 20 %Cu).
The amounts for 1g of lignin@brochantite10%_M are reported: in a 80ml agata jar 0.6g of lignin (BioPiva100) and 0.3g of $CuSO_4 \cdot 5H_2O$ were pre-ground for 2 minutes (inversion time =1min, break time =5s) with 5 agata spheres with diameter of 10 mm, at 300 rpm. Subsequently, solid NaOH (0.08 g) was added. To ensure homogeneous wetting of the solid mixture, 2mL of distilled water were added. The grinding at 300 rpm lasted 1h with an inversion time of 30minutes and a break time 5s[36]. Inversion time is the time after which the rotation of the planetary mill is reversed. The paste was washed by filtration with water and, subsequently dried at 60°C overnight. To obtain the powder the material was ground at 300 rpm for 2 min.

In general, to obtain materials with different percentages of copper the lignin/$CuSO_4 \cdot 5H_2O$ mass ratio was modified, see table 2.1, while the molar ratio $CuSO_4 \cdot 5H_2O$/NaOH=1/2 was kept constant.

Table 2.1: different lignin/ $CuSO_4 \cdot 5H_2O$ mass ratio for lignin@brochantite by wet and mechanochemical synthesis. The percentage value in the column refers to the copper content measure by inductively coupled plasma atomic emission spectrometry analysis (ICP-AES).

Sample	**Lignin/$CuSO_4 \cdot 5H_2O$ mass ratio g/g**	**Cu % ± SD**
Lignin@brochantite3%_W	1/0.12	2.93 ± 0.06
Lignin@brochantite6%_W	1/0.25	6.90 ± 0.20
Lignin@brochantite10%_W	1/0.50	11.45 ± 0.03
Lignin@brpchantite15%_W	1/0.80	15.30 ± 0.10
Lignin@brochantite20%_W	1/1.20	21.30 ± 0.20
Lignin@brochantite3%_M[1]	1/0.12	2.49 ± 0.03
Lignin@brochantite10%_M[1]	1/0.50	8.45 ± 0.04
Lignin@brochantite20%_M[1]	1/1.20	19.8 ± 0.3
[1]for 1g of final material 2mL of water guaranteed the homogeneous wettability		

The scale up procedure for the preparation of 30g of lignin@brochantite10%_M was conducted with a 500ml zirconia jar and 5 zirconia spheres with a diameter of 20mm. 20,86g of lignin (BioPiva395), and 6,36g of anhydrous $CuSO_4$ are pre-ground for 2 minutes. Subsequently, 2,78g of NaOH and 60mL of H_2O were added. The grinding was conducted at 300rpm for 1 hour with an inversion time of 30 minutes. The material was washed with water and dried overnight at 60°C.
The brochantite phase was identified by means of X-Ray Powder Diffraction (XRPD) and Transmission Electron Microscopy (TEM), see figure 2.2.

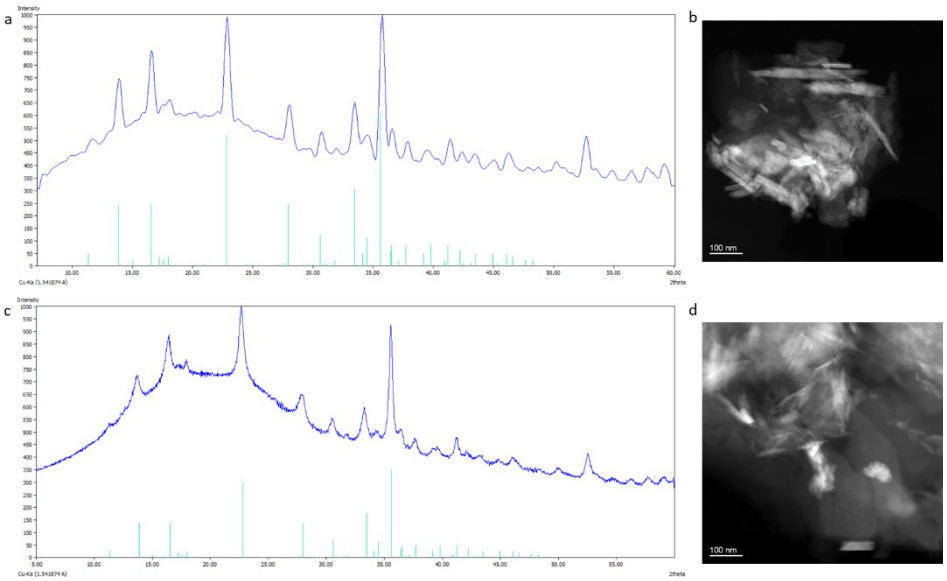

Figure 2.2. XRPD patterns (blue) and TEM images of lignin@brochantite10%_W (a,b), and lignin@brochantite10%_M (c,d); green peaks are theoretical peaks of brochantite.

Treatments:

BioPiva395 grinding

BioPiva395 was ground using 500ml zirconia jar and 5 spheres of the same material with diameter of 20 mm. 30g of BioPiva395 were milled for 2 minutes and then for 1 hour after the addition of 60mL of water. Sample named BioPiva395_M, were dried at 70°C overnight.

Treatments with HCl

BioPiva395 and lignin@brochantite10%_M were treated as follow: 5g of sample were soaked in 500ml of a HCl solution 0,02M. A vigorous stirring was maintained for 24 hours at room temperature. Materials were washed with water until the

pH was neutral, and subsequently dried at 70°C overnight. Materials are named: BioPiva395-HCl, and lignin@brochantite-HCl.

Stability of the material in water

250mg of lignin@brochantite20%_W were stirred in 25mL of acetate buffers (pH=4 and pH=5), phosphate/phthalate buffer (pH=7), aqueous solution of sodium hydroxide (pH=10) and distilled water for 24 hours at room temperature. The contact solutions were recovered and analysed by means of inductively coupled plasma atomic emission spectroscopy analysis (ICP-AES). The percentage of copper released in solution is presented in table 2.6 in the Results and Discussion paragraph "Stability of the material in water"[35].

Results and Discussion

Synthesis and characterization

The wet synthesis of the material lignin@brochantite was based on previous studies in which different copper salts, such as $Cu(CH_3COO)_2 \cdot H_2O$, $Cu(NO_3)_2 \cdot 3H_2O$, $CuSO_4 \cdot 5H_2O$ and $CuCl_2 \cdot 2H_2O$, were evaluated[35]. The best results, obtained in terms of copper loading, led to the choice of copper sulphate as the source of the metal and the use of sodium hydroxide to fix the pH at 7. The heterogeneous synthesis consists in suspending lignin in water and adding copper sulphate and sodium hydroxide, which always led to the exclusive formation of brochantite as mineral phase. Instead, it was observed that, in the absence of lignin, dissolving the copper sulphate in water and adding dropwise the same amount of sodium hydroxide used for the synthesis, the pH increased beyond 12 and a mixture of tenorite, CuO, and brochantite, $Cu_4(OH)_6(SO_4)$, was obtained[35] (figure S2.1). Lignin proved to be fundamental for the selectivity towards the formation of brochantite. The lignin suspension, in fact, controls the pH of the system neutralizing the addition of sodium hydroxide. The same amount of sodium hydroxide, in fact, leads to completely different pH with (pH=7) or without (pH=12) lignin in suspension. This is due to the slightly acid pH of the kraft lignin

water suspension (about 4-5) that causes the exclusive formation of brochantite when lignin is present. It is possible to tune the percentage of uploaded copper, defining the lignin/copper salt/NaOH mass ratio[35].
Based on these premises my work started focusing on the optimization of reaction times. Initially, the suspension was left to stir for 24 hours after the addition of sodium hydroxide[35]. It was then confirmed that a stirring of 2 hours was sufficient for the formation of brochantite and a complete copper loading[36] (see figureS2.2).

To further simplify the synthetic procedure, the next step was to obtain the same material through mechanochemistry (identified as lignin@brochantiteX%_M, with X= 3, 10, 20 % Cu)[36]. This synthetic protocol has some undisputed advantages. Among the others, the use of little amount of solvent and low reaction times that make it more suitable for scale up.
For the optimization of the grinding procedure, conducted on the material with 10% of copper and identified as lignin@brochantite10%_M, the amount of solid reagents was kept constant and equivalent to 1g. The number and size of spheres was kept constant too, using 5 spheres of agata with a diameter of 10 mm, and a jar of 80 mL.
Initially, the syntheses were conducted under *neat grinding* conditions (no solvent added), grinding the material at 300 rpm for 30 minutes (trial 1), 1h (trial 2), 2h (trial 3) and 4h (trial 4). All the syntheses led to the formation of posnjakite, which corresponds to the hydrate phase of brochantite, $Cu_4(SO_4)(OH)_6 \cdot H_2O$, as exclusive crystalline phase (figure 2.3). While with 30 minutes the signals of posnjakite are not well defined (figure 2.3a), the complete upload of copper was observed with 1h of grinding, as stated by ICP analysis: 11.5% ± 0.5.

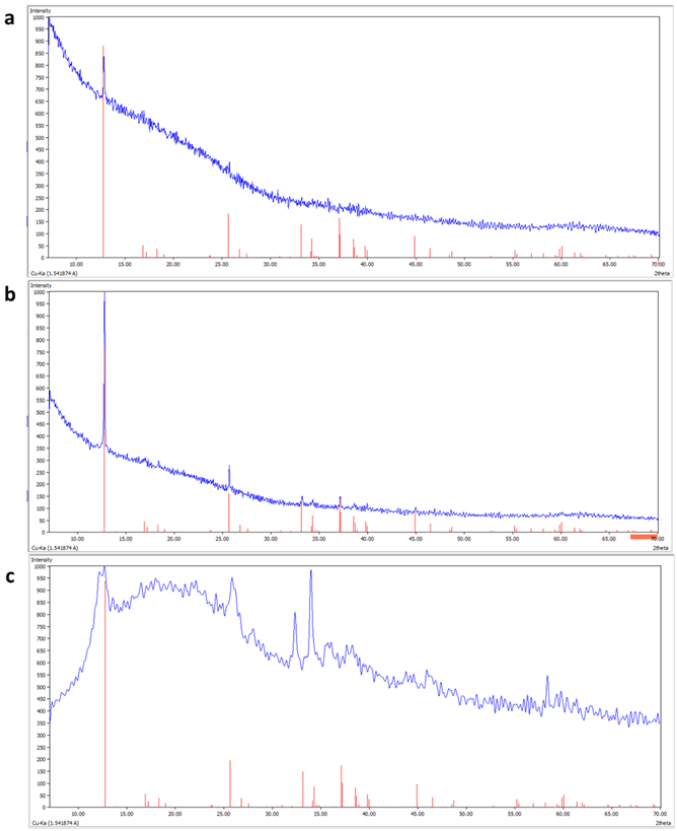

Figure 2.3. XRPD analysis of the materials obtained by mechanochemistry under neat grinding conditions at different reaction times: a) 30 minutes, b) 1 hour and c) 4 hours; red peaks are the expected peaks for posnjakite

Zittlau et al. describe posnjakite as the kinetic product[37]. The conversion of posnjakite to brochantite, the thermodynamically stable phase, occurs when the former is left in contact with mother liquors[37,38]. Accordingly, we have seen that with a dry grinding the exclusive phase formed is always posnjakite regardless of reaction times (figure 2.3), while the addition of water leads to the posnjakite-brochantite transition (figure 2.4).

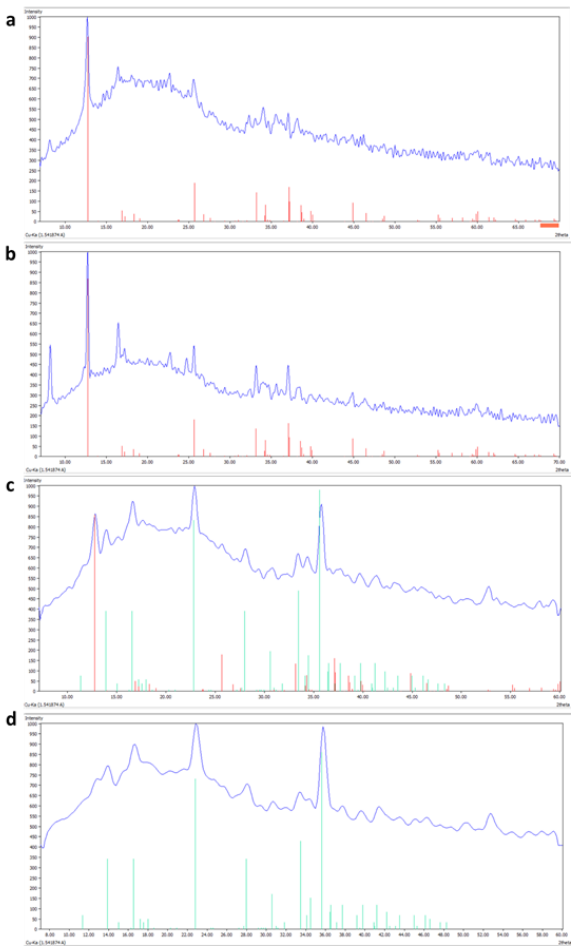

Figure 2.4. XRPD of the synthesis obtained with 2g of reagents and a) 200 µl, b) 600 µl, c) 900 µl and d) 1 ml of water. Colour code: red peaks, expected peaks of posnjakite; green peaks, expected peaks for brochantite.

In figure 2.4 we can appreciate the influence of the amount of water on posnjakite-brochantite conversion. With the same quantity of solid reagents (2g) and grinding time (2h), in fact, 200 µl (figure 2.4a) and 600 µl (figure 2.4b) are not sufficient for the brochantite formation that starts to occur only with 900 µl of water, but posnjakite is still present (figure 2.4c). The exclusive formation of brochantite is observed with 1ml of water, as shown in figure 2.4d.

In the attempt to isolate materials containing lower weight percentages of copper, the use of 1 mL of water revealed to be not sufficient to ensure the complete wetting of the solids during grinding. To overcome this problem, we decided to use 2mL of water for 1g of total solid reagents, in such a way to have slurry conditions. To assure a homogeneous distribution of copper a pre-grinding phase was conducted, and the time parameters settled to have an inversion time after 30 minutes as reported in experimental part section in the dedicated paragraph "Mechanochemical procedure". Under these conditions, the exclusive formation of brochantite was observed, irrespective of the lignin/$CuSO_4$ mass ratio, see TEM images in figure 2.6.

Table 2.2. Influence of water and grinding time in the optimization of the synthesis of lignin@brochantite10%_M

Trials	Grinding time			Mass of reagents	Water	Crystalline phase
	Total time	Inversion time	Break time			
Trial 1	30 min	NO	NO	1 g	NO	Posnjakite
Trial 2	1h	NO	NO	1 g	NO	Posnjakite
Trial 3	2h	NO	NO	1 g	NO	Posnjakite
Trial 4	4h	2h	5s	1 g	NO	Posnjakite
Trial 5	2h	NO	NO	2 g	200 µl	Posnjakite
Trial 6	2h	NO	NO	2 g	400 µl	Posnjakite
Trial 7	2h	NO	NO	2 g	600 µl	Posnjakite
Trial 8	2h	1h	5s	2 g	800 µl	Posnjakite
Trial 9	2h	1h	5s	2 g	900 µl	Posnjakite Brochantite
Trial 10	2h	1h	5s	2 g	1ml	Brochantite
Trial 11	15 min	NO	NO	1g	2ml	Posnjakite
Trial 12	30 min	15 min	5s	1g	2ml	Posnjakite Brochantite
Trial 13	1h	30 min	5s	1g	2ml	Brochantite
Posnjakite = $Cu_4(OH)_6(SO_4)\cdot H_2O$, Brochantite = $Cu_4(OH)_6(SO_4)$						

A screening on the grinding time was also conducted. In this case 1g of solid reagents (lignin, $CuSO_4 \cdot 5H_2O$ and NaOH) added of 2mL of water was grinded for 15 minutes (trial 10 in table 2.2), 30 minutes (trial 11 in table 2.2) and 60 minutes, (trial 12 in table 2.2) revealing that the conversion of posnjakite into brochantite is complete within 1 hour (figure 2.5.).

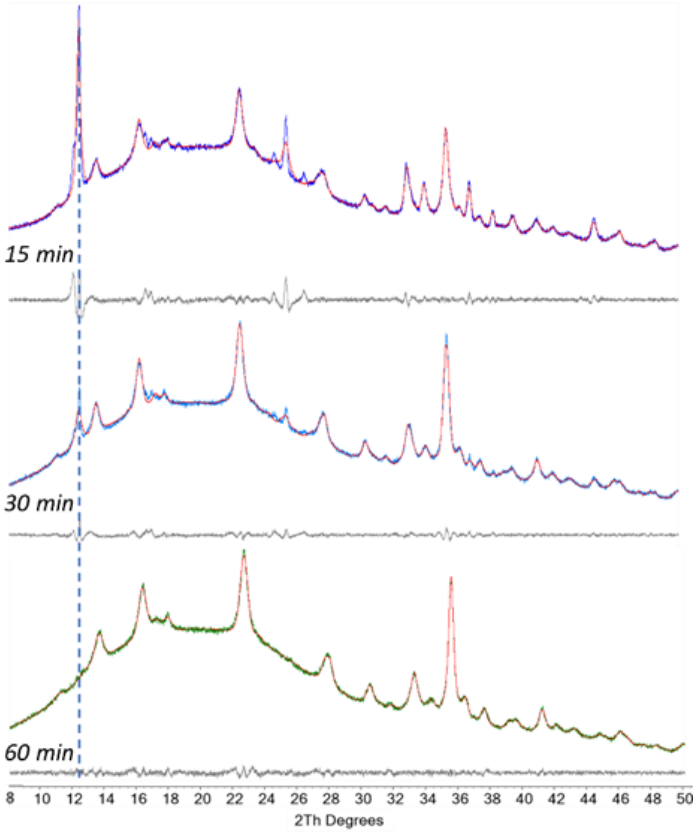

Figure 2.5. Pawley fit (red lines) against experimental pattern of lignin@brochantite10%_M, at different grinding times; 15 minutes (top, blue lines), 30 minutes (middle, cyan line) and 60 minutes (bottom, green line). Vertical blue dashed line represents the position of the (010) reflection of posnjakite that progressively decreases as a function of the grinding time. After 60 minutes, there is a perfect match between the experimental and simulated patterns for brochantite. Grey lines represent the difference between the experimental and calculated patterns.

These observations highlight how the fundamental parameter for obtaining the lignin@brochantite material is an appropriate amount of water in order to make the mixture homogeneously wet. By using slurry conditions, in fact, it is possible to obtain brochantite as an exclusive phase within 60 minutes.

TEM analysis allowed a more detailed description of the material revealing brochantite crystals embedded in lignin matrix. Furthermore, a correlation between copper concentration and the morphology and dimension of crystals was highlighted for both procedures (figure 2.6 and table 2.3).
Crystals of lignin@brochantite3%_W obtained by wet procedure are nanospheres with a diameter around 2-20 nm while already with 6% of copper a change in morphology can be noted. In this case brochantite rods with a thickness of 10-20 nm and a length of about 120 nm formed. Using higher percentages of copper, the crystals tend to grow more in length than in width giving sticks with a thickness always around 20 nm and a length ranging from 50 to 250 nm. Vilminot et al. report a detailed description of the crystalline structure of brochantite characterized by monoclinic symmetry with space group $P2_1/a(14)$ and cell parameters: a=13.1206(5) Å, b=9.8551(3)Å, c=6.0295(2)Å, β=103.432(3)°[39]. The structure of brochantite crystals is characterized by double chains of edge-sharing copper octahedra that are connected each other by corners forming corrugates planes along *bc*. Planes are bridged by the μ^7-sulfate tetrahedra to give the 3D-structure[39].
Table 2.3 reports a comparison in morphology of crystals for both procedures along with the different copper content.
It is interesting to note that, with the same copper concentration, brochantite crystals obtained by mechanochemistry are slightly larger compared to those obtained by wet procedure. In this regard, we can notice that already with 3% of copper, sticks with a thickness of 10-20 nm and a length of 40-150 nm formed under mechanochemical conditions, against the nanospheres observed under wet conditions (see figure 2.6 and table 2.3).
The crystallization process can be rationalized in two steps: nucleation and growth. Otálora et al. tried to give an explanation about the existence of a cave in Mexico with few giant crystals (even 11 m) of gypsum (dihydrate calcium sulphate) while not far away the so-called “cave of the swords” is characterized from many smaller crystals[40]. In their interesting work, they report how the

difference depends on the nucleation rate. In fact, in the cave of giant crystals, the concentration of calcium sulphate in water is only slightly higher than the saturation concentration. This involves a very slow nucleation (about one per year), so nuclei do not have to compete with each other. In other words, therefore, slower nucleation, larger crystals. By evaluating the two systems with which the synthesis of lignin@brochantite was carried out, we can reach different conclusions. On the one hand, in fact, our experimental observation seems to contrast with what has just been stated, because it is in the wet system that we have a greater dilution of reagents. On the other hand, we must also consider the presence of lignin as additional component which could somehow physically hinder crystallization because of its “folded” structure. In light of this, the most accepted hypothesis would be that in the wet procedure, nucleation is facilitated because lignin is more “diluted” than in the mechanochemical procedure. This, despite of the less concentration of the reagents in wet, could give a faster crystallization process than the grinding procedure, leading to smaller crystals.

When, in the wet procedure, the NaOH solution was dropped into the aqueous suspension of lignin and copper sulphate, a dark brown area formed as soon as the drop entered in contact with the suspension. When the solution of sodium hydroxide is completely added, the suspension assumed the same dark colour. This observation suggests that, in the case of the wet synthesis, nucleation is immediate every time the drop of NaOH solution encounters the suspension. Probably, dropping the basic solution favours the formation of a greater number of nuclei with consequently smaller crystals. The choice of adding dropwise the basic solution was taken to avoid filtrations problems during washing, since pouring the NaOH solution in the lignin suspension caused the formation of a very fine material.

We can also notice that, both in the wet and mechanochemical procedure the dimensions of crystals at higher copper concentrations are quite similar. This may be due to the lignin matrix that, beyond a certain concentration of copper, limits the size of the crystals.

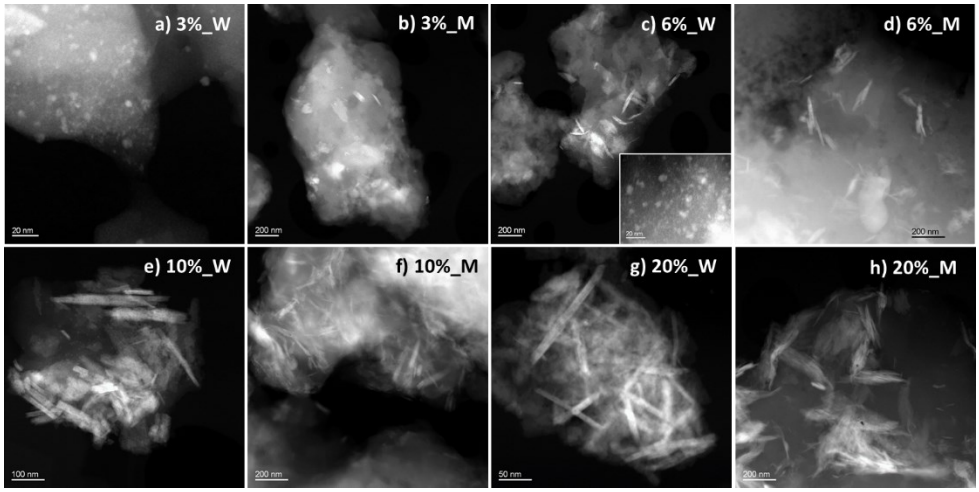

Figure 2.6. STEM-HAADF images of lignin@brochantite materials. The brochantite crystals are brighter than the lignin matrix.

Table 2.3. Correlation between copper concentration and dimension of brochantite crystals for lignin@brochantiteX%_W and lignin@brochantiteX%_M.

Sample	Morphology	Dimension- Thickness/Length (nm)
Lignin@brochantite3%_W	Spheres	2-20
Lignin@brochantite6%_W	Spheres Sticks	2-10 10-20/50-150
Lignin@brochantite10%_W	Sticks	10-30/50-200
Lignin@brochantite15%_W	Sticks	10-30/100-250
Lignin@brochantite20%_W	Sticks	10-20/40-150
Lignin@brochantite3%_M	Sticks	10-20/40-150
Lignin@brochantite6%_M	Sticks	8-40/30-200
Lignin@brochantite10%_M	Sticks	10-50/60-300
Lignin@brochantite20%_M	Sticks	10-50/60-300

The homogeneous distribution of copper in lignin matrix was evaluated by means of EDS mapping analysis, both for the material lignin@brochantite20%_W and lignin@brochantite10%_W, figure 2.7.

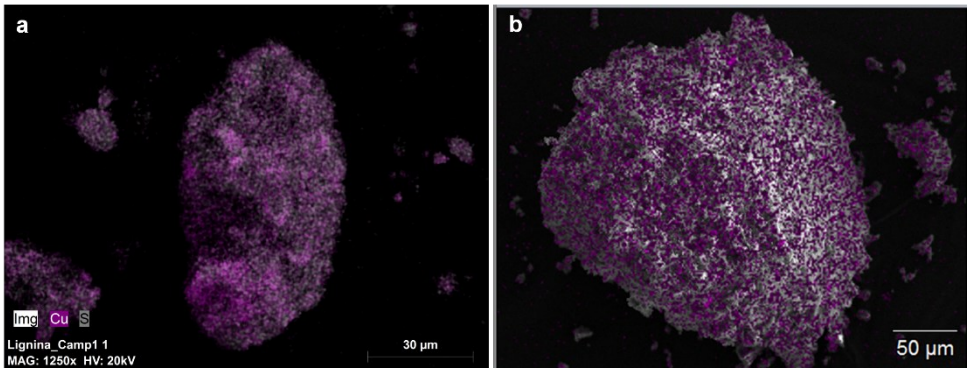

Figure 2.7. EDS mapping, with Cu metal in purple for a) lignin@brochantite20%_W, and b) lignin@brochantite10%_M

The next step was to characterize lignin@brochantite focusing on the polymer. The aim was to understand if lignin underwent some modifications after the synthesis. The use of sodium hydroxide and $CuSO_4$, as well as the grinding in the mechanochemical procedure could lead to a lignin fragmentation or a change in its structure, thus modifying its properties. To do this, materials lignin@brochantite10% by wet and mechanochemical procedures were characterized by means of Gel Permeation Chromatography (GPC), Infrared Spectroscopy (IR), Pyrolysis-Gas Chromatography coupled with Mass Spectrometry (Py-GC/MS) and Nuclear Magnetic Resonance (NMR).

For lignin@brochantite10%_W we used BioPiva100 as reference, because the synthesis was conducted using this type of lignin, while lignin@brochantite10%_M was synthesized with the scale upped procedure in ZrO_2 jar (see experimental part), using BioPiva395. The same analysis for control were conducted also for both BioPiva395 and BioPiva395 milled as reported in experimental part. The grinding of BioPiva395 was conducted considering a dry pre-grinding of lignin alone for 2 minutes and subsequently the grinding was conducted for 1h with water to evaluate the influence of the inorganic phases on the grinding.

As already explained in the dedicated section in chapter 1 “Lignin materials used in this work”, BioPiva100 and BioPiva395 differs for the drying step, and there are no characterization differences except for Gel Permeation Chromatography which reveals a slightly higher molecular weight distribution for BioPiva395 (see figure

S1.4 in “Supporting Information”). This aspect will be important therefore, in the comparison of GPC results of the respective materials.

The wet procedure consists in a heterogeneous reaction in which to the water lignin suspension, a water solution of copper sulphate is added. The pH of the system is then set to 7 with 1M sodium hydroxide solution. In figure 2.8 IR spectra of BioPiva100 and lignin@brochantite10%_W, are reported.

The two profiles are very similar. We can identify OH groups band in the region 3700-3200 cm^{-1} and the C-H aliphatic band at 2936 cm^{-1} for both samples[41]. Some differences are presented in the region between 1800-600 cm^{-1}. The stretching band of the carbonyl at 1704 cm^{-1} is not observed in lignin@brochantite10%_W[41]. This is due to the deprotonation of carboxylic acid during the synthesis that reduced the double bond character of the carbonyl function. Other differences are due to the copper sulphate bands. Bands at about 1122 cm^{-1}, 628 and 597 cm^{-1} are related to the SO_4^{2-} group[42].

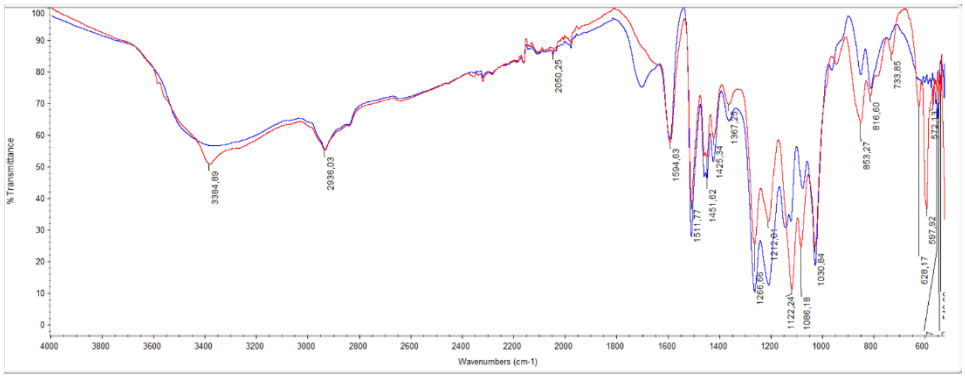

Figure 2.8. IR spectra of BioPiva100 (blue), and lignin@brochantite10%_W (red)

Pyrolysis-GC/MS analysis are showed in figure 2.9 for BioPiva100 and lignin@brochantite10%_W. The analyses were conducted twice, and samples weighed to make a more correct comparison. The retention of the structure is confirmed by the presence of the same organic fragments.

By means of gel permeation chromatography we demonstrated if lignin underwent some fragmentations by evaluating its molecular weight distribution. The two chromatograms are presented in figure 2.10 with the number average, M_n, the weight average, M_w and polydispersity data. The molecular weight

distributions are quite stackable, while an increasing of about 600 is revealed in M_w of the material lignin@brochantite10%_W.

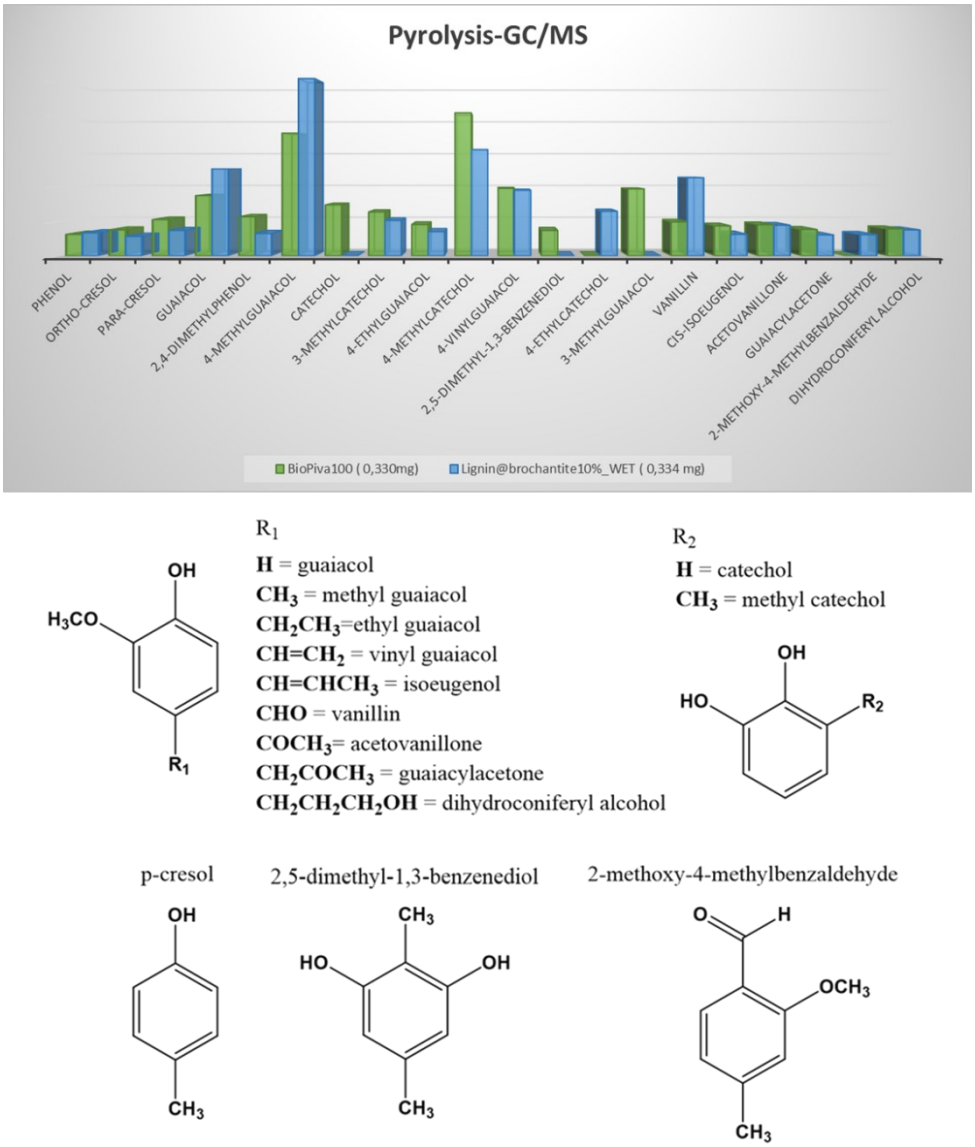

Figure 2.9. Main fragments from pyrolysis-GC/MS of BioPiva100 and lignin@brochantite10%_W. The bars represent the relative area percentages of the single analytes.

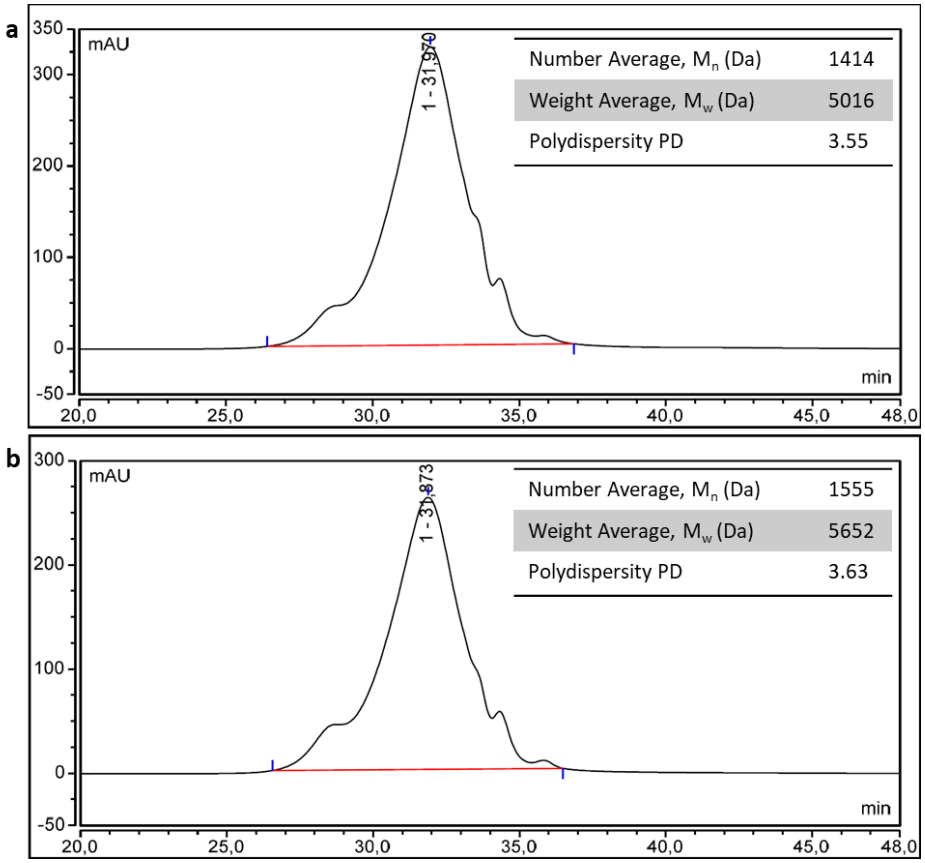

Figure 2.10. Chromatograms and molecular weight distributions of a) BioPiva100 and b) lignin@brochantite10%_W.

The scale-upped procedure for the material lignin@brochantite10%_M was conducted considering 30g of total reactants and using a 500 mL ZrO_2 jar and 5 spheres of the same material with diameter of 20 mm. As reported in the experimental part, this synthesis consists in a 2 minutes pre-grinding of lignin (BioPiva395) and copper sulphate, to homogeneously distribute the inorganic phase. Subsequently solid NaOH and water are added and the mixture ground for 1 hour (see experimental section “Mechanochemical procedure”)

Following the same procedure 30g of BioPiva395 were ground in dry conditions for 2 minutes and with the addition of water for 1 hour in order to evaluate the effect of the inorganic phases. The details of the procedure are reported in the

experimental section. The treated lignin is identified as BioPiva395_M. As reference also BioPiva395 were characterized.

There are no differences in IR spectra neither between BioPiva395 and milled BioPiva395 (see figure 2.11) nor between lignin@brochantite10%_M and the material obtained by wet procedure, (figure S2.3 in "Supporting information").

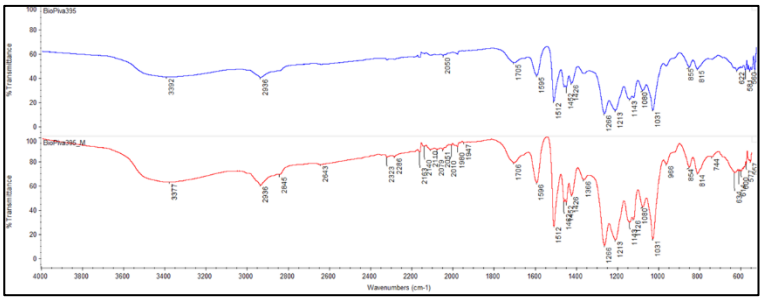

Figure 2.11. IR spectra of BioPiva395 (blue) and BioPiva395 milled (red).

In figure 2.12 IR spectra of the milled BioPiva395 and the material lignin@brochantite10%_M are shown. For lignin alone, the main peaks are at 3377 cm^{-1} (OH group), at 2936 cm^{-1} the band of (aliphatic C-H) and at 1706 cm^{-1} (the stretching of the carbonyl group)[41]. At 1595 and 1512 cm^{-1} we have the aromatic unit peaks and at 1266 and 1213 cm^{-1} the aromatic C-O stretching[41]. As previously reported the main differences between milled BioPiva395 and lignin@brochantite10%_M are due to the SO_4^{2-} bands[42].

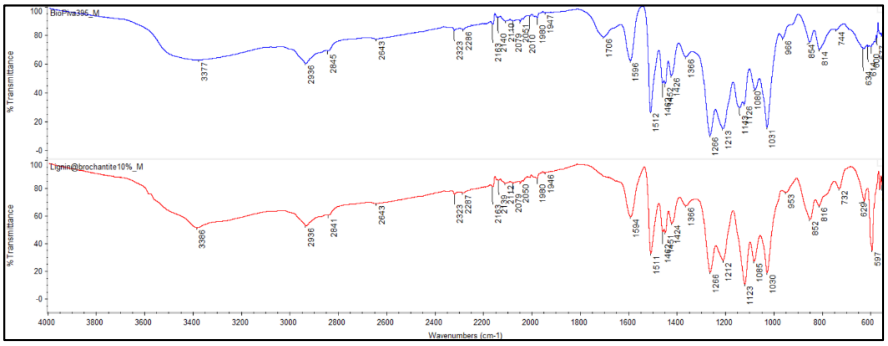

Figure 2.12. IR spectra of milled lignin, BioPiva395_M and lignin@brochantite10%_M

Py-GC/MS data for lignin@brochantite10%_M and BioPiva395 are shown in figure 2.13.

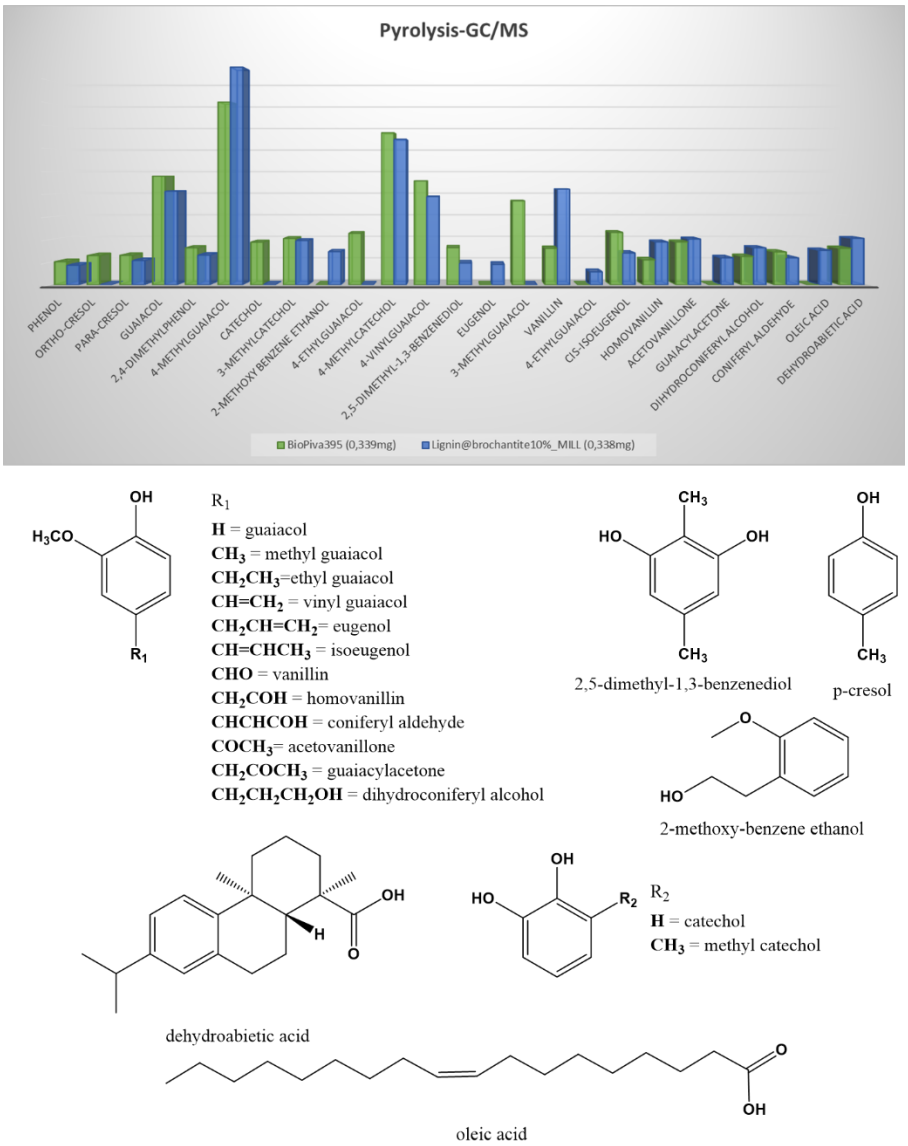

Figure 2.13. Main fragments from pyrolysis-GC/MS of BioPiva395 and lignin@brochantite10%_M. The bars represent the relative area percentages of the single analytes.

In Py-GC/MS analysis, we can notice again how the main fragmentations are phenol-derived molecules and there is a good agreement between pyrolysis profile of BioPiva395 and the material lignin@brochantite10%_M thus confirming the retention of lignin structure.

Gel Permeation Chromatography results for BioPiva395, milled BioPiva395, and lignin@brochantite10%_M are presented in table 2.4.

Table 2.4. Gel Permeation Chromatography results for BioPiva395, milled BioPiva395 and lignin@brochantite10%_M

Parameters	BioPiva395	BioPiva395_M	Lignin@brochantite10%_M
Number Average, M_n (Da)	1565	1414	1591
Weight Average, M_w (Da)	**5975**	**5796**	**7161**
Polydispersity, PD	3.82	4.10	4.50

The slight difference between BioPiva395 and milled BioPiva395 reveal no significant fragmentation because of the grinding. This is confirmed also by identical IR spectra (figure 2.11).
For what concern the comparison between lignin and the material lignin@brochantite10%_M, GPC results revealed an unexpected result. The material, in fact, presents a considerably increasing in the M_w value. A similar trend, to a lesser extent, was observed also in the material synthesized by the wet procedure, as shown in figure 2.10. The hypothesis is that the presence of the inorganic phase could influence the hydrodynamic radius of lignin molecules. For the analysis, samples were dissolved in a water solution of NaOH (0.1M) and the mobile phase is a 0.1M solution of NaOH. Experiments conducted soaking lignin@brochantite material in a basic solution (pH=10) revealed that no copper leaching occurs (see paragraph “Stability of the material in water”). Analogous experiments demonstrated that the dissolution of brochantite phase occurs, instead, when the material is soaked in an acid solution. Thus, to confirm our hypothesis, lignin@brochantite10%_M was soaked in a HCl solution (pH=2) for 24h (see experimental part “Treatment with HCl” for details) to remove the

inorganic phase and analyse the corresponding lignin matrix. The same treatment was conducted also for BioPiva395, as reference. The new samples identified as BioPiva395-HCl and lignin@brochantite-HCl were plenty washed with water and analysed by means of GPC (table 2.5), NMR (figure 2.14), and IR (figure 2.15).

Table 2.5. Comparison of GPC results for BioPiva395, and lignin@brochantite treated with a HCl solution.

Samples	Number Average, Mn (Da)	Weight Average, Mw (Da)	Polydispersity, PD
BioPiva395	1560	5959	3.82
BioPiva395-HCl	1316	5209	3.96
Lignin@brochantite-HCl	1188	5210	4.39
Lignin@brochantite	1591	7161	4.50

GPC results revealed that after the acid treatment the two samples, lignin@brochantite-HCl and BioPiva395-HCl, have similar M_w values. This confirmed our hypothesis about the interference of the inorganic phase on molecular weight distribution. Furthermore, it is worthy to note that the weight average of BioPiva395 treated with HCl is dropped compared to its original value. Thus, also HCl seems to have some effects in the GPC analysis. This result agrees with literature. In particular, when lignin is subjected to acid treatment, two processes compete: the depolymerization, that occurs for acid hydrolysis of β-O-4 bonds, and the re-polymerization related to the acid catalysed condensation between aromatic carbon atoms (C_6 or C_5) and a carbonium ion (usually localized on C^{α} of the side chain)[43–45]. Li et al. investigated the contribution of these two processes[44]. They treated lignin with an aqueous solution of acetic acid at 3%, heating at reflux for a total time of 1h and 30minutes and monitoring the products at regular time intervals. Through size exclusion chromatography they showed how in reduced treatment times the molecular weight distribution of lignin is reduced as a result of acid hydrolysis. An increased in molecular weight is instead observed if the treatment is continued longer, confirming the re-polymerization as the dominant process[44]. In our experiments, samples were soaked in a 0,02M solution of HCl (pH=2) for 24h at room temperature. Probably, the low

temperature of the treatment caused hydrolysis to prevail over condensation, leading to a decrease in the molecular weight.
Anyway, the decreasing in the molecular weight distribution did not lead to a significant structural change as we can see from $^{13}C\{^{1}H\}$-NMR analysis of BioPiva395-HCl and lignin@brochantite-HCl (figure 2.14). NMR spectra are, in fact, perfectly superimposable to that of the original lignin.

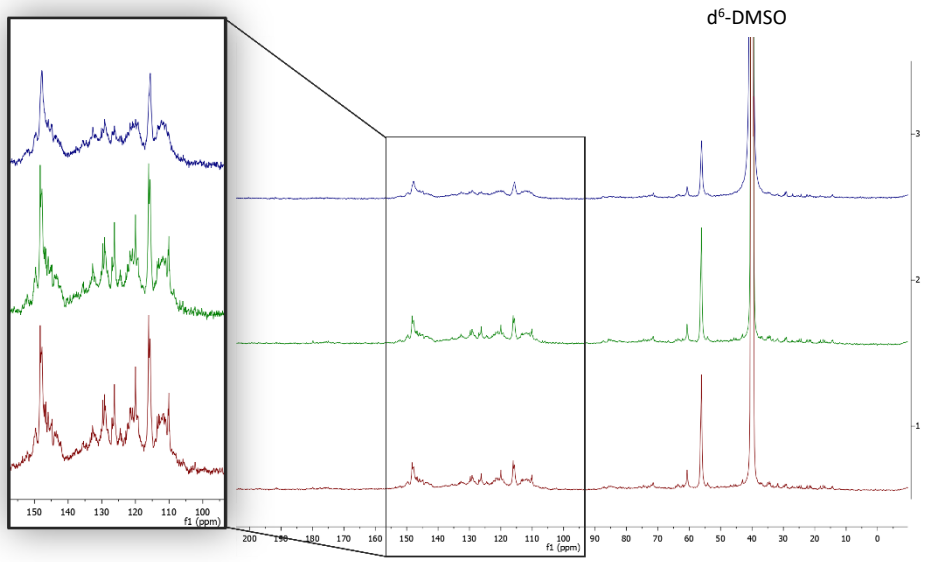

Figure 2.14. $^{13}C\{^{1}H\}$-NMR spectra of lignin@brochantite-HCl (blue), BioPiva395-HCl (green) and BioPiva395 (red).

Figure 2.14 shows the aromatic carbon signals in the interval 160-110 ppm, the carbon of methoxy groups at 56 ppm, while the carbon in γ position of the aliphatic chain, $-CH_2OH$ (or the carbon of aliphatic hydroxyl group), are visible at 60 ppm[41]. Also, between the ^{1}H-NMR spectra of BioPiva395 and BioPiva395-HCl no differences were observed (figure S2.4 in "Supporting information").

IR spectra of BioPiva395, BioPiva395-HCl and lignin@brochantite-HCl are also superimposable, thus confirming NMR results. In figure 2.15 the carbonyl band of the COOH groups are visible at about 1700 cm^{-1}; this signal is found also in the spectrum of lignin@brochantite-HCl due to the protonation following the acid

treatment while, as expected, the peaks of SO_4^{2-} groups are absent (1122, 628 and 597 cm^{-1}).

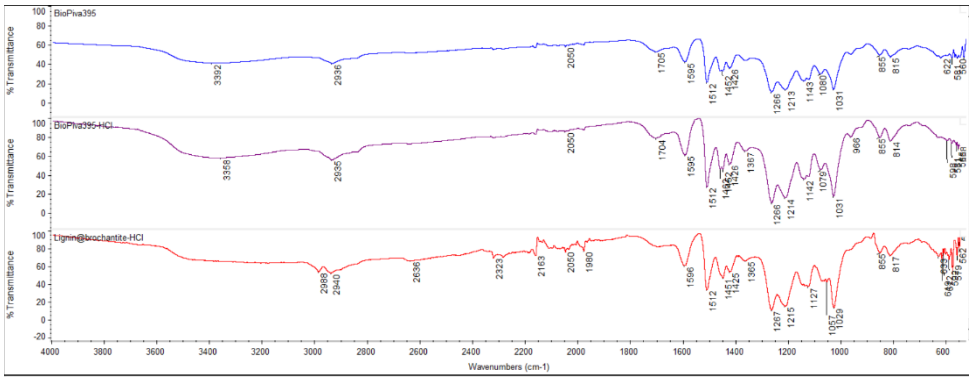

Figure 2.15. IR spectra of BioPiva395 (blue), BioPiva395-HCl (purple), and lignin@brochantite-HCl (red)

Properties of lignin@brochantite materialXX%_W

The characterization of the material lignin@brochantiteXX%_W was completed with the following measurements.

Stability of the material in water

The aim of these experiments was to assess the stability of the material in water at different pHs. In agricultural field this is important because products sprayed on plants must adhere adequately to leaf surfaces, in such a way that the material is not easily washed off by rain, always having a certain degree of acidity due to the dissolved carbon dioxide[11]. This could, in fact, cause reduction of activity and dangerous leaching in the soil[11]. Moreover, the formulations necessary to render the product sprayable on plants considers the use of basic solutions. Thus, a knowledge of the stability of the material against pH is fundamental.

In agreement with the solubility of brochantite,[46] treatments in acid water (pH=4 and 5, see table 2.2) revealed a complete release of copper, while at higher pH values the material is stable, see table 2.6.

Table 2.6 Stability of lignin@brochantite20%_W in water at different pH

Lignin@brochantite20%_W	
Experimental conditions	% Cu released
pH=4*	91%
pH=5*	93%
pH=7**	0.1%
pH=10***	0.1%
Distilled water	0.3%
* acetate buffers ** phosphate/phthalate buffer ***aqueous solution of sodium hydroxide	

Wettability

The wettability of materials is an important parameter for industrial processes involving interaction between solid and liquid phases as it provides information on the adhesion and cohesion forces at the solid-liquid interface[47,48]. Knowing if the wettability properties of our material have changed compared to the starting lignin can be useful in the storage phase of the solid material (tendency to absorb water) and in the formulation of the final product to be sprayed on the leaf.
Wettability measurements were conducted on lignin@brochantite10%_W using Biolin Scientific Sigma 700/701 instrument with the setting for powder samples, a cylindrical filter with 5,5 mm radius (details are reported in Characterization techniques paragraph “Wettability measurements”). Samples are gently manually ground in such a way to have a homogeneous powder. Subsequently, 0.3 g of sample are introduced as follow. Initially 0.2g of sample are introduced and they are packed by tapping the filter on the table for 1 minute. The remaining 0.1 g is, then, added and the packing procedure conducted again. For all samples two measurements must be conducted. The first one, using n-hexane or n-heptane (as

completely wetting liquid) to calculate the material constant, C, a parameter for the powder packing[49]. The idea is measuring the powder wettability against low surface tension liquid in such a way to have zero contact angle against powder. Subsequently, a second measurements is conducted with water that leads to the definition the contact angle.

These must be considered preliminary results because the technique needs several measurements conducted with the same parameters to evaluate the data reproducibility, and a complete set of results has not yet been collected.

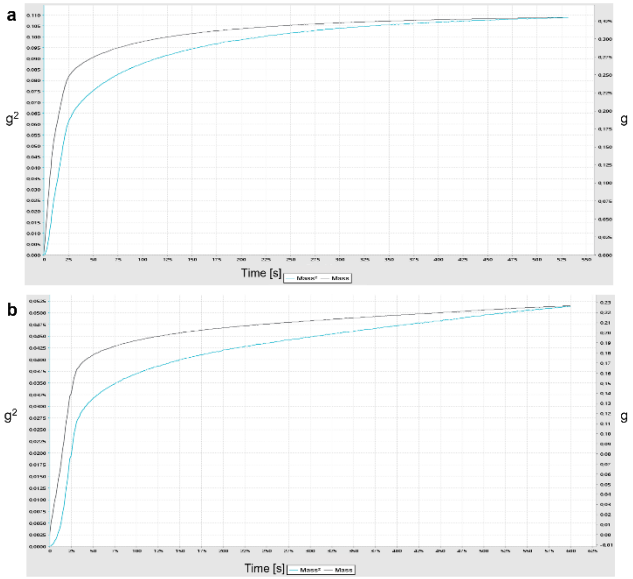

Figure 2.16. Wettability profiles of a) BioPiva100 and b) lignin@brochantite10%_W

Table 2.7. Results of wettability measurements

Parameters	BioPiva100	Lignin@brochantite10%_W
Slope [g^2/s]	0.003	0.001
cos(θ)	0.505	0.457
Θ [deg]	**59.7**	**62.8**

As we can see from table 2.7, the contact angles of BioPiva100 and lignin@brochantite10%_W are very similar confirming the retention of wettability grade after the synthesis.

Morphology

SEM images of BioPiva100 and lignin@brochantite10%_W did not reveal significative surface differences between the two materials, as can observed in figure 2.17.

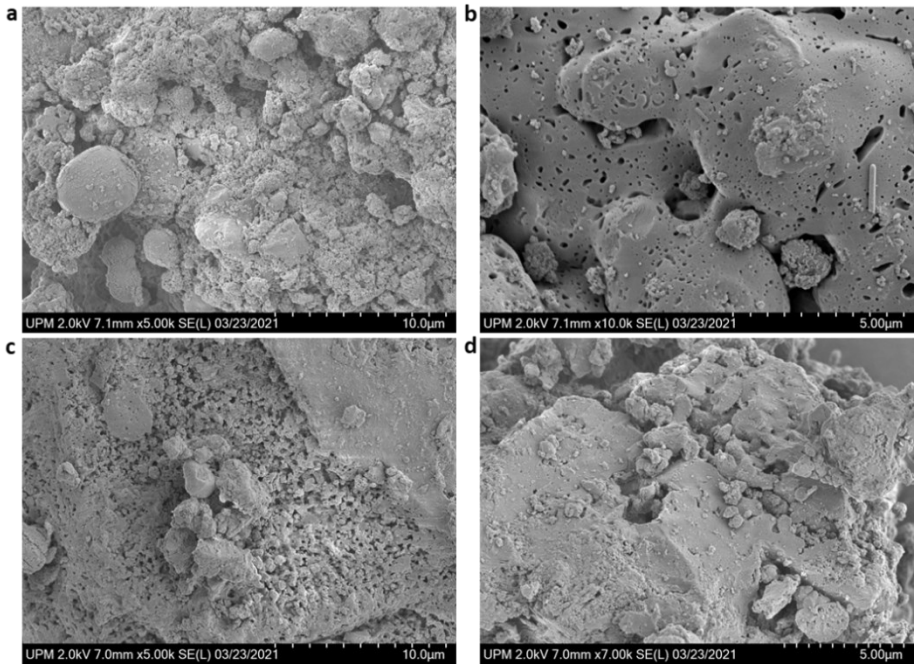

Figure 2.17. SEM images of BioPiva100 (a-b) and lignin@brochantite10%_WET

Thermal analysis

Thermo Gravimetric Analysis (TGA) and Differential Scanning Calorimetry (DSC) were conducted on both BioPiva100 (figure 2.18) and lignin@brochantite10%_W (figure 2.19).

Figure 2.18 shows TGA and DSC traces of BioPiva100. The TGA profile presents a dehydration process around 100°C, also confirmed by DSC analysis, with a maximum weight loss of 46,06% at about 370°. The glass transition temperature detected by DSC analysis occurs at 140°C, in agreement with literature for kraft lignin[50].

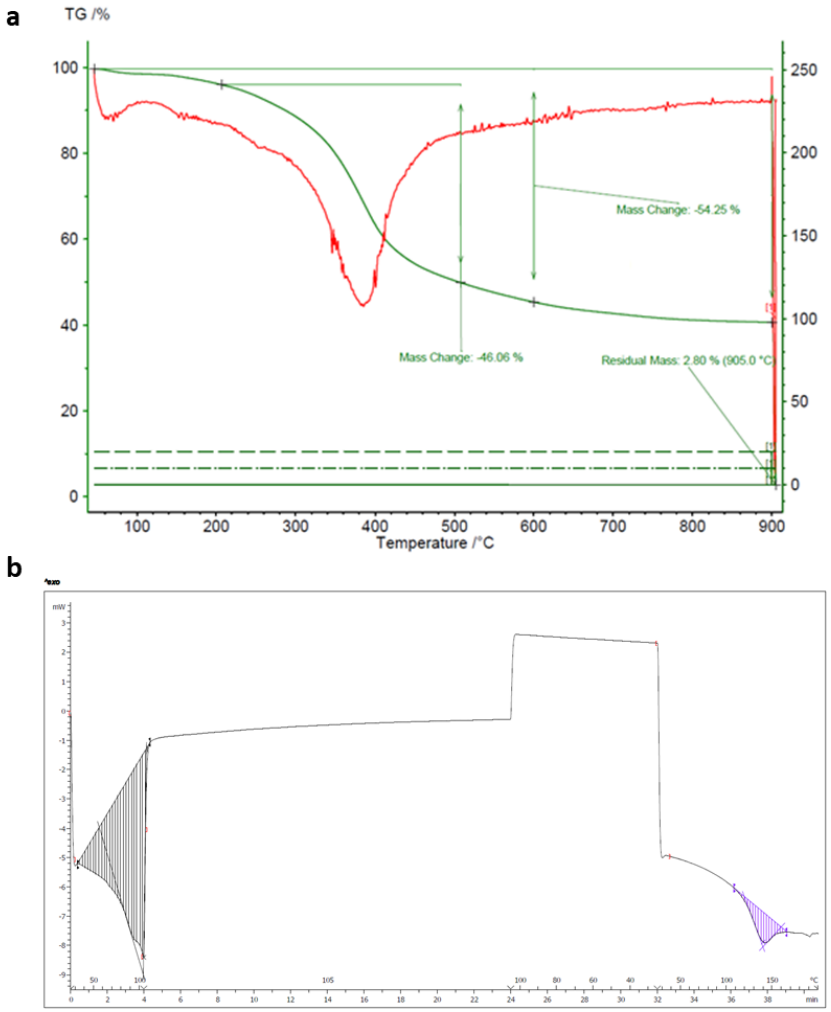

Figure 2.18. Thermal characterization of BioPiva100; a) TGA and b) DSC profile, with exothermic processes up. The DSC profile is expressed both in °C (above the x axis) and in minutes (below the x axis). Glass transition temperature, 139,67°C.

In figure 2.19 are reported the same analyses conducted on lignin@brochantite10%_W; these reveal a different situation due to the presence of the inorganic phase.

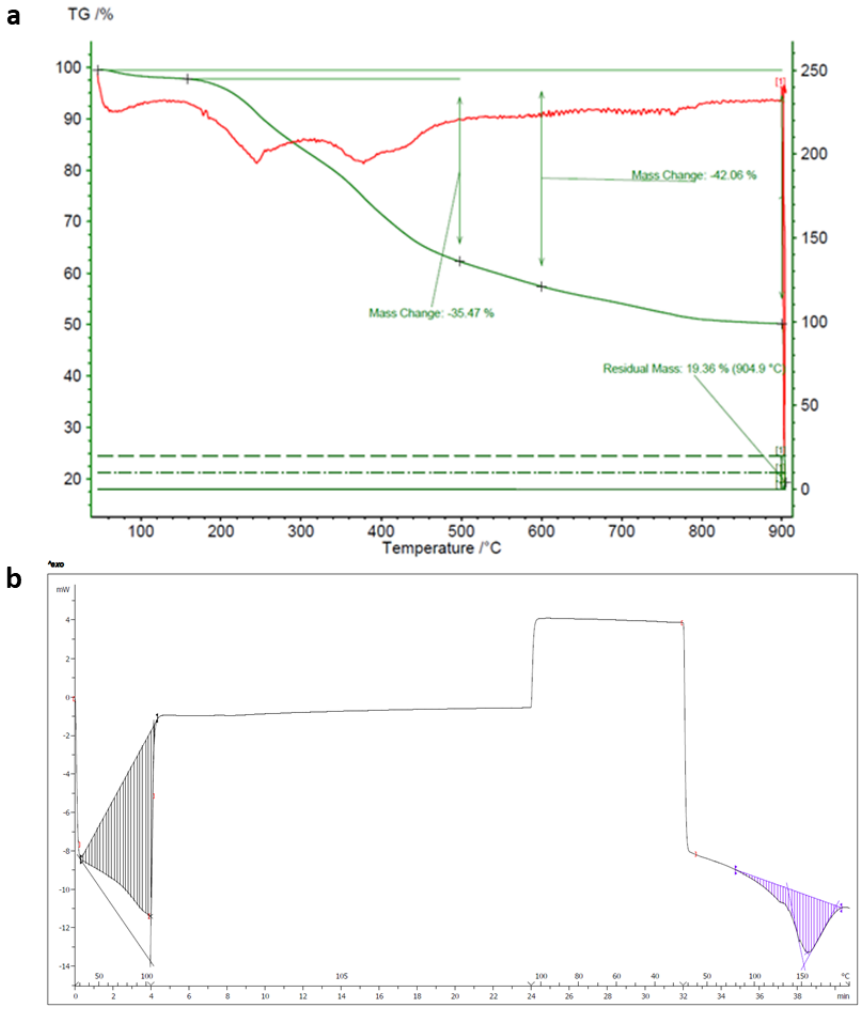

Figure 2.19. Thermal characterization of lignin@brochantite10%_W: a) TGA and b) DSC analysis with exothermic processes up. The DSC profile is expressed both in °C (above the x axis) and in minutes (below the x axis). The peak at 154,75°C is a likely combination of the glass transition temperature of the polymer with a process related to the inorganic phase.

TGA profile is in fact now more complicate. After the water loss at about 100°C, there are two main degradation steps, at 250°C and at 410°C, respectively.
For what concern DSC analysis, the peak at about 150°C presents an unusual shape to be the peak of the glass transition temperature. This transition is, in fact, normally characterized by a very small curve as the one present in BioPiva100 profile (figure 2.18b). It might be possible that in this case the curve does not correspond exclusively to the lignin glass transition, but some processes involving the inorganic phase could be also present.
In the thermal decomposition process of brochantite the main steps are dehydration to an amorphous phase followed by in-situ crystallization of CuO and CuSO4 and finally to thermal desulferation leading to CuO[51]. The dehydration process occurs between 200 and 400°C, while the decomposition of the oxy-sulphate takes place above 600°C[52]. Although the large endothermic peak observed at 150°C in the DSC of lignin@brochantite10%_W (figure 2.19) does not correspond properly to what reported in literature, it cannot be excluded that it comes from the initial stage of the thermally induced brochantite decomposition.

Antimicrobial activity - in vivo tests

The antimicrobial activity of lignin@brochantiteX%_W was evaluated by tests on plants in greenhouse. Following a previous work demonstrating the good efficacy of the material against a wide range of pathogens, the study was further extended[35]. Three trials in vivo were conducted[36]. The first trial was aimed at evaluating the material on different plants and against different pathogens in such a way to evaluate its range of activity. In the previous work, in fact, good results, shown in section "Trial 1-experiment 1", were obtained on tomato plants against *Rhizoctonia solani*. The next step was, then, to test the efficacy of lignin@brochantite10%_WET on strawberry against *Botrytis cinerea* (Trial 1-experiment 2). In both cases, the concentration of the active material was 10 g/L. In the trial 2, two different dosages of the material were evaluated: 3L/ha and 10L/ha. Finally, trial 3 was aimed to evaluate the correlation between the morphology of brochantite crystals and their activity. TEM analysis, conducted on lignin@brochantite at different percentages of copper (from 3% to 20%), in fact revealed the presence of a correlation between the metal concentration and the morphology of brochantite crystals. Increasing the metal content, brochantite

crystals become larger. In this case, materials with 3%, 10% and 20% of copper were tested against *Pseudomonas Infestans* on tomato plants, keeping the same copper concentration in the three formulations, thus assuring the same amount of metal distributed per hectar (30g/ha of metal).
The material lignin@brochantite is properly formulated before its use on plants. XRPD and TEM analysis, conducted on the formulate of lignin@brchantite10%_WET, allowed to confirm that no variation to the inorganic phase occurred following the formulation (see figure 2.20).

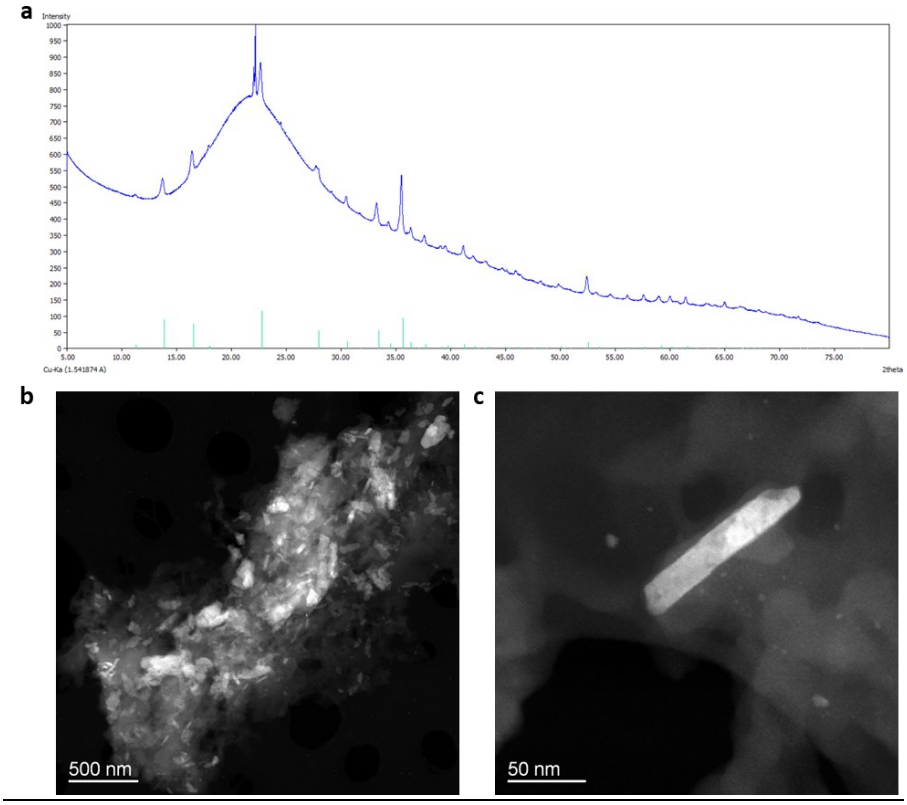

Figure 2.20. Characterization of lignin@brochantite10%_W formulated a) experimental XRPD pattern, with dark green brochantite peaks, and b-c) STEM-HAADF images. Crystals have an average thickness of 20nm and a length between 30-150 nm.

Operating conditions

Tests were conducted by Soc. Agr. AGOFLOR S.C.-via delle Messi, 101-64014 Martinsicuro (TE)-ITALY and at the Centro Ricerche Agronomiche ed Ambientali, ResAgraria srl, via A. Canova 19/2, 64018 Tortoreto Lido (TE)-ITALY (climatic chambers).

Trial 1- activity assessment

Experiment 1. The first experiments were conducted on tomato plants, variety "Cuore di Ponente" against *Rhizoctonia solani*[35]. The final copper concentration of the formulation was 10g/L for a dosage rate of 3L/ha. As reference was used the commercial product $Cu(OH)_2$ (copper concentration, 20g/100g and dosage rate 3.0 kg). 24/48h after the first artificial inoculum the first application (A) was conducted at transplanting of the products. 15 days later, application B followed. 7-10 days after the second application (B) and 48h after the second artificial inoculum the third application (C) was conducted. In this trial we evaluated the number of plants attacked and dead, following the inoculum of the pathogen (day 0), and the efficacy of the products in term of incidence percentage corresponding to the percentage of attacked leaves.

Experiment 2. The second experiment was conducted in greenhouse on 54 plots, each counting 11 strawberry plants (variety Four Seasons), against *Botrytis cinerea*[36]. The efficacy was evaluated taking into account the percentage of fruits attacked in the field and during the storage. The formulated material, whose concentration was 10g/L for a dosage of 3L/ha, was applied three times: application A, after 24/48h from the inoculum of the pathogen, application B, after 7-10 days from application A and application C, after 7-10 days from application B. 24/48h before application C a second artificial inoculum of the pathogen was done. For comparison, the lignin alone (10g/ha), the commercial products Iprodione (75g/100g) and *Bacillus amyloliquefaciens* (50g/kg), were also evaluated.

Trial 2 - evaluation of different dosages of material lignin@brochantite10%_WET

The tests were conducted on tomato plants, variety Optima, in a climatic chamber with abiotic parameters under control and sterile soil[36]. In this case the material was sprayed on the leaf (spray volume 500L/ha). The evaluated parameters were the incidence (percentage of attacked leaves on 60 leaves per plot) and the severity (percentage of attacked foliar area). While the copper concentration was always maintained 10g/L, the material was applied with two different dosages: 3L/ha and 10L/ha. For each dosage the material was applied three times (identified as applications/treatments A, B, C) as follows: the first application (A) was done 24/48h after the artificial inoculation at transplanting. After 15 days from application A, the second application (B) was conducted. Application C was carried out 7-10 days after application B. 48 h before the third application a second artificial inoculation was done. In these trials the tested pathogens are *Pseudomonas syringae*, *Xanthomonas campestris*, *Xanthomonas arboricola fragrari*, *Botrytis cinerea*. As reference, the commercial product based on $Cu(OH)_2$ (Coprantol Hi Bio 2.0, Sygenta) was used.

Trial 3 - crystals morphology and activity correlation

Tests were carried out on 11 tomato plants, variety Optima, in a climatic chamber with abiotic parameters under control and sterile soil[36]. By means of foliar method (spray volume 300L/ha), the efficacy and the severity were evaluated against *Pseudomonas infestans*. The correlation between crystals morphology and activity was performed testing lignin@brochantiteX%_WET with X= 3%, 10% and 20%. The copper concentration in the final formulates for all three products was 30g/ha. The products were applied as follow: application A, three days after the artificial inoculation of the pathogens, application B, 7 days after application A and application C, 7 days after application B. Additional information on tested products: lignin@brochantite3%_W, copper concentration 3g/L and dosage rate 10L/ha; lignin@brochantite10%_W, copper concentration 10g/L and dosage rate 3L/ha; lignin@brochantite20%_W, copper concentration 20g/L, dosage rate 1.5L/ha.

Results and Discussion

Trial 1 - activity assessment

The formulated material lignin@brochantite10%_WET at the concentration of 10g/L was tested against *Rhizoctonia solani* on tomato plants (experiment 1) and against *Botrytis cinerea* on strawberries (experiment 2).
All experiments were carried out in such a way to have environmental conditions favourable to the growth of the pathogens.

Experiment 1

The tested products were applied three times (applications A, B and C), as reported in the experimental part. The first sign of sick appeared after 8 days from application A, that is 9/10 days from the inoculation.
Figure 2.21a shows the activity of the material expressed as number of attacked and dead plants out of a total of 30 plants, while figure 2.21b presents the incidence percentage on 35 days after application A.

The material lignin@brochantite10%_WET has an undoubted efficacy against the tested pathogen, even surpassing the commercial product used as reference. The potential of lignin@brochantite is not limited to its effectiveness, but also affects the final copper concentration used. While in the case of the commercial product the final metal concentration is 600g/ha, with lignin@brochantite10%_WET it is lowered to 30g/ha, confirming a successful combined effect between the metal and lignin which allows to obtain better performances by reducing the metal content.

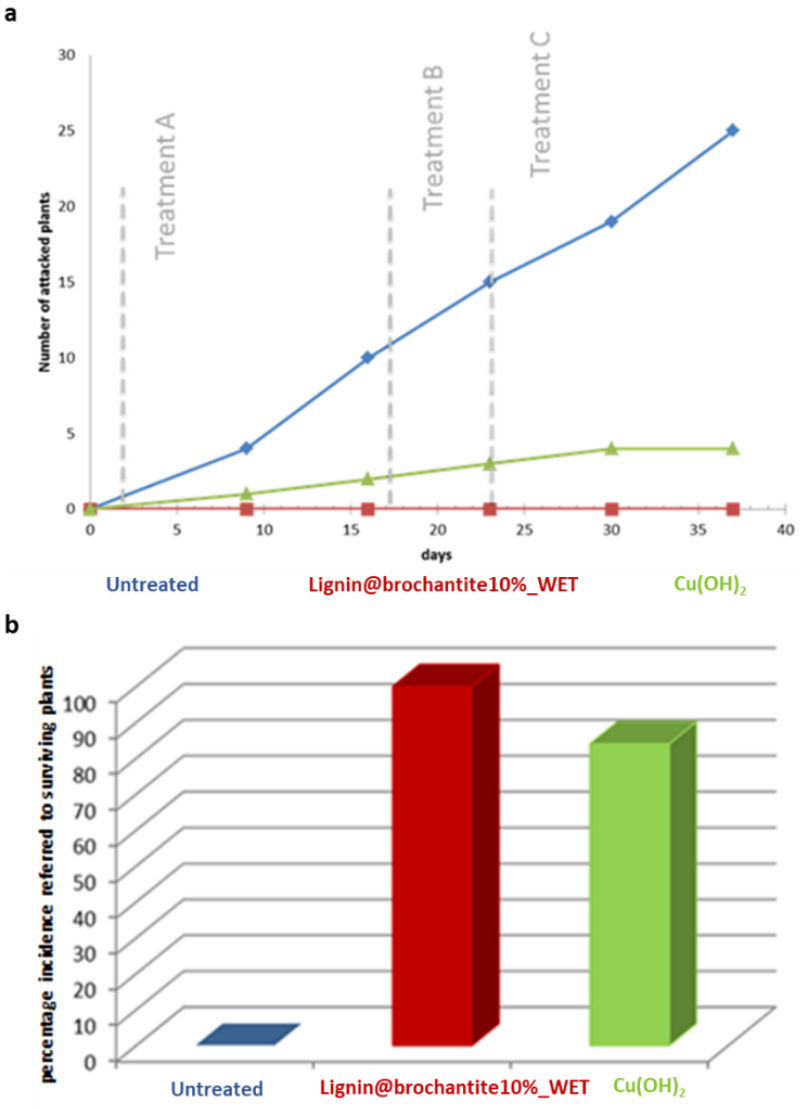

Figure 2.21 test against *Rhizoctonia solani*, a) number of attacked and dead plants on 30 plants with day 0 as the day of the inoculum of pathogen, b) incidence % on 35 days after application A.

Experiment 2

The promising results against *Rhizoctonia solani* encouraged us to further investigate the activity of lignin@brochantite material. The second experiment was conducted to evaluate the material lignin@brochantite10%_WET at the final concentration of 10g/L, for strawberries, Four Seasons variety, against *Botritis cinerea*. In this case lignin alone, iprodione (a contact fungicide) and *Bacillus amyloliquefaciens* (a biopesticide) were used as references. The efficacy of the products was evaluated during and immediately after the treatments, figure 2.22a (7 days after application A and 7 days after application C; see Experimental for details regarding the protocol followed for the applications on plants) and after 3 days of storage to evaluate the postharvest phase, figure 2.22b. By setting the untreated check as 0% efficacy, the activity of the material is evident once compared to lignin alone as well as to *Bacillus amyloliquefaciens* (figure 2.22a). An activity similar to that of Iprodione was instead found, the last being slightly more effective after 3 days of storage (figure 2.22b).

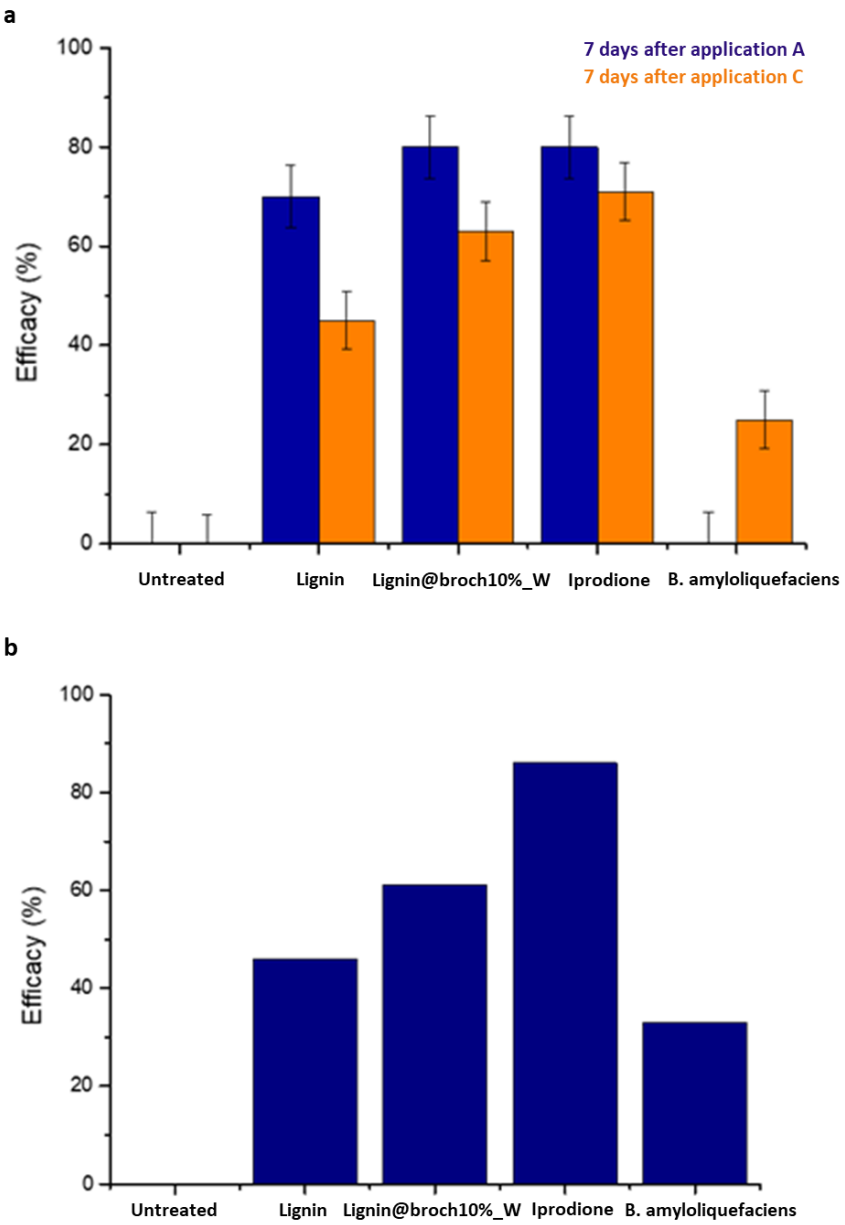

Figure 2.22 Efficacy of the treatments against *Botrytis cinerea* on strawberries: a) during and immediately after the applications and b) after three days of storage. In both graphs untreated check is settled as 0% efficacy.

Trial 2 - evaluation of different dosages of material lignin@brochantite10%_WET

As explained in detail in the experimental part dedicated to this section, this test was aimed at evaluating the effectiveness of lignin@brochantite10%_W with two different dosages, 3L/ha and 10L/ha. The tests were carried out on tomato plants, variety Optima, against the following pathogens: *Pseudomonas syringae*, *Xanthomonas campestris*, *Xanthomonas arboricola fragrari* and *Botrytis cinerea*. Results, in terms of efficacy percentage and of incidence and severity, are shown in figure 2.23 and 2.24, respectively.

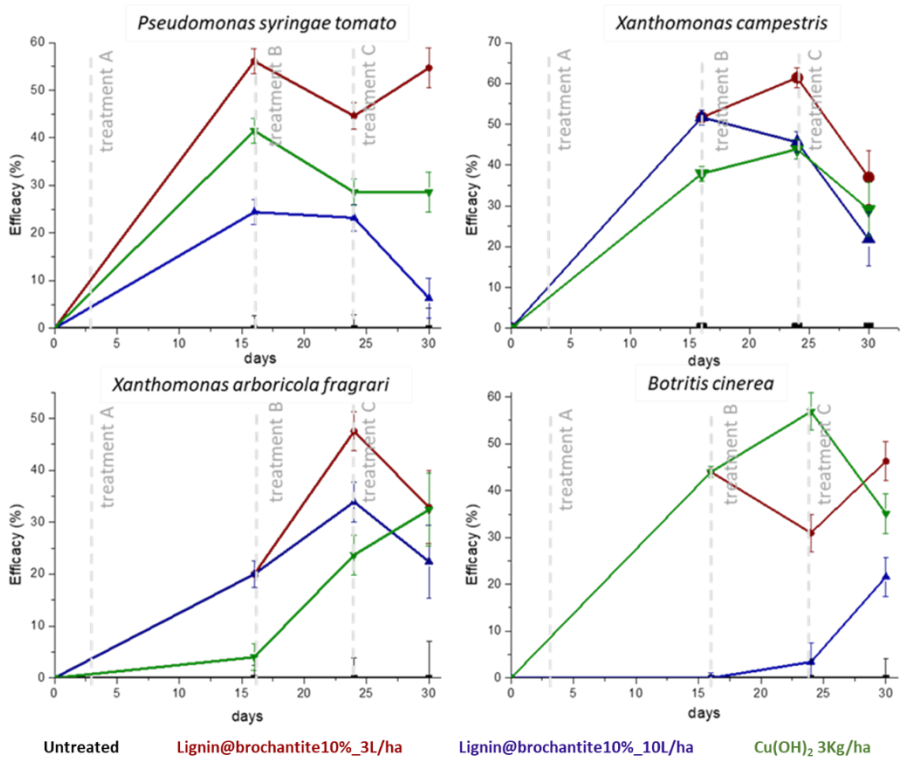

Figure 2.23. Assessment of the efficacy of the material with different dosages on tomato plant against several pathogens. The efficacy is expressed as percentage of attacked leaves on 60 leaves per plot; the untreated check is settled at 0%.

The efficacy percentage is obtained considering the percentage of attacked leaves on 60 total leaves per plot. The untreated check was settled at efficacy 0% and day 0 corresponds to the inoculum of the pathogen. The incidence, instead, refers to the percentage of attacked leaves, while the severity corresponds to the percentage of attack on the leaves (are interested by the attack). As reference the commercial product $Cu(OH)_2$ was used, while lignin alone was not tested due to the low activity found in the previous tests (figure 2.22).

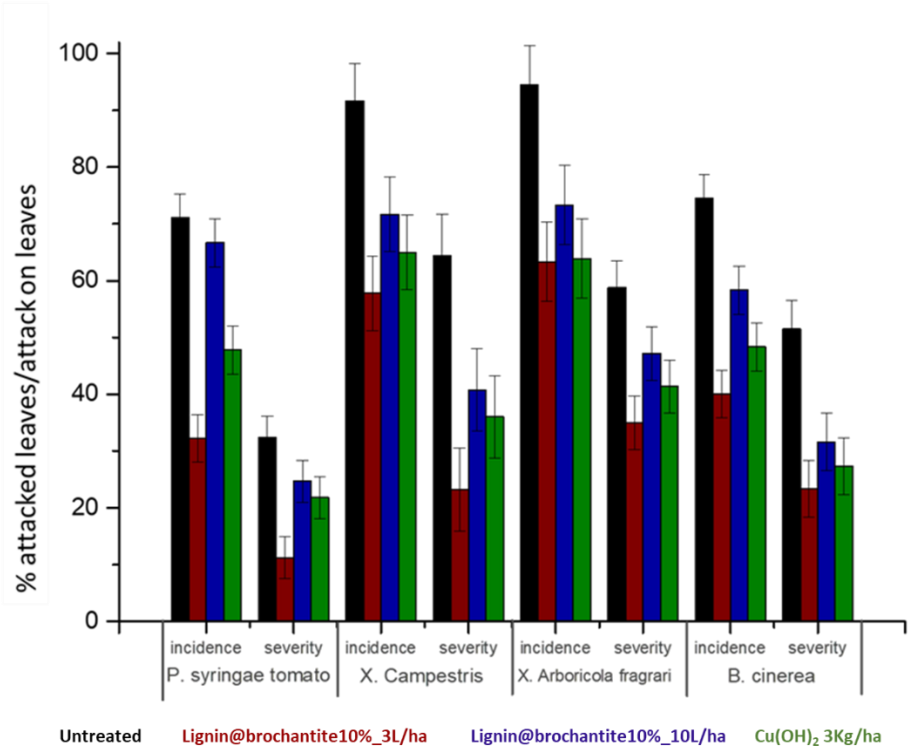

Figure 2.24. Assessment of different dosages for material lignin@brochantite10%_W considering the incidence (percentage of attacked leaves) and the severity (percentage of attack on leaves). The results are refereed to 30 days after the first artificial inoculum.

Even against these pathogens the material lignin@brochantite10%_W compares well with the commercial product. Moreover, surprisingly, in all cases the best performances were obtained with the lower dosage of 3L/ha, bringing the final concentration of copper to 30 g/ha, again much lower than that usually applied with the commercial product, corresponding to 600 g/ha. Once again, the hybrid material lignin@brochantite shows its high potential as a pesticide thanks to the combined lignin-copper effect. Comparing the biocidal activity of inorganic copper-based products and our hybrid material, it is clear that the combination of copper and lignin is more effective than the individual components.
The reasons for this successful combination may lie in the nature of the hybrid materials presented here. The crystals are, in fact, embedded in the lignin matrix, and this could allow a more controlled release of copper. In this sense, lignin could act as a protecting matrix toward Cu-containing crystals slowing down their solubilization and then prolonging their biocidal action. This aspect will be investigated in the future in order to understand the mechanism of action of the Lignin@Cu hybrid materials.

Trial 3 - crystals morphology and activity correlation

The next step was to assess the influence of the morphology of brochantite crystals on the activity. As explained in the dedicated paragraph "Synthesis and characterization", as the concentration of the metal increases, the brochantite crystals become larger, starting from spherical nanocrystals up to isolate rods with a length between 150 and 250 nm in the material lignin@brochantite20%_WET. These finding gives the possibility to study a crystal dimension-activity correlation, helpful for the definition of the best protective material. Three materials featured by different size of brochantite crystals were then compared as pesticides: lignin@brochantite3%_WET, containing crystalline nanospheres with a diameter between 2 and 20 nm, lignin@brochantite10%_WET, containing rods with a length of approximately 100 nm and a width of 20 nm and, finally, lignin@brochantite20%_WET, characterized by brochantite rods slightly larger than 10% material (thickness between 10-20nm and a length between 40-150nm). To evaluate the effectiveness of the crystals' morphology, the three materials were formulated in such a way to have the same final copper concentration (30g/ha). Tests were conducted on tomato plants

(Optima variety) against *Pseudomonas infestans* by evaluating the number of affected leaves and the percentage of attack on the leaves (figure 2.25).
As reported by several authors, the particle dimension is not always the dominant factor in toxicity[8,53]. El Badawy et al., for example, studied the toxicity of silver nanoparticles underling as, in their cases, the surface charge has a greater effect on toxicity[53].
Furthermore, a key factor is also the shape of nanoparticles. As explained by Slavin et al, in fact, the presence of corners, edges or defects can lead to an increase in toxicity due to a greater surface area-volume ratio[8]. This, in fact could allow the nanoparticle to be more easily adsorbed by cells or to facilitate the attachment to the molecules constituting the cell membrane.

Our results clearly show that the greatest activity is found for the materials with 10% and 20% of copper, while the 3% copper material has less control over the pathogen (figure 2.25). This suggests, therefore, that larger brochantite rods have a greater effect than nanospheres present in lignin@brochantite3%_WET. Furthermore, in figure 2.25a we can see the effectiveness of the materials over time. Larger brochantite crystals not only have better efficacy, but also have longer-term activity than materials containing smaller crystals, as can be seen from the curve trends. The red curve, in fact, referred to the material lignin@brochantite with bigger crystals has a less steep rise over time than the other two materials. These unexpected results made us reflect on what happens to the leaf once the product has been sprayed. While it is common to consider that smaller nanocrystals may be more available to the plant being, therefore, able to exert a greater activity[8], in our case it seems that what matters is the permanence of the products on the leaf. To a higher permanence of the product on the leaf corresponds a higher control of Cu^{2+} ions release over time. From this point of view, therefore, it is not difficult to think that larger rods cannot only have greater adhesion, but also constitute a better copper reservoir compared to nanospheres, which can be dissolved/removed more easily by water, whose acid character is expected to be more effective onto small crystals[4].

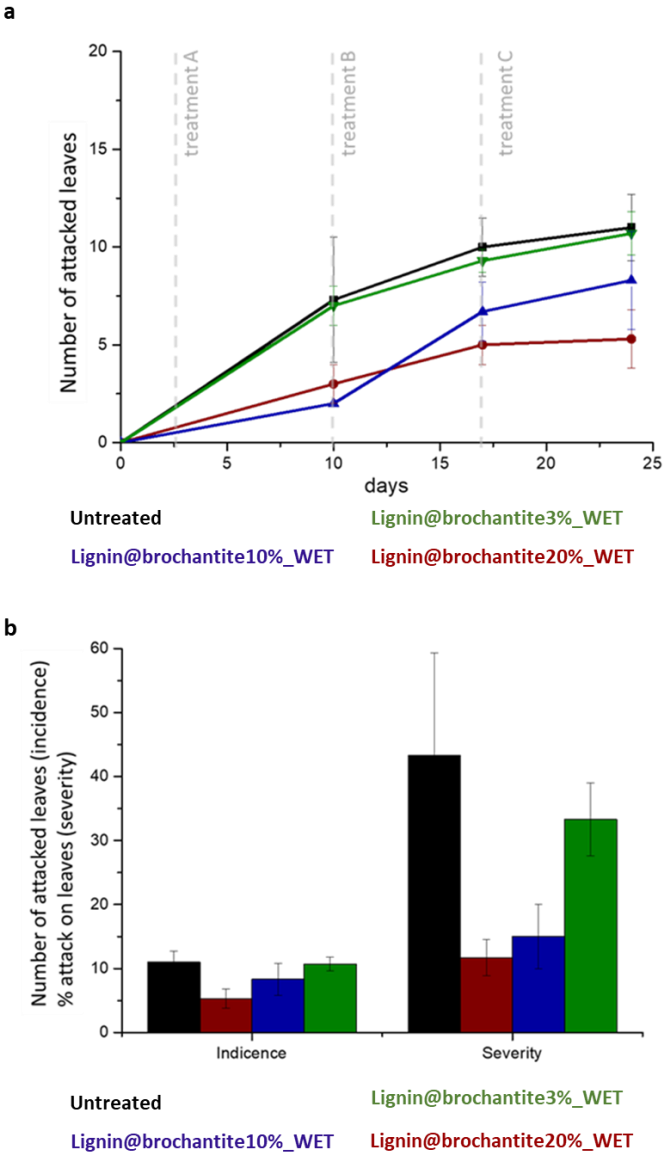

Figure 2.25. Crystals' morphology and activity correlation by tests conducted on 11 tomato plants. a) Number of attacked leaves, with day 0 referred to the inoculum of the pathogen; b) incidence: number of attacked leaves; severity: percentage of attack on leaves; the results are refereed to 30 days after the first artificial inoculum.

Ac-lignin@brochantite

In this paragraph the synthesis and characterization of the product Acetylated-lignin@brochantite, hereinafter identified as Ac-lignin@brochantite, is presented. In order to obtain this product, BioPiva395 was firstly acetylated and subsequently the same wet procedure followed for the synthesis of lignin@brochantite was adopted.
Acetylation is a complete functionalization that occurs on both aliphatic and aromatic OH groups[54]. Many of the properties of lignin, such as antibacterial activity and antioxidant activity, as well as its pH in aqueous suspension, are closely related to its alcoholic functional groups[15]. Therefore, the evaluation of their influence both in the antibacterial activity, and in the formation of brochantite, has aroused our interest.

Experimental Part

Acetic anhydride, pyridine, $CuSO_4$ (anhydrous), and NaOH were purchased from Sigma Aldrich and used without further purification.
The pH-meter used was a Crison pHmeter basic 20 equipped with an Ag/AgCl electrode.

Acetylated lignin

20.48 g of BioPiva395 dried overnight at 60°C were dissolved in 80ml of pyridine at 26°C with a stirring of 4Hz under inert atmosphere. After 10 minutes 32.2mL of acetic anhydride was added slowly (10mL at a time) keeping the inert atmosphere. The reaction was conducted at room temperature for 18 hours in a 2L jar. The mixture was quenched with cold HCl (0.4M). Acetylated lignin precipitated and it was washed with water by filtration until neutral pH. The drying step was conducted at 40°C in a vacuum oven overnight.
The product was characterized by means of Infrared spectroscopy (IR) and Nuclear Magnetic Resonance (NMR).

Figure 2.26 shows IR spectra of BioPiva395 and acetylated lignin.

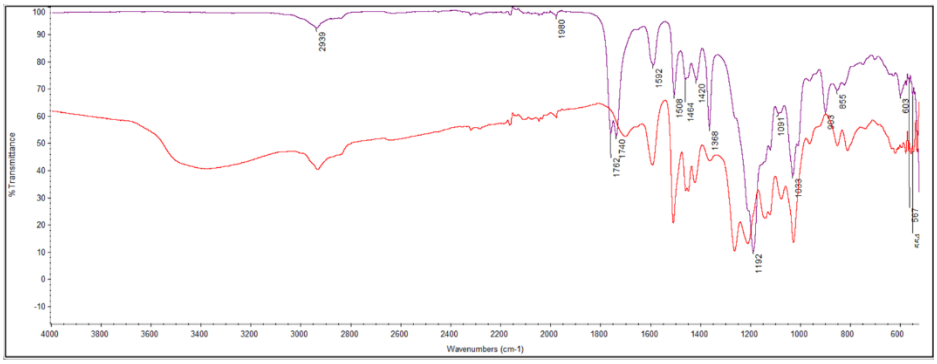

Figure 2.26. IR spectra of BioPiva395 (red) and Ac-lignin (purple).

The main differences between the IR spectra of Ac-lignin and its precursor are related to the disappearance of the broad OH band at 3000 cm^{-1} and to the appearance of carbonyl stretching signals at 1700 cm^{-1}, figure 2.26[54]. These findings confirm the occurred acetylation.

NMR data obtained dissolving the sample in deuterated DMSO are presented in figures 2.27, and 2.28. In figure 2.27 the ^{1}H-NMR spectra of Ac-lignin is shown. The aromatic protons are found in the region 6-8 ppm, while the protons of methyl and methoxy groups are found in the region 4-3 ppm. The most characteristic peaks are those belonging to the acetyl groups at about 2.25 ppm and 1.95 ppm, not present in the ^{1}H-NMR spectra of original lignin (see paragraph "Results and discussion"). The peak at 2.25 ppm corresponds to the protons of the acetyl groups linked to the phenolic functions while the peak at 1.95 ppm is related to the acetyl groups bound to aliphatic alcohol functions. A not identified peak at 8.62 ppm is present. Figure 2.28 reports the ^{13}C-NMR spectra of acetylated lignin. The peaks of aromatic carbons are in the region 110-160 ppm while at about 56.26 ppm the carbons of methoxy groups can be identified. The quaternary carbon of acetyl groups is at about 170 ppm while the methyl carbon of the acetyl group is at 20 ppm.

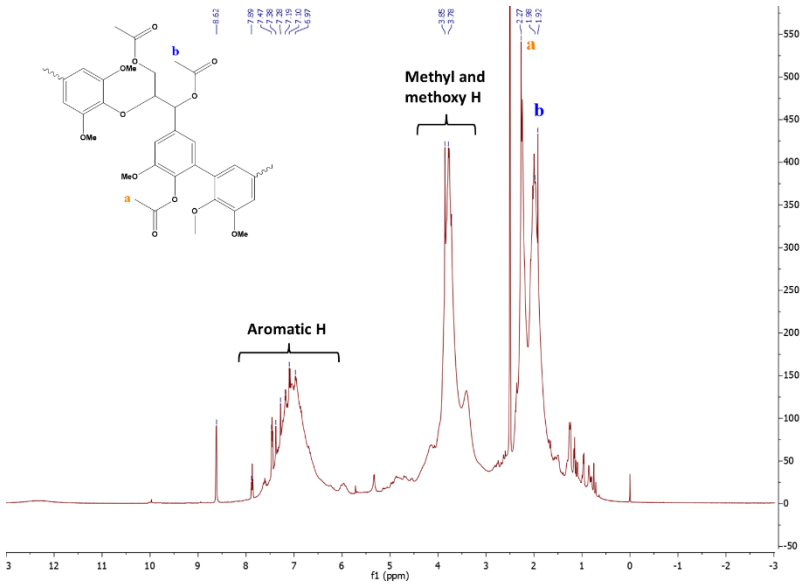

Figure 2.27. ^{1}H-NMR spectra of acetylated lignin_1 obtained in DMSO-d^{6} (solvent signal at 2.5 ppm).

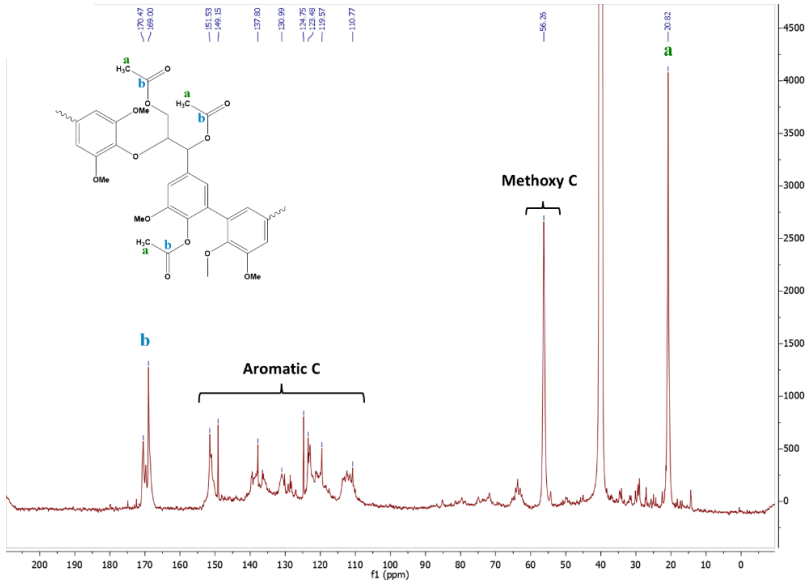

Figure 2.28. ^{13}C-NMR spectra of acetylated lignin_1 obtained in DMSO-d^{6} (solvent signal at 40 ppm).

Acetylated-lignin@brochantite

In a 100 ml bottle, 2.788 g of Ac-lignin were dispersed in 30mL of distilled water. Under vigorous stirring a water solution of copper sulphate was added. This solution was prepared dissolving 0.85g of anhydrous $CuSO_4$ in 10 mL of water. Subsequently, 9.1 mL of a 1M solution of NaOH was added dropwise.
After 2h of stirring the solid was filtered out and washed with water.
In table 2.8 are reported the reagent ratios adopted for the synthesis. The mass ratio between lignin and $CuSO_4$ was used in such a way to have a material with 10% of copper.

Table 2.8. Ratio between the reagents applied for the synthesis of Ac-lignin@brochantite

Reagents	Ratio
Mass ratio lignin/$CuSO_4$ (10%Cu)	3.28
Molar ratio $CuSO_4$/NaOH	0.6

The pH of the system was checked (table 2.9).

Table 2.9. pH of the system at different steps of the synthesis

Synthesis step	**pH**
Acetylated lignin suspension	5.68
Addition of $CuSO_4$ solution	4.22
Addition of NaOH solution	11.75
After 2h of stirring	10.73

The identification of the formed mineral phase was done by XRPD analysis (figure 2.29a), while EDS analysis revealed a rather homogeneous distribution of copper into lignin (figure 2.29b). By ICP analysis a copper content of 10.1 % ± 0.1 was detected.

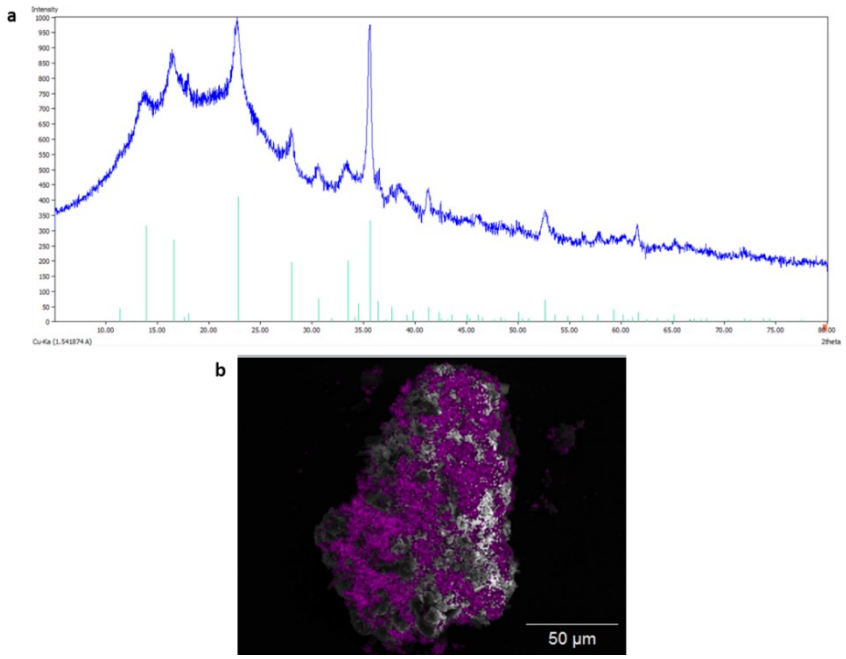

Figure 2.29. Characterization of Ac-lignin@brochantite10%_WET: a) XRPD analysis (green peaks correspond to the expected peaks of brochantite; b) EDS mapping conducted by SEM analysis; Cu element is in purple.

Results and discussion

Acetylated lignin

Lignin acetylation was conducted following the procedure describe by Buono et al. to have a complete functionalization of the OH groups[54], and the corresponding material, identified as Ac-lignin_1 was isolated. This is confirmed by IR (figure 2.26) and NMR analyses (figures 2.27 and 2.28) that evidence how functionalization occurs on both aromatic and aliphatic OH groups. IR spectrum, in fact, does not show the broad band of the OH groups around 3000 cm^{-1}, while in the ^{13}C-NMR spectrum the peak related to the C^{γ} of the function -CH_2OH (G

unit) at 60.69 ppm is absent[41]. Figure 2.30 shows the overlap between ^{13}C-NMR spectra of Ac-lignin_1 and BioPiva395.

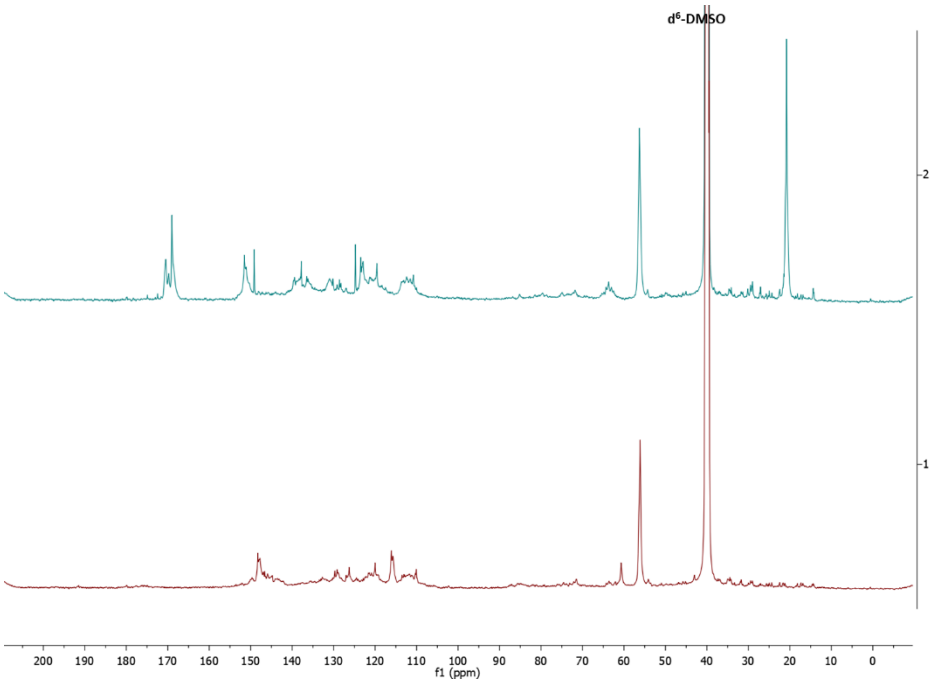

Figure 2.30. ^{13}C-NMR spectra of Ac-lignin_1 (green) and BioPiva395 (brown) conducted in d^6-DMSO (signal at 40ppm).

The two NMR profiles are quite similar except for the two peaks related to the acetyl groups at 170 ppm for the quaternary carbon and at 20 ppm for the methyl carbon. In the aromatic region we can notice a new sharp peak in the spectrum of Ac-lignin_1 at about 149.15 ppm, which could be related to traces of pyridinium chloride. However, this hypothesis is discharged by the elemental analysis results conducted on the isolated sample, which gives back a very low percentage of nitrogen, as can be inferred from Table 2.10. The N% found in Ac-lignin, although higher than that found in BioPiva395, is indicative of at maximum traces of pyridinium chloride.

Table 2.10. Elemental analysis of BioPiva395 and Ac-lignin_1

Sample	**Weight (mg)**	**Nitrogen**	**Carbon**	**Hydrogen**	**Sulphur**
BioPiva395	2.022	0.13%	63.28%	6.66%	1.91%
Ac-lignin	2.035	0.3%	63.71%	5.59%	1.29%

To evaluate the reproducibility of the procedure, other two syntheses were conducted, the corresponding samples being identified as Ac-lignin_2 and Ac-lignin_3. Figure 2.31 reports the completely superimposable IR spectra of the three Ac-lignins, the same being true also for the ^{13}C-NMR spectra, Figure 2.32.

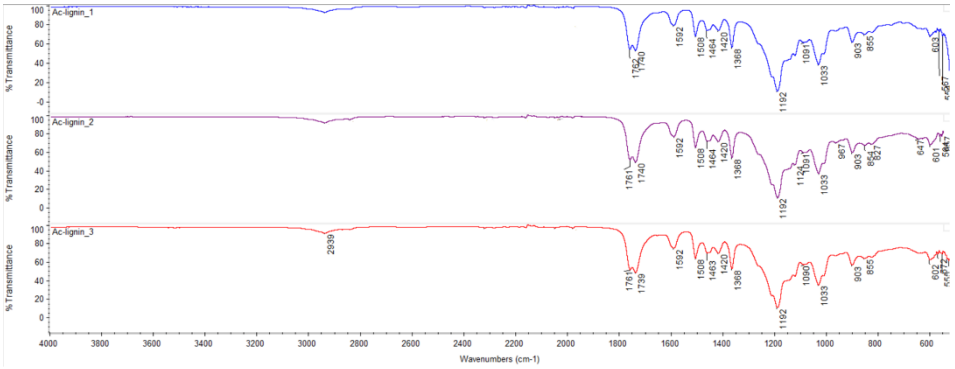

Figure 2.31. Over imposition of the IR spectra of Ac-lignin_1 (blue), Ac-lignin_2 (purple), and Ac-lignin_3 (red) confirming the reproducibility of the functionalization reaction.

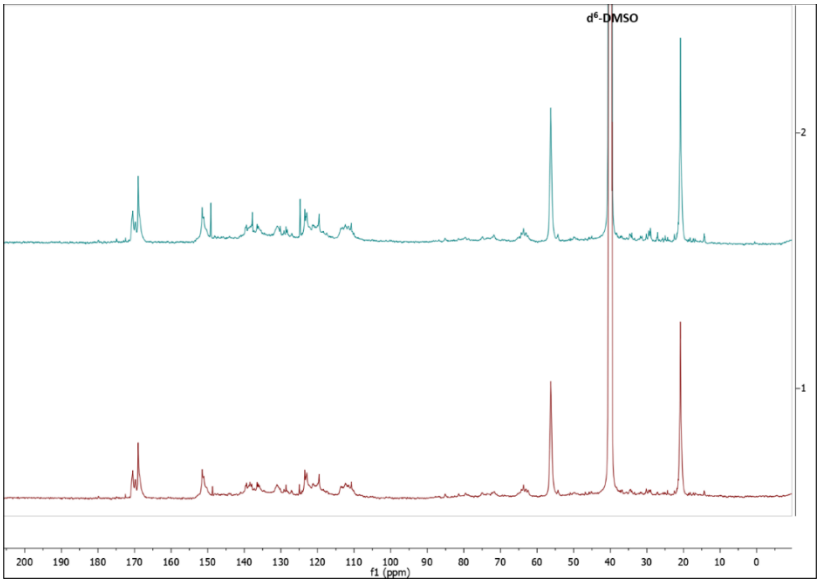

Figure 2.32. Comparison of ^{13}C-NMR spectra of Ac-lignin_1 (green) and Ac-lignin_3 (brown) conducted in d^6-DMSO.

The fragmentation profile of acetylated lignin was obtained by means of pyrolysis-GC/analysis; the main peak, as expected, is related to acetic acid (figure 2.33), while the typical signals deriving form phenol-derivatives are very low, once compared with the pyrogram obtained with BioPiva395.

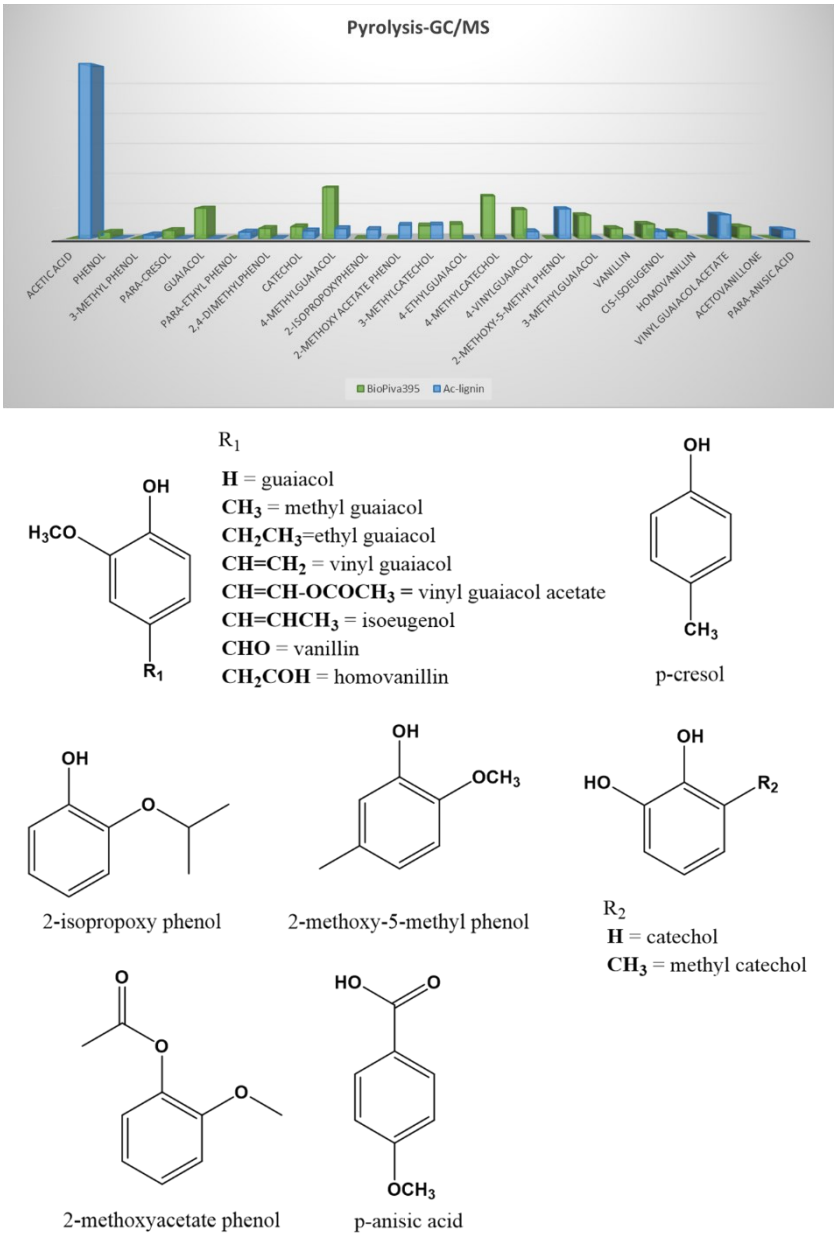

Figure 2.33. Main fragments from pyrolysis-GC/MS results of BioPiva395 and Ac-lignin. The bars represent the relative area percentages of the single analytes.

The molecular weight distribution by means of GPC analysis was not possible because of the high insolubility of acetylated lignin in aqueous basic solution (up to 1M NaOH). For GPC analysis in fact a 0.1M NaOH solution was used as eluent (see dedicated section “Gel permeation chromatography” in chapter “Characterization techniques”).

Further investigations on acetylated lignin were also conducted to describe the morphology, and the thermal proprieties.
Morphological studies carried out by SEM microscopy revealed a completely different surface for acetylated lignin compared to the one of the original BioPiva395. The surface of functionalized lignin, in fact, is clearly porous as shown in figure 2.34.

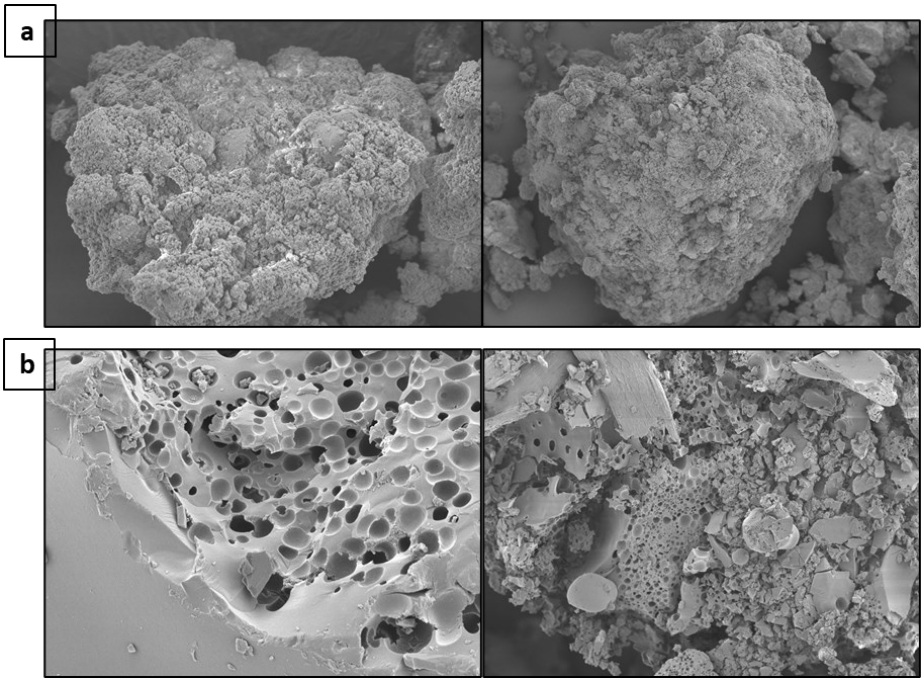

Figure 2.34. SEM images of a) BioPiva395, and b) Ac-lignin

The hydrophobicity of acetylated lignin was also investigated by means of wettability measurements with the same method described in the paragraph

"Properties of the material lignin@brochantite-Wettability" and detailed in the chapter "Characterization techniques", paragraph "Wettability measurements". Table 2.11 reports the results that are consistent with the ones reported in literature[54]. Ac-lignin has a contact angle with water of about 90°, thus confirming the expected higher hydrophobicity than BioPiva395, owing to the acetylation of the OH groups.

Table 2.11. Wettability results for BioPiva395 and Ac-lignin_1

Parameters	BioPiva395	Ac-lignin_1
Slope [g^2/s]	0.00021601	0.00001375
cos(θ)	0.373	0.018
Θ [deg]	**68.1**	**89.0**

For what concern thermal properties, figure 2.35 compares TGA profiles of BioPiva395 and Ac-lignin. Both profiles present a small mass loss between 90 and 120°C related to the removal of the residual water, the maximum weight loss being found at about 370 °C. The residual mass is similar for acetylated lignin (2.40%) and for BioPiva395 (2.28%).
DSC analyses were also conducted (figure 2.36). DSC profiles revealed a different glass transition temperature (Tg) between BioPiva395 and Ac-lignin. Glass transition temperature strongly depends on the structure of lignin. More precisely, functional groups creating hydrogen bonds, broad molecular weight distribution of the polymer and the presence of free volume can highly change the glass transition temperature[50]. In this case we can appreciate how the Tg of acetylated lignin is lower (120°C) than Tg of BioPiva395 (141°C). These data agree with literature references[54], and it can be related with the reduction of the number of hydrogen bonds as well as the increasing of free volume caused by the presence of acetyl groups, as evidenced by the presence of holes on the surface of Ac-lignin, as seen by SEM morphological analysis (figure 2.34).

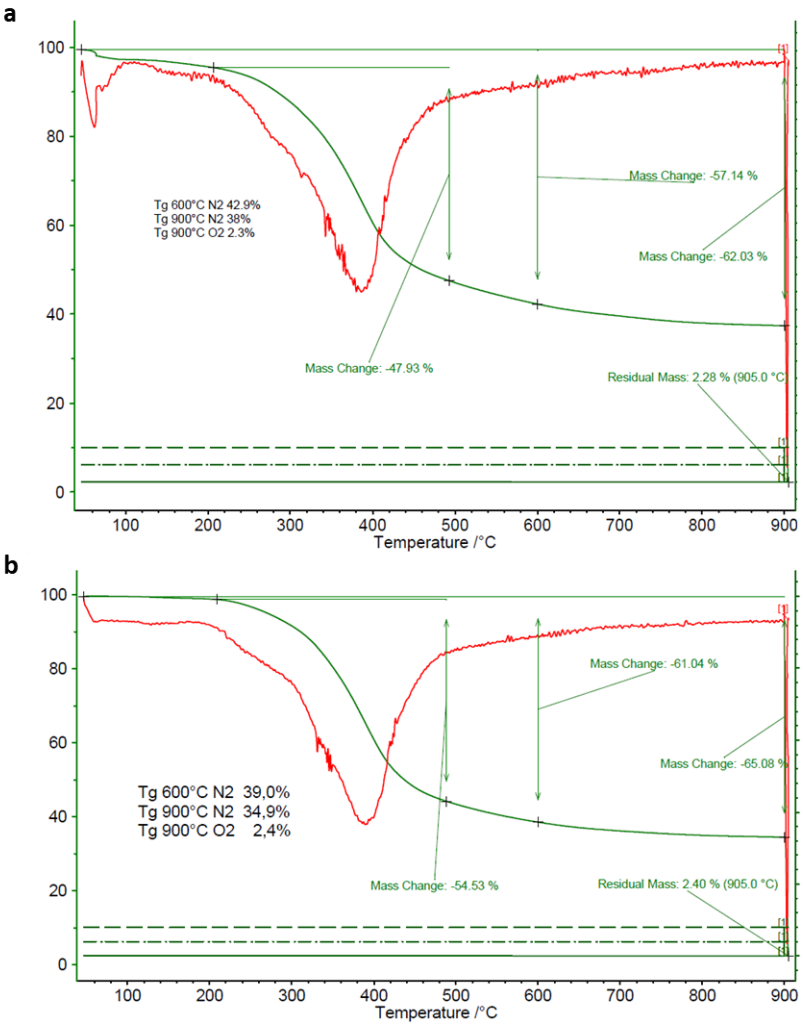

Figure 2.35. TGA of a) BioPiva395 and b) Ac-lignin.

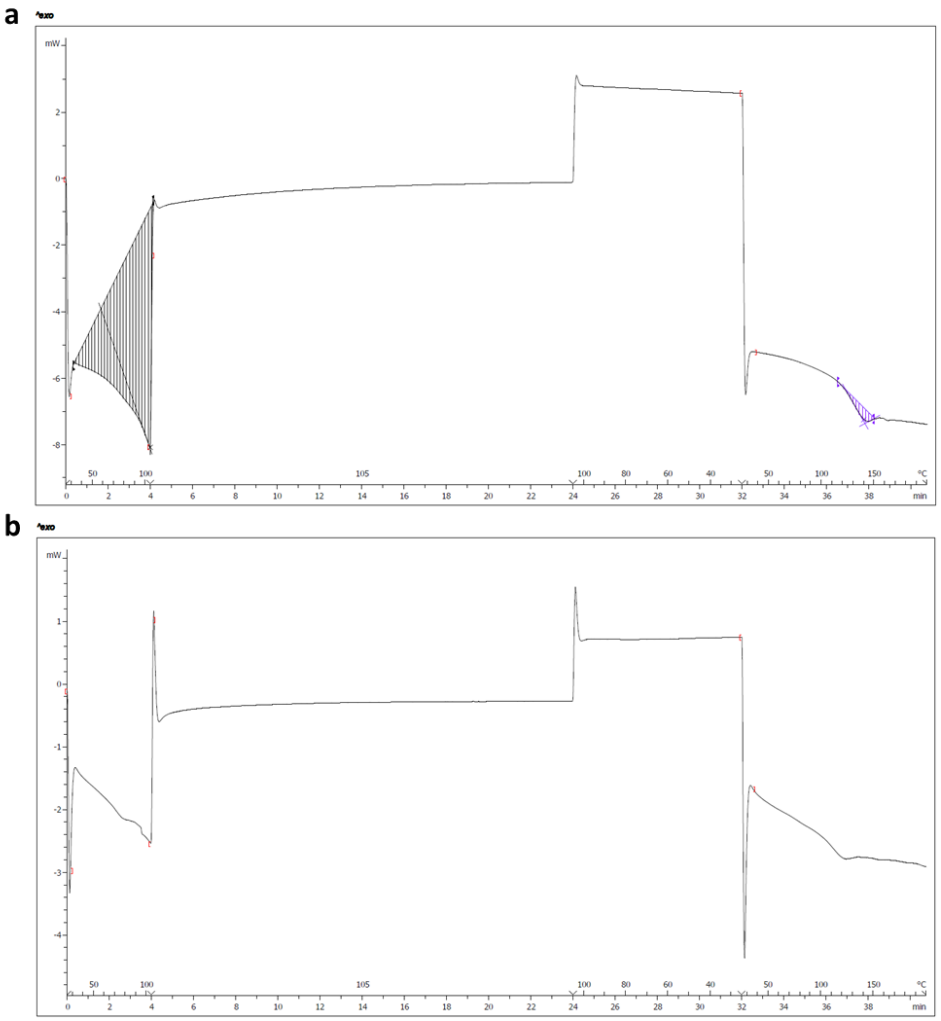

Figure 2.36. DSC profile expressed both in °C (above the x axis), and in minutes (below the x axis) of a) BioPiva395, Tg 139,70°C and b) Ac-lignin, Tg 125°C.

In vitro antibacterial tests on acetylated lignin

After the complete characterization of the material, its biological activity was evaluated by *in vitro* tests. Gyawali et al. have mentioned on the antibacterial activity of acetylated model molecules due to the increased lipophilic properties that these groups can impart to the molecules[15,16].
Lipophilic compounds can, in fact, inhibit the transport of electrons, cause proteins translocation and influence enzymatic activities leading to the destruction of the cell membrane[16].
However, several works report on how the antibacterial activity of lignin is closely related to the presence of hydroxyl groups[13,14,18,20]. It is therefore extremely interesting to evaluate the antibacterial activity of acetylated lignin in order to understand, at least approximately, how much the hydroxyl groups impact on its activity.
Preliminary investigations were done through *in vitro* tests.

Operating conditions

In vitro tests were conducted using an agar dilution method (CLSI protocol – Clinical and Laboratory Standard Institute) to determine the minimum inhibitory concentrations (MICs). All the in vitro tests were conducted by BICT-Bioindustry Innovation srl. The agar dilution assay, preferred to the liquid method because of the insolubility of the samples was performed into 24-well plates with 2mL of medium.
Acetylated lignin and BioPiva100 were suspended in the melted agar medium at a concentration of 50g/L and then, by 12 serial dilutions 1:2, dispensed into successive wells. The tested concentration range was from 50 g/L to 0.024 g/L. Once the medium solidified, the microorganisms were inoculated into the plates following specific growth conditions reported in table 2.12.
The following controls were evaluated:
-Positive control of growth: microorganisms were plated in the agar medium in the absence of the compounds
-Control of sterility: the agar mediums were not inoculated with the microorganisms

-Control of antimicrobial activity: microorganisms were plated with serial dilutions of antimicrobial agent, Ceftriaxone (64 µg/mL concentration) against bacteria and fluconazole (512 µL/mL concentration).

Table 2.12. Growth conditions of microorganisms, for TSA= Tryptic soy agar, SDA= Sabouraud dextrose agar, PDA = phenylalanine deaminase test.

Microorganism	Inoculum	Medium	Temperature	Incubation time
S. aureus	10^5	TSA	37 °C	24h
P. aeruginosa	10^5	TSA	37 °C	24h
L. monocytogenes	10^5	TSA	37 °C	24h
E. coli	10^5	TSA	37 °C	24h
C. albicans	10^5	SDA	37 °C	24h
B. Cinerea	10^4	PDA	25 °C	48h
R. Solani	10^4	PDA	25 °C	48h

Results and discussion

The MIC values were identified at the end of the incubation time evaluating the first well in which no visible growth was present. Results are summarized in table 2.13.

Table 2.13. MIC values for each microorganism and sample

Microorganism	----------MIC----------		
	Acetylated lignin	BioPiva100	[1]Ceftriaxone/ [2]Fluconazole
S. aureus[1]	>50 g/L	25 g/L	64 µg/ml
P. aeruginosa[1]	**25 g/L**	50 g/L	32 µg/ml
L. monocytogenes[1]	**1.56 g/L**	6.25 g/L	8 µg/ml
E. coli[1]	25 g/L	25 g/L	4 µg/ml
C. albicans[2]	>50 g/L	50 g/L	> 512 µg/ml
B. cinerea[2]	>50 g/L	>50 g/L	> 512 µg/ml
R. solani[2]	>50 g/L	>50 g/L	16 µg/ml

As reported in table 2.13, the most interesting results were obtained against bacteria *P. aeruginosa and E. coli*, with a MIC of 25 g/L, and against *L. monocytogenes* with a MIC of 1.56 g/L. Only in the case of *S. aureus* BioPiva100 has a lower MIC than Ac-lignin, thus confirming that not only phenol groups of lignin are responsible of the biocidal activity of this biopolymer.
However, the antimicrobial activity of the two polymers is several orders of magnitudes lower than that shown by the two references Ceftriaxone and Fluconazone. For this reason, once again, we combine Ac-lignin with copper to try to reinforce its biocidal activity.

Acetylated-lignin@brochantite

BioPiva395 dispersed in water (10% slurry) gives a pH around 4. The same dispersion obtained with Ac-lignin gives a pH of 5.68 (table 2.9). This is reasonable because of the replacement of the OH functions of lignin with acetyl groups. Considering that the reaction with copper is conducted in the presence of NaOH, the absence of the OH groups is expected to bring to strongly basic conditions of the reactant medium. Several studies correlate the formation of different copper phases in aqueous solution with the Cu^{2+} /OH^- molar ratio, strictly related to the pH of the systems and the temperature at which the reaction is carried out[37,38,55].
In particular, Zittlau et al. conducted titration experiments in which a 0.001M copper sulphate solution was titrated with a solution of sodium hydroxide varying the temperature between 20 and 85°C and monitoring the pH[37]. The importance of pH and temperature in the formation of brochantite was highlighted, revealing that this phase is obtained at 55°C and at a pH of 6.2. The formation of brochantite was observed again at pH 7.5 increasing the temperature up to 85°C. Same pH conditions but lower temperatures, such as room temperature, led instead to the formation of posnjakite, while higher pHs favoured the formation of tenorite[37].
Under our experimental conditions, in which to an Ac-lignin suspension a water solution of copper sulphate and 9.1 mL of NaOH 1M were added we observed the rather unexpected formation of brochantite. In fact, after the addition of NaOH solution a pH of 11.75 was recorded (table 2.9), which remained remarkably basic even after two hours of stirring (pH=10.73, table 2.9) and far from the conditions described in the literature for the formation of brochantite. Thus, once again, the

action of the polymer in the exclusive formation of brochantite was confirmed, no traces of tenorite were, in fact, found.

The possibility of a deacetylation of Ac-lignin through basic hydrolysis can be excluded, on the basis of its low solubility in basic solutions and by IR analysis. The IR spectrum of Ac-lignin@brochantite, shown in figure 2.37, reveals, in fact, the typical stretching band of the carbonyl group deriving from acetyl functions at about 1750 cm^{-1}, while the broad band deriving from the OH groups is not observed. The characteristic peaks deriving from brochantite (3580 cm^{-1}, 3565 cm^{-1}, 3389cm^{-1}, 1087 cm^{-1}, 945 cm^{-1}, the broad peak at 853 cm^{-1}, 783 cm^{-1} and 598 cm^{-1}) are well visible[37].

The complete copper upload revealed by ICP clearly confirms that the reaction occurred completely (see Experimental Part "Acetylated-lignin@brochantite").

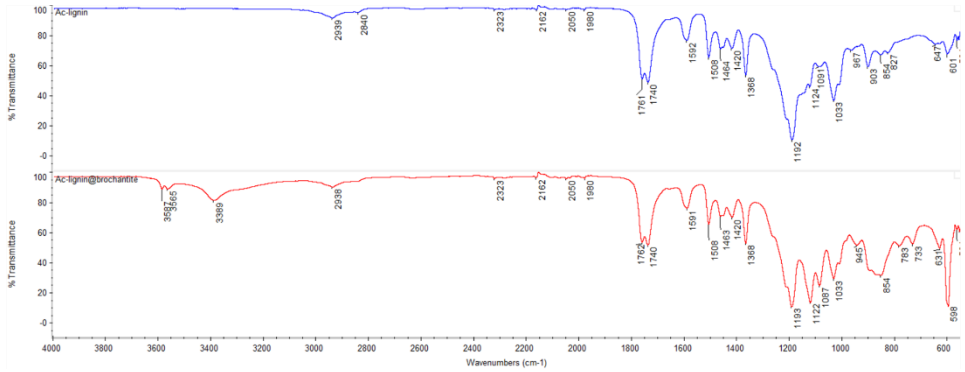

Figure 2.37. IR spectra of acetylated lignin (blue) and Ac-lignin@brochantite10% (red).

The evaluation of biocidal activity of Ac-lignin@brochantite by *in vitro* tests are in progress.

Conclusions

The hybrid material lignin@brochantite paved the way for the use of lignin for agronomic purposes, highlighting its potential when combined with copper.
Two synthetic procedures have been optimized to obtain this product characterized by brochantite crystals embedded in the lignin matrix.
The wet procedure "lignin@brochantite_W" consists of a heterogeneous system in which water solutions of copper sulphate and sodium hydroxide are added to a water lignin suspension. The formation of brochantite as exclusive crystalline phase is possible only in the presence of lignin suspension which, after the addition of sodium hydroxide, keeps the system at pH = 7, avoiding the formation of tenorite (CuO).
To further simplify the synthesis and make it more scalable for possible future development on pilot plants, the material was also obtained through mechanochemistry, "lignin@brochantite_M". Mechanochemistry can be considered a scalable production method because it simplifies the recovery steps of the product compared to the wet synthesis which must necessarily consider tedious filtration steps. In particular, with a view to large-scale production, cylindrical twin screw extruders appear particularly well suited to guarantee continuous production[56,57].
In this case lignin, copper sulphate and sodium hydroxide are added as solids in the jar and for 1g of total reagents 2mL of water are used, in order to have slurry conditions. The optimization of the mechanochemical procedure has highlighted the importance of the slurry conditions for the selective formation of brochantite rather than its hydrated phase, posnjakite.
In vivo tests conducted on tomato and strawberry plants against several pathogens have highlighted the promising efficacy of the combined activity between lignin and copper. The lignin@brochantite_W material, suitably formulated and sprayed on plants, in fact, exerts a better pesticidal activity with a reduced copper content compared to the copper-based commercial products.
Hybrid materials lignin@brochantite with different copper concentrations, from 3% to 20%, were obtained with both syntheses, and by increasing the metal content larger crystals formed. In vivo tests, then, made it possible to evaluate the correlation between crystals' morphology and their activity and the best performances were observed with bigger crystals. Probably larger crystals adhere

better to the leaf thus having a longer-term protective action than smaller crystals.

A comprehensive evaluation of the materials was possible using IR, NMR, Pyrolysis-GC / MS and GPC analyses which allowed to evaluate the actual integrity of lignin after both syntheses. The presence of the metal salt, the base and the grinding did not, in fact, cause fragmentation or other changes in the structure of lignin. This agrees with what reported by Sipponen et al. regarding the negligible degradation of lignin observed during mechanochemical treatment of maize stem.[58]. Also, Guerra et al. evaluated the effects of grinding on the molecular weight of lignin during wood pulverization, highlighting that there are no significant variations[59].

A structural modification of lignin was, on the other hand, carried out through its complete acetylation (Ac-lignin) confirmed by IR and NMR analyses. By means of wettability measurements its hydrophobic character was confirmed and a characterization was carried out also through thermal and morphological analyses. Preliminary *in vitro* tests conducted on acetylated lignin revealed the potential of lignin as antibacterial agent even when deprived of the hydroxyl groups.

Finally, by combining Ac-lignin with copper sulphate and sodium hydroxide, according to the wet procedure, the hybrid material Ac-lignin@brochantite, with 10% of copper, was surprisingly obtained despite the basic pH of the heterogeneous system (10.7). The XRPD analysis did not reveal, in fact, any trace of copper oxides and IR analysis of the Ac-lignin@brochantite confirmed that during the synthesis the hydrolysis of the acetate groups did not significantly occur.

The promising in vitro tests conducted on acetylated lignin and the formation of Ac-lignin@brochantite make the exploration of the combined effect between acetylated lignin and copper intriguing for future studies.

Lignin@cuprite

The antimicrobial activity of copper oxide nanoparticles makes this species suitable not only for agronomical applications, but also applicable in paints, fabrics and in the health sector, both as constituent powders and as coated films[60].

The action of copper oxides against microorganisms is still not well understood. Surapaneni et al. evaluated the concentration of radical species that are formed following the action of copper (II) oxide and copper (I) oxide to understand how these species damage cells, if there are any differences between them, contributing, therefore, to clarify the mechanisms of action[60].

In their study they show that cupric oxide generates superoxide radical ions, while cuprous oxide leads to an increase in the concentration of hydroxyl radicals. The development of hydroxyl radicals would be linked to the Fenton chemistry, according to which Cu (I) oxidizing to Cu (II) by reaction with H_2O_2 would generate hydroxyl ions and hydroxyl radical ions. The latter, very reactive, attack indiscriminately all the molecules present in the cells.

Other studies show that Cu (I) damages enzymes such as fumarase[61]. Furthermore, the main action of copper (I) oxide is related to its ability to bind to the thiol groups of the amino acids in the intracellular proteins[62].

Once again, the scope of my work is the development of antibacterial material to be applied in the agronomic sector. In the following paragraph, a new lignin-based material containing copper (I) oxide in the form of cuprite is presented.

Obtained from $CuSO_4$ as a metal source, the reducing properties of lignin were exploited. The material is characterized by ICP, XRPD, and by GPC, Py-GC / MS to evaluate any changes occurred to the lignin structure.

Finally, the activity is evaluated through *in vitro* and *in vivo* tests.

Experimental Part

The technical lignin was Kraft lignin from *Pinus taeda*, provided by UPM-Kymmene Oyj and Green Innovation GmbH, BioPiva395 (M_w=5950-6000 g/mol, M_n= 1560-1565 g/mol) which was employed without further purification. Its features are

presented in the dedicated section in chapter 1, “Lignin materials used in this work”.
$CuSO_4 \cdot 5H_2O$ and NaOH were purchased from Sigma Aldrich and used as received. The distilled water was degassed by boiling for about 1 h and subsequently cooled under a gentle flux of nitrogen.
pH was measured with a Crison pHmeter basic 20 equipped with an Ag/AgCl electrode.

Synthesis and characterization

100 mg of BioPiva395 were suspended in 5 mL of oxygen-free deionized water in a 50 mL two necked round bottom flask. Under vigorous stirring 350 µl of a 1M NaOH solution were added in such a way to reach pH 11. After the complete dissolution of lignin, 10mL of a solution containing 20 mg of $CuSO_4 \cdot 5H_2O$ were added dropwise. After the addition the pH dropped at 10.2. The reaction was conducted under nitrogen atmosphere to avoid the formation of carbonates which hinder its characterization.
After 5 minutes from the complete addition of copper sulphate, water was removed under stirring at 50°C by a gentle flux of nitrogen. When a brown dried powder formed, the material was washed twice with distilled water by centrifugation and dried again at 50°C.

The same procedure was followed using 50 mg of copper salt in such a way to increase the metal content; after the addition of copper sulphate solution, the pH of the system dropped from 11 to 5.8.
Table 2.14 reports the amount of $CuSO_4 \cdot 5H_2O$, the percentage of Cu calculated with respect to the mass of lignin and the percentage of Cu determined by ICP analysis, as well as the inorganic phase detected by XRPD analysis.

Table 2.14. synthesis with basic lignin solution.

$CuSO_4 \cdot 5H_2O$ (mg) in 10ml	% Cu respect to the lignin mass	% Cu (from ICP-AES)	XRPD
20 mg	5%	3.64[1]±0.05	cuprite
50 mg	13%	-----	posnjakite
[1]the material was washed as describe in the procedure			

Figure 2.38 reports the XRPD trace, TEM image and EDS mapping of lignin@cuprite5% .

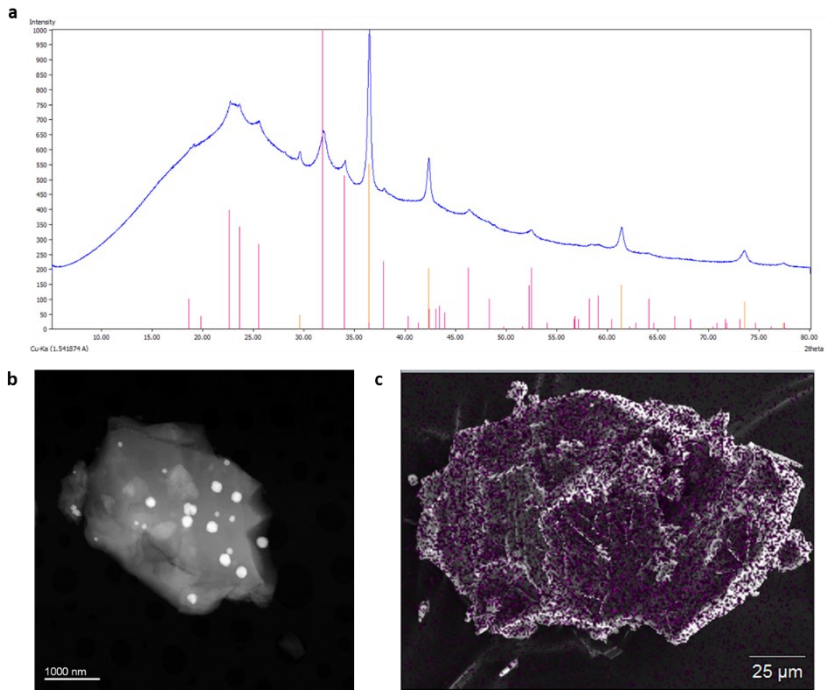

Figure 2.38. a) XRPD pattern of lignin@cuprite5% prior washing with water: the orange trace corresponds to expected signals of cuprite, while the pink traces correspond to sodium sulphate, the byproduct of the reaction; b) TEM image of lignin@cuprite5%: the bright spots correspond to nanoparticles of cuprite distributed in the lignin matrix (grey), c) EDS mapping of lignin@cuprite5% particle: copper is depicted in purple.

Synthesis and characterization

Dissolution of BioPiva395 under basic conditions makes possible to exploit the reducing property of lignin towards copper. The reduction of the metal occurs at the expense of the phenolic groups, as describe by Fiss et al[63].

Two syntheses with a different percentage of metal (5% and 13%, see table 2.12) were evaluated. The reaction conducted with the highest amount of copper led to a drastic lowering of the pH causing the precipitation of posnjakite, as reported in table 2.14 and shown in figure 2.39.

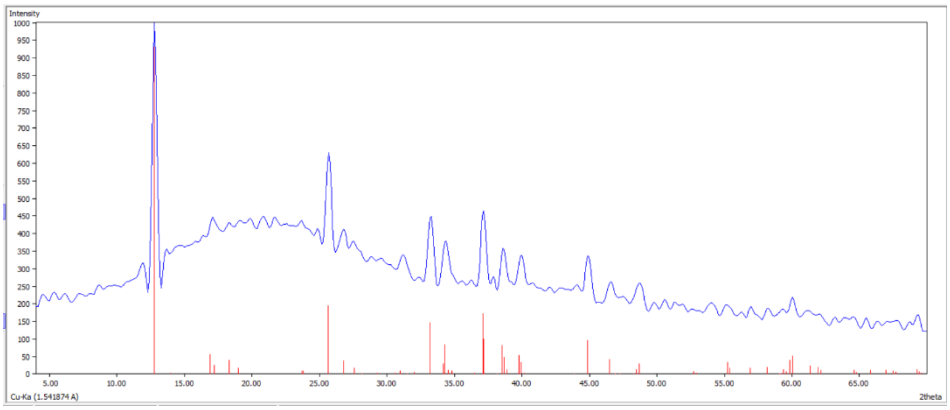

Figure 2.39. XRPD trace of the material synthesizes using 13% of copper, corresponding to lignin@posnjakite.

This observation is in complete agreement with what reported by literature regarding the relative stability of different phases of basic copper sulphates at different temperatures and pHs. At room temperature and close to neutral pH, the formation of posnjakite is in fact expected[37,38]. Furthermore, as already mentioned, posnjakite is the kinetically favoured product with respect to brochantite, and the sudden drop of the pH from 11 to 5.8 promotes its fast crystallization[37].

The drop of the pH provokes the concomitant precipitation of lignin leading to the formation of a material identical in appearance to the previously synthesized lignin@brochantite and lignin@posnjakite. No further investigations were conducted on this sample, focusing the attention on the new hybrid material lignin@cuprite5%.
In this case, the raw material collected at the end of the reaction, once put in contact with water, gives rise to a dispersion, making very difficult the washing step. This is the reason why figure 2.38a reports the XRPD trace of the material containing the by-product sodium sulphate (cuprite corresponds to the orange trace, while sodium sulphate corresponds to the pink trace). As we can see from table 2.12, ICP analysis conducted on the washed samples reveals a lower percentage of copper (3.64%) than the expected one (5%). Since XRPD analysis conducted on the raw material excludes the presence of unreacted copper sulphate, the incomplete copper upload must be imputed to the partial loss of cuprite during washing. As will be highlighted in the section "Stability of the dispersion in water", in fact, the release of pure cuprite NPs from the material dispersed in water occurs within a few days standing the sample at room temperature.

As seen for the other Cu-containing materials previously described, lignin@cuprite5% is characterized by the presence of nanoparticles of the inorganic phase embedded in the lignin matrix. No coordination of the metal to lignin can be invoked, the material thus having a hybrid, heterogeneous character, as shown in figure 2.38. The nanoparticles have a diameter between 50 and 250 nm, determined by TEM dimensional analysis. A statistical analysis, conducted on 70 crystalline specimens, revealed two populations of cuprous oxide particles according to their average size. The first one presents particles with an average diameter of 100±10 nm, and the second one is characterized by bigger particles with an average size of 200±10 nm.

To complete the characterization of lignin@cuprite5% the next step was to investigate possible modifications occurred at expense of lignin.
Zhao et al. evaluated the effect of oxidant agents, among them copper oxide, on alkali lignin[64]. They dissolved lignin in NaOH treating it with different concentration of oxidant at 90°C for 2h. According to their study, the presence of the oxidant agent can provoke the hydrolysis of β-O-4 bonds, with a consequent

increase in aromatic hydroxyl groups, leads to the formation of carbocation intermediates with consequent recondensation or causes the cleavage of C-C bonds in the side chain of the phenylpropanoic units, generating new carboxyl groups and causing a drop in the molecular weight distribution.
Thus, despite our synthesis conditions are much milder than those presented in this work, we decided to evaluate, by IR, GPC, and Py-GC/MS, if even in our case the lignin could undergo some structural changes.

Figure 2.40 reports IR spectra of lignin@cuprite5% (prior to be washed) and BioPiva395. The main differences are related to the disappearance of the carbonyl stretching band at 1705 cm^{-1} present in the spectrum of the biopolymer and to the presence of SO_4^{2-} anion bands, in the spectrum of lignin@cuprite5%, at about 1121 cm^{-1} and 600 cm^{-1}. The absence of the carbonyl stretching band of carboxylic acid groups is related to the basic environment present during the synthesis that causes their deprotonation, while the sulphate band is indicative of the formation of sodium sulphate. Thus, with this technique no substantial differences were revealed in the structure of lignin after synthesis.

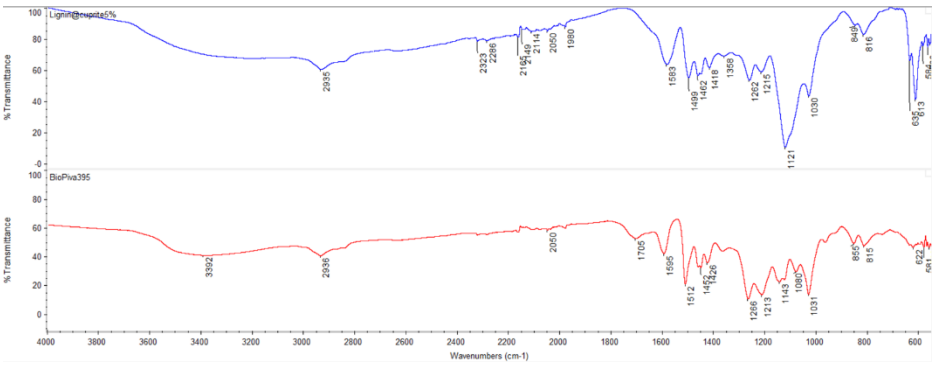

Figure 2.40. IR spectra of lignin@cuprite5% before washing (blue) and BioPiva395 (red).

Py-GC/MS results for BioPiva395 and lignin@cuprite5% are shown in figure 2.41. With Py-GC/MS analysis no major differences were revealed from the fragmentation profiles of BioPiva395 and lignin@cuprite5%.

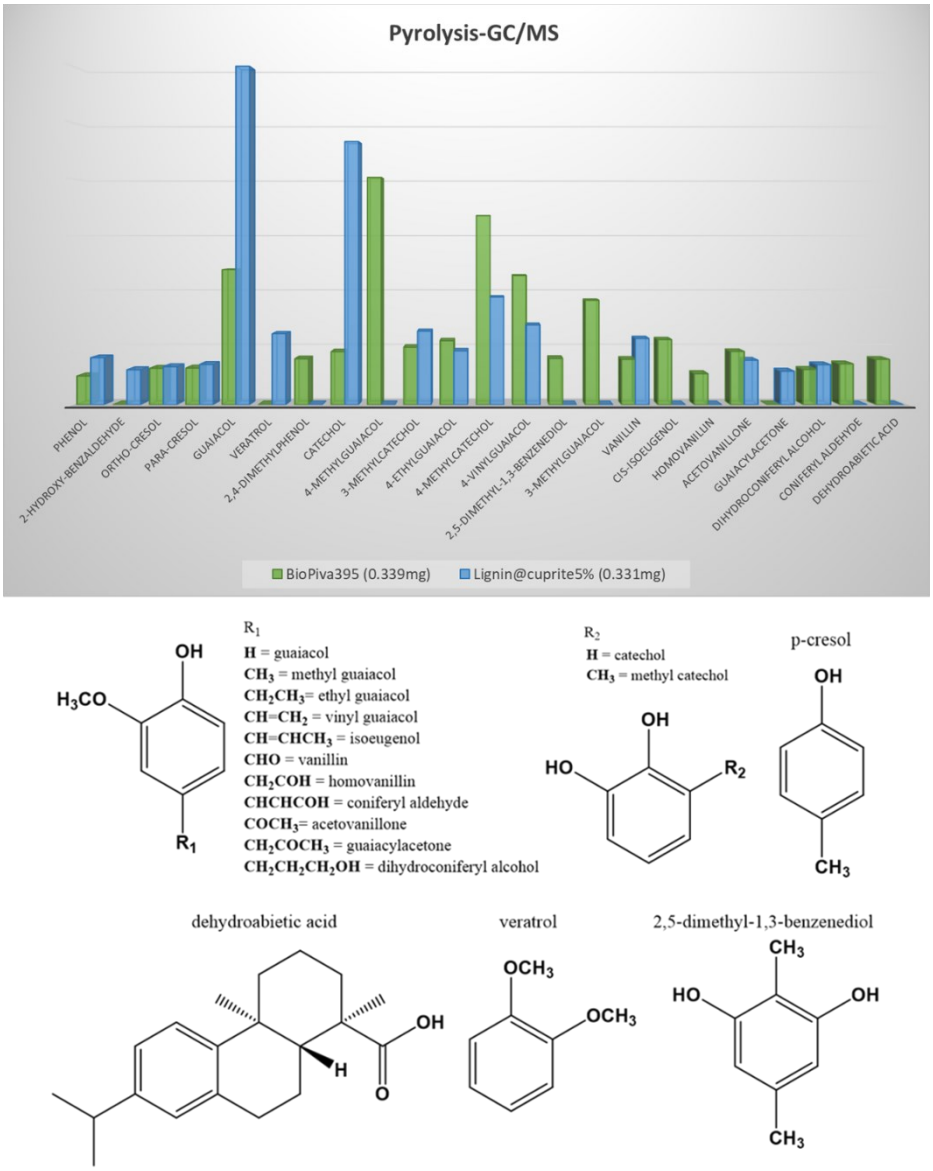

Figure 2.41. Main fragments from pyrolysis-GC/MS profiles of BioPiva395 and lignin@cuprite5%. The bars represent the relative area percentages of the single analytes.

GPC analysis instead revealed the same trend already observed for the materials lignin@brochantite. The average mass molecular weight (M_w) value increases by 1000 Da compared to the M_w value of the original lignin, (figure 2.42). An increase in molecular weight could be due to recondensation phenomena, as described by Zhao et al[64]. Such phenomena, due to the recombination between carbocation intermediates, would be generated at copper oxide concentrations higher than 2% by weight[64].

These recondensation phenomena appear, however, a fairly unlikely hypothesis given our mild synthesis conditions. In fact, recondensation occurs following the hydrolysis of β-O-4 bonds[64] and it is difficult to think that this hydrolysis can be caused by a basic solution at room temperature, since kraft lignin is extracted through a hard basic process (see chapter 1-Kraft lignin). This, combined with what was observed from the GPC analysis of lignin@brochantite material deprived of the inorganic phase (page 68), makes more likely to suppose an aggregation effect due to the copper phase rather than a structural change of the polymer.

Furthermore, by the comparison of the chromatographic profiles, we can assert that lignin has not undergone significative structural changes. The profiles are, in fact, very similar, as we can see in figure 2.42.

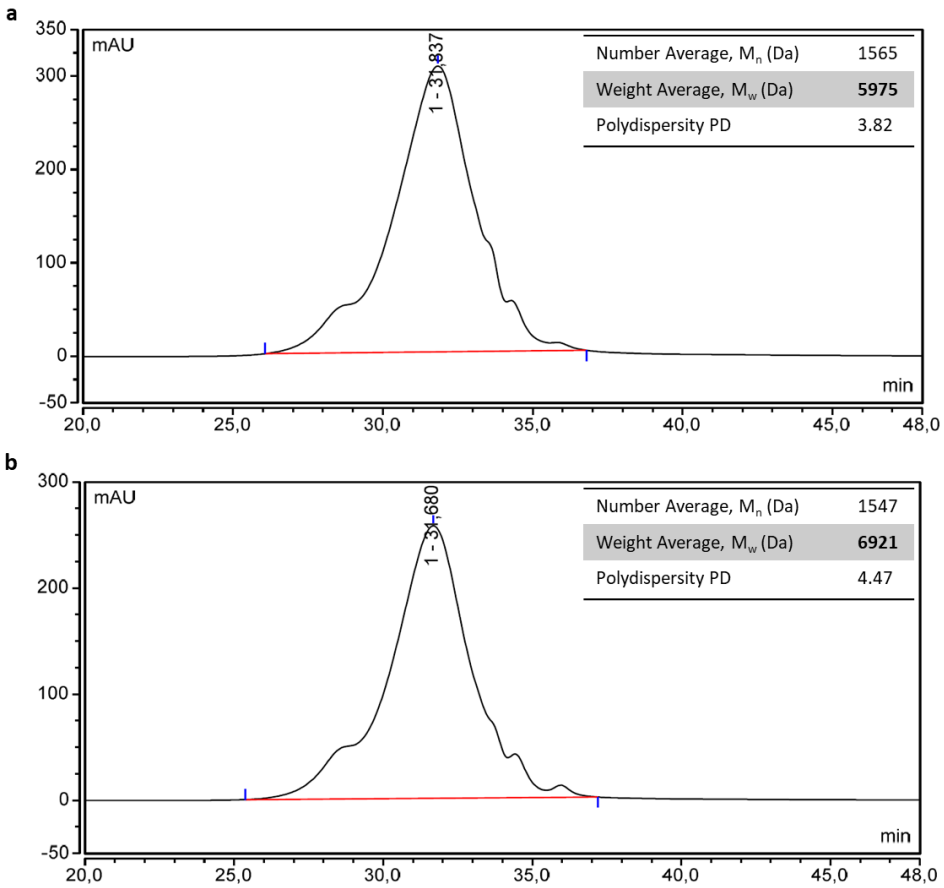

Figure 2.42. Chromatograms and GPC parameters of a) BioPiva395 and b) lignin@cuprite5%

Properties of lignin@cuprite material

Some properties of lignin@cuprite5% were investigated. Firstly, the stability of its dispersion in water by means of DLS measurements was stated. Subsequently, morphological analysis by means of SEM analysis allowed to characterize its surface, while thermal analyses (TGA and DSC) completed the characterization.

Stability of the dispersion in water

The investigation of the stability in water of the material lignin@cuprite5% was conducted by means of DLS analysis carried out on the properly diluted original solution. For this analysis, the material was not dried, or washed, and the water for the synthesis was previously filtered with 0.22µm nylon filters to make it suitable for the analysis. 1 mL of the original solution was diluted to 5 mL with fresh and filtered distilled water. The DLS analysis of the solution, shown in figure 2.43, reveals NPs with an average size of 183.7 nm (red curve), in agreement with TEM results. After 5 days, the same solution was analysed again, figure 2.43, green curve, showing an averaged size increasing at 282.2 nm.

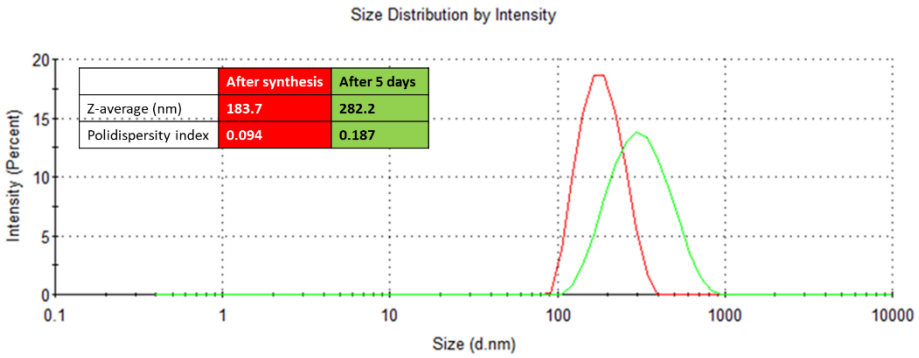

Figure 2.43. DLS analysis of a properly diluted solution of lignin@cuprite5%. Red curve refers to the analysis conducted immediately after the synthesis; the green curve refers to the analysis conducted after 5 days of storage.

Dynamic light scattering evidenced the tendency of the cuprite nanoparticles to aggregate in water suspension which results in the precipitation of a yellow powder within one week of storing. XRPD analysis of the yellow powder revealed the presence of pure cuprite, highlighting how only the inorganic phase precipitated (figure 2.44).

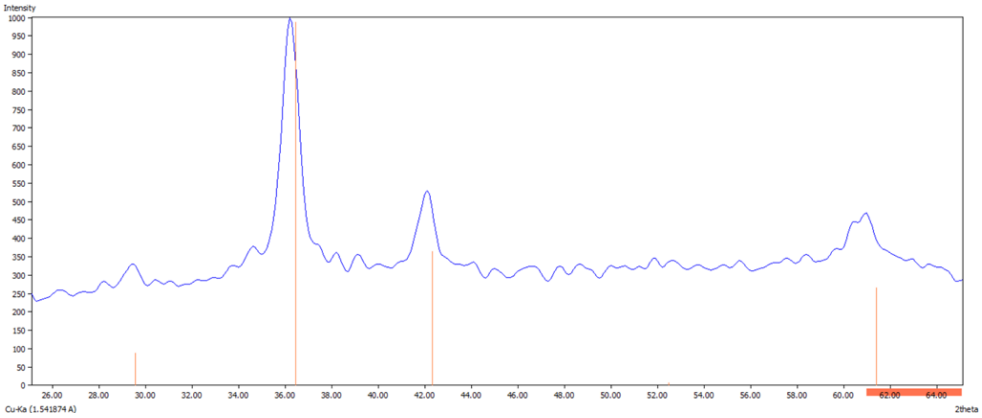

Figure 2.44. XRPD of the yellow powder precipitated within 1 week from the suspension of lignin@cuprite5%.

Morphology

SEM images of lignin@cuprite5% are shown in figure 2.45.

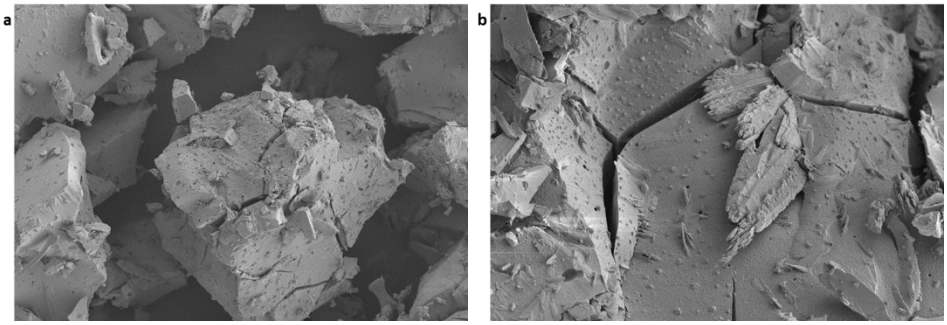

Figure 2.45. SEM images of the material lignin@cuprite5% with an enlargement of a) 100 µm and b) 20 µm.

Thermal analysis

Figure 2.46a reports TGA analysis of lignin@cuprite5%. The first weight loss is at about 100°C corresponding to the loss of the residual water, the second one starts at 200°C and ends at 400°C. The third weight loss is at 750°C. The residual mass,

due to the presence of the inorganic phase, is 25.07%, considerably higher than that found for BioPiva395, corresponding to 2.28%. DSC analysis is shown in figure 2.46b.

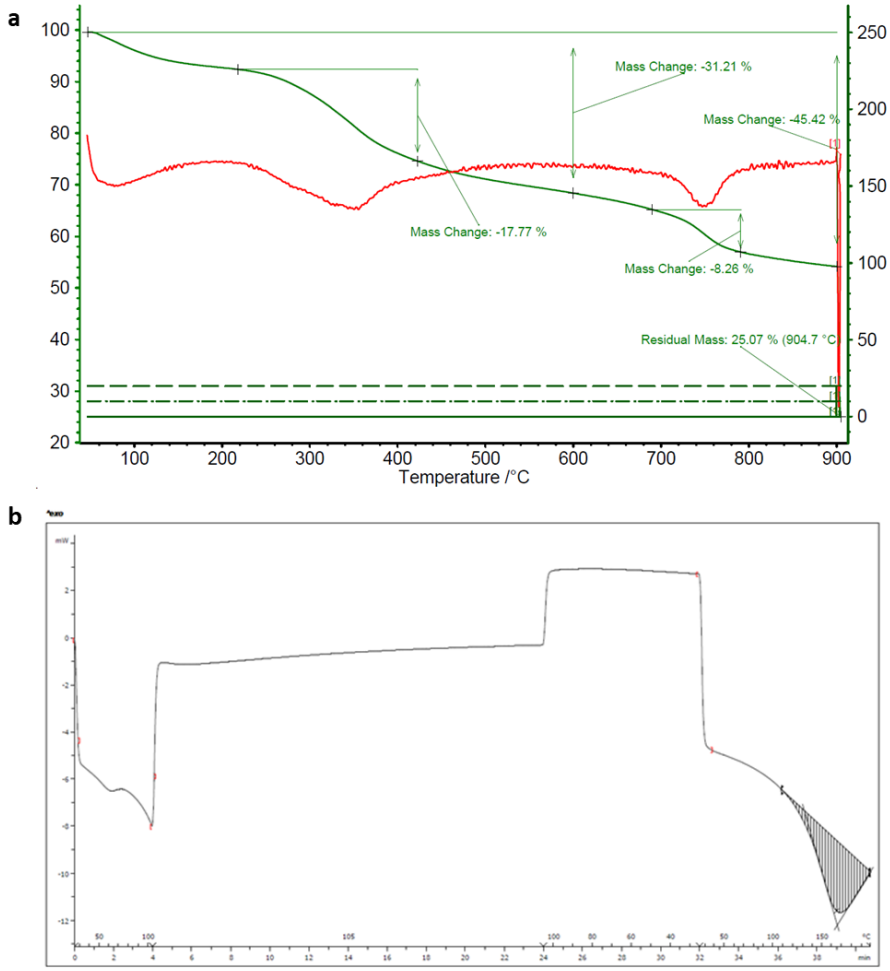

Figure 2.46. a) TGA and b) DSC analyses of lignin@cuprite5%. The DSC profile is expressed both in °C (above the x axis) and in minutes (below the x axis). The peak at 164,47°C is likely a combination of the glass transition temperature of the polymer with a process related to the inorganic phase.

DSC analysis (figure 2.46b) reveals the presence of an endothermic peak at 164,47°C. This peak cannot correspond to the glass transition temperature (Tg) of the polymer because this transition is represented by a sort of inflection point than by a real peak. Same results were observed also in the case of DSC analysis of lignin@brochantite_W material. Probably the interference of the inorganic phase activated some endothermic process.

Antimicrobial activity - In vitro tests

Aware of the potential activities of copper (I) oxide, a preliminary investigation of its activity was done through *in vitro* tests conducted by BICT-Bioindustry Innovation.

Operating conditions

The antimicrobial activity was evaluated by an agar dilution method to determine the minimum inhibitory concentrations (MICs) of the compound and related controls. The agar dilution assay, preferred to the liquid dilution method because of the insolubility of the material, was performed into 24-well plates with 2mL of medium.
All assays were performed in triplicate. For each triplicate, the same microbial suspension of known titer was used, inocula were quantified by determination of viable colonies upon agar plate method. To avoid solubility problems and related reproducibility issues, MIC index determination was performed following the protocol CLSI-M7, modified for visually observing the growth of viable colonies on the agar surface. MIC was defined as the lowest concentration of the compounds that inhibits visible growth of the microorganism after incubation. The compounds were tested at serial dilutions factor 2, each concentration of the triplicate gave the same result in terms of microbial growth.

Lignin, BioPiva100, and copper (I) oxide were used as controls. The concentrations used are listed in table 2.15.

Table 2.15. List of the compounds tested and relative concentrations

Materials	**Initial concentrations (g/L)**	**Starting copper concentration (g/L)**
BioPiva100	50.00	0.00
Lignin@cuprite5%	50.00	1.75
Cu_2O	1.95	1.75

The starting amount of lignin@cuprite5% and Cu_2O were chosen in such a way to have the same copper amount.

The microorganisms tested with their specific parameters of growth were bacteria, such as *Staphylococcus aureus*, *Listeria monocytogenes*, *Escherichia coli*, *Xanthomonas campestris*, *Pseudomonas syringa pv. Actinidiae,* and fungi such as *Botrytis cinerea* and *Rhizoctonia solani*. For each microorganisms the following controls were included:

- positive control of growth: microorganisms were plated in the agar medium in the absence of the compounds
- control of sterility: the agar mediums were not inoculated with the microorganisms
- control of antimicrobial activity: microorganisms were plated with 6 serial dilutions of antimicrobial agent, Ceftriaxone (64 µg/mL starting concentration) against bacteria and Fluconazole (512 µg/mL starting concentration) against fungi.

Results and discussion

The results are reported in table 2.16.

Table 2.16. List of the MIC values (minimum inhibitory concentration) of the compounds tested; the copper concentration is reported in brackets.

		---------- MIC g/L ----------			
	microorganisms	lignin	lignin@Cu_2O	Cu_2O	antimicrobial agent*
Bacteria	*Staphylococcus aureus*	0,78	0,78 (0.027)	0,49 (0.438)	>64 µg/L
	Listeria monocytogenes	3,13	1,56 **(0.055)**	0,49 (0.438)	8 µg/L
	Escherichia coli	3,13	12,50 (0.438)	>1,95 (1.7)	2 µg/L
	Xanthomonas campestris	1,56	3,13 (0.109)	1,95 (1.70)	4 µg/L
	Pseudomonas syringae pv. actinidiae	1,56	3,13 (0.109)	>1,95 (1.7)	16 µg/L
Fungi	*Botrytis cinerea*	>50	>50	>1,95 (1.7)	>512 µg/L
	Rhizoctonia solani	0,20	**0,02 (0.001)**	>1,95 (1.7)	16 µg/L
* Ceftriaxone for bacteria, fluconazole for fungi					

The tests allowed to identify the minimum inhibitory concentrations (MICs) of the tested materials. MIC is the lowest concentration that inhibits the visible growth of a microorganism. The most interesting data was obtained with the fungus *Rhizoctonia solani.* In fact, in this assay a strong combined effect of lignin and copper was evident. In particular, lignin@cuprite5% is active at a concentration 10 times lower than lignin and has a lower MIC than cuprous oxide alone.
Regarding the bacteria, the trial with *Listeria monocytogenes* is significant and, also in this case, the combined effect lignin-copper is evident. In fact, despite the MIC is lower with copper (I) oxide alone, the copper concentration used is

significantly higher than that used with lignin@cuprite5% (values in brackets). Generally, lignin shows a clear inhibitory effect and all strains tested are inhibited at relatively low concentrations, with the only exception of *Botrytis cinerea*. This, however, showed strong resistance to all the tested compounds (included the antibiotic) and the minimum inhibitory concentrations could not be detected.

In the light of these results, the antimicrobial properties of lignin@cuprite material are confirmed by the selectivity towards *Listeria monocytogenes* and *Rhizoctonia solani*.

UPM Solargo™ 100@Cu

As already mentioned, the materials must be formulated before being used. In particular, our products are applied on the leaves or on the fruits and, therefore, they must be made sprayable, avoiding problems such as sedimentation and clogging of the nozzle. In the synthesis of lignin@cuprite5% we observed the tendence of cuprite NPs to aggregate when the material is dispersed in water. This aggregation, appreciable after 5 days through dynamic light scattering (figure 2.43), causes the precipitation of cuprite within a week (figure 2.44). Having had confirmation of the effectiveness of cuprous oxide through the in vitro tests presented in the previous paragraph, the next step was to try to improve the synthesis in such a way to produce the material directly in the field. In addition to the undoubted practical advantage linked to an easier synthetic procedure, the possibility of having a product immediately ready for use would also solve the problems related to the instability of the cuprite nanoparticles. To do this, it was decided to use a pre-formulated lignin, named UPM Solargo™ 100, supplied by UPM-Kymmene and Green Innovation. UPM Solargo™ 100 is a commercial product by UPM/Green Innovation in which lignin is mixed with propylene glycol, KOH, and water.

Always starting from copper sulphate, the reducing properties of lignin lead once again to cuprite (cuprous oxide) nanoparticles embedded in the lignin matrix. The materials, indicated as solargo@copper phaseX%, with X= 5%, 13% and 18%, contain different percentages of copper referred to the mass of lignin contained in the formulate. All the materials were characterized by XRPD, TEM and DLS analysis and tested by in *vivo tests* in the greenhouse.

Two different synthetic procedures will be presented here, aimed at making the preparation of the materials as practical as possible in the field. In the first, an aqueous solution of copper sulphate is added dropwise to UPM Solargo™ 100; the products are indicated as UPM Solargo™ 100@CuX%_1. In the second case, solid copper sulphate is added to 1 mL of UPM Solargo™ 100, previously diluted with 99 mL of water. The materials thus obtained will be identified as UPM Solargo™ 100@CuX%_2.

Experimental part

UPM Solargo™ 100 provided by UPM-Kymmene and Gren Innovation is a lignin formulated with lignin (100g), water (325g), potassium hydroxide, (KOH) 50% (75g), and propylene glycol (500g) for 1L of Solargo100.
$CuSO_4 \cdot 5H_2O$ was purchased from Sigma Aldrich and used without further purification.

Synthesis and characterization of the materials

UPM Solargo™ 100@CuX%_1

To 50 mL of UPM Solargo™ 100 (5g of lignin), a copper sulphate water solution was added dropwise at room temperature and under stirring (see Table 2.17 for the amounts of copper sulphate used in the syntheses). For the characterization of the samples an aliquot of the reactant mixture was withdrawn after 10 minutes from the end of the copper sulphate addition and dried by heating at about 120°C until a lacquered solid formed. This was washed with water and dried again at 100°C overnight.

The XRPD and TEM characterizations for the materials UPM Solargo™ 100@CuX%_1 with X= 5% and 13% of copper, are presented in figure 2.47. TEM and SAED (selected area electron diffraction) analyses reveal cuprite nanoparticles with a dimension between 2-5 nm that aggregate in spheres with a diameter of 20-100 nm for both samples.

Table 2.17. Details of the procedure for the preparation of UPM Solargo™ 100*@CuX%_1*

Sample	$CuSO_4 \cdot 5H_2O$ mg in ml of water	%Cu referred to lignin	%Cu from ICP-AES	XRPD results
UPM Solargo™ 100@cuprite5%_1	1g in 5mL	5%	2.42% ± 0.06	cuprite
UPM Solargo™ 100@cuprite13%_1	2.5g in 11mL	13%	11.3% ± 0.1	cuprite
UPM Solargo™ 100 @cuprite-brochantite18%_1	3.5g in 15mL	18%	13.8% ± 0.2	cuprite-brochantite
UPM Solargo™ 100 @brochantite-posnjakite23%_1	4.5g in 20ml	23%	----------	Brochantite-posnjakite

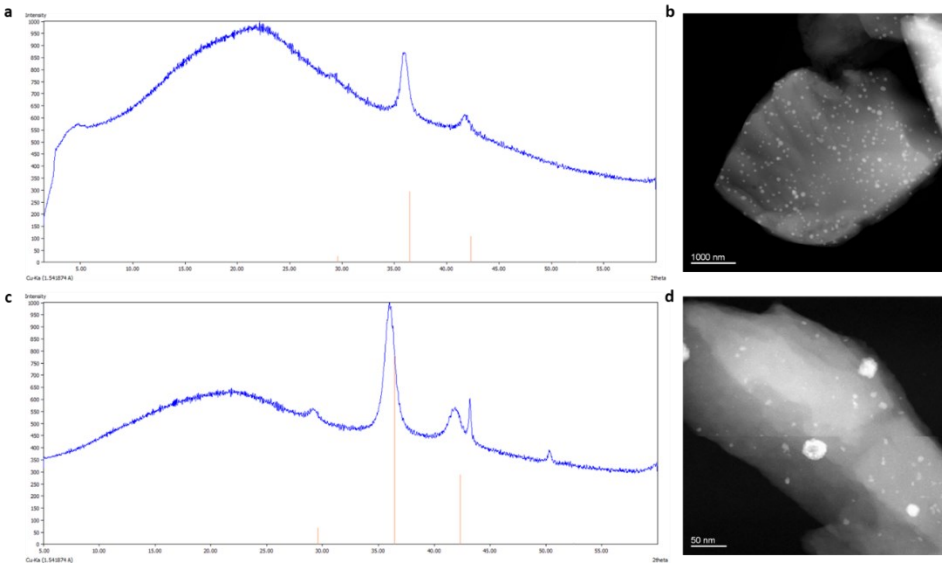

Figure 2.47. XRPD and TEM images of the materials UPM Solargo™ 100@cuprite5%_1 (a-b) and UPM Solargo™ 100@cuprite13%_1 (c-d). Orange bars are theoretical peaks of cuprite.

UPM Solargo™ 100@CuX%_2

1mL of UPM Solargo™ 100 (100 mg of lignin) was diluted with 99 mL of distilled water. Subsequently, solid $CuSO_4 \cdot 5H_2O$ was added under stirring. After 5 minutes from the addition the suspension was dried at 100°C overnight. The solid obtained was washed with water, dried again, and analysed by means of XRPD and TEM analysis (figure 2.48).

Table 2.18 collects the syntheses conducted with dilution.

Table 2.18. Experimental conditions of synthesis UPM Solargo™ 100*@CuX%_2 and ICP and XRPD results.*

Sample	$CuSO_4 \cdot 5H_2O$ (mg)	%Cu referred to the lignin	XRPD results
UPM Solargo™ 100@cuprite5%_2	20 mg	5%	cuprite
UPM Solargo™ 100@cuprite13%_2	50 mg	13%	cuprite
UPM Solargo™ 100@Cu18%_2	70 mg	18%	crystalline phase not identified

TEM images in figure 2.48 (b, c) shows cuprite nanoparticles, identified by means of SAED analysis, with a dimension between 20-50 nm in the case of UPM Solargo™ 100@cuprite5%_2 and between 10-30 nm for UPM Solargo™ 100@cuprite13%_2.

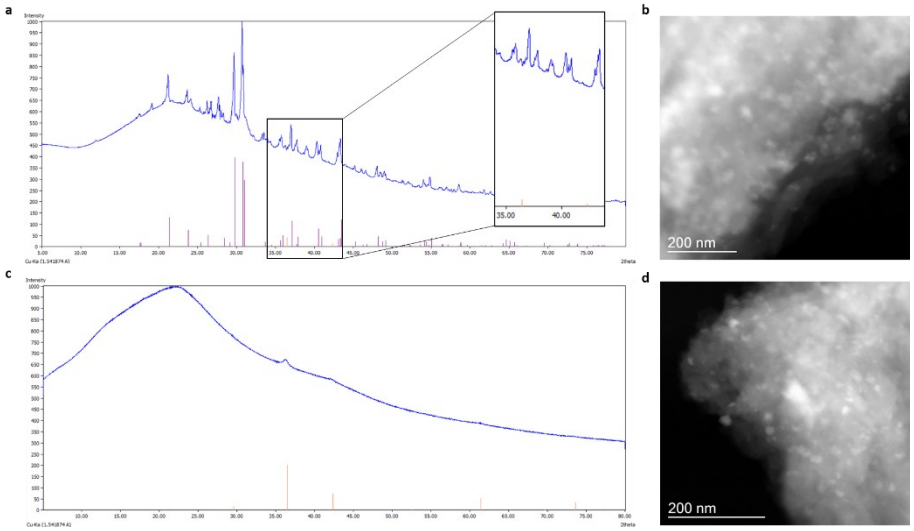

Figure 2.48. Characterization of UPM Solargo™ 100@cuprite5%_2 (not washed) and UPM Solargo™ 100@cuprite13%_2 (washed): a) and c), XRPD traces (orange bars are the theoretical peaks of cuprite, purple bars are the theoretical peaks of potassium sulphate); b) and d): TEM images

Results and discussion

Synthesis and characterization

Two different syntheses starting from the pre-formulated lignin UPM Solargo™ 100 were conducted. In the first one, a solution of copper sulphate was added dropwise to the UPM Solargo™ 100 as it is (materials indicated as UPM Solargo™ 100@cupriteX%_1), while in the second synthesis, in order to further simplify the procedure, solid copper sulphate was added to UPM Solargo™ 100 previously diluted with water (dilution ratio = 1:100, materials indicated as UPM Solargo™ 100@cupriteX%_2). The dilution was chosen to reach the optimal activity conditions of lignin formulation. The ICP analysis was conducted only on the material UPM Solargo™ 100@cupriteX%_1. The difficulty met during washing and the presence of other not volatile organic/inorganic components have discouraged the use of this technique for the characterization of UPM Solargo™

100@cupriteX%_2. However, it must be taken into account that the adopted procedure assures that all copper is applied in the field. From table 2.17 it can be inferred that only in the case of UPM Solargo™ 100@cuprite13%_1 there is a good correspondence between the calculated percentage of copper and the ICP result. The lower percentages found in the case of UPM Solargo™ 100@cuprite5%_1 and UPM Solargo™ 100@cuprite-brochantite18%_1 are due to the difficulty of washing and/or to the separation of different fractions, as explained below.

The attention was therefore focused on the definition of the inorganic phase. In both cases, the use of the formulation made possible to obtain cuprite as inorganic phase with a higher percentage of copper than those reached in the synthesis in aqueous medium. In fact, using UPM Solargo™ 100, cuprite is the exclusive copper-containing phase up to 13% of copper (see figures 2.47c and 2.48c), with complete conversions of the starting copper sulphate. In the case of the reaction corresponding to 18% of copper a first precipitation led to a material containing a mixture of brochantite and cuprite (UPM Solargo™ 100@cuprite-brochantite18%_2), as indicated by XRPD analysis (figure 2.49a) and confirmed by TEM analysis (figure 2.50). The diffractogram seems in favour of brochantite as the main phase. From the supernatant suspension it was instead isolated a material containing only cuprite (see figure 2.49 b).

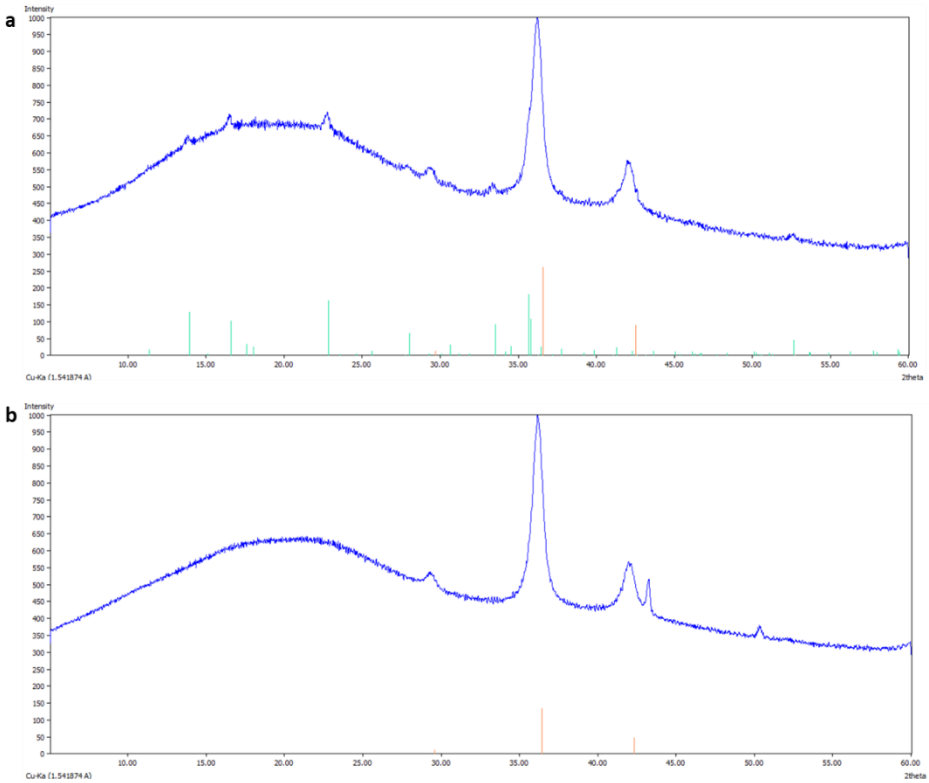

Figure 2.49 XRPD traces of solargo@cuprite-brochantite18%_1, a) filtered material, and b) supernatant solution. Theoretical peaks of brochantite, green, and theoretical peaks of cuprite, orange.

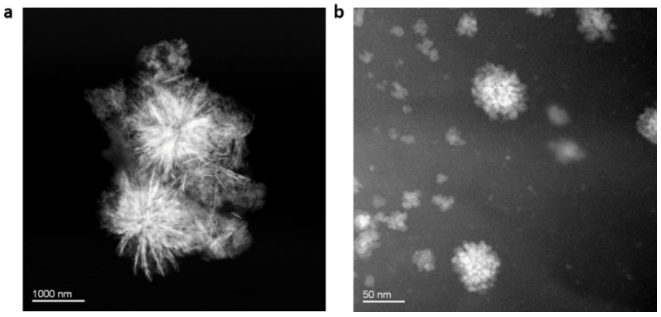

Figure 2.50. TEM images of solargo@cuprite-brochantite18%, a) crystals of brochantite and b) crystals of cuprite

A different result was obtained in the synthesis with the highest copper concentration (23%) a mixture of brochantite and posnjakite was revealed by XRPD, (see figure S2.5 in "Supporting Information").
The second procedure led to a reduced crystallinity of the materials as can be seen from XRPD and TEM analysis in figure 2.48. In the case of UPM Solargo™ 100@cuprite5%_2 and UPM Solargo™ 100@cuprite13%_2, albeit with some difficulty, the cuprite phase was identified, while in the case of UPM Solargo™ 100@cuprite18%_2 it was not possible to define the Cu-containing phase due to the low crystallinity of the material. The reduced crystallinity could be due to the addition of copper sulphate as solid, which could have led to a fast nucleation with formation of amorphous particles.
It is then clear that the speed of addition of the copper source to the formulate (dropwise or solid) has a profound effect on the crystallinity of the inorganic phases that form. A quick addition leads to the fast formation of amorphous phases, while a slow addition favours the formation of crystalline phases.
The nature of the phase is undoubtedly governed by the metal concentration: the higher the metal content the higher the probability to form brochantite. It is clear that several factors participate in determining the nature of the final inorganic phase, but the metal content is expected to have an impact on the pH of the reactant medium. High copper concentrations tend to lower the pH thus favouring the formation of brochantite, while low copper concentrations, or high dilutions, favours the formation of cuprite. These observations allow anyway to conclude that, depending on the adopted procedure, it is possible to prepare different "already-formulated" materials containing different active phases, making possible more selective applications.

Regarding the size of the nanoparticles, neither significant differences are observed between the two syntheses, nor a correlation between size and copper concentration was noted. Table 2.19 summarizes the dimensions of the nanoparticles defined by TEM analysis in the different materials.

Table 2.19. Lists of the dimension of the inorganic phases nanoparticles in the materials obtained with UPM Solargo™ 100.

sample	Size of particles
UPM Solargo™ 100@cuprite5%_1	cuprite NPs of 2-5 nm which aggregate in 50-100nm spheres
UPM Solargo™ 100@cuprite13%_1	cuprite NPs of 2-5 nm which aggregate in 50-100nm spheres
UPM Solargo™ 100@cuprite-brochantite18%_1	brochantite crystals 100 nm x 50 nm and cuprite crystals of 20-50 nm
UPM Solargo™ 100@cuprite5%_2	cuprite NPs with d= 20-50nm
UPM Solargo™ 100@cuprite13%_2	cuprite NPs with d= 10-30 nm
UPM Solargo™ 100@Cu18%_2	aggregates of Cu and O with d= 5-20 nm

Compared to the synthesis in aqueous medium, however, cuprite nanoparticles are smaller. This may be due to the presence of propylene glycol acting as a capping agent controlling their size. The analysis of the size of nanoparticles was also conducted through dynamic light scattering (DLS) carried out by taking a fraction of the original solution, after dilution with water (volume ratio = 1:40). Figure 2.51 shows the DLS analyses of UPM Solargo™ 100@cuprite5%_1 and UPM Solargo™ 100@cuprite-brochantite18%_1 which agree with what reported by TEM analyses. Unfortunately, the analyses carried out on UPM Solargo™ 100@cuprite13%_1 did not give reproducible results.

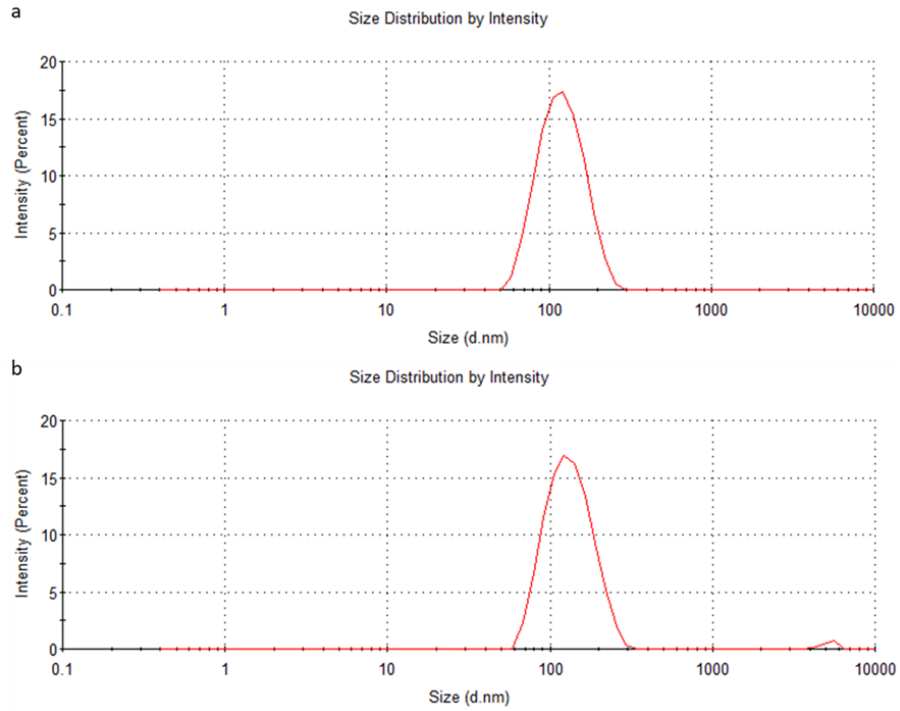

Figure 2.51 DLS analyses of a) UPM Solargo™ 100@cuprite5%_1 (Z-average of 112.6 nm and polydispersity index of 0.085) and b) UPM Solargo™ 100@cuprite-brochantite18%_1 (Z-average of 126.5 nm and polydispersity index 0.176)

Antimicrobial activity-in vivo tests

Operating conditions

Until now the tests have been conducted on materials synthesized by us in the laboratory which were then appropriately formulated before being applied.
The advantage of using the lignin formulation, on the other hand, was aimed at developing a synthesis that could be produced in the field once the phases have been characterized.

Tests were carried out by Azienda Agricola Vallese Alessandro, via Roma, 709-64014 Martinsicuro (TE)-ITALY and at the Centro Ricerche Agronomiche ed Ambientali, Res Agraria srl, via A. Canova 19/2, 64018 Tortoreto Lido (TE)- ITALY. The commercial product Coprantol WG ($CuCl_2 \cdot 3Cu(OH)_2$, 32% of copper) was purchased by Sygenta, while $CuSO_4 \cdot 5H_2O$ (with 25% of copper), by Manica.

The materials were prepared in situ according to our previously described procedures. Table 2.20 reports the materials with the synthetic procedures and the dosages used.

Table 2.20. Dosages of products used in the trial and synthetic procedures "in the field" of UPM Solargo™ 100@Cu materials

Entry	Materials	Dosage
1	Coprantol WG	165g/ha
2	UPM Solargo™ 100	20L/ha
3	UPM Solargo™ 100	10L/ha
4	Copper sulphate	200g/ha
Procedure 1: copper sulphate, previously diluted with the minimum amount of water, is added to Solargo100. The solution obtained is diluted to reach a volume of 40L. The solution was prepared in excess compared to the volume to be sprayed (800L/ha) in such a way to assure a homogeneous spraying for all plots. Different percentages of copper were obtained maintaining copper sulphate dosage at 200 g/ha and changing the amount of Solargo100.		
5	UPM Solargo™ 100@cuprite_5%	10 L/ha
6	UPM Solargo™ 100@cuprite_13%	4 L/ha
7	UPM Solargo™ 100@cuprite/brochantite	2.8 L/ha
8	UPM Solargo™ 100@brochantite/posnjakite	2.2 L/ha
Procedure 2: for each thesis (4 plots), Solargo100 is diluted with 2L of water. Copper sulphate, diluted with 100mL of water is added. The solution is, then, diluted up to 4L. Different percentages of copper were obtained maintaining copper sulphate dosage at 200 g/ha and changing the amount of Solargo100.		
9	UPM Solargo™ 100@cuprite_2.5%dil	20 L/ha
10	UPM Solargo™ 100@cuprite_5%dil	10 L/ha
11	UPM Solargo™ 100@cuprite_13%dil	4 L/ha

Tests were conducted in field on 48 plots with 28 plants per plot, against *Rhizoctonia solani*, using tomato plants variety Kero. Several foliar applications were carried out according to the procedure described below. The first application of the product (application A) is preventive. After 7 days from application A, the second application, B, follows, and, after two days from B, the first artificial inoculum is conducted. Application C happens, after 7 days from B, and then, after 5 days from the first inoculum. Application D occurs after 7 days from C, and a second artificial inoculum is conducted after 2 days from application D. Then application E takes place 7 days after D and 5 days after the second inoculation. 7 days after E, application F is performed, and after 7 days from F, application G.
In the case of Coprantol WG only applications A, C, E and G were conducted.

The parameters evaluated in these trials were: the incidence that is the percentage of attacked plants, the severity consisting in the average of the attacked area per plant in the field, the yield per plot at harvest, the content of chlorophyll, water and nitrogen on leaves, and vigour and phytotoxicity of the plants. For the comparison of the incidence and severity values with the untreated control, statistical analyses were used. For each assessment date the homogeneity of variance was tested by Bartlett's test. The content of chlorophyll, nitrogen and water on leaves were evaluated using the foliar instrument Chlorophyll Meter FK-YL02. Vigour and phytotoxicity of the plants were instead assessed by the visual comparison with the untreated check.

Results and discussion

The promising results observed with lignin@cuprite5% with *in vitro* tests against Rhizoctonia solani encouraged the in vivo trials against this pathogen. Trials were conducted on tomato plants, variety "Kero" using the UPM Solargo™ 100@Cu materials synthesized directly on the field according to the procedures reported in the section "Operating conditions". Briefly, the first procedure (entries 6-9) involves the addition of copper sulphate dissolved in the minimum amount of water to not diluted Solargo100. The solution formed is then diluted up to 40L volume with water. The second synthetic procedure (entries 10-12), on the other hand, consists in mixing UPM Solargo™ 100 and copper sulphate after having

diluted them separately with water. When the two solutions are mixed, a further addition of water is conducted to reach 40L of volume. The different copper percentages in materials have been obtained fixing the amount of copper sulphate at 200g/ha (50g/ha of copper) and using a different amount of UPM Solargo™ 100, as reported in table 2.20 in "Operating Conditions".
Entry10 (UPM Solargo™ 100@cuprite_2.5%dil) with a lower copper percentage than the materials obtained in laboratory, was synthesized to further explore the ratio between UPM Solargo™ 100 and copper and, then the combined activity between the two components.
Trials were carried out by spraying the materials on the leaves for a total of seven applications (A-G) interspersed with two artificial inoculations of the pathogen, according to the scheme represented in figure 2.52.

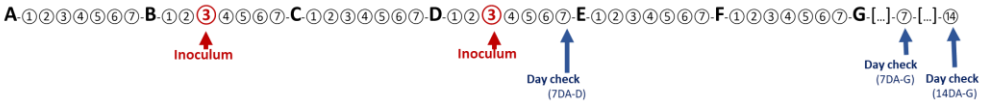

Figure 2.52. Foliar application scheme of the materials UPM Solargo™ 100@Cu materials. The seven foliar applications (A-G) are conducted every 7 days, two artificial inoculums are carried out the third day after application B and after application D. In figure the days in which the trials were evaluated (day check) are also reported.

UPM Solargo™ 100@copper materials were applied keeping constant the copper concentration at 50g/ha, while the dosages for Coprantol WG and copper sulphate were respectively 165g/ha and 200g/ha. UPM Solargo™ 100 was instead applied using the dosages of 10L/ha and 20L/ha.
In the case of Coprantol WG only the applications A, C, E, and G were conducted, following the standardized protocol for this commercial product.
Seven days after the first application the first signs of diseases appear. In fact, the natural disease infection was already present, and the two artificial inoculations contributed to the natural disease infection.
The first artificial inoculum was conducted after 10 days from the first application. 14 days after the first inoculum a second artificial inoculum was carried out, after two days from the fourth application (D). The highest levels of infection were

observed after 14 days from the last application (G) revealing an incidence percentage of 43% and a severity percentage of 30%.
The selectivity and efficacy assessments on *Rhizoctonia solani* were made 7 days after (7DA) each application and 14 days after the last application (14DA-G).
The efficacy percentage of treatments after 7 days from the application D (7DA-D) and after 7 and 14 days from the last applications (7DA-G and 14DA-G) is reported in term of incidence, in figure 2.53, and in term of severity, in figure 2.54.
From a first analysis it is clear that all treatments provide good control of the infection. The lignin formulation in the two different dosages showed a very good efficacy that, in the case of the dosage at 20L/ha is greater than the efficacy of both Coprantol and copper sulphate. Preliminary studies, aimed to evaluate the effect of propylene glycol on pathogens, highlighted that propylene glycol at the concentrations used in the formulation has no effects, thus confirming that the pesticide activity in UPM Solargo™ 100 derives from lignin. Also, the materials UPM Solargo™ 100@Cu have a greater efficacy of the exclusive copper-based products.
From the point of view of both incidence and severity the best results were obtained with the inorganic phase cuprite. The best ratio lignin formulation-copper was also found. The UPM Solargo™ 100@Cu materials were in fact applied maintaining constant the copper concentration at 50g/ha, thus adapting the UPM Solargo™ 100 dosage. In this regard we can see how the materials with the lowest copper concentration, UPM Solargo™ 100@cuprite_5% (entry 6), UPM Solargo™ 100@cuprite _2.5%dil (entry 10), UPM Solargo™ 100@cuprite_5%dil (entry 11), present the best performances. The combined effect between lignin and copper is then confirmed and the aim to reduce the use of the metal has been reached since the best ratio between the two component is based on the use of UPM Solargo™ 100 in excess.

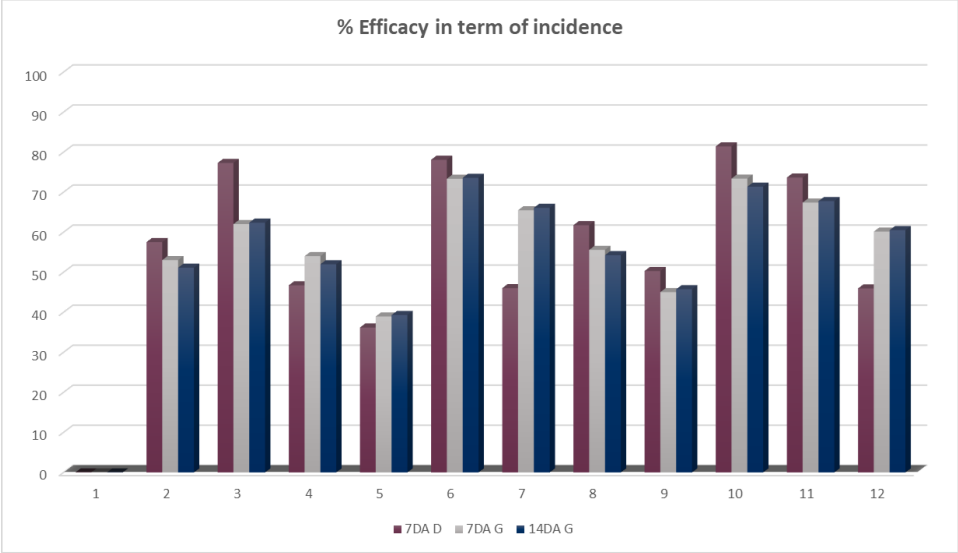

(1) Untreated check
(2) Coprantol 30 WG
(3) UPM Solargo™ 100-20L/ha
(4) UPM Solargo™ 100-10L/ha
(5) Copper sulphate
(6) UPM Solargo™ 100@cuprite5%_1
(7) UPM Solargo™ 100@cuprite13%_1
(8) UPM Solargo™ 100@cuprite/brochantite_1
(9) UPM Solargo™ 100@brochantite/posnjakite_1
(10) UPM Solargo™ 100@cuprite2.5%_2
(11) UPM Solargo™ 100@cuprite5%_2
(12) UPM Solargo™ 100Solargo@cuprite13%_2

Figure 2.53. Efficacy in term of incidence of attack against *Rhizoctonia solani* on tomato. The untreated check is set at 0% of efficacy. For each material the results 7 days after application D (7DA-D) and 7 and 14 days after application G (7DA-G and 14DA-G) are presented.

Comparing the two different synthetic procedures, instead, the best results were obtained with the second procedure, in which UPM Solargo™ 100 and copper sulphate were separately diluted before to be mixed (entries 10 and 11).

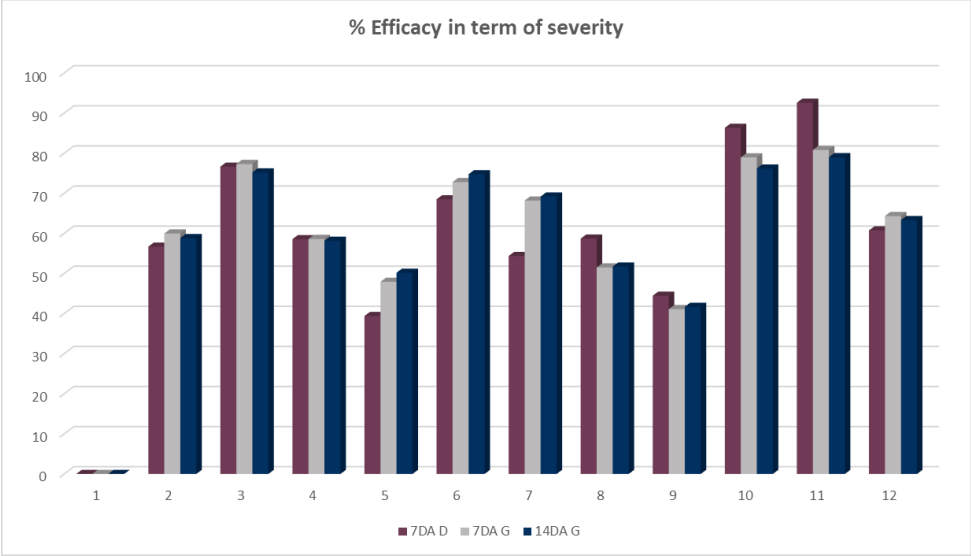

(1) Untreated check
(2) Coprantol 30 WG
(3) UPM Solargo™ 100-20L/ha
(4) UPM Solargo™ 100-10L/ha
(5) Copper sulphate
(6) UPM Solargo™ 100@cuprite5%_1
(7) UPM Solargo™ 100@cuprite13%_1
(8) UPM Solargo™ 100@cuprite/brochantite_1
(9) UPM Solargo™ 100@brochantite/posnjakite_1
(10) UPM Solargo™ 100@cuprite2.5%_2
(11) UPM Solargo™ 100@cuprite5%_2
(12) UPM Solargo™ 100Solargo@cuprite13%_2

Figure 2.54. Efficacy in term of severity of attack against *Rhizoctonia solani* on tomato. The untreated check is set at 0% of efficacy. For each material the results 7 days after application D (7DA-D) and 7 and 14 days after application G (7DA-G and 14DA-G) are presented.

In figure 2.55 the results referred to the yield per plot at harvest are showed. Although all materials have shown a good efficacy, also in this case the best yield were obtained with UPM Solargo™ 100@cuprite and, in particular, with UPM Solargo™ 100@cuprite_2.5% (entry 10) the yield percentage reached the 75%.
Among treatments no significative difference was observed for what concern vigour plants, content of chlorophyll, water and nitrogen on leaves, and no phytotoxicity was observed.

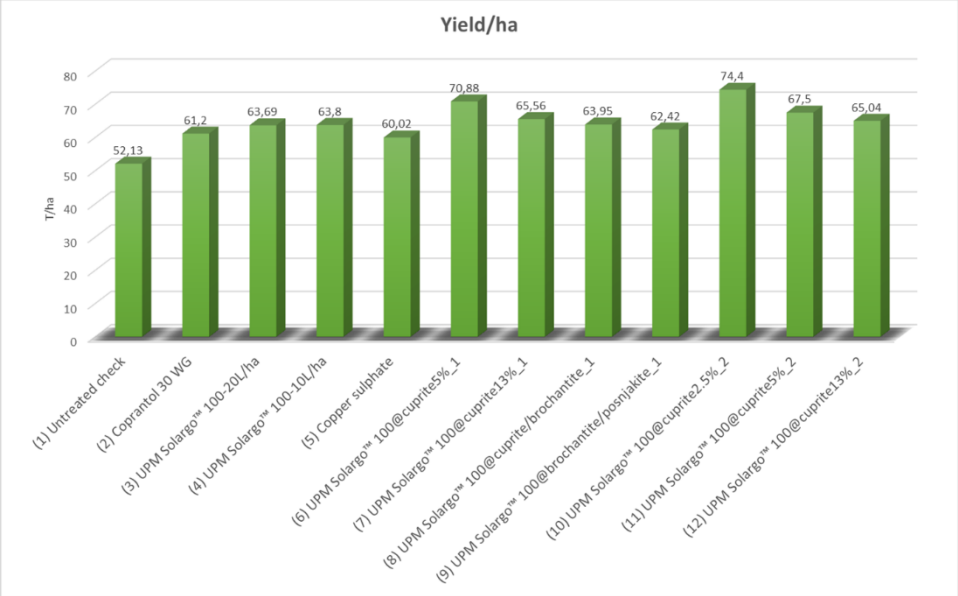

Figure 2.55. Yield/ha achieved by assessment on weight of harvestable fruits per plot accomplished 35 days after the last application.

Conclusions

The strongly basic pH allowed to obtain a homogeneous system in which the lignin was completely dissolved in water. Subsequently, the addition of a copper sulphate solution led to the formation of copper (I) oxide, identified by XRPD, EDS and TEM analyses as cuprite nanoparticles, embedded in the lignin matrix. A new hybrid material lignin@cuprite was then synthesized by exploiting the reducing properties of lignin.

Under these conditions it was possible to obtain cuprite with only 5% of copper because further additions of the metal lowered the pH causing the precipitation of basic copper sulphates (posnjakite).

An extensive characterization of the material lignin@cuprite5% was carried out by GPC, IR, Py-GC / MS analysis, confirming that the strongly basic pH did not cause important structural changes to the polymer.
The known antibacterial properties of copper (I) oxide directed research towards the evaluation of the antimicrobial activity of this new hybrid material. Through *in vitro* tests, the combined effect between lignin and cuprite was found to be very high against *Rhizoctonia solani* and *Listeria monocytogenes*.
The promising results obtained from these preliminary trials have therefore spurred the development of a simpler synthesis in such a way to obtain the material directly in the field, solving the problem of the cuprite nanoparticles aggregation when the material is dispersed in water.
In this regard, the liquid lignin formulation, UPM Solargo™ 100, containing lignin, water, KOH and propylene glycol, was used in combination with copper sulphate at different concentrations (from 5% to 23% of copper). Under these conditions it was possible to obtain cuprite as exclusive crystalline phase up to 13% of copper, while with 18% and 23% a mixture of cuprite / brochantite and brochantite / posnjakite was respectively obtained. In order to evaluate simple syntheses that can be carried out in the field, two different synthetic procedures have been evaluated. The first synthesis is based on the addition of copper sulphate in solution to the formulation, while the second, which led to a reduced crystallinity of the inorganic phases, consists in the addition of solid copper sulphate to the previously diluted UPM Solargo™ 100.
All the materials UPM Solargo™ 100@copper thus obtained were then tested by *in vivo* tests against *Rhizoctonia solani*. The already high efficacy of UPM Solargo™ 100 was further amplified by the presence of the copper phase and, in particular, the best results were obtained with the materials UPM Solargo™ 100@cuprite. The tests also allowed to evaluate the best UPM Solargo™ 100-copper ratio, demonstrating how the materials with the lowest concentration of copper (UPM Solargo™ 100@ cuprite with 2.5 and 5% of copper) showed the best performances confirming once again the combined effect between lignin and copper.

Lignin@goethite

Like copper, iron is also an essential element for most biological systems[65] but when present in high concentrations it can damage living organisms[30]. This means that iron, especially in nano particle form, is studied both as a fertilizer[6] and as a pesticide[30,66].

As fertilizer, iron increases the seed germination via enhancement of water adsorption capacity of seeds, enhances enzyme activity as nitrate reductase and has a positive impact on the growth of the plant roots[6].

Once again, our research focuses on the use of iron as a possible pesticide. Although the mechanism by which iron exerts its biocidal action is not yet clear, recent studies have made a profound contribution to the understanding of this aspect. At the base of its action there would be, as in the case of copper, the damage of DNA by means of ROS generated through the Fenton reactions, consisting in the reduction of hydrogen peroxide promoted by transition metals to give reactive hydroxyl radicals[66]. The damage caused by these species affects all cellular biological macromolecules, such as protein fragmentation, lipid peroxidation and carbohydrates degradation[66]. There is growing evidence that transition metals can interact with the genetic material by altering it through an oxidative mechanism[66]. About that, Lloyd et al. investigated the DNA lesions by transition metals, including iron (II), setting up two different experiments[30]. In the first, the DNA is joined to the metal ion, and only subsequently the complexing agent EDTA is added, while in the second, the metal is first complexed with EDTA and then the DNA is added. The goal of this research is to understand whether the DNA damage, mediated by Fenton chemistry, originates from a site-specific mechanism which involves a metal ion-DNA interaction before reacting with hydrogen peroxide to produce ROS. If an interaction between the metal and DNA were required, then the action of the metal ion would be further reduced in the case of pre-complexation with EDTA. If the two experiments instead lead to the same degree of DNA damage, then this would mean that the mechanism is not site specific and would only require the generation of reactive oxygen species. The generation of ROS by reaction with hydrogen peroxide takes place, in fact, even when the metal is complexed by EDTA, while the metal-DNA interaction is prevented. What emerged from this work is that in the case of copper (II) and iron (II) DNA lesions such as formation of putatile intrastrand cross-link, the formation

of 8-hydroxy-deoxyguanosine and both single and double strand breaks are due to specific interactions between the metal and the DNA which would then lead to the generation of ROS[30].
Other researchers deal with iron (III) complexes and their nuclease activity[67,68]. Ghosh et al., for example, synthesized an iron (III) complex of which they study the ability to break DNA, highlighting how the species produced in greater quantities and, therefore, responsible for the nuclease activity, are hydroxyl radicals[67].
Furthermore, thanks to its versatile coordination chemistry and redox properties, iron is also able to bind to the peptides that make up proteins through nitrogen or carbonyl function coordination [67]. All these considerations make this metal a good entry point in the agronomic field, hence the idea of developing new materials deriving from its combination with lignin.
In this paragraph, therefore, a new material based on lignin and iron is presented. Lignin@goethite is characterized by crystals of goethite, a basic iron (III) oxide with formula FeO(OH), embedded in the lignin matrix. Obtained through mechanochemistry, its antibiocidal activity is evaluated by *in vitro* tests.

Experimental Part

The technical lignin employed without further purification was the Kraft lignin from *Pinus taeda*, provided by UPM-Kymmene Oyj and Green Innovation GmbH: BioPiva100 (M_w=4400-5000 g/mol, M_n= 1200-1300 g/mol). See dedicated section in chapter 1 for details.
$FeSO_4 \cdot 7H_2O$ and KOH were purchased from Sigma Aldrich and used without further purification.
Mechanochemical syntheses were conducted through a planetary ball mill Retsch PM100 using an 80 mL agate jar and 8 spheres of the same material with a diameter of 10 mm.
A scale up of the mechanochemical synthesis was conducted using a 450 ml agata jar and 5 agata spheres with diameter of 20 mm.

Synthesis and characterization

Two syntheses are reported for the preparation of lignin@goethite using a weight ratio lignin-iron sulphate equal to 1.69, corresponding to 10% of iron and a molar ratio between iron sulphate and potassium hydroxide of 0.5. The second synthesis consisted in a scale up to have the sufficient amount of material for *in vitro* tests. Both syntheses consisted in a pre-grinding between lignin and iron sulphate at 300 rpm for 2 minutes (inversion time 1 minute). Subsequently, after the addition of potassium hydroxide and water the grinding lasted 1 h (inversion time 30 minutes) at 300 rpm. The materials were washed with water by filtration and dried at 60°C overnight.

Synthesis I

2.19 g of lignin were pre-ground with 1.29 g of $FeSO_4 \cdot 7H_2O$ at 300 rpm for 2 minutes, with an inversion time of 1 minute. Subsequently, 0.52 g of KOH and 4 ml of distilled water were added. The grinding was conducted at 300 rpm for 1 hour with an inversion time of 30 minutes using 8 spheres of agata with a diameter of 10 mm. The material was washed with water by filtration and characterized by means of ICP and XRPD analyses.
To evaluate the reproducibility of the synthesis the procedure was repeated twice. The ICP analyses revealed a complete upload of iron in both syntheses, with 9.81% ± 0.03 and 12.4% ± 0.1 of iron. In figure 2.56 the XRPD is reported.

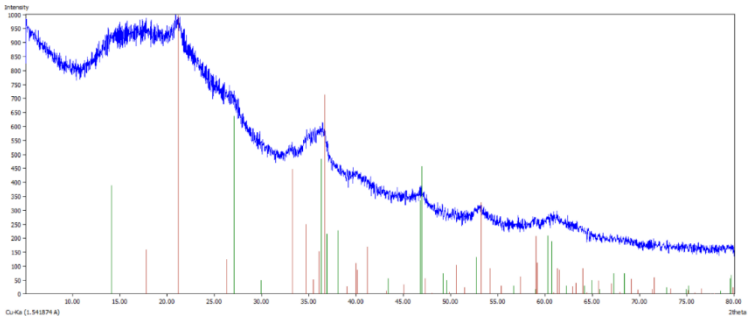

Figure 2.56. Experimental pattern of the material lignin@goethite; Bordeaux peaks are theoretical peaks of goethite, dark green peaks, theoretical peaks of lepidocrocite.

Synthesis II

The scale up synthesis was conducted starting from 40g of total reagents. 22.65 g of BioPiva100 and 12.87 g of $FeSO_4 \cdot 7H_2O$ were pre-ground for 2 minutes at 300 rpm with an inversion of rotation after 1 minutes. Subsequently 4.48 g of KOH and 40 mL of water were added to the mixture. Grinding occurred for 1 hour at 300 rpm, with an inversion of rotation after 30 minutes. 5 spheres of agate with a diameter of 20 mm were used.
The material was washed with water by filtration and dried at 60°C overnight. The brown powder was analysed by ICP, XRPD and TEM analysis.
ICP analysis revealed a percentage of iron of 7.06% ± 0.12, slightly lower than the expected percentage of 9.66%. XRPD analysis (figure 2.57) shows a quite amorphous material compared to the material lignin@brochantite obtained by mechanochemical synthesis. Furthermore, two mineral phases of FeO(OH) were detected, corresponding to goethite (α-FeO(OH) and lepidocrocite (γ-FeO(OH)).
In table 2.21 the unit cell parameters and the space groups of the two polymorphic forms are listed.

Table 2.21. Unit cell parameters and space groups of goethite and lepidocrocite

Phase	Unit cell parameters			Space group
	a	b	c	
Goethite[69]	4.59 Å	9.95 Å	3.01 Å	Pbnm
Lepidocrocite[70]	3.87 Å	12.51 Å	3.06 Å	Amam

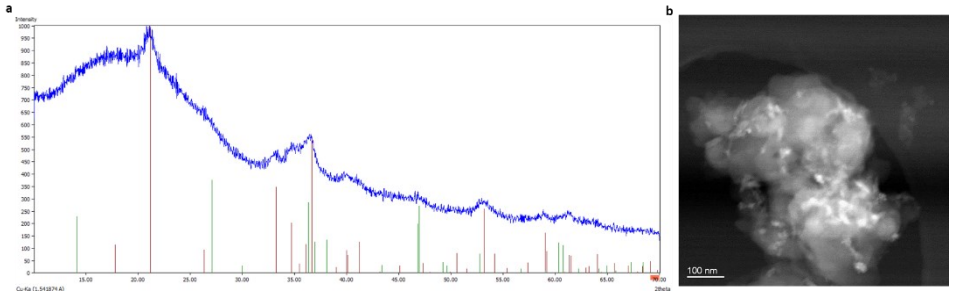

Figure 2.57. a) XRPD of lignin@goethite; bordeaux peaks are theoretical peaks of goethite, dark green are peaks of lepidocrocite; b) TEM image of the material

Electron diffraction analysis conducted during TEM inspection confirmed goethite as the main mineral phase. Only in one plate it was possible to clearly identify the presence of a spot (d=0.38 nm) indexable unequivocally as lepidocrocite. The EDS analysis conducted on crystals of goethite gave back data in agreement with the expected stoichiometry. Goethite crystals are sticks with a length between 30 and 80nm and a thickness between 10 and 20 nm. There are also rounded clusters of crystals with a size between 10 and 30 nm. TEM image is shown in figure 2.57b.

Results and discussion

Synthesis and characterization

Following the same procedure adopted for the preparation of lignin@brochantite, a new hybrid material based on iron was obtained. Starting with iron(II) sulphate we observed the oxidation of the metal that formed an iron(III) specie identified by XRPD as goethite (main phase) and lepidocrocite (minority phase). TEM analysis, conducted on the scale up procedure, revealed smaller crystals than the brochantite ones. However, the synthesis led due to a material featured by low crystallinity of the inorganic component.
Furthermore, ICP analysis conducted on the material obtained by scale up procedure, revealed a not complete upload of the metal. All these observations led to conclude that the synthetic procedure needs to be optimized.
In vitro tests were conducted using the material obtained from the scale up procedure, considering the percentage of iron found by ICP analysis (7%).

Antimicrobial activity- in vitro test

To evaluate the antimicrobial activity of the material lignin@goethite, a preliminary investigation of its activity was done through *in vitro* tests conducted by BICT-Bioindustry Innovation.

Operating Conditions

The material lignin@goethite was synthesized with a scale up reported in the experimental section as synthesis II.
The antimicrobial activity was evaluated by an agar dilution method to determine the minimum inhibitory concentrations (MICs) of the compound and related controls.
The agar dilution assay, preferred to the liquid dilution method because of the insolubility of the material, was performed into 24-well plates with 2mL of medium. As controls, lignin and FeO(OH) were also tested; the concentrations used are listed in table 2.22.

Table 2.22. List of the compounds tested and relative concentrations

Materials	**Initial concentrations (g/L)**	**Starting iron concentration (g/L)**
Lignin	50.00	0.00
Lignin@goethite	50.00	3.50
FeO(OH)	5.55	3.50

The starting concentration of FeO(OH) (5.55 g/L) was chosen in such a way to have the same iron concentration (3.50 g/L) used with lignin@goethite.
The microorganisms tested with their specific parameters of growth were *Staphylococcus aureus*, *Listeria monocytogenes*, *Escherichia coli*, *Xanthomonas campestris*, *Pseudomonas syringa pv. actinidiae* as bacteria, while *Botritis cinerea* and *Rhizoctonia solani* as fungi. For each microorganisms the following controls were included:
- positive control of growth: microorganisms were plated in the agar medium in the absence of the compounds
- control of sterility: the agar mediums were not inoculated with the microorganisms
- control of antimicrobial activity: microorganisms were plated with 6 serial dilutions of antimicrobial agent, Ceftriaxone (64 µg/mL starting concentration) against bacteria and Fluconazole (512 µg/mL starting concentration) against fungi.

Results and discussion

The results are reported in table 2.23.

Table 2.23. List of the MIC (minimum inhibitory concentration) found for the of materials tested, the copper concentration is reported in brackets.

		---------- MIC g/L ----------			
	microorganisms	lignin	lignin@goethite	FeO(OH)	antimicrobial agent
Bacteria[1]	*Staphylococcus aureus*	0.78	1.56 (0.109)	5.550 (3.500)	>64 µg/mL
	Listeria monocytogenes	3.13	3.13 (0.219)	5.550 (3.500)	8 µg/mL
	Escherichia coli	3.13	6.25 (0.438)	5.550 (3.500)	2 µg/mL
	Xanthomonas campestris	1.56	3,13 (0.219)	5.550 (3.500)	4 µg/mL
	Pseudomonas syringae pv. actinidiae	1.56	1.56 (0.109)	5.550 (3.500)	16 µg/mL
Fungi[2]	*Botritis cinerea*	>50	>50	5.550 (3.500)	> 512 µg/mL
	Rhizoctonia solani	0.20	**0.05 (0.003)**	3.550 (3.500)	16 µg/mL
Antimicrobial agents: [1]Ceftriaxone, [2]Fluconazole					

The tests allowed to identify the minimum inhibitory concentrations (MICs) of the target compounds. MIC is the lowest concentration of the compound that inhibits the visible growth of a microorganism.

The lignin@goethite material did not show a particular activity against microorganisms, always showing higher MICs than lignin or, at best, equivalent values MIC, like in the case of *Pseudomonas syringae pv. actinidiae*. The only exception was observed for the fungus *Rhizoctonia solani*. In this case, in fact, a

strong combined effect between lignin and iron leads to the lowest MIC for lignin@goethite, with a very low iron concentration.
Generally, lignin shows a clear inhibitory effect and all strains tested are inhibited at relatively low concentrations except *Botrytis cinerea*.
The fungus *Botritis cinerea* showed strong resistance to the tested compounds (included the antibiotic) and the minimum inhibitory concentrations could not be detected.
These results did not show the desired results for the material lignin@goethite. Probably, the presence of an iron (III) species negatively affected the results because ROS generation is favoured by lower oxidation states of the metal. Ghosh et al., in fact, highlight how the lyase activity of iron (III) complexes is greater in the presence of reducing agents[67]. Here, the reducing properties of lignin does not appear sufficient to stabilize the +2 oxidation state of the metal, at least when a mechanochemical synthetic approach is followed. The reactivity of lignin towards iron(II) under homogeneous conditions appears then quite attractive, in light of the possibility to stabilize low oxidation states of the metal, as seen with copper.

Conclusions

Another metal extremely important for life is iron[65], widely used in the agronomic field as a fertilizer, but also for its potential antimicrobial activity[6,30,66].
In this paragraph the mechanochemical synthesis of the hybrid material lignin@goethite obtained by mixing lignin and $FeSO_4 \cdot 7H_2O$ has been described and discussed. Goethite, crystalline phase of FeO(OH), is present in the form of rods with a length between 30 and 80 nm and a thickness between 10 and 20nm.
Preliminary in vitro tests were carried out on the hybrid material lignin@goethite but no satisfactory results were found, probably because of the iron (III) specie formation. One of the main mechanisms of the pesticidal action of iron is, in fact, based on the formation of hydroxyl radicals through the Fenton reactions, but these are promoted by low oxidation states.
However, the use of hybrid materials lignin@Fe for agronomic purposes must remain an open question, aiming at a synthetic procedure that prevents the oxidation of the metal.

Conclusions

The antibacterial properties of three hybrid materials based on lignin were evaluated by means of *in vitro* and *in vivo* tests. Each material is characterized by a different inorganic phase: brochantite $Cu_4(SO_4)(OH)_6$, cuprite Cu_2O, and goethite FeO(OH). In all cases, the crystals of these inorganic phases are embedded in the lignin matrix.

Copper and iron are both essential elements for living organisms, and their antimicrobial properties are widely known[30]. On the other hand, lignin, currently considered a waste from paper mills and bioethanol industries[71], hides many important properties in its polyphenolic structure[72]. Among the others, its potential biocidal action has an important role in the agrochemical field as well as in packaging sector[11].

The idea to combine the polymer with the inorganic phases arises from the need to find new performing pesticides with a low environmental impact. The use of metals as pesticides has, in fact, dangerous issues related to their accumulation in the soil that can cause the death of soil bacteria flora and pollutions[7]. For these reasons we wished to evaluate the combined activity between the polymer and the inorganic components.

The best results have been obtained with the copper-based hybrid materials which have shown high efficacy against several pathogens, significantly reducing the copper content compared to the copper based commercial products.

The materials, obtained with green reagents and sustainable procedures, were completely characterized in their inorganic and organic components. XRPD and TEM analyses allowed to identify the inorganic phases, while the extent of the metal upload was determined by ICP analysis. GPC, GC-pyrolysis, IR and NMR analyses were able to give back important information on the integrity of the biopolymer contained in the isolated materials.

If with copper the *in vitro* and *in vivo* tests were successful, no satisfactory results were obtained with the iron-based material. Probably, this is caused by the oxidation state of the metal, which, during the synthesis, oxidized from iron(II) to iron(III). It is known, in fact, that Fenton chemistry is promoted by low oxidation states. Other attempts could be made to prevent the oxidation of iron during the synthesis in such a way to evaluate the combined action between lignin and iron(II).

In the meantime, given the poor results of lignin@goethite as pesticide, we went in search of other possible applications always aimed at improving the quality of life. Future works will therefore focus on the adsorbing capacity of lignin@goethite towards heavy metals in water.

To date, heavy metal pollution is one of the main environmental problems. Among them, chromium, due to its high toxicity in its highest oxidation state, must be constantly monitored[73]. Over the years there have been several industrial applications of this metal[73]. It is, for example, a constituent of textile manufacturing plants, it is also used in stainless steel factories as well as in the leather and paint industries. It is also easily found in pipes because it inhibits corrosion. Unfortunately, all these processes produce Cr(VI), the high toxicity of which is now well known. Cr(VI), due to its high oxidation state and relatively small ionic radius, penetrates through the membrane and is carcinogenic and mutagenic to humans[73]. Cr(VI) exposure causes, among the others, ulcers, respiratory problems and can affect almost any organ.

In the light of these premises, it is clear how to find a system for the reclamation of Cr (VI) wastewater is a subject that is as scientifically intriguing as it is important from an environmental point of view. The possibility of using the hybrid material lignin@goethite for this purpose opens a new scenario on the use of these materials, so far only conceived for agronomic purposes. Phases of iron may, in fact, play a role in the absorption of chromium[74–76] and, on the other hand, the reducing properties of lignin could help to reduce the dangerous Cr(VI) to the more friendly Cr(III).

References

1. youmatter. Causes of deforestation. https://youmatter.world/en/definition/definitions-what-is-definition-deforestation-causes-effects/.

2. Worldometer. Current World Population. https://www.worldometers.info/world-population/.

3. Cameron, A. & Sarojini, V. Pseudomonas syringae pv. actinidiae: Chemical control, resistance mechanisms and possible alternatives. *Plant Pathol.* **63**, 1–11 (2014).

4. Battiston, E., Antonielli, L., Marco, S. Di, Fontaine, F. & Mugnai, L. Innovative delivery of Cu(II) ions by a nanostructured hydroxyapatite: Potential Application in Planta to Enhance the Sustainable Control of Plasmopara viticola. *Phytopathology* **109**, 748–759 (2019).

5. Ding, Q. *et al.* Impact of low molecular weight organic acids and dissolved organic matter on sorption and mobility of isoproturon in two soils. *J. Hazard. Mater.* **190**, 823–832 (2011).

6. Chhipa, H. *Applications of nanotechnology in agriculture*. *Methods in Microbiology* vol. 46 (Elsevier Ltd., 2019).

7. Lamichhane, J. R. *et al.* Thirteen decades of antimicrobial copper compounds applied in agriculture. A review. *Agron. Sustain. Dev.* **38**, (2018).

8. Slavin, Y. N., Asnis, J., Häfeli, U. O. & Bach, H. Metal nanoparticles: Understanding the mechanisms behind antibacterial activity. *J. Nanobiotechnology* **15**, 1–20 (2017).

9. Siegbahn, P. E. M. & Blomberg, M. R. A. Transition-Metal Systems in Biochemistry Studied by High-Accuracy Quantum Chemical Methods. *Chem. Rev.* **100**, 421–437 (2000).

10. Mitra, D., Kang, E. T. & Neoh, K. G. Antimicrobial Copper-Based Materials and Coatings: Potential Multifaceted Biomedical Applications. *ACS Appl. Mater. Interfaces* **12**, 21159–21182 (2020).

11. Solihat, N. N. *et al.* Lignin as an Active Biomaterial: A Review. *J. Sylva Lestari*

9, 1–22 (2021).

12. Klein, S. E. *et al.* Antimicrobial activity of lignin-derived polyurethane coatings prepared from unmodified and demethylated lignins. *Coatings* **9**, (2019).

13. Alzagameem, A. *et al.* Antimicrobial activity of lignin and lignin-derived cellulose and chitosan composites against selected pathogenic and spoilage microorganisms. *Polymers (Basel).* **11**, 670–688 (2019).

14. El-Nemr, K. F., Mohamed, H. R., Ali, M. A., Fathy, R. M. & Dhmees, A. S. Polyvinyl alcohol/gelatin irradiated blends filled by lignin as green filler for antimicrobial packaging materials. *Int. J. Environ. Anal. Chem.* **100**, 1578–1602 (2020).

15. Dorman, H. J. D. & Deans, S. G. Antimicrobial agents from plants: Antibacterial activity of plant volatile oils. *J. Appl. Microbiol.* **88**, 308–316 (2000).

16. Gyawali, R. & Ibrahim, S. A. Natural products as antimicrobial agents. *Food Control* **46**, 412–429 (2014).

17. Espinoza-Acosta, J. L., Torres-Chávez, P. I., Ramírez-Wong, B., López-Saiz, C. M. & Montaño-Leyva, B. Antioxidant, antimicrobial, and antimutagenic properties of technical lignins and their applications. *BioResources* **11**, 5452–5481 (2016).

18. Kai, D. *et al.* Towards lignin-based functional materials in a sustainable world. *Green Chem.* **18**, 1175–1200 (2016).

19. Barber, M. S., McConnell, V. S. & DeCaux, B. S. Antimicrobial intermediates of the general phenylpropanoid and lignin specific pathways. *Phytochemistry* **54**, 53–56 (2000).

20. Jung, H.G. and Fahey, G. C. Nutritional Implications of Phenolic Monomers and Lignin: A Review. *J. Anim. Sci.* **57**, 206–219 (1983).

21. Cazacu, G., Capraru, M. & Popa, V. I. *Advances concerning lignin utilization in new materials*. *Advanced Structured Materials* vol. 18 (2013).

22. Griffin, S. G., Wyllie, S. G. & Markham, J. L. Antimicrobially active terpenes cause K+ leakage in E. Coli cells. *J. Essent. Oil Res.* **17**, 686–690 (2005).

23. Vincent, M., Hartemann, P. & Engels-Deutsch, M. Antimicrobial applications of copper. *Int. J. Hyg. Environ. Health* **219**, 585–591 (2016).

24. Johnson, G. F. The Early History of Copper Fungicides. *Agric. Hist. Soc.* **9**, 67–79 (1935).

25. Warnes, S. L., Caves, V. & Keevil, C. W. Mechanism of copper surface toxicity in Escherichia coli O157:H7 and Salmonella involves immediate membrane depolarization followed by slower rate of DNA destruction which differs from that observed for Gram-positive bacteria. *Environ. Microbiol.* **14**, 1730–1743 (2012).

26. Compilated by A. D. McNaught and A. Wilkinson. *IUPAC. Compendium of Chmical Terminology, 2nd ed. (the 'Gold Book')*. (Blackwell Scientific Publications, Oxford (1997).). doi:https://doi.org/10.1351/goldbook.

27. Alemán, J. *et al.* Definitions of terms relating to the structure and processing of sols, gels, networks, and inorganic-organic hybrid materials (IUPAC recommendations 2007). *Pure Appl. Chem.* **79**, 1801–1829 (2007).

28. Li, J. *et al.* Physiological effects of magnetic iron oxide nanoparticles towards watermelon. *J. Nanosci. Nanotechnol.* **13**, 5561–5567 (2013).

29. Ren, H. X. *et al.* Physiological investigation of magnetic iron oxide nanoparticles towards Chinese Mung bean. *J. Biomed. Nanotechnol.* **7**, 677–684 (2011).

30. Lloyd, D. R. & Phillips, D. H. Oxidative DNA damage mediated by copper(II), iron(II) and nickel(II) Fenton reactions: Evidence for site-specific mechanisms in the formation of double-strand breaks, 8-hydroxydeoxyguanosine and putative intrastrand cross-links. *Mutat. Res. - Fundam. Mol. Mech. Mutagen.* **424**, 23–36 (1999).

31. Singh, V. K. *et al.* Multigram Mechanochemical synthesis of a Salophen Complex: A Comparative Analysis. *ACS Biomater. Sci. Eng.* **9**, 1152–1160 (2021).

32. Schneider, F., Szuppa, T., Stolle, A. & Hopf, H. Energetic assessment of the Suzuki – Miyaura reaction : a curtate life cycle assessment as an easily understandable and applicable tool for reaction optimization †. *Green Chem.* **11**, 1894–1899 (2009).

33. Rosenkranz, S., Breitung-Faes, S. & Kwade, A. Experimental investigations and modelling of the ball motion in planetary ball mills. *Powder Technol.* **212**, 224–230 (2011).

34. Schneider, F., Stolle, A., Ondruschka, B. & Hopf, H. The Suzuki-Miyaura reaction under mechanochemical conditions. *Org. Process Res. Dev.* **13**, 44–48 (2009).

35. Sinisi, V. *et al.* A Green Approach to Copper-Containing Pesticides: Antimicrobial and Antifungal Activity of Brochantite Supported on Lignin for the Development of Biobased Plant Protection Products. *ACS Sustain. Chem. Eng.* **7**, 3213–3221 (2019).

36. Gazzurelli, C. *et al.* Making Agriculture More Sustainable: An Environmentally Friendly Approach to the Synthesis of Lignin@Cu Pesticides. *ACS Sustain. Chem. Eng.* **8**, 14886–14895 (2020).

37. Zittlau, A. H., Shi, Q., Boerio-Goates, J., Woodfield, B. F. & Majzlan, J. Thermodynamics of the basic copper sulfates antlerite, posnjakite, and brochantite. *Chemie der Erde - Geochemistry* 2–13 (2013) doi:10.1016/j.chemer.2012.12.002.

38. D. Marani, J. W. P. and P. R. A. ALKALINE PRECIPITATION AND AGING OF Cu(II) IN THE PRESENCE OF SULFATE. *Elsevier Sci. Ltd* **29**, 1317–1326 (1995).

39. Vilminot, S. *et al.* Nuclear and magnetic structures and magnetic properties of synthetic brochantite, Cu4(OH)6SO4. *J. Chem. Soc. Dalt. Trans.* **6**, 1455–1462 (2006).

40. Otálora, F. & García-Ruiz, J. Nucleation and growth of the Naica giant gypsum crystals. *Chem. Soc. Rev.* **43**, 2013–2026 (2014).

41. Stephen Y. Lin, C. W. D. *Methods in Lignin Chemistry*. (Springer Series in Wood Science: Wood structure and enviroment, 1992).

42. Makreski, P., Jovanovski, G. & Dimitrovska, S. Minerals from Macedonia: XIV. Identification of some sulfate minerals by vibrational (infrared and Raman) spectroscopy. *Vib. Spectrosc.* **39**, 229–239 (2005).

43. Allison Tolbert, Hannah Akinosho, Ratayakorn Khunsupat, Amit K. Naskar, A. J. R. Characterization and analysis of the molecular weight of lignin for

biorefining studies. *Biofuels, Bioprod. Biorefining* (2014) doi:10.1002/bbb.

44. Li, J., Henriksson, G. & Gellerstedt, G. Lignin depolymerization/repolymerization and its critical role for delignification of aspen wood by steam explosion. *Bioresour. Technol.* **98**, 3061–3068 (2007).

45. Samuel, R., Pu, Y., Raman, B. & Ragauskas, A. J. Structural characterization and comparison of switchgrass ball-milled lignin before and after dilute acid pretreatment. *Appl. Biochem. Biotechnol.* **162**, 62–74 (2010).

46. Nassau, K. Miller, A. E. and Graedel, T. E. THE REACTION OF SIMULATED RAIN WITH COPPER , COPPER PATINA , AND SOME COPPER COMPOUNDS. **27**, 703–719 (1987).

47. Buckton, G and Newton, J. M. Assessment of the Wettability of Powders by Use of Compressed Powder Discs. **46**, 201–208 (1986).

48. Depalo A. and Santomaso A. C. Caratterizzazione della bagnabilità di polveri alimentari e farmaceutiche mediante risalita capillare in letti impaccati. (2012).

49. Biolin Scientific Oy, Espoo, F. Force tensiometer: Sigma 700/701-operation manual.

50. Glasser, W. G. Classification of lignin according to chemical and molecular structure. *ACS Symp. Ser.* **742**, 216–238 (1999).

51. Koga, N., Criado, J. M. & Tanaka, H. Reaction pathway and kinetics of the thermal decomposition of synthetic brochantite. *J. Therm. Anal.* **49**, 1467–1475 (1997).

52. Alcaraz, D., Arana, R., Gàlvez, J. & Palazòn, J. Thermal studies of minerals of metallurgical interest. V. Kinetics of the thermal decomposition of chrysocolla and brochantite and mineralogical study. **39**–**40**, 55–67 (1983).

53. El Badawy, A. M. *et al.* Surface charge-dependent toxicity of silver nanoparticles. *Environ. Sci. Technol.* **45**, 283–287 (2011).

54. Buono, P., Duval, A., Verge, P., Averous, L. & Habibi, Y. New Insights on the Chemical Modification of Lignin: Acetylation versus Silylation. *ACS Sustain. Chem. Eng.* **4**, 5212–5222 (2016).

55. Tanaka, I. I., Kawano, M. & Koga, N. Thermogravimetry of basic copper(II) sulphates obtained by titrating NaOH solution with CuSO4 solution. **182**, 281–292 (1991).

56. Crawford, D. E. & Casaban, J. Recent Developments in Mechanochemical Materials Synthesis by Extrusion. *Adv. Mater.* **28**, 5747–5754 (2016).

57. Crawford, D. E., Miskimmin, C. K. G., Albadarin, A. B., Walker, G. & James, S. L. Organic synthesis by Twin Screw Extrusion (TSE): Continuous, scalable and solvent-free. *Green Chem.* **19**, 1507–1518 (2017).

58. Sipponen, M. H., Laakso, S. & Baumberger, S. Impact of ball milling on maize (Zea mays L.) stem structural components and on enzymatic hydrolysis of carbohydrates. *Ind. Crops Prod.* **61**, 130–136 (2014).

59. Guerra, A. *et al.* Toward a better understanding of the lignin isolation process from wood. *J. Agric. Food Chem.* **54**, 5939–5947 (2006).

60. Meghana, S., Kabra, P., Chakraborty, S. & Padmavathy, N. Understanding the pathway of antibacterial activity of copper oxide nanoparticles. *RSC Adv.* **5**, 12293–12299 (2015).

61. Cho, M., Kim, J., Kim, J. Y., Yoon, J. & Kim, J. H. Mechanisms of Escherichia coli inactivation by several disinfectants. *Water Res.* **44**, 3410–3418 (2010).

62. Semisch, A., Ohle, J., Witt, B. & Hartwig, A. Cytotoxicity and genotoxicity of nano - and microparticulate copper oxide: role of solubility and intracellular bioavailability. *Part. Fibre Toxicol.* **11**, 1–16 (2014).

63. Fiss, B. G. *et al.* Mechanochemical methods for the transfer of electrons and exchange of ions: Inorganic reactivity from nanoparticles to organometallics. *Chem. Soc. Rev.* **50**, 8279–8318 (2021).

64. Zhao, Z. & Ouyang, X. Effect of oxidation on the structures and properties of lignin. *Adv. Mater. Res.* **550**–**553**, 1208–1213 (2012).

65. Dutta, A. K. *et al.* Syntheses, structural, spectroscopic and magnetic properties of polynuclear Fe(III) complexes containing N and O donor ligands. *Inorganica Chim. Acta* **444**, 141–149 (2016).

66. Lloyd, D. R., Phillips, D. H. & Carmichael, P. L. Generation of putative intrastrand cross-links and strand breaks in DNA by transition metal ion-

mediated oxygen radical attack. *Chem. Res. Toxicol.* **10**, 393–400 (1997).

67. Ghosh, K., Tyagi, N., Kumar, P., Rathi, S. & Singh, U. P. Efficient nuclease activity of dinuclear iron(III) complex with ligand having carboxamido nitrogen donors. *Inorg. Chem. Commun.* **20**, 167–171 (2012).

68. Ghosh, K., Tyagi, N., Kumar, P. & Singh, U. P. Synthesis, structure, redox properties and DNA interaction studies on mononuclear iron(III) complexes with amidate ligand. *Inorganica Chim. Acta* **412**, 20–26 (2014).

69. Yang, H., Lu, R., Downs, R. T. & Costin, G. Goethite, α -FeO(OH), from single-crystal data. *Acta Crystallogr. Sect. E* **62**, i250–i252 (2006).

70. Ewing, F. J. The crystal structure of lepidocrocite. *J. Chem. Phys.* **3**, 420–424 (1935).

71. Beisl, S., Friedl, A. & Miltner, A. Lignin from micro- To nanosize: Applications. *Int. J. Mol. Sci.* **18**, (2017).

72. Lora, J. H. & Glasser, W. G. Recent industrial applications of lignin: A sustainable alternative to nonrenewable materials. *J. Polym. Environ.* **10**, 39–48 (2002).

73. Yousefi, S. M. & Shemirani, F. Selective and sensitive speciation analysis of Cr (VI) and Cr (III) in water samples by fiber optic-linear array detection spectrophotometry after ion pair based-surfactant assisted dispersive liquid – liquid microextraction. *J. Hazard. Mater.* **254**–**255**, 134–140 (2013).

74. Huang, D. L. *et al.* Synthesis and Application of Modified Zero-Valent Iron Nanoparticles for Removal of Hexavalent Chromium from Wastewater. *Water. Air. Soil Pollut.* **226**, (2015).

75. Lazaridis, N. K. & Charalambous, C. Sorptive removal of trivalent and hexavalent chromium from binary aqueous solutions by composite alginate-goethite beads. *Water Res.* **39**, 4385–4396 (2005).

76. Song, Z. *et al.* Novel magnetic lignin composite sorbent for chromium(vi) adsorption. *RSC Adv.* **5**, 13028–13035 (2015).

Chapter 3: Lignin functionalization, phosphorylation

We have already seen how the intrinsic heterogeneity of lignin can limit its use[1]. Various problems in this regard are for example related to its miscibility with other polymers when it is used as additive for the preparation of new materials[1]. To improve the dispersion of lignin in polymeric systems, among the possible alternatives, there is the polymerization with poly(methyl methacrylate), and tailored functionalizations[1]. The possibility to modify lignin structure is mainly based on the reaction between aliphatic and aromatic hydroxyl groups with different types of organic molecules. Among the possible functionalizations, it must be mentioned acetylation[2], to incorporate lignin in polypropylene[1], sulfonation, to improve its solubility in water[3], and phosphorylation, useful both to increase the dispersion in polymers and to improve thermal properties[1].

To date, in fact, phosphorylated lignin is thought as a flame retardant in polypropylene, polybutylene succinate, polyurethane, and polylactic acid[1].

Phosphorylated lignin is also evaluated for another important function: the adsorption of metals in an aqueous environment. Thanks to the high surface area and its functional groups such as carboxylic acid and hydroxyl groups, lignin can already have potential for this purpose[4]. The introduction of phosphorylated molecules or phosphate groups can increase its effectiveness[4]. In this regard Nada et al. compared the sodium binding capacity and the metal ions adsorption of peroxyacid lignin, kraft lignin and the respective phosphorylated ones with phosphorous oxychloride[5]. They showed that between the two lignins, the one with the greatest efficacy is the peroxyacid lignin precisely due to its higher degree of oxidation deriving from the hardest extraction process. Unlike kraft lignin, in fact, peroxyacid lignin has a greater number of COOH groups. Comparing, instead, the starting lignins with the phosphorylated ones, both the peroxyacid lignin and the kraft lignin showed a greater activity after functionalization[5]. In particular, the most promising is the phosphorylated peroxyacid lignin, thanks to the higher phosphorous content. The introduction of phosphate groups, in the case of peroxyacid lignin, was in fact facilitated by the most extensive fragmentation deriving from the pulping process because it made the hydroxyl groups more available. At the basis of the adsorption of metals on ion exchangers there are intrinsic adsorption, closely related to the surface area of the material, and the Coulombic interactions[6]. In fact, the electrostatic energy between adsorbents and adsorbates as well as the matching based on the hard soft theory

between the coordinating functional groups of the adsorbent and the metal ion of interest determine the amount of adsorption[6]. In this regard the charge and the hydration metal radius are two important factors[6]. Comparing the adsorption in aqueous medium of Cr(III), Fe(III), Cu(II), Ni(II), Cd(II), and Pb(II), the worst results are obtained with cadmium and lead[5,6]. The main reason is, therefore, the low charge/radius ratio of cadmium and lead, which makes them soft metals, unlike harder Cr(III) and Fe(III), with a higher charge/radius ratio, are the two metals[5,6] best adsorbed. Furthermore, steric factors and electronegativity can be crucial in tuning the adsorption capability[4,5,7].

Lignin phosphorylation proceeds through a SN_2 mechanism on both aliphatic and aromatic hydroxyl groups of the polymer[8]. Several procedures have been developed using different types of lignins and phosphorylating agents[8], such as orthophosphoric acid [9,10], hypophosphorous acid[9], dihydrogen ammonium phosphate[11,12], phosphorous oxychloride[5], phosphorous pentoxide[13,14], diethyl phosphite[15,16], tributyl phosphate[9] , and diphenyl phosphoryl chloride[1].

Gao et al., for example, used ammonium dihydrogen phosphate in aqueous solution with urea, and functionalization takes place by impregnation of lignin at 70°C[11]. The same method was also used by Bykov et al. which showed how urea favours the phosphorylation of lignin by phosphoric acid thanks to the formation of unstable compounds characterized by cyanic acid, deriving from urea decomposition, and lignin[9]. The decomposition of these compounds subsequently leads to the functionalization of the polymer with phosphoric acid.

Mendis at al. used, instead, diphenyl phosphoryl chloride as phosphorylating agent, under solventless conditions as well as using pyridine as solvent[1]. They showed how pyridine improves functionalization through swelling of the polymer making the functional groups more accessible, as well as functioning as nucleophilic catalyst for the esterification reaction.

In light of these premises, together with the reducing properties of the polymer, phosphorylated lignin drew our attention on the possibility of using it as an effective material for the remediation of Cr(VI) polluted waters. The idea, in fact, is to evaluate not only the adsorption of Cr(VI) by phosphorylated lignin, but also the possible reduction of the metal, before adsorption. The number of OH groups involved in the functionalization is expected to be rather limited and this allows to maintain the reducing ability of the biopolymer. In this regard, the kraft BioPiva395 lignin, whose characteristics are presented in chapter 1-Lignin

materials used in this work, has been functionalized following the procedure of Prieur and co-workers, based on the use phosphorous pentoxide as phosphorylating agent in THF[13]. In this chapter, which collects preliminary results still needing optimization, the phosphorylation of lignin is presented, focusing attention on the characterization of the isolated material.

Experimental Part

Kraft lignin (*Pinus taeda*) BioPiva395 (M_w=5950-6000 g/mol), was provided by UPM-Kymmene Oyj and Green Innovation GmbH. Its features are listed in Chapter 1-Lignin materials used in this work.
Phosphorous pentoxide and THF were purchased from Sigma Aldrich and used without further purification.

Synthesis

The reaction was conducted following the procedure reported by Prieur et al[13]. After drying at 60°C in a vacuum oven, BioPiva395 was dissolved in THF. After few minutes phosphorous pentoxide was added, and reaction lasted 8h at reflux. During the reaction phosphorylated lignin precipitates. After quenching with cold water in an ice bath, lignin is washed by filtration with water to remove phosphoric acid. After the washing step, phosphorylated lignin was dried at 60°C overnight. To evaluate the reproducibility of the procedure three syntheses were conducted under the same conditions, isolating P_LIG1, P_LIG2, and P_LIG3. A scale up of the reaction was also carried out, named P_LIGx5_1. Table 3.1 reports the experimental details.

Table 3.1. Amount for reagents and solvent used in the lignin phosphorylation reactions

Sample	**Lignin**	**P4O10**	**THF**
P_LIG1, P_LIG2, P_LIG3	2.00 g	2.13 g	20 ml
P_LIGx5_1	10.00 g	10.646 g	100 ml

The characterization of the isolated materials was done by means of IR spectroscopy, SEM-EDS technique, and ^{31}P-NMR spectroscopy.

Results and discussion

Prieur et al. report a rather simple and high-performance phosphorylation procedure for Kraft lignin, using phosphorous pentoxide as a phosphorylating agent[13,14]. This procedure was chosen because it does not require the intervention of other chemicals other than the source of phosphorous and the solvent. Alternative procedures involving the use ammonium dihydrogen phosphate[11] or phosphoric acid[9], use in fact an excess of urea to facilitate functionalization. These procedures lead to the partial modification of lignin structure due to incorporation of nitrogen, as evidenced by the elemental analysis. Since the aim of our work is to evaluate the ability of phosphorylated lignin to remove Cr(VI) from aqueous medium in comparison with unfunctionalized lignin, it is necessary to avoid the introduction of additional coordinating functions, such as those deriving from N-containing fragments.

Phosphorylation is expected to occur on both aromatic and aliphatic OH groups, according to the scheme shown in figure 3.1. In their work, Gao et al. report on the possibility of forming phosphate groups or phosphate ester groups[11]. The lignin, dissolved in THF, is reacted with phosphorous pentoxide at reflux for 8 hours, during which the reacted lignin precipitates.

Quenching with water allows to transform the unreacted phosphorous pentoxide into phosphoric acid, which must be carefully removed by repeated washing with water. By using this procedure, a final 3% of phosphorous is expected to be found in the functionalized material, as reported in the original paper[13].

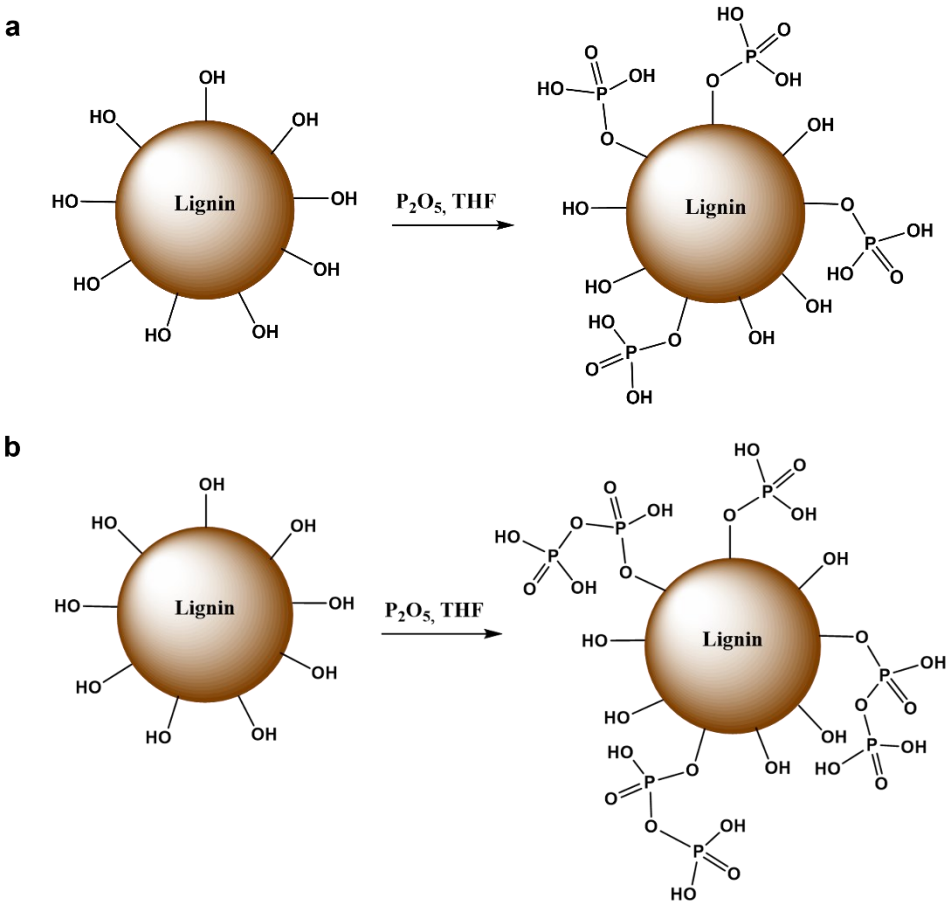

Figure 3.1. Schematic representation of a) phosphorylation and b) formation of phosphate esters.

Characterization

Three gram-scale syntheses were conducted, corresponding to the products P_LIG1, P_LIG2, and P_LIG3, to evaluate the reproducibility of the procedure; a scale up referred to the use of 10 grams of lignin led to P_LIGx5_1. The experimental conditions were kept constant for all the syntheses, using an excess of phosphorous pentoxide with respect to the OH groups present in lignin.

Infrared Spectroscopy

IR spectra of P_LIG1, P_LIG2, P_LIG3 and P_LIGx5_1, reported in figure 3.2, are perfectly superimposable.

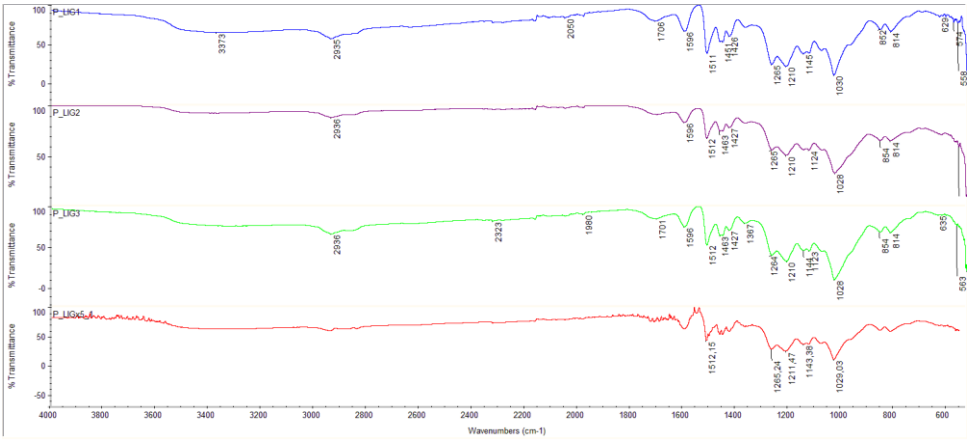

Figure 3.2. Comparison of the IR spectra of P_LIG1 (blue), P_LIG2 (purple), P_LIG3 (green) and P_LIGx5_1 (red).

In figure 3.3 the IR spectrum of P_LIG1 is compared with that of BioPiva395. From the spectrum of the latter, it is possible to recognize all the typical bands of the polymer[11,14]. In particular, the bands at 1596 cm^{-1}, 1512 cm^{-1}, and 1427 cm^{-1} correspond to the stretching vibrations of the aromatic C-C bonds of the phenyl propanoic units. The wide band around 3364 cm^{-1} is related to the OH groups, while the adsorption bands at 2936cm^{-1}, 2843 cm^{-1} and 1462 cm^{-1} are related to the CH stretching vibrations of the methyl and methylene groups. At 1266 cm^{-1}, 1125 cm^{-1} and 1031 cm^{-1} the stretching of the C-O bond and ethereal C-O-C bonds are visible.

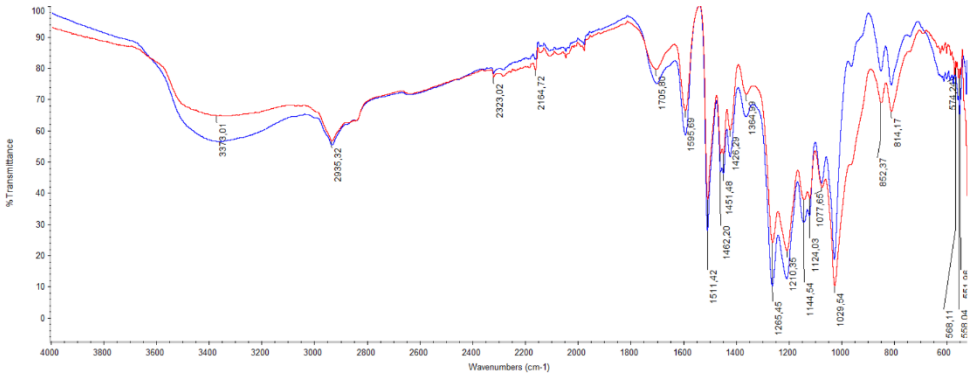

Figure 3.3. Overlap between IR spectrum of BioPiva395, blue and P_LIG1, red.

Prieur attributes the band at around 1000 cm^{-1} to the stretching vibration of the bond LigO-P[14]. However, in our case the IR characterization is not definitive in establishing the occurred installation of P-containing groups, since even in the spectrum of pristine lignin there is a clear band at around 1000 cm^{-1}. The only difference can be a broadening of the signal observable after functionalization.
Gao et al. attribute to the P-O-C groups deriving from aliphatic OHs a band at about 830 cm^{-1}, while at the P-OH bond stretching is attributed a band around 922 cm^{-1} [11]. The same assignments for P_LIG1 are not immediate, indeed, the band related to the aliphatic bond P-O-C, cannot be well identified, being present two bands at 852,37 cm^{-1} and at 814,17 cm^{-1} which are also found in the IR spectrum of the starting lignin. The P-OH bond stretching band could be the shoulder of the broad band at 1000 cm^{-1}, placed around 968,90 cm^{-1}.
However, a decrease in the intensity of the band at 3364 cm^{-1} can be noted passing from lignin to phosphorylated lignin. This is in agreement with what Prieur and Gao observed in their works[11,14].
It is clear that IR spectroscopy is not sufficient to confirm the occurrence of phosphorylation, as the phosphate groups do not have intense bands in IR spectroscopy[17].

Nuclear Magnetic Resonance

The ^{31}P-NMR signal for lignin functionalized with phosphate groups is expected to generate signals comprised between 0 and -2 ppm[11,13].

From the ^{31}P-NMR spectrum recorded in d^6-DMSO, Gao and co-workers excluded the formation of phosphate esters, previously hypothesized, since no peak were found at around -7 ppm[11].

Prieur et al., in one of their works, showed the ^{31}P NMR spectrum in d_6-DMSO of phosphorylated lignin with and without proton decoupling[14]. Two different peaks were observed at -1.11 ppm and at -1.17ppm, inevitably belonging to two different phosphorous atoms. One signal, which couples with two protons of CH_2 groups of lignin, was attributed to the functionalization of the aliphatic OH, while the second most intense signal, not showing any coupling, is related to P atoms bound to the aromatic oxygen[14]. In the same work, the ^{31}P-NMR spectrum of phosphoric acid is reported to exclude its presence in the phosphorylated lignin. The peak relative to the acid, when DMSO is used as solvent, is at -0,35ppm.

While in many works the phosphorylated lignin is considered soluble or partially soluble in DMSO[11,14], in our case a significantly obstacle was represented by the complete insolubility of P_LIG samples in this solvent. In fact, in the attempt to record the liquid ^{31}P{^{1}H}-NMR spectrum of our functionalized lignin, 10 mg of P_LIG1 were placed in a NMR tube and added of 0,6 mL of d^6-DMSO; the sample was heated and sonicated for at least 5 minutes, without appreciable solubilization. The insolubility in DMSO could be explained by the fact that the phosphate groups, covalently linked to lignin, can interact with each other through hydrogen bonds, greatly modifying its solubility[14]. The spectrum, recorded with extended accumulations, did not reveal any signal, as can be seen from figure 3.4a.

The complete insolubility of phosphorylated lignin in DMSO was also observed by Mendis et al. which, however, functionalized the polymer using phosphoryl chloride as a phosphorylating agent[1]. The absence of signals in the spectrum of P_LIG1 is however indicative also of the absence of phosphoric acid in the sample, whose formation would derive from hydration of P_2O_5 during washing with water.

To overcome the solubility issues, the solid state ^{31}P{^{1}H}-MAS-NMR spectrum of P_LIGx5_1 was then recorded (figure 3.4b). The spectrum exhibited a large peak centred at about 0 ppm, as can be inferred from figure 3.4b. Although equivalent with the signal expected for orthophosphoric acid, the chemical shift is also in agreement with the presence of orthophosphate groups[18].

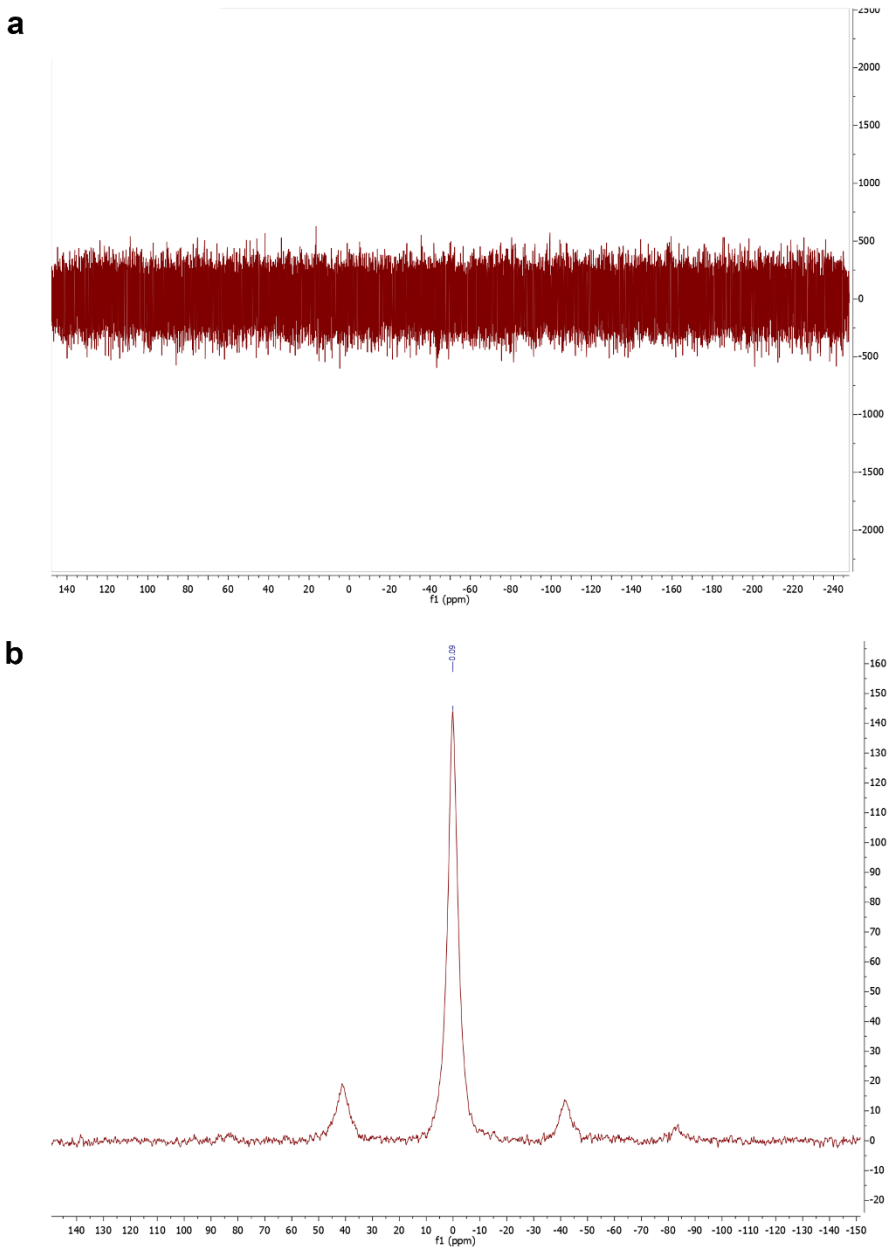

Figure 3.4. $^{31}P\{^{1}H\}$-NMR spectra of P_LIG: a) in d^{6}-DMSO, b) in the solid state.

The solid state $^{13}C\{^{1}H\}$-NMR spectra of pristine and phosphorylated lignin are shown in figure 3.5. The two spectra do not present significative differences and, as reported in literature for kraft lignin, it is possible to identify the aromatic carbons region between 150 and 110 ppm, the most intense peak at 55,02 ppm related to the carbon atoms of the methoxy group, and the peak at about 61 ppm which is referred to the carbon of the CH_2OH[19] groups.

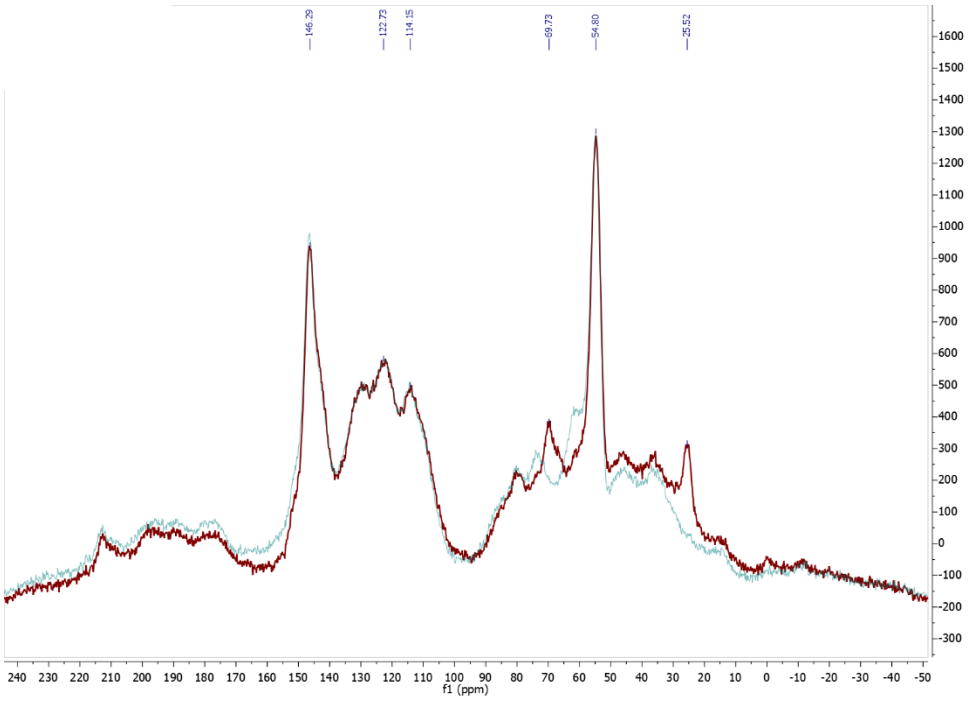

Figure 3.5. Solid state $^{13}C\{^{1}H\}$-NMR of BioPiva395 (green) and P_LIG (red).

Morphological analysis and phosphorous content

Scanning Electron Microscopy, Energy Dispersive X-ray Spectrometry and Elemental analysis

In figure 3.6 SEM images of pristine lignin and P_LIG are reported with different enlargements.

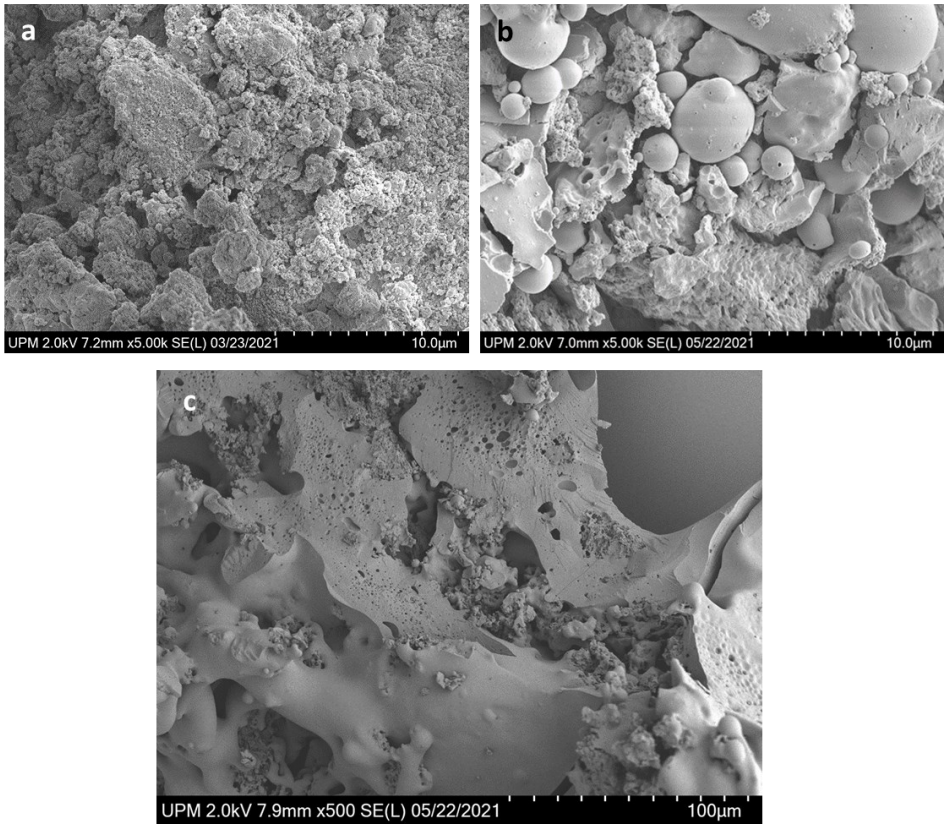

Figure 3.6. SEM images of BioPiva395 (a) and P_LIG (b and c).

The surface of lignin treated with phosphorous pentoxide appears to contain larger particles than the original lignin. This agrees with what was observed by Prieur and co-workers[14]. The particle size depends not only on the synthesis

conditions (temperature, concentration, work up), but may also be due to the capability of the phosphate groups to promote aggregation and then triggering the precipitation of phosphorylated lignin during the synthesis and the formation of agglomerates[14]. We can also observe, especially from figure 3.6c, that the surface of lignin treated with phosphorous pentoxide has featured by holes, in accordance with the literature[13].

Combining elemental analysis with EDS results it was possible to estimate the amount of P element in P_LIG samples. This was determined to be comprised between 1-2% in weight, as shown in table 3.2, for P_LIG1, P_LIG2 e P_LIG3. Each data is the mean value of two different scans on the same specimen.

Table 3.2. Elemental analysis results for P_LIG samples, and percentage of phosphorous by combining elemental analysis and EDS measurements

	From elemental analysis				
Sample	**N**	**C**	**H**	**S**	**%P**
P_LIG1	0,14	60,44	5,65	1,56	**1,23%**
P_LIG2	0,14	58,57	5,83	1,45	**1,90%**
P_LIG3	0,14	60,78	5,69	1,54	**1,53%**
BioPiva395	0,13	63,28	6,66	1,91	----

The relative weight percentages of phosphorous and sulphur determined by EDS analysis are multiplied by the respective atomic weights and then the ratio between the obtained values (P/S) is calculated. From this value, considering the weight percentage of S determined by elemental analysis, a weight percentage of P was estimated. The corresponding values are reported in table 3.2.
The low yield of phosphorylation agrees with the data reported in literature. In fact, lignin phosphorylation reaches a maximum of 3-4% in weight of phosphorous[13,14].
By means of EDS mapping we assessed the homogenous distribution of phosphorous on lignin particles, as can be appreciated from figure 3.7.

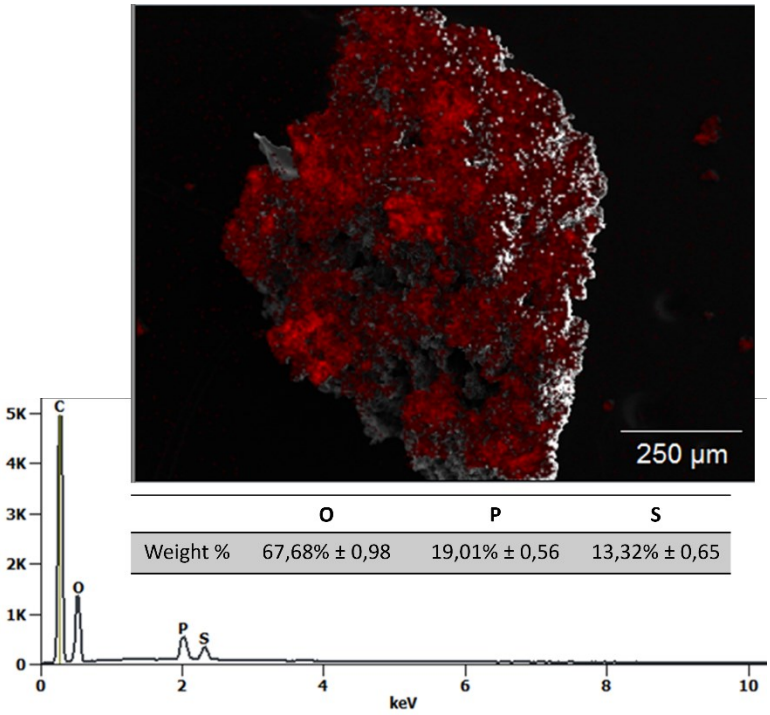

Figure 3.7. EDS analysis and EDS mapping for P_LIG2, phosphorous is represented by red.

Thermogravimetric analysis:

The thermogravimetric analysis of BoPiva395 and P_LIG1 run under inert atmosphere are shown in figure 3.8. The TGA profile of P_LIG1 is very similar to that reported by Prieur et al.[13,14].

In the case of P_LIG1 after a first weight loss around 100°C, caused by residual water, the thermal decomposition begins earlier than what observed with BioPiva395, starting close to 200°C. instead of 250°C. It is also noted that, during the decomposition process, weight loss is more pronounced in the case of lignin than in phosphorylated lignin. The greater stabilization at high temperatures (about 400°C) of phosphorylated lignin is a direct consequence of

functionalization, which is why phosphorylated lignin is being studied as a flame retardant[14].

From the thermogravimetric profile it is also possible to derive the ignition temperature of a given substance, which, being the critical point between pyrolysis and combustion, is related to its thermal stability[11]. The temperature at which weight loss begins (around 190°C, in our case) and the temperature at which weight loss reaches its maximum must be considered in the thermal profile. The ignition temperature is the point of intersection between the tangents of the thermal profile at these two temperatures[11,20]. While the ignition temperature of the starting lignin is about 320°C, the ignition temperature of our phosphorylated lignin is 355°C. The increase in the ignition temperature after phosphorylation is in accordance with what is reported in the literature[11].

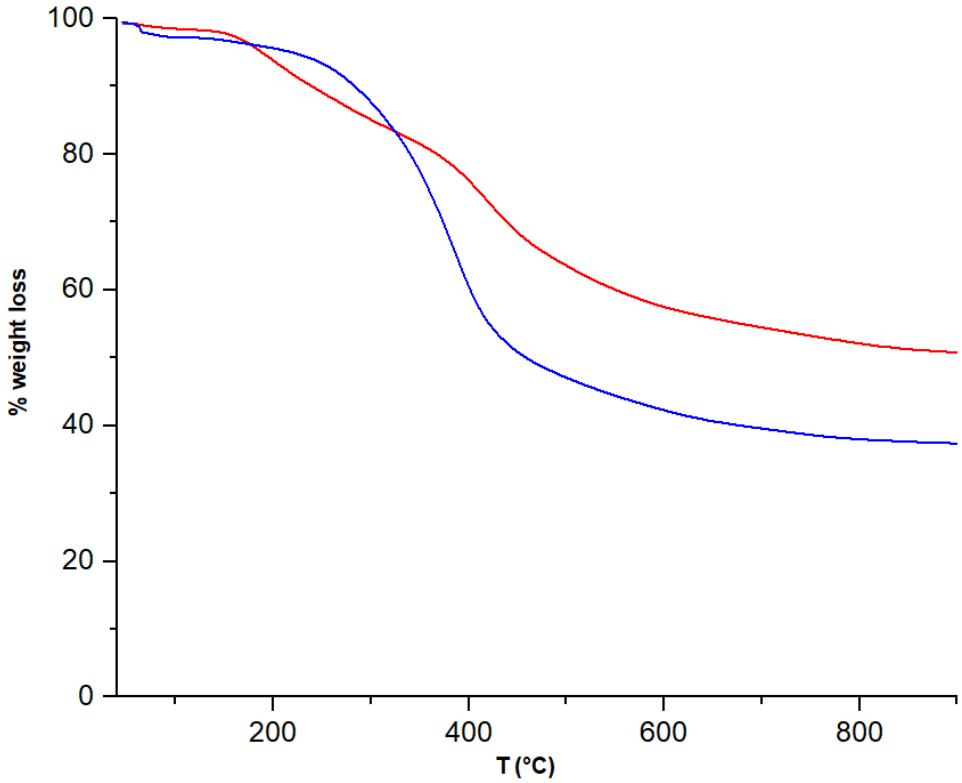

Figure 3.8. TGA profiles of BioPiva395 (blue) and P_LIG1 (red).

Contact angle measurements

Preliminary wettability measurements were also carried out on P_LIG, revealing a contact angle with water of about 65° slightly higher than the one of BioPiva395 (54°).

Conclusions

Phosphorylated lignin is a promising material both as a flame retardant for polymers or polymer blends and as a heavy metal adsorbent in aqueous medium[1,6]. The latter is precisely the reason why we decided to functionalize our BioPiva395 Kraft lignin with phosphate groups. In particular, the phosphorylated lignin will be tested for the adsorption/reduction of Cr(VI) in water. The synthesis of phosphorylated lignin, referred to as P_LIG, follows a simple procedure optimized by Prieur and co-workers, which consists in the use of phosphorous pentoxide as a phosphorylating agent[13,14]. The characterization of the material revealed to be quite difficult. The main problem was related to the possibility to discharge the presence of free orthophosphoric acid eventually embedded in the polymer, acid that can form after reaction quenching with water. Although some characterization data are not conclusive, especially those deriving from NMR analysis, several findings are in favour of the occurred installation of phosphate groups in the polymer chains: i) the product precipitates from THF after the addition of P_2O_5; ii) the product was plenty washed with water just to be sure of the complete removal of free inorganic P-containing species; iii) contrarily to the starting lignin, the product is insoluble in DMSO; iv) $^{31}P\{^1H\}$-NMR recorded in DMSO did not show any trace of orthophosphoric acid; v) TGA trace of P_LIG samples shows a lower weight loss than starting lignin, contrarily to what expected in the presence of orthophosphoric acid which is known to sublime at around 800K[18]; vi) the amount of P element found in the samples is in agreement with literature reported data; vii) the morphological analysis conducted by SEM shows an extremely similar situation to that reported in literature[13]. Finally, the formation of polyphosphate species can be ruled out because the dehydration of orthophosphoric acid occurs at temperature much higher than those involved in the followed experimental procedure[18].

References

1. Mendis, G. P. *et al.* Phosphorylated lignin as a halogen-free flame retardant additive for epoxy composites. *Green Mater.* **4**, 150–159 (2016).

2. Buono, P., Duval, A., Verge, P., Averous, L. & Habibi, Y. New Insights on the Chemical Modification of Lignin: Acetylation versus Silylation. *ACS Sustain. Chem. Eng.* **4**, 5212–5222 (2016).

3. Guo, Y., Gao, W. & Fatehi, P. Hydroxypropyl sulfonated kraft lignin as a coagulant for cationic dye. *Ind. Crops Prod.* **124**, 273–283 (2018).

4. Ads, E. N., Nada, A. M. A. & El-Masry, A. M. Use and evaluation of lignin as ion exchangers. *J. Korean Chem. Soc.* **55**, 86–91 (2011).

5. Nada, A. M. A., Kassem, N. F. & Mohamed, S. H. Characterization and properties of ion exchangers produced from lignin precipitated after peroxyacid pulping. *BioResources* **3**, 538–548 (2008).

6. Abd-Allah M. A. Nada, M. L. H. Phosphorylated cation-exchangers from cotton stalks and their constituents. *J. Appl. Polym. Sci.* **89**, 2950–2956 (2003).

7. Lehrfeld, J. Conversion of agricultural residues into cation exchange materials. *J. Appl. Polym. Sci.* **61**, 2099–2105 (1996).

8. Eraghi Kazzaz, A., Hosseinpour Feizi, Z. & Fatehi, P. Grafting strategies for hydroxy groups of lignin for producing materials. *Green Chem.* **21**, 5714–5752 (2019).

9. Bykov, G. L. & Ershov, B. G. A sorbent based on phosphorylated lignin. *Russ. J. Appl. Chem.* **83**, 316–319 (2010).

10. Alalykin, A. A., Vesnin, R. L. & Kozulin, D. A. Preparation of modified hydrolysis lignin and its use for filling epoxy polymers and enhancing their flame resistance. *Russ. J. Appl. Chem.* **84**, 1616–1622 (2011).

11. Gao, C., Zhou, L., Yao, S., Qin, C. & Fatehi, P. Phosphorylated kraft lignin with improved thermal stability. *Int. J. Biol. Macromol.* **162**, 1642–1652 (2020).

12. Ferry, L. *et al.* Chemical modification of lignin by phosphorus molecules to

improve the fire behavior of polybutylene succinate. *Polym. Degrad. Stability, Elsevier* **113**, 135–143 (2015).

13. Prieur, B. *et al.* Phosphorylation of lignin: characterization and investigation of the thermal decomposition. *RSC Adv.* **7**, 16866–16877 (2017).

14. Prieur, B. *et al.* Phosphorylation of lignin to flame retard acrylonitrile butadiene styrene (ABS). *Polym. Degrad. Stab.* **127**, 32–43 (2016).

15. Liu, L., Huang, G., Song, P., Yu, Y. & Fu, S. Converting industrial alkali lignin to biobased functional additives for improving fire behavior and smoke suppression of polybutylene succinate. *ACS Sustain. Chem. Eng.* **4**, 4732–4742 (2016).

16. Liu, L. *et al.* Fabrication of Green Lignin-based Flame Retardants for Enhancing the Thermal and Fire Retardancy Properties of Polypropylene/Wood Composites. *ACS Sustain. Chem. Eng.* **4**, 2422–2431 (2016).

17. Nourry, G., Belosinschi, D., Boutin, M. P., Brouillette, F. & Zerrouki, R. Hydrophobization of phosphorylated cellulosic fibers. *Cellulose* **23**, 3511–3520 (2016).

18. Karrasch, A., Wawrzyn, E., Schartel, B. & Jäger, C. Solid-state NMR on thermal and fire residues of bisphenol A polycarbonate/silicone acrylate rubber/bisphenol A bis(diphenyl-phosphate)/(PC/ SiR/BDP) and PC/SiR/BDP/zinc borate (PC/SiR/BDP/ZnB) - Part I: PC charring and the impact of BDP and ZnB. *Polym. Degrad. Stab.* **95**, 2525–2533 (2010).

19. Stephen Y. Lin, C. W. D. *Methods in Lignin Chemistry*. (Springer Series in Wood Science: Wood structure and enviroment, 1992).

20. Cao, Wenhan Li, Jun Lue, L. Study on the ignition behavior and kinetics of combustion of biomass. *Energy Procedia* **142**, 136–141 (2017).

Chapter 4: Coordinative studies of lignin-inspired ligands.

The synthetic procedures between lignin and metal salts presented until now, led to the formation of inorganic phases embedded in the lignin matrix, despite the different conditions investigated.

It is well known that one of the ways to fix metals in the soil, in order to avoid their release into the aquifers and reduce pollution, is through coordination with organic molecules[1].

The antibacterial activity of metals and organic molecules, such as phenol derivatives, can also be improved with the formation of organo-metal complexes. This is because through complexation, for example, the chemical and biological properties of phenolic compounds can be modified in such a way to make them more available thus increasing their antibacterial power[2].

To decontaminate sites polluted by heavy metals, or to clean wastewater, one of the common way of intervention is the possibility of a coordinative link between the target metal and proper ligands[3,4].

In this regard, the use of lignin to reclaim water contaminated by heavy metals is gaining more and more interest in research[5]. Potentially endowed with coordination capacity thanks to functional groups such as carboxylic acids and hydroxyl groups, together with its reducing power, lignin is considered for these purposes also thanks to its high surface area[5,6].

From this perspective, therefore, the possibility of a complexation of metal cations by lignin is particularly intriguing, both from a scientific and an application point of view. Potentially, lignin could coordinate metals, thanks to its phenolic and carboxylic functions (see figure 1.5 and details about its structure in Chapter 1). The folded and complex structure of lignin, together with its low solubility, however, make difficult a detailed characterization of interactions occurring between metal cations and specific coordinative sites present on the polymer[1]. In order to study the coordinative properties of the polymer the attention was then directed to the use of model compounds that could mimic some coordinative pockets present in lignin.

To date, in the literature there are few examples of structurally characterized complexes or coordination polymers based on lignin-inspired ligands, such as hydroxycinnamic acid derivatives.

Kitanovski et al. reported the structures of two complexes based on copper and ferulic acid. In both cases the coordination occurs through the carboxylate functions of ferulic acid that bridge two Cu^{2+} ions[7].

Starting from copper sulphate, the sodic salt of ferulic acid and ethylenediamine, an ionic complex was isolated, and its structure determined by Single Crystal X-ray Diffraction analysis (SC-XRD)[8]. The crystal packing is characterized by layers consisting of alternating anionic (ferulate ligand) and [trans-$Cu(en)_2(H_2O)_2]^{2+}$ cationic units. The two ionic units are held together by means of electrostatic forces and hydrogen bonds between phenolate oxygens of the deprotonated ferulic acids and the hydrogens of ethylenediamine and water molecules coordinated to the metal[8].
With vanillic acid a binuclear compound of Co(II) was obtained by Spekreijse et al. In this case the two cobalt atoms, both with an octahedral geometry, are coordinated to the methoxy and phenolate groups of vanillic acid and the remaining coordination positions are completed by water molecules[9].
To the best of our knowledge, the only ferulic acid-based coordination polymer isolated so far has been obtained by Demir et al. with a solvothermal synthesis using zinc nitrate[10]. The isolated compound is a Metal Organic Framework (MOF) characterized by three Zn^{2+} ions, each with a different coordination geometry (tetrahedral, octahedral, and trigonal bipyramidal), bridged by ferulic acid ions that coordinate with the carboxylate group, the methoxy function and the phenolate group. The high void volume (3517Å) made this MOF attracting both for gas adsorption[10] and for the encapsulation of drugs[11]. Zhou et al., instead, studied it for the photocatalytic degradation of organic dyes in aqueous medium[12].

Based on the scarcity of data regarding the coordination properties of hydroxycinnamic derivatives towards transition metal ions, and the importance of data deriving from the knowledge of the coordination properties of lignin to understand its heavy metal adsorption properties, we focused our attention on ferulic acid, whose structure is shown in figure 4.1. Ferulic acid, that is the acid of coniferyl alcohol, one of lignin monolignols, contains the guaiacyl unit (unit G, see figure 1.3 on page 4), significantly present in BioPiva, the lignin used in this work (see table 1.2). Synthetic screening, carried out in combination with transition metal salts such as Co(II), Cu(II), Mn(II), Fe(II) and Ni(II), led to the isolation of a coordination polymer with Co^{2+}, hereinafter referred to as CG3, whose crystalline structure is here presented. A mechanochemical procedure for the obtaining of CG3 was also conducted starting from ammonium ferulate instead of ferulic acid.

The investigation was then extended to other phenol-propanoic carboxylic compounds, such as coumaric acid (figure 4.1), mimicking the p-hydroxyphenyl unit of lignin (unit H, see figure 1.3) and caffeic acid, having two OH groups on the aromatic ring (figure 4.1).

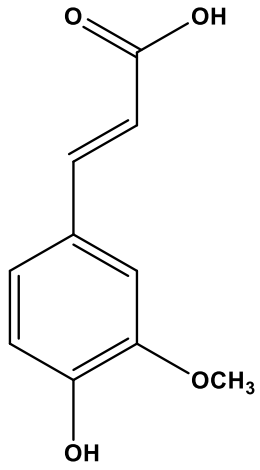

ferulic acid

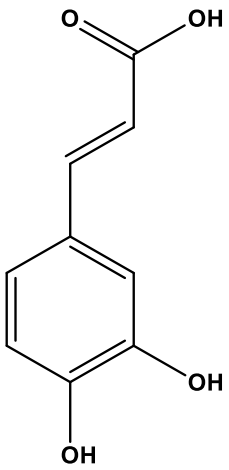

caffeic acid

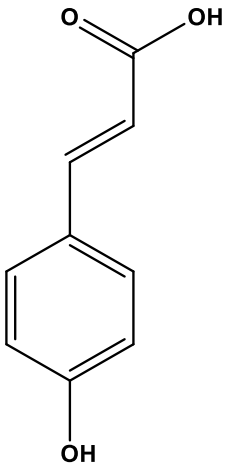

coumaric acid

Figure 4.1. Lignin-inspired ligands.

Experimental part

$CoCl_2 \cdot 6H_2O$, $Co(NO_3)_2 \cdot 6H_2O$, $MnCl_2 \cdot 4H_2O$, $NiCl_2 \cdot 6H_2O$, $Ni(NO_3)_2 \cdot 6H_2O$, $Cu(NO_3)_2 \cdot 3H_2O$, and anhydrous $FeCl_2$ were purchased from Sigma Aldrich and used without further purifications.

Ferulic acid, caffeic acid and coumaric acid were purchased from TCI (Tokyo Chemical Industry Co., LTD), while dimethyl formamide was purchased by VWR International.

Illustration and crystal data of the coordination polymer CG3 were obtained from means of Mercury 4.3.1 software (Build 273970).

Solvothermal synthesis

In a 17 mL screw cap tube the organic ligand (ferulic acid, coumaric acid or caffeic acid) was dissolved in 10 mL of DMF. Subsequently, the metal salt was added to the solution. The clear solution was then heated at 80°C for 6 days. Only in the case of ferulic acid (1mmol) with $CoCl_2 \cdot 6H_2O$ (0,5mmol), prismatic blue crystals formed (trial 1). These were collected, washed with fresh DMF, and stored under this solvent to prevent any damage. Subsequently a structural characterization was carried out by means of SC-XRD (see paragraph "CG3 from solvothermal synthesis").
In table 4.1. the details of the syntheses are reported.

Table 4.1. Solvothermal screening with different metal salts for coordination studies of ferulic acid, coumaric acid and caffeic acid.

Trial	Ligand	Metal salt	Molar ratio	Results
1	Ferulic acid	$CoCl_2 \cdot 6H_2O$[2]	2:1	CG3 blue crystals, yield 56%
2	Ferulic acid	$CoCl_2 \cdot 6H_2O$[2]	4:1	CG3 blue crystals, 45%
3	Ferulic acid	$CoCl_2 \cdot 6H_2O$[2]	1:1	CG3 small blue crystals, yield, 24%
4	Coumaric acid	$CoCl_2 \cdot 6H_2O$[2,3]	2:1	[2] no product [3] fuchsia powder, cobalt formate hydrate
5	Caffeic acid	$CoCl_2 \cdot 6H_2O$[1,2]	2:1	[2] heterogeneous solid [1] darkening of the solution
6	Ferulic acid	$Co(NO_3)_2 \cdot 6H_2O$[2]	2:1	no product
7	Ferulic acid	$MnCl_2 \cdot 4H_2O$[2]	2:1	no product
8	Ferulic acid	$NiCl_2 \cdot 6H_2O$[2,3]	2:1	[2,3] nothing
9	Ferulic acid	$Ni(NO_3)_2 \cdot 6H_2O$[2]	2:1	no product
10	Ferulic acid	$Cu(NO_3)_2 \cdot 3H_2O$[3]	2:1	darkening
11	Caffeic acid	$Cu(NO_3)_2 \cdot 3H_2O$[1]	2:1	black powder
12	Ferulic acid	$FeCl_2$[2]	2:1	no product
mmol metal salt: [1]0.25, [2]0,5, [3]1				

Mechanochemical synthesis

Mechanochemical syntheses were conducted through a planetary ball mill Retsch PM100 using an 80 mL steel jar and 3 spheres of the same material with a diameter of 10 mm.
Diammonium ferulate was obtained by reacting ferulic acid with ammonia vapour as follows. 1 g of ferulic acid was placed in a petri dish and introduced in a desiccator together with 25 mL of a concentrate NH_3 solution (33% in weight) placed in a beaker. The desiccator was then closed and left at room temperature for 24 hours. The yellow solid formed was dried under vacuum overnight and characterized by means of IR and NMR analysis (see figures S4.1 and S4.3 in "Supporting Information").

CG3 was then obtained by means of a mechanochemical procedure as follows. 228 mg (1 mmol) of diammonium ferulate and 476 mg (2 mmol) of $CoCl_2 \cdot 6H_2O$ were introduced as solids in the steel jar. Subsequently, 231 µL of DMF were added dropwise. After the addition of three steel spheres the grinding was carried out at 500 rpm for 1 hour with 4 rotation inversions every 15 minutes.
At the end of the grinding the blue powder was washed with fresh DMF by centrifugation, dried under vacuum and characterized by means of XRPD (figure 4.9).

CG3 moisture exposure

To study the reactivity of CG3 towards moisture, several approaches were followed.

- CG3 crystals were placed on a microscope slide and exposed to air for 25 days, monitoring the colour change.
- Two experiments were carried out with ground CG3 (microcrystalline powder): in the first experiment, crystals were ground, dried with filter paper, and exposed to air for 15 days.
The second experiment consisted in monitoring the hydration process by X-Ray Powder Diffraction analysis. CG3 crystals were dried under vacuum overnight, before to be ground in such a way to avoid the formation of the paste. Dried

powder was placed on a sample holder for X-ray powder diffraction analysis, and the diffractogram recorded every day for 21 days. A further control was conducted after about 6 months.

Results and Discussion

With the aim to study the coordination properties of lignin-inspired ligands, a series of solvothermal syntheses were carried out combining ferulic acid with different metal salts (table 4.1). Previous synthetic attempts have also been conducted under reflux conditions using mainly methanol and ethanol as solvents. These syntheses leading to poor soluble and, therefore, not easily to characterize products, were abandoned in favour of solvothermal synthesis. Solvothermal synthesis is one of the main synthetic routes to promote crystallization[13]. Frequently used to obtain Metal Organic Framework, it allows to obtain polymeric species more easily than methods that occur at atmospheric pressure. The success is due to the combination of high temperatures and autogenous pressure that lead kinetic and thermodynamic exclusive conditions that cannot be reached under reflux conditions and allow the framework to continuously rearrange during crystallization up to the most stable thermodynamic one[13]. Initially, the structures with lower density are formed which then, to maximize contacts and achieve the highest stability, evolve into more compact and higher density frameworks[13].
In many cases, combining the ligands with different metal salts (copper, nickel, manganese, and iron) in a 2:1 molar ratio did not lead to satisfactory results, irrespective to the concentration of the metal present in the reactant solution and reaction time (see Table 4.1). In most cases, the use of ferulic acid did not lead to the formation of a precipitate, even after 2 weeks of heating and the solvent maintained the typical colour of the dissolved starting salt (trials 6-9, 12). With copper, a darkening of the solution was observed (trial 10), imputable to the metal-promoted oxidation of the ligand. Only in one case, corresponding to the reaction between coumaric acid and cobalt dichloride (trial 4), fuchsia single crystals were isolated corresponding to $Co(HCOO)_2 \cdot H_2O$, as evidenced from the comparison between the cell parameters of isolated crystals and literature data[14]. Its formation is then imputable to the DMF decomposition occurring during the reaction.

The best results were obtained combining ferulic acid with cobalt chloride. Using a 2:1 ligand to metal molar ratio, CG3 was isolated in 56% yield, as blue prismatic X-ray quality single crystals (trial 1). The same material was obtained also varying the molar ratio between reagents (trial 2-3), using a solvent mixture of DMF:EtOH= 8:2, and bipyridine and isonicotinamide as additional ligands highlighting how CG3 is a thermodynamically stable product. However, prismatic blue crystals were obtained with the best yield following the synthesis reported as trial 1 in table 4.1.

CG3 from solvothermal synthesis

From the reaction corresponding to trial 1, already after 4 days from the beginning of the solvothermal synthesis, blue prismatic crystals formed (figure 4.1). Heating was maintained until the amount of crystals was constant, (6 days). At the end of the reaction, crystals were collected and washed with fresh DMF for at least three times. After vacuum drying, the yield, referred to cobalt, was 56%.
To avoid damages, the crystals were stored in DMF, where are completely stable. As shown in figure 4.2., prismatic blue crystals tend to aggregate forming agglomerate of twinned crystals.

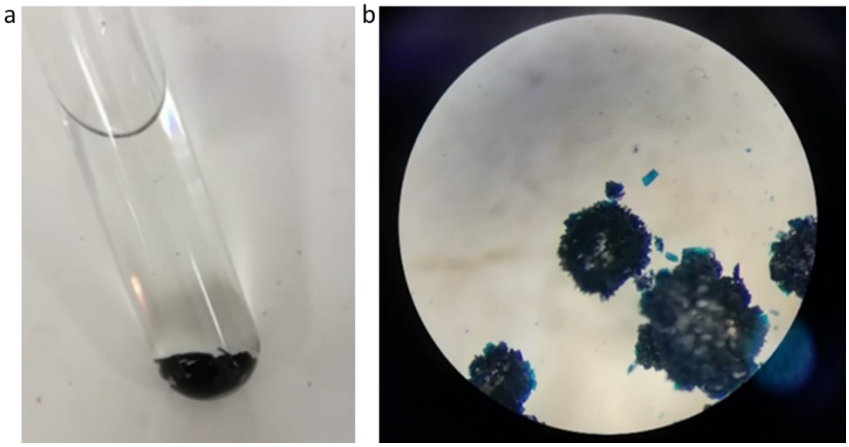

Figure 4.2. a) CG3 crystals stored under fresh DMF, b) microscope image of the blue prismatic crystals.

CG3 presents an asymmetric unit (figure 4.3) that contains two Co(II), a bi-deprotonated ferulic acid (fer), two chloride anions and three DMF molecules leading to the formula $[Co_2(fer)Cl_2]\cdot 3DMF$.
Single crystal X-ray diffraction revealed the presence of a Secondary Building Unit (SBU) characterized by two adjacent cobalt atoms having different coordination geometry (figure 4.4). The tetrahedral Co is coordinated by the oxygen of the deprotonated hydroxyl group of one ferulic acid, by a carboxylate oxygen of a second ferulic acid and by two chloride anions. The octahedral Co is coordinated by the phenolate oxygen that bridges the two cobalt atoms, by the methoxy oxygen of the same ferulic acid and by the other carboxylate oxygen of the second ligand bridging the two cobalt atoms. The octahedral geometry is completed by three DMF molecules (figure 4.4).
The framework is characterized by chains running between a and c axis in which the organic ligand bridges four cobalt atoms. In figure 4.5 is depicted a single chain built thanks to the ferulate dianion that coordinates the two adjacent cobalt atoms using its carboxylate and deprotonated guaiacol functions.

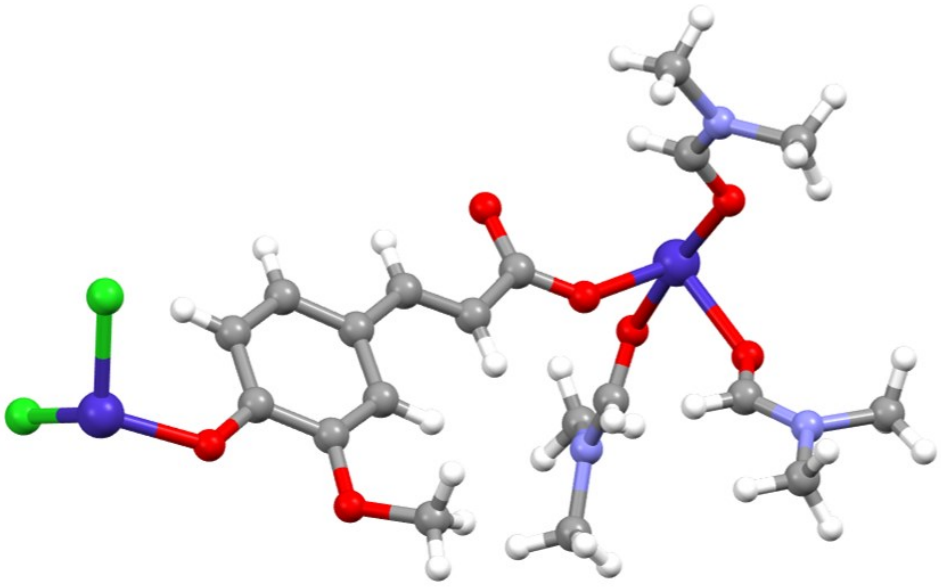

Figure 4.3. Asymmetric unit of CG3 of formula $Co_2LCl_2\cdot 3DMF$ (L = ferulate dianion).

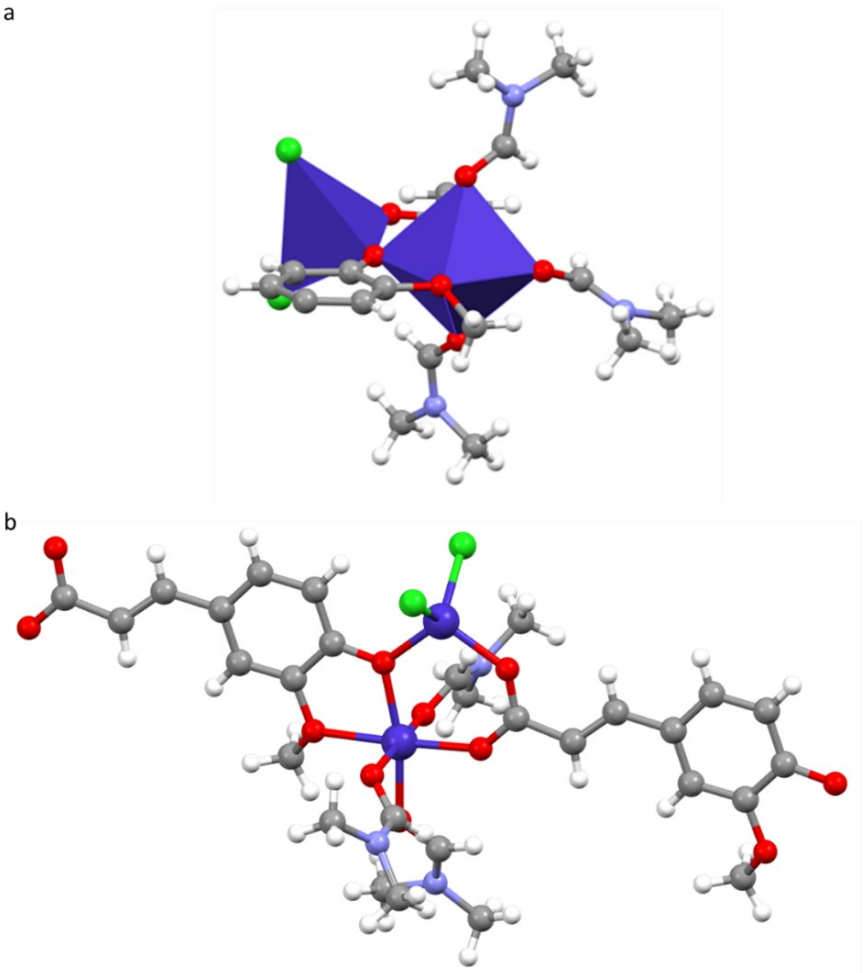

Figure 4.4. Secondary Building Unit of CG3 a) the tetrahedral and octahedral Co coordination geometries, b) coordination bonds featuring the SBU of CG3; colour code: blue, Co atoms; green, Cl atoms; red, O atoms; light violet, N atoms; grey, C atoms; white, H atoms.

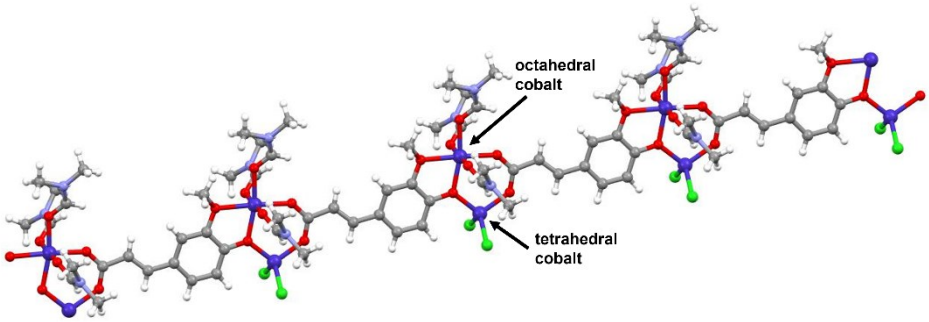

Figure 4.5. Single chain of CG3

Each chain contacts those adjacent through weak interactions between chloride ligands and hydrogens of the ferulate dianion of the neighbouring chain, figure 4.6. CG3 is, therefore, a mono-dimensional coordination polymer, avoid of porosity as can be inferred from figure 4.7. The packing along the crystallographic axis b, figure 4.7a, shows the interactions between chains, while the representation with "space fill" mode by Mercury software highlights the completely cavity free structure, figure 4.7b. The distances and bond angles are listed in table 4.2 while the crystallographic details in table 4.3. In figure 4.8. the diffractogram of CG3 is shown.

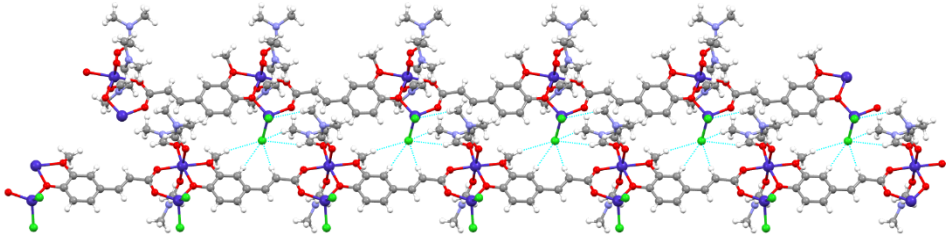

Figure 4.6. Weak interactions (light blue) involving adjacent polymeric chains.

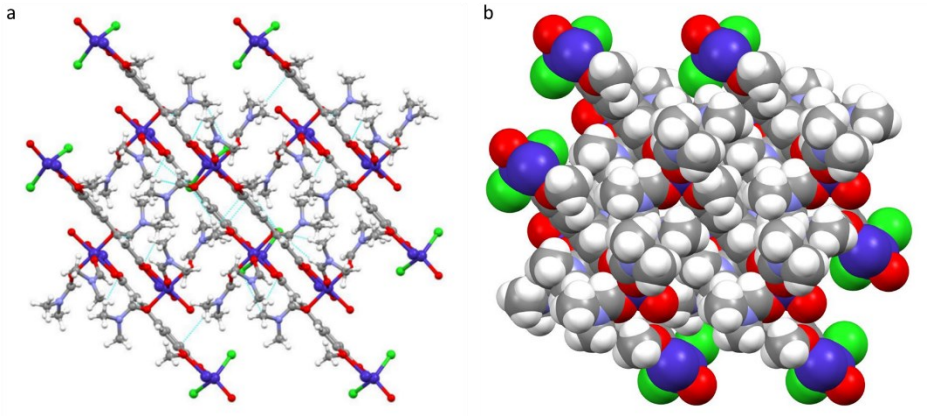

Figure 4.7. Framework of CG3: a) packing along b axe and interchain weak interactions (light blue); b) view of the framework in "space fill" mode which highlights the total absence of voids.

From literature, there are few examples in which the bridging nature of ferulic acid is exerted through coordinative bonds with both the carboxylic and guaiacol functions. Kitanovski et al., for example, report the formation of copper complexes via the carboxylate group of ferulic acid, while phenolate groups participate in the formation of a H-bonding network[7].

With our procedure, we were instead able to obtain a real polymer in which all the functional groups of ferulic acid participate in the coordination giving an SBU not yet present for Co atom in the Cambridge Crystallographic Database Centre (CCDC).

A similar SBU, with metals characterized by different coordinations, was also obtained by Demir et al. in their PhytoMOF-1 based on Zn and ferulic acid[10]. In this case the framework contains three Zn^{2+} atoms with octahedral, tetrahedral, and trigonal bipyramidal coordination geometry, bridged by two bi-deprotonated ferulic acid molecules.

Attempts to increase the dimensionality of the framework were pursued by using a higher ferulic acid to cobalt chloride molar ratio (trial 2), with the aim to avoid coordination of the chloride anions. However, CG3 was obtained again, although in lower yield (trial 3). The use of modulators, such as 2,2'-bipyridine or isonicotinamide, aimed to isolate molecular species, resulted unsuccessful,

irrespective to the molar ratio employed. In all cases, XRPD analysis revealed the formation of CG3.

Table 4.2. Bond distances and bond angles in CG3

Octahedral Co	**Tetrahedral Co**
Bond distances (Å)	
Co-O (carboxyl) 2.040 (2)	Co-O (carboxyl) 1.961 (2)
Co-O (OH) 2.033 (2)	Co-O (OH) 1.955 (2)
Co-O (OCH_3) 2.169 (2)	Co-Cl 2.232 (15)
Co-O(DMF) 2.083 (2)	Co-Cl 2.240 (18)
Co-O (DMF) 2.071 (2)	
Co-O (DMF) 2.071 (2)	
Bond angles (°)	
O (DMF)-Co-O (DMF) 84.99 (8); 175.16 (8); 90.79 (8)	Cl-Co-Cl 114.30 (7)
O (OCH_3)-Co-O (OH) 77.35 (7)	Cl-Co-O (carboxyl) 107.34 (10)
O (OH)- Co-O (carboxyl) 99.92 (8)	Cl-Co-O (carboxyl) 110.49 (9)
O (OCH_3)-Co-O (carboxyl) 177.25 (7)	Cl-Co-O (OH) 108.54 (9); 109.44 (8)
O (OH)-Co-O (DMF) 90.83 (8); 166.64 (7); 92.76 (8)	O-Co-O 106.42 (9)
O (OCH_3)-Co-O (DMF) 89.20 (11); 89.83 (7); 88.41 (11)	
Co(Td)-O(OH)-Co(Oh) 118.79 (10)	

Table 4.3. Crystal data and structure refinement for CG3.

Identification code	CG3
Empirical formula	$C_{19}H_{29}Cl_2Co_2N_3O_7$
Formula weight	600.21
Temperature/K	150.03
Crystal system	monoclinic
Space group	$P2_1$
a/Å	9.012(9)
b/Å	13.548(11)
c/Å	10.975(12)
α/°	90
β/°	111.20(2)
γ/°	90
Volume/Å^3	1249(2)
Z	2
ρ_{calc}g/cm^3	1.596
μ/mm^{-1}	1.585
F(000)	616.0
Crystal size/mm^3	0.04 × 0.03 × 0.02
Radiation	MoKα (λ = 0.71073)
2Θ range for data collection/°	4.848 to 59.482
Index ranges	-12 ≤ h ≤ 12, -18 ≤ k ≤ 18, -15 ≤ l ≤ 15
Reflections collected	46619
Independent reflections	7088 [R_{int} = 0.0305, R_{sigma} = 0.0251]
Data/restraints/parameters	7088/1/305
Goodness-of-fit on F^2	1.060
Final R indexes [I>=2σ (I)]	R_1 = 0.0224, wR_2 = 0.0527
Final R indexes [all data]	R_1 = 0.0243, wR_2 = 0.0534
Largest diff. peak/hole / e Å^{-3}	0.45/-0.40
Flack parameter	0.027(3)

CG3 from mechanochemistry

Mechanochemistry is an important alternative synthetic route for the obtaining of coordination polymers[15]. It usually allows to reach highest yields using greener conditions than the usual solvothermal synthesis because reactions can be conducted with few amounts of solvent or even in solventless conditions[15,16]. Furthermore, among the advantages of mechanochemistry there are also the possibility to obtain huge amount of product with very short reaction times[16]. In the attempt to obtain CG3, a synthesis was before conducted using ferulic acid.
The mechanochemical reaction between ferulic acid and cobalt chloride in a 1:2 molar ratio was conducted at 500 rpm for 1 h. The reaction did not lead to the formation of CG3. Through IR spectrophotometry the presence of ferulic acid as main component was in fact evidenced (figureS4.4).
For this reason, we tried to use an activated form of the ligand, under the form of ammonium salt, obtained from ferulic acid for reaction with ammonia vapour. The NMR spectra of ferulic acid and of the salt are shown in figures S4.2 and S4.3 in “Supporting Information”. The reaction was carried out under the same experimental conditions applied in the first experiment. From the comparison with the CG3 diffractogram calculated from the solid-state structure it was possible to confirm the formation of the coordination polymer in 95% yield, although featured by a reduced crystallinity (figure 4.8).

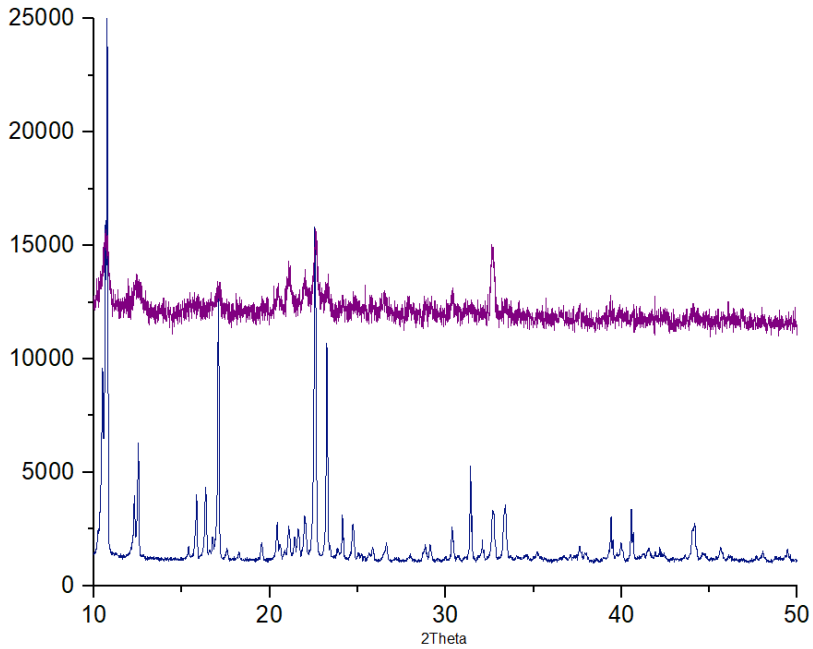

Figure 4.8. XRPD of CG3 from solvothermal synthesis (dark blue trace) and from mechanochemistry (dark purple trace).

Further characterization of CG3

Elemental analysis

Elemental analysis was conducted on the sample deriving from solvothermal synthesis. The results are reported in table 4.4, and perfectly correspond to the formula Co_2(fer)Cl_2·3DMF.

Table 4.4. Elemental analysis of CG3

	%C	**%H**	**%N**
% calculated	38.02	4.87	7.00
% from analysis	38.16	4.92	7.27

Thermogravimetry analysis

The analysis was carried out after vacuum drying of the crystals at room temperature for about 5 hours, to remove any trace of physically adsorbed DMF and reveals a weight loss of 36.66%, between 108 and 246°C, corresponding to the three coordinated DMF molecules (expected value = 36.54%); thermal decomposition occurred at about 300°C, as can be inferred from figure 4.9, and it can be imputed to decarboxylation of the COOH group or HCl elimination.

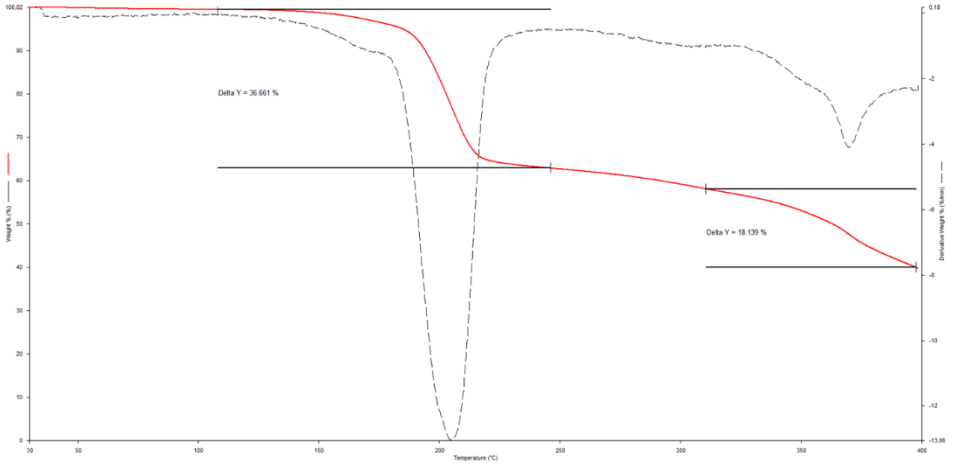

Figure 4.9. TGA of CG3 crystals.

CG3 moisture exposure

As often reported in literature, coordination polymers containing Co(II) tend to change colour through hydration de-hydration processes[17,18]. In several cases the transition process reveals to be reversible. At the basis of this phenomenon there is a change in the coordinative environment of the Co atom that leads to a change in the d-orbital energy level during the hydration-dehydration processes[18].
The same phenomenon was observed by exposing CG3 crystals to air (figure 4.10). The presence of twinned crystals under the form of agglomerates made the process particularly long (more than one month). However, the process is

significantly faster when involving single crystals. The process is accompanied by loss of crystallinity and a prolonged exposure (about three months) causes complete amorphization.

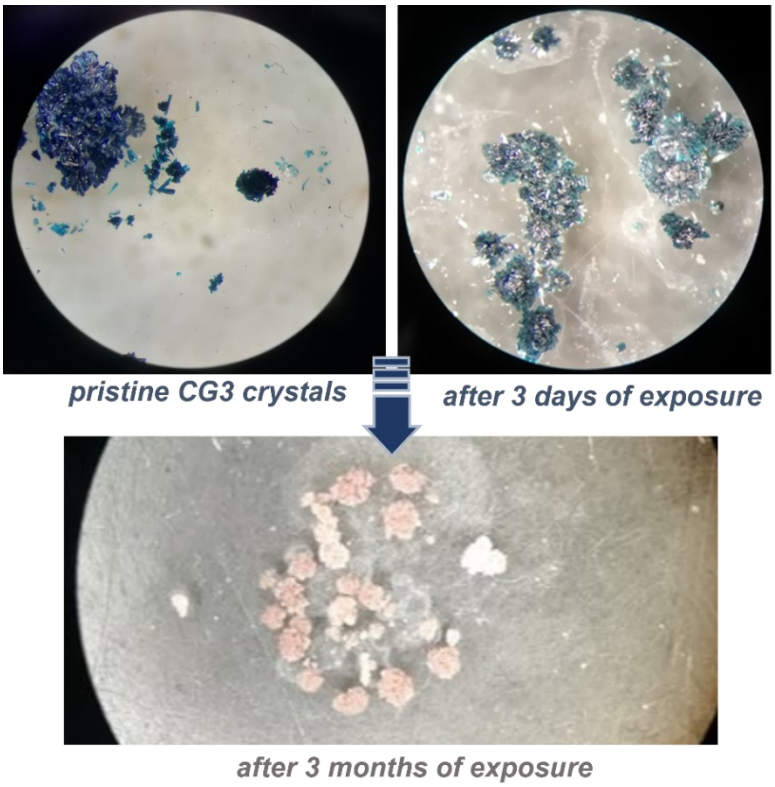

Figure 4.10. CG3 crystals behaviour upon prolonged exposure to air.

With the attempt to structurally characterize the new pink crystals, further trials were conducted on native CG3 crystals.

Further exposure experiments

In figure 4.11a the monitoring of a single CG3 crystal exposed to air up to 11 days is reported. After 4 days the crystal is only partially pink (figure 4.11b), while it becomes completely pink within 11 days (figure 4.11c). The crystal agglomerates maintain a partial blue colour, to indicate a slower kinetic for the more inaccessible crystals (see figure 4.11c).

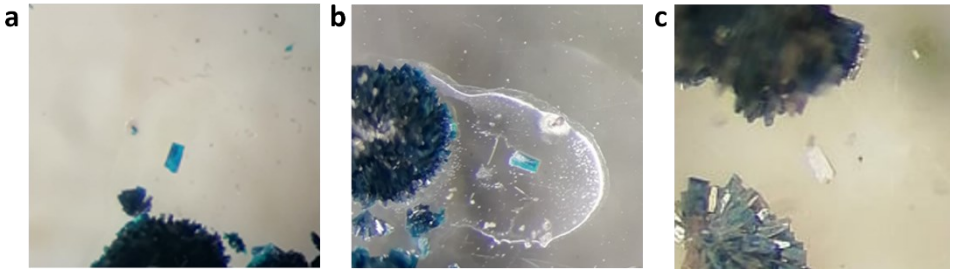

Figure 4.11. Exposure to air of a single CG3 crystal a) after 2 days, b) after 4 days, and c) after 11 days.

Pink crystals were suitable for single crystal X-ray diffraction analysis and were identified as cobalt dichloride hexahydrate, where four out of the six water molecules are coordinated to the metal ion, as can be inferred from figure 4.12.
The formation of the inorganic specie after exposure to air led us to hypothesize a process of hydrolysis of the coordination polymer during which together with the formation of cobalt chloride hydrate also an unknown specie with hypothetical formula CoL is obtained.

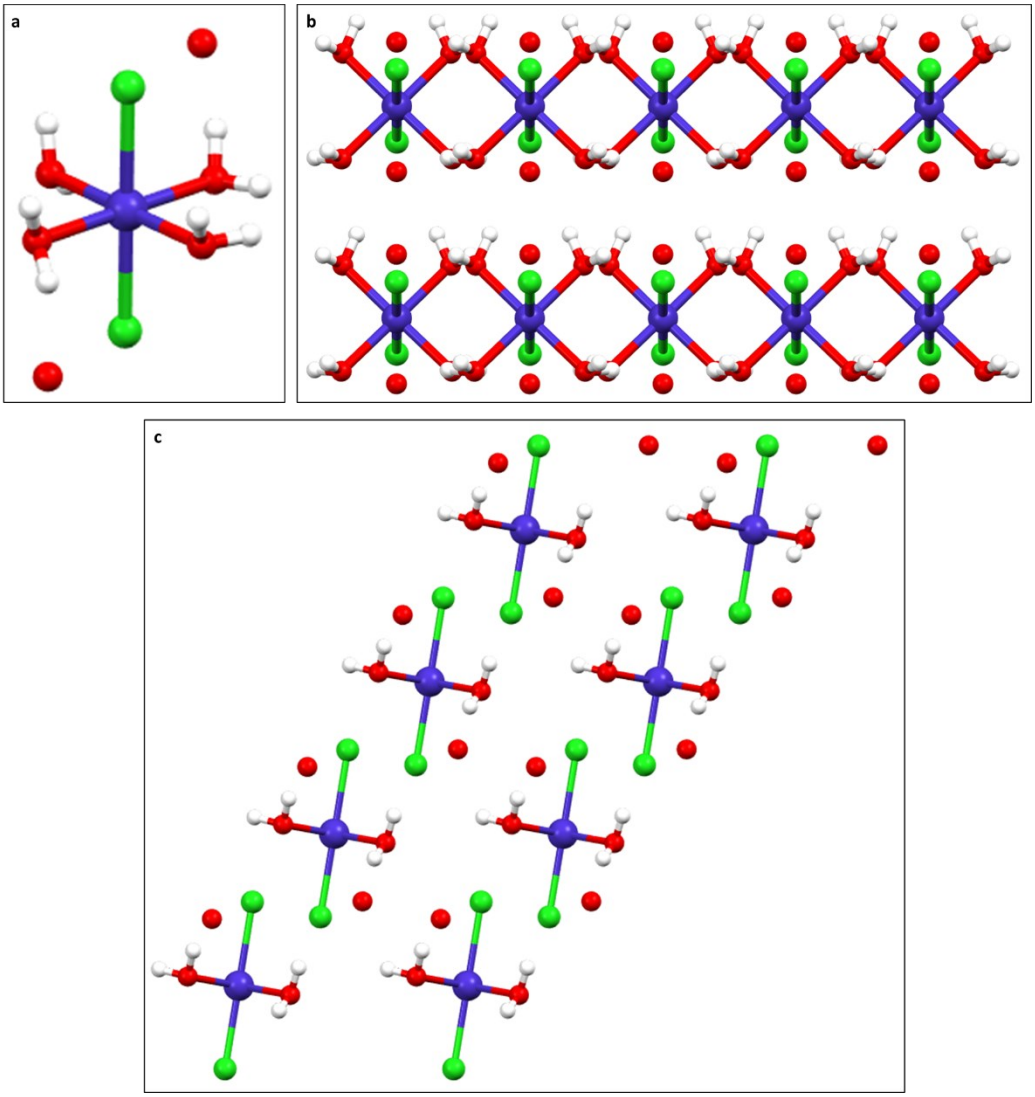

Figure 4.12. Solid state structure of the pink crystals that were identified as cobalt dichloride hexahydrate of formula $[Co(H_2O)_4Cl_2]\cdot 2H_2O$: a) coordination sphere of cobalt; the two uncoordinated water molecules are indicated as red spheres; b) packing along crystallographic axis a; c) packing along crystallographic axis b

Exposure of microcrystalline CG3

Experiment 1

CG3 crystals, after grinding, were exposed to air for 15 days.
Figure 4.13 shows the colour changes undergone by the powders within 15 days. During the first two days no appreciable changes were noted (figure 4.13a), except the evaporation of DMF that has probably disfavoured the adsorption of moisture. After three days of exposure (figure 4.13b) the colour change becomes to be appreciable, and after 7 days the solid appears almost completely turned pink (figure 4.13c). As can be seen from figure 4.13d, after 15 days the powder is homogeneously pink (see the enlargement of figure 4.13e).

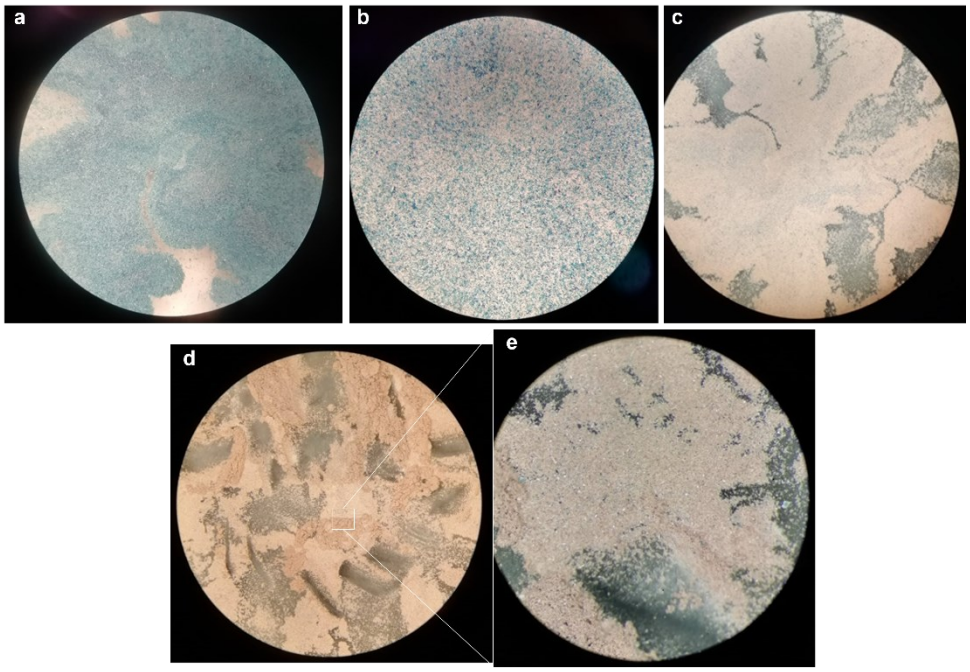

Figure 4.13. Exposure to air of microcrystalline CG3: a) after 2 days, b) after three days, c) after 7 days, d) after 15 days, e) enlargement of the sample after 15 days.

The pink powder was analysed by means of XRPD, and the diffractogram compared with the experimental pattern of CG3 and with the calculated pattern of $[CoCl_2 \cdot (H_2O)_4] \cdot 2H_2O$, (figure 4.14).
Although the low crystallinity of the pink powders does not allow an easy comparison, a good match with the signal featuring the inorganic phase was found. Unfortunately, no signals attributable to the hypothesized new species CoL were clearly visible, that must then correspond to an amorphous phase.

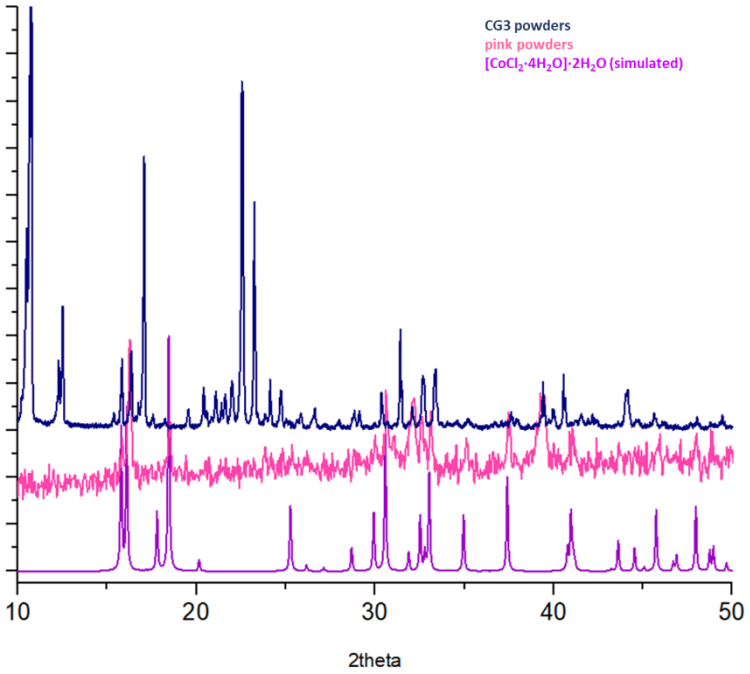

Figure 4.14. X-ray powder diffraction of $[CoCl_2 \cdot 4H_2O] \cdot 2H_2O$ (simulated pattern from Mercury, light purple, on the bottom), pink powders (pink trace, in the middle), and CG3 powders (blue trace, on the top).

Experiment 2

In the second experiment, CG3 crystals were dried overnight under vacuum prior to be ground. CG3 powders were placed in a XRPD sample holder and colour change was monitored by diffraction analysis for 21 days. A further collection was

repeated after 6 months (due to the lockdown imposed by Covid-19 pandemic) powders were analysed again.
Figure 4.15 shows the diffractograms of CG3 powders (dark blue), after 17 days (blue), after 21 days (light blue) and after about 6 months (lilac) from exposure. The pattern of pink powders from experiment 1 is also shown for comparison.
Surprisingly, the hydration process took completely different times compared to experiment 1. From figure 4.15 we can appreciate a progressive lowering of some peaks passing from CG3 powders and powders after 6 months, but there is not match with the pattern registered in experiment 1 (pink trace). The different timing may be due to the different relative humidity of the room in which the experiments were carried out. CG3 is sensitive to moisture, but its behaviour changes considerably according to the environmental conditions, and this did not allow a complete understanding of the hydration process.

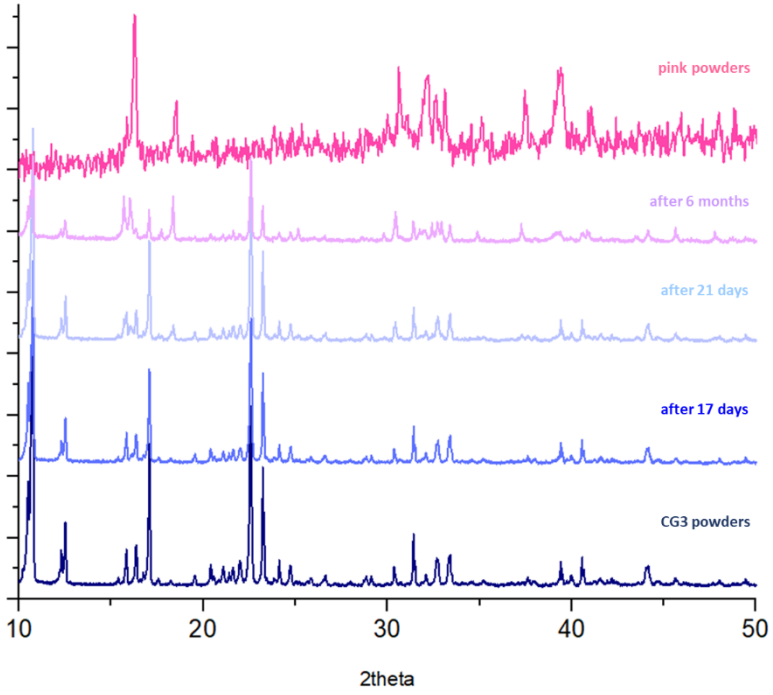

Figure 4.15. X-ray powder diffraction of CG3 powders, dark blue, CG3 powders exposed to air after 17 days, blue, after 21 days, light blue, after about 6 months, lilac, and pink powders from experiment 1, pink.

Then, we can conclude that the hydration process of CG3 leads to pink crystals of cobalt chloride hexahydrate and an amorphous phase corresponding to a not yet defined CoL species. Further studies aimed at defining the nature of this species are in progress.

Other attempts of exposure

In the attempt to have a more accurate control of the hydration process, two other tests were carried out.

Soaking of CG3 crystals in water

The advantage of this test lies in the possibility of having a more homogeneous situation than just exposure to air which, as we have seen, is not effective enough to have a single phase.
CG3 crystals were washed with fresh DMF and subsequently dried under vacuum to remove the DMF in excess. Dried CG3 crystals were soaked in 2mL of water, figure 4.16 reports the process.

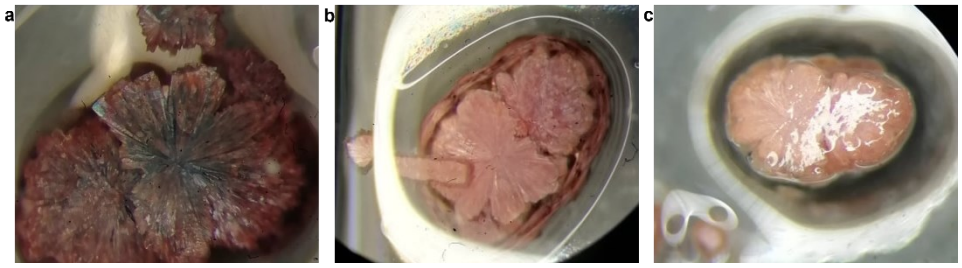

Figure 4.16. CG3 crystals soaked in water a) after 1 minute, b) after 40 minutes, and c) after 5 hours.

In figure 4.16a, we can see the diffusion of water molecules from the external boundaries of a CG3 crystals agglomerate. After 40 minutes (figure 4.16b) the agglomerate is completely pink, with reduced crystallinity. 5 hours of soaking (figure 4.16c) lead to visually faded crystals.

The solid material after water soaking was dried under vacuum for 2 hours and analysed with IR spectroscopy. Figure 4.18 shows IR spectra of CG3 after water soaking and CG3 after exposure in air.

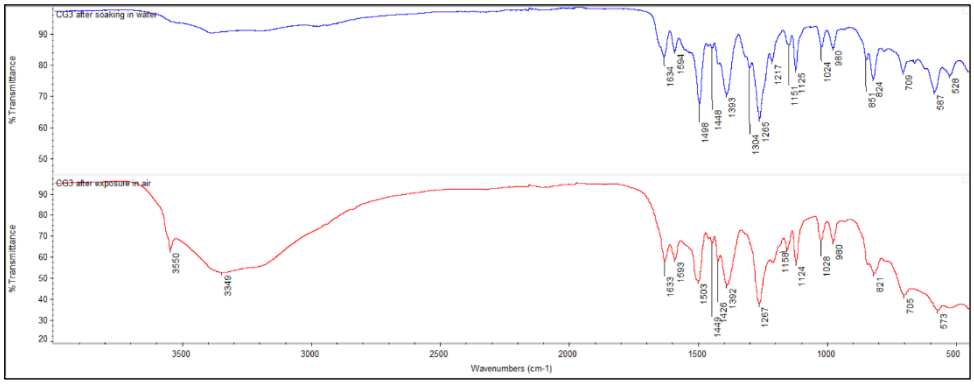

Figure 4.17. IR spectra of CG3 after water soaking (blue, on the top) and CG3 after exposure in air (red, on the bottom).

After 5 hours of water soaking the solid material was collected and dried under vacuum for 2 hours. This step was not conducted in the case of powder exposed to air, this caused the presence of a broader OH band in CG3 after exposure in air. Figure 4.17 reveals a very similar profile between the two spectra, despite the soaking in water may dissolve the cobalt chloride phase.

IR spectrum of $CoCl_2 \cdot 6H_2O$ (see figure S4.5) presents bands at around 3520 cm^{-1}, 3386 cm^{-1}, 3170 cm^{-1}, 1599 cm^{-1}, 787 cm^{-1}, 531 cm^{-1} and 447 cm^{-1}. In the spectra of CG3 after water treatments we can notice the presence of bands at about 1600 cm^{-1} that can be related to the presence of cobalt chloride phase.

Furthermore, by the comparison of IR spectra of CG3 after water soaking and ferulic acid (figure 4.18), we can notice a not perfect match between the two spectra thus confirming the possible presence of an unknown Co-L phase.

Unfortunately, the soaking treatment led to an amorphous material and XRPD analysis was not possible.

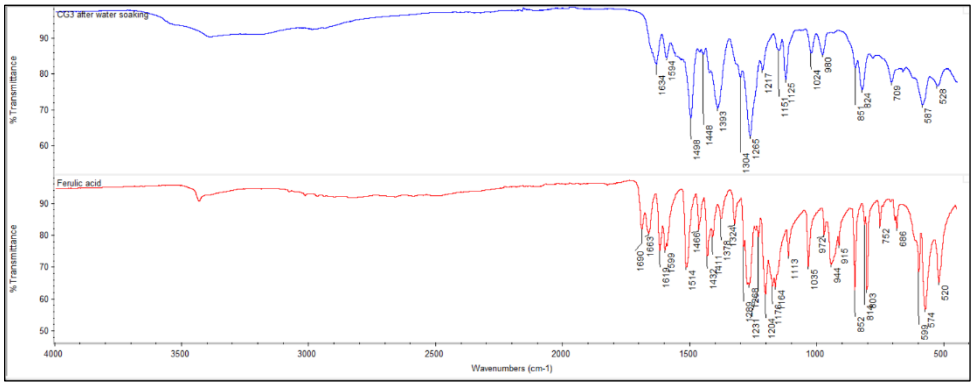

Figure 4.18. IR spectra of CG3 after water soaking, on the top, and ferulic acid, on the bottom.

CG3 exposure to water vapour

To improve the control over the hydration process, a second attempt was to expose both crystals and powder of CG3 to water vapour.
As reported in figure 4.19a, the crystals and powders of CG3 were collected in vials and on microscope slides and then placed in a dryer with a beaker containing water (not shown in the figure). The application of the vacuum for a few minutes allowed to saturate the dryer with the water vapours. After only 24hours both samples were turned to pink, figure 4.19b.

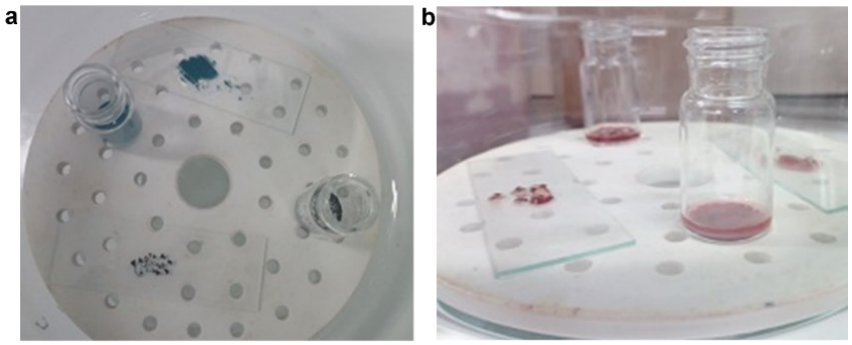

Figure 4.19. Experimental setting for water vapour exposure of CG3, a) CG3 crystals and powders are collected in vials and on microscope slides b) after 24 hours of exposure, all samples have completely changed colour.

Figure 4.20 shows the XRPD pattern of pristine CG3, CG3 after air exposure, the simulated pattern of cobalt dichloride and the one of CG3 after adsorption of water vapours.

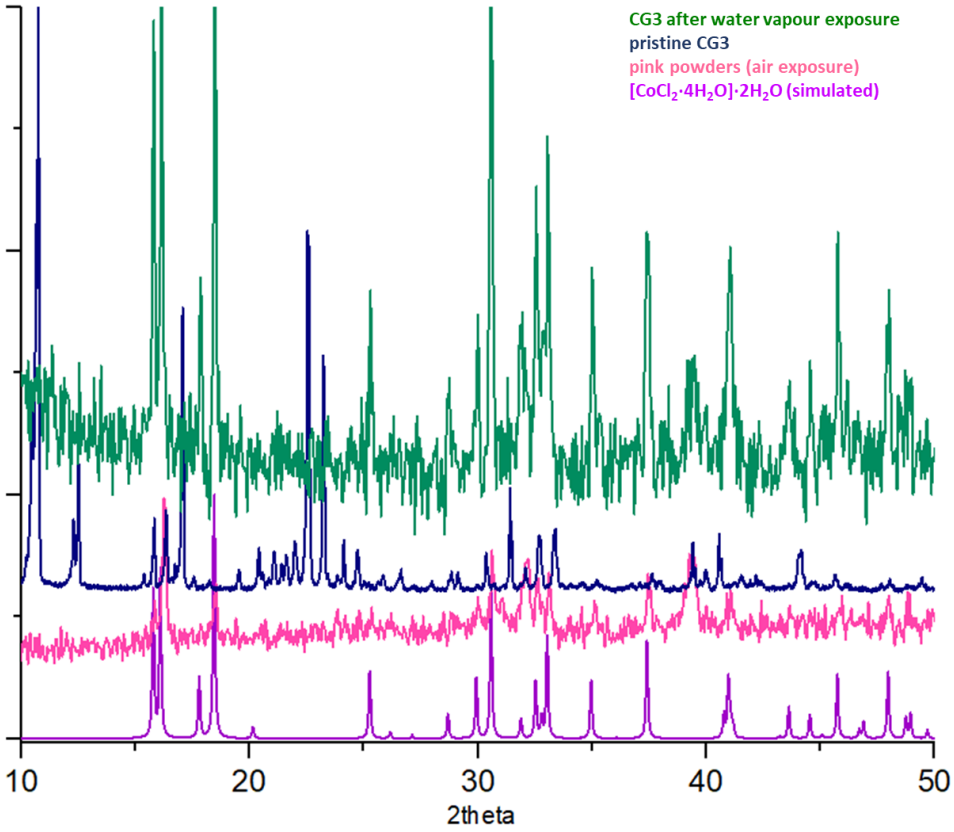

Figure 4.20. XRPD of CG3 after water vapour exposure (green-the first from the top), pristine CG3 (blue-the second), CG3 after air exposure (pink-the third) and simulate pattern of cobalt chloride phase (purple-on the bottom).

Comparing the two patterns after water exposure we can notice that the use of water vapours led to a slightly more crystalline product. However, the main peaks come from inorganic cobalt chloride confirming that hydrolysis leads to an unknown amorphous species containing the organic ligand.

Conclusions

Synthetic screening involving lignin-inspired hydroxycinnamic ligands and different metal salts did not lead to the formation of many crystalline species. From the solvothermal synthesis between ferulic acid and cobalt chloride hexahydrate, however, the coordination polymer CG3 was obtained in the form of blue prismatic crystals. The intriguing SBU featuring this product contains a tetrahedral and an octahedral cobalt atom, bridged by the carboxylate, phenolate and methoxy groups of a bideprotonated ferulate dianion. Although ferulic acid is not featured by a linear geometry, as usual for the most used ditopic ligands for the synthesis of coordination polymers, it shows the ability to use all its donors to bridge two different metal nuclei, giving rise to a rather intriguing SBU.

Exposed to air CG3 changes from blue to pink following a hydration process that has been monitored by both single crystal and powders. The structural analysis of the pink crystals, however, revealed the formation of a completely inorganic specie based on cobalt chloride. The low crystallinity of the CG3 powders exposed to air and the high dependence of the process on the environmental humidity conditions did not allow to fully understand whether it is possible to isolate a crystalline hydrated phase of CG3. To understand this, the soaking of CG3 crystals in water and exposure of the same to water vapours were also carried out, but both methods failed to give conclusive results.

Anyway, what we can conclude is that the hydrolysis process took place only on the tetrahedral cobalt giving the isolated species $[Co(H_2O)_4Cl_2]\cdot 2H_2O$. This is because no signals of free ferulic acid were observed in the IR spectrum of pink powder, thus confirming that a Co-ferulate species is present. Furthermore, this species is most likely amorphous as indicated by the absence of new peaks in the XRPD monitoring.

References

1. Merdy, P., Guillon, E., Aplincourt, M. & Duomonceau, J. Interaction of metallic cations with lignins. Part 1: Stability of iron (III), manganese (II) and copper (II) complexes with phenolic lignin model compounds: coumaric, ferulic and sinapic acids and coniferyl alcohol. *J. Chem. Res. - Part S* **05**, 76–77 (2000).

2. Kalinowska, M. *et al.* Spectroscopic (FT-IR, FT-Raman, 1H, 13C NMR, UV/VIS), thermogravimetric and antimicrobial studies of Ca(II), Mn(II), Cu(II), Zn(II) and Cd(II) complexes of ferulic acid. *Spectrochim. Acta - Part A Mol. Biomol. Spectrosc.* **122**, 631–638 (2014).

3. Yang, R. & Van Den Berg, C. M. G. Metal complexation by humic substances in seawater. *Environ. Sci. Technol.* **43**, 7192–7197 (2009).

4. Linnik, P. N. Complexation as the most important factor in the fate and transport of heavy metals in the Dnieper water bodies. *Anal. Bioanal. Chem.* **376**, 405–412 (2003).

5. Ads, E. N., Nada, A. M. A. & El-Masry, A. M. Use and evaluation of lignin as ion exchangers. *J. Korean Chem. Soc.* **55**, 86–91 (2011).

6. Nada, A. M. A., Kassem, N. F. & Mohamed, S. H. Characterization and properties of ion exchangers produced from lignin precipitated after peroxyacid pulping. *BioResources* **3**, 538–548 (2008).

7. Kitanovski, N., Pevec, A. & Kozlevčar, B. Copper(II) coordination compounds with ferulic acid. *Polyhedron* **28**, 3642–3646 (2009).

8. Sharma, R. P., Kumar, S., Kumar, J., Venugopalan, P. & Aree, T. First structural evidence of biologically important dinegative ferulate ion: Synthesis, characterization, single crystal X-ray structure and DFT calculation of [Cu(en)2(H2O)2](fer). *Polyhedron* **126**, 245–251 (2017).

9. Spekreijse, J., Inge, A. K. & Öhrström, L. Lignin Based Molecular Materials – a Zinc Vanillate with a Hydrogen Bonded 4- and 8-connected Net with a New Topology. *Isr. J. Chem.* **58**, 1127–1130 (2018).

10. Demir, S., Merve Çepni, H., Topcu, Y., Hołyńska, M. & Keskin, S. A phytochemical-containing metal–organic framework: Synthesis,

characterization and molecular simulations for hydrogen adsorption. *Inorganica Chim. Acta* **427**, 138–143 (2015).

11. Li, F. *et al.* Encapsulation of pharmaceutical ingredient linker in metal-organic framework: Combined experimental and theoretical insight into the drug delivery. *RSC Adv.* **6**, 47959–47965 (2016).

12. Zhou, E. H. *et al.* Photocatalytic degradation of organic dyes by a stable and biocompatible Zn(II) MOF having ferulic acid: Experimental findings and theoretical correlation. *J. Mol. Struct.* **1149**, 352–356 (2017).

13. Lai, J., Niu, W., Luque, R. & Xu, G. Solvothermal synthesis of metal nanocrystals and their applications. *Nano Today* **10**, 240–267 (2015).

14. Kaufman, A., Afshar, C., Rossi, M., Zacharias, D. E. & Glusker, J. P. Metal ion coordination in cobalt formate dihydrate. *Struct. Chem.* **4**, 191–198 (1993).

15. Friščić, T. *et al.* Ion- and liquid-assisted grinding: Improved mechanochemical synthesis of metal-organic frameworks reveals salt inclusion and anion templating. *Angewandte Chemie - International Edition* vol. 49 712–715 (2010).

16. Friščić, T., Halasz, I., Štrukil, V., Eckert-Maksić, M. & Dinnebier, R. E. Clean and efficient synthesis using mechanochemistry: Coordination polymers, metal-organic frameworks and metallodrugs. *Croat. Chem. Acta* **85**, 367–378 (2012).

17. Chisca, D. *et al.* From pink to blue and back to pink again: Changing the Co(II) ligation in a two-dimensional coordination network upon desolvation. *CrystEngComm* **18**, 384–389 (2016).

18. Ke, S. Y. *et al.* Self-assembly of four coordination polymers in three-dimensional entangled architecture showing reversible dynamic solid-state structural transformation and color-changing behavior upon thermal dehydration and rehydration. *Cryst. Growth Des.* **14**, 4011–4018 (2014).

Characterization techniques

This chapter resumes all the details of the characterization techniques used in this thesis.

X-ray powder diffraction (XRPD):
Data were collected on a Thermo Scientific ARL X'TRA diffractometer in theta−theta Bragg−Brentano geometry with Cu Kα radiation.

XRPD data were collected on lignin@Cu10%_MILL milled at different time scales, namely 15, 30, and 60 min, in Bragg−Brentano (BB) geometry with Cu Kα radiation on a Rigaku Smartlab XE diffractometer equipped with a solid-state Hypix3000 2D detector. To increase the limit of detection (LoD) of any crystalline impurity, data were collected with 5° Soller slits and variable vertical slits, which guarantee the same volume of sample under the beam along the measurement. Data were then normalized to the counting time. To evaluate the content of the materials, Pawley refinements were performed against cell parameters reported in the literature.

XRPD analysis on lignin@brochantite10%_WET after formulation was performed on a Rigaku SmartLab XE diffractometer equipped with a CBO parabolic mirror (parallel beam, Cu Kα) and a 2D HyPix3000 solid state detector. Data were collected overnight in the 3−80 2Θ (deg) range in transmission geometry. The sample was loaded into a 1.0 mm glass capillary and aligned against the beam position (vertical direction) before data acquisition.

The inorganic phases of the hybrid materials lignin@metals were identified with the software Match!, version 1.9g.

XRPD analysis on coordination polymer CG3 ($[Co_2(fer)Cl_2]\cdot 3DMF$) was conducted on a Rigaku Smartlab XE diffractometer in theta−theta Bragg−Brentano geometry. Soller with 5° were used both on the incident beam and on the diffracted beam. CG3 powders were placed on a sample holder in microcrystalline silicon (Zero Background). Sample is automatically aligned along the vertical direction to minimize sample displacement. The diffraction data are collected with the Hypix3000 2D solid state detector. The data are collected using the Rigaku SmartLab software.

Single Crystal X-ray Diffraction (SC-XRD):

SCXRD (Single Crystal X-ray Diffraction) analysis was performed on single crystal samples on a Bruker D8 Venture diffractometer equipped with a kappa goniometer and an Oxford cryostream. Low temperature data collections were performed under nitrogen flux. Microfocused MoKa radiation was used for the data collection. Lorentz polarization and absorption correction were applied. Data were reprocessed using APEX v3 software. Structure was solved by direct methods using SHELXT and refined by full-matrix least-squares on all F2 using SHELXL implemented in Olex2.2. Anisotropic displacement parameters were refined except for hydrogen atoms. Chiesi Farmaceutici s. p. a. is acknowledged for the use of D8 Venture equipment.The images of the structures were made using Mercury software (https://www.ccdc.cam.ac.uk/Community/csd-community/freemercury/).

Inductively Coupled Plasma - Atomic Emission Spectroscopy (ICP-AES):

The metal content in hybrid materials was determined by means of a JY 2501 of the HORIBA Jobin Yvon, ULTIMA2 model. Solid samples were treated as reported: 100 mg of solid sample were suspended in 5 mL of HNO3 65% and 1 mL of H2O2 30%, then digested in a Milestone microwave MLS-1200 MEGA (digestion sequence: 1 min at 250-Watt, 1 min at 0 Watt, 5 min at 250 Watt, 5 min at 400 Watt, 5 min at 650 Watt, 5 min of cooling). The solutions were diluted to 50 mL with bi-distilled water and analysed by using an emission spectrometer JY 2501 with coupled plasma induction in radial configuration HORIBA Jobin Yvon (Kyoto, Japan), ULTIMA2 model. Instrumental features: monochromator Model JY 2501; focal length 1 m; resolution 5 pm; nitrogen flow 2 l/min. ICP source: nebulizer Meinhard, cyclonic spraying chamber; argon flow 12 l/min; wavelengths range 160-785 nm; optical bench temperature 32 °C. The wavelength used for quantitative analysis was chosen by examining the emission line with greater relative intensity, ensuring that there was no spectral interference with the Argon emission lines. Acquisition parameters for lignin@Cu materials: wavelength Cu (nm): 224.700; Voltage (V): 580; gain: 100. Acquisition parameters for lignin@Fe materials: wavelength Fe (nm): 238.204; Voltage (V): 700; gain: 10. The quantitative analysis was performed after the acquisition of a calibration line using standard solutions in HNO3 10%, to simulate the final acidity of the samples; the concentration range of the standards varied from 1 mg/L to 100 mg/L. Data

acquisitions and processing were performed using the ICP JY v 5.2 software (Jobin Yvon). Measurements were performed in triplicate.

Transmission electron microscopy (TEM) and Energy dispersive X-ray spectrometer (EDS):

Transmission electron microscopy (TEM) was carried out using a FEI TECNAI F20ST microscope operating at 200 kV and equipped with an EDAX PV9761-SUTW energy dispersive X- ray spectrometer (EDS). Scanning transmission (STEM) pictures were recorded using a high angle annular dark field (HAADF) detector: in this imaging mode, the intensity I of an image point is proportional to Z1.7t, where Z is the mean atomic number and t is the thickness of the specimen. The specimens were prepared by grinding the powders in isopropyl alcohol. The solution was subsequently sonicated for 15 min and drop casted on a holey carbon film heated at 50 °C.

Scanning Electron microscopy (SEM) and Energy dispersive X-ray spectrometer (EDS):

SEM analyses were performed on a field emission scanning electron microscope Hitachi FE-SEM (model SU5000) while EDS was carried out with Thermo Scientific NORAN System 7 with an energy resolution (HWHM) ≤ 126eV (Mn-Kα @ 10 000 count per second) and using PathFinder X-ray Microanalysis Software. Images are taken in high vacuum mode. Morphological analyses were performed detecting the signal of secondary electrons (SE) or of backscattered electron (BSE), operating with an acceleration voltage of 2.0kV. Spectra were acquired at 15kV.

Dynamic Light Scattering (DLS)

DLS analyses were conducted on lignin@cuprite, solargo@cuprite_5% and solargo@cuprite/brochantite samples by means of a Malvern Zetasizer Nano ZSP. Each sample was diluted with deionized water and then subjected to the measure.

Infrared Spectroscopy (IR):

IR spectra were recorded with a Nicolet 5PCFT-IR spectrophotometer equipped with ATR accessory (diamond), range 4000−400 cm−1.

Nuclear Magnetic Resonance (NMR):
NMR experiments on lignins were conducted at Technical Research Centre of Finland Ltd (VTT, Helsinki, Finland).

Liquid state NMR were carried out at room temperature with a Bruker Avance III 500, 5 mm double resonance BBFO probe. All samples were dissolved in d^6-DMSO in an approximate concentration of 100 mg/mL. To assure a good solubilization, samples were left under stirring, overnight before analysis.
^{1}H-NMR spectra were collected with 16 scans, a delay between scans of 1.5 s and 30-degree excitation pulse. While ^{13}C-NMR were conducted using 16 384 scans with 1.5 s of delay between scans and 30-degree excitation pulse. Proton decoupled, pulse sequence with NOE enhancement.
BioPiva; ^{1}H-NMR: 9.8 ppm (Ar-OH), from 8 to 6 ppm (Ar-H), from 3.83 to 3.41 ppm (CH_3 and OCH_3), 2.5 ppm (d^6-DMSO). ^{13}C{^{1}H}-NMR: from 148.29 to 110.08 ppm (Ar C), 60.69 ppm (-(γ)CH_2OH)), 56.08 ppm (OCH_3), 40 ppm (d^6-DMSO).
Acetylated lignin; ^{1}H-NMR: from 8 to 6 ppm (Ar-H), from 3.83 to 3.41 ppm (CH_3 and OCH_3), 2.24 ppm (acetyl groups bound to aromatic rings), 1.92 (acetyl groups linked to aliphatic chain), 2.5 ppm (d^6-DMSO). ^{13}C{^{1}H}-NMR: 170 ppm (C=O of acetyl groups), from 151.53 to 110.76 ppm (Ar C), 56.26 ppm (OCH_3), 20.02 ppm (CH_3 of acetyl groups), 40 ppm (d^6-DMSO).

Solid state ^{31}P-NMR was recorded using a magic angle spinning rate of 10 kHz, 1024 scans with 20s of delay between scans. The experiment was conducted with a direct pulsing, 90-degree excitation pulse. Chemical shift referencing externally via adamantane by setting the low field signal at 38.48 ppm.

Liquid state ^{1}H-NMR on ammonium ferulate, and ^{31}P-NMR on P_LIG were conducted using 400 MHz Bruker Avance III spectrometer with 16 scans for proton and 1160 scans for phosphorous experiments. 10mg of phosphorylated lignin were suspended in 0,6mL of d^6-DMSO. Sample was sonicated and heated for at least 5 minutes.
Ammonium ferulate: ^{1}H-NMR: 7.26 ppm (d, 1H, $^-$OOC-CH=C**H**-), 7.16 (s, 1H, Ar), 6.97 ppm (dd, 1H, Ar), 6.78 (d, 1H, Ar), 6.30 ppm (d, 1H, $^-$OOC-C**H**=CH-), 3.8 ppm (s, 3H, -OCH_3), 2.5 ppm (d^6-DMSO), 3.67 (H_2O).

Gel permeation chromatography (GPC):

Solid lignin samples were dried in the oven at 60°C overnight prior to dissolve about 10-12 mg in 10mL of a 0.1M NaOH solution (up to 1M NaOH solution), then filtered with 0.2µm nylon HPLC filter. Measures were conducted in duplicate by means of Thermo Scientific DIONEX UltiMate 3000 equipped with two detectors: a refractive index detector (RefractoMax520) and a UV detector (Dionex Ultimate 3000 diode array detector at 280nm). The columns were PSS MCX analytical 1000Å and 100000Å and a 0.1M NaOH solution was used as eluent. The system operated at a flow rate of 0.5ml/min and 30˚C. The measurements were conducted with isocratic run for a run time of 50 minutes. Calibration was done for UV-detector (280nm): The PSS-standard, poly(styrenesulfonate)sodium salt, is used with different molar mass (65400,29500,15800, 6430 and 891 Da). Standard samples were dissolved to ultra-pure water with a concentration of 5mg/ml and injection volume 20µL.

Pyrolysis-GC/MS (Py-GC/MS):

Lignin pyrolysis was carried at 600°C temperature using Frontier Lab pyrolizer EGA/Py-3030D connected to an Agilent GC/MS- system consisting of 7890B GC and 5977A MSD. The separation column was a HP-5ms capillary column (30m, 250 µm inner diameter and 0,25µm film thickness) and the GC-parameters the following: injector temperature 250°C, split ratio 1:20, oven program starting from 70°C with 4 minutes isothermal and continuing with a heating rate of 10°C/min until finishing with a 20 min hold time at 300°C final temperature. For MS, the transfer line temperature was 300°C, scan range 40-550m/z and the ionizing voltage 70eV. Software used for instrument control and data processing was Agilent Chemstation. Compounds generated in pyrolysis were identified by comparing the MS-spectra against commercial MS-libraries (Wiley and NIST.)

Elemental analysis:

Elemental analysis was conducted using CHNS Thermo Fisher model FlashSmart.

Thermogravimetric analysis (TGA):

TGA analyses were conducted using a NETZSCH TG 209F1 Libra instrument. About 10 mg of sample was placed in a Al_2O_3 crucible and the heating was conducted under nitrogen from 50°C to 900°C at 10°C/min. The last step consisted in heating from 900°C to 905°Cat 0.5°C/min in oxygen.

TGA analyses of the coordination polymer CG3, $[Co_2(fer)Cl_2]\cdot 3DMF$, was conducted using a NETZSCH TG 209F1 Libra instrument equipped with platinum crucible. The measurement was carried out heating from 25°C to 400°C at 10°C/min under air atmosphere. The heating was only brought up to 400°C to avoid damage to the platinum crucible.

Differential scanning calorimetry (DSC):

DSC analysis was conducted using Mettler Toledo DSC1 STAR System. Around 10mg of sample were heated from 25°C to 105°C with a heating rate of 20°C/min. After 20 minutes at 105°C, the cooling process from 105°C to 25°C takes place at 10°C/min. Subsequently sample is heated again from 25°C to 200°C with 20°C/min. DSC measurements were carried out under nitrogen atmosphere.

Wettability measurements:

Wettability measurements on powder samples were carried out using the force tensiometer Biolin Scientific Sigma 700/701.

The measurements consist in packing the sample according to a precise procedure (shown below) in a glass round rod with radius R = 5,5 mm equipped with a filter on the bottom. Under the hanging sample holder there is a movable stage on which the beaker containing the ultrapure water is placed. The position of the stage can be suitable before starting the measurement so that the sample holder is close to the water level. The stage has a position resolution of 0.015 µm, maximum stoke of 100 mm, an input range of 85 VAC and a frequency of 47-440 Hz. When the measurement starts the sample holder is immersed in water for 0,5 mm and one measurement data per second is recorded. The instrument measures the change in weight caused by the capillarity of the water through the sample. The speed with this process occurs is strictly related to the degree of wettability of the material.

Sample preparation: after a manual grinding 0.2g of sample are placed in the glass round rod. The powder is then packaged by gently tapping the cylinder against the table for one minute. 0.1 g of sample is added, and the tapping procedure is repeated.

Before conducting measurements with water, it is necessary to calculate the constant of the samples using a liquid with low surface tension in such a way to assume that the contact angle of the materials with this solvent is zero. Table XX

reports the constants of the samples analysed in this thesis using n-hexane as solvent.

	BioPiva100	Lignin@brochantite	BioPiva395	Ac-lignin	P_LIG
Constant [mm^5]	0.079288	0.037330	0.008030	0.010400	0.098165

Supporting information

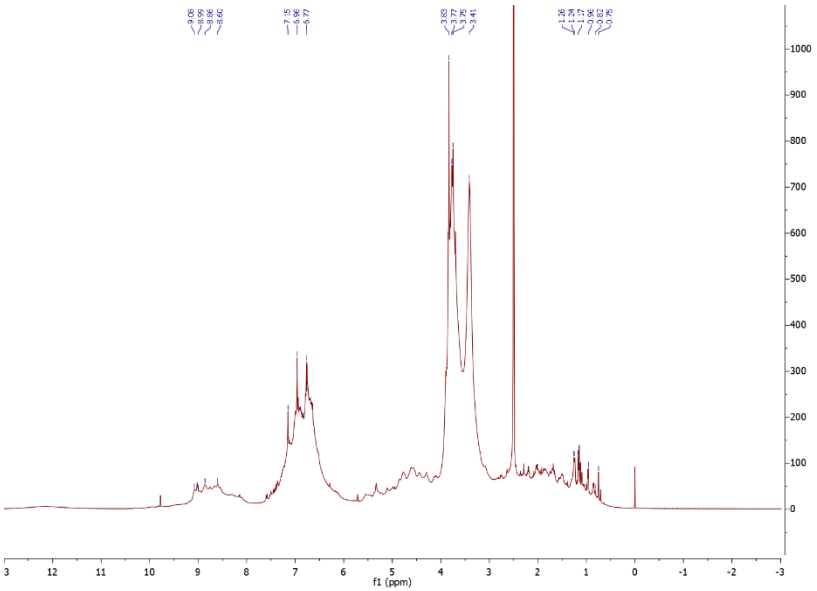

Figure S1.1. ^{1}H-NMR BioPiva395.

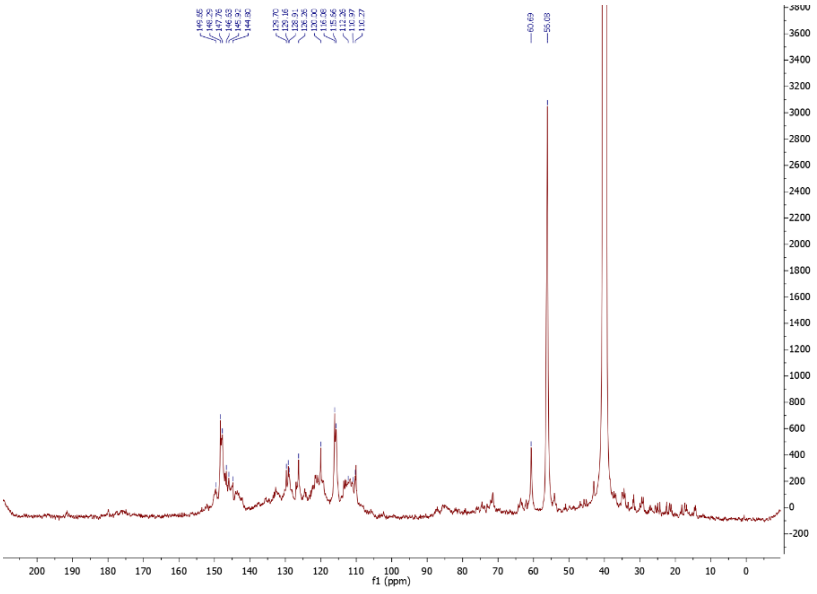

Figure S1.2. ^{13}C{^{1}H}-NMR BioPiva395.

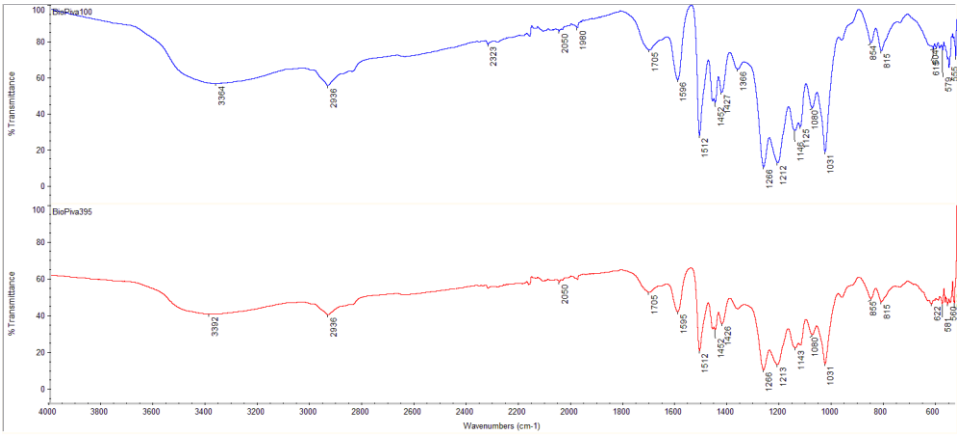

Figure S1.3. IR BioPiva100 and BioPiva395.

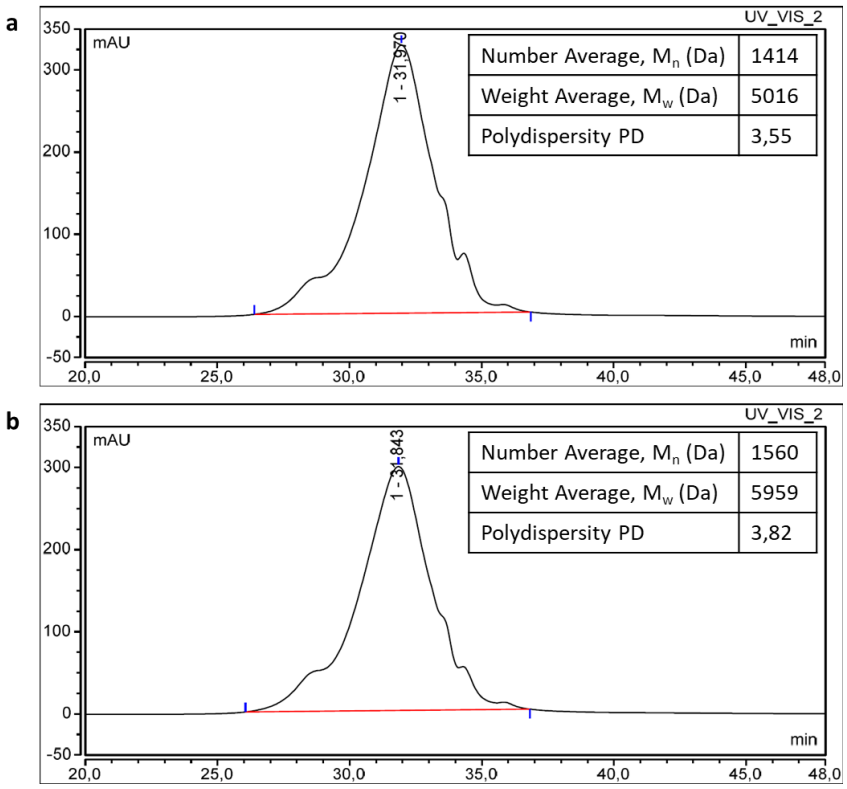

Figure S1.4. GPC analysis of BioPiva100 (a) and BioPiva395 (b).

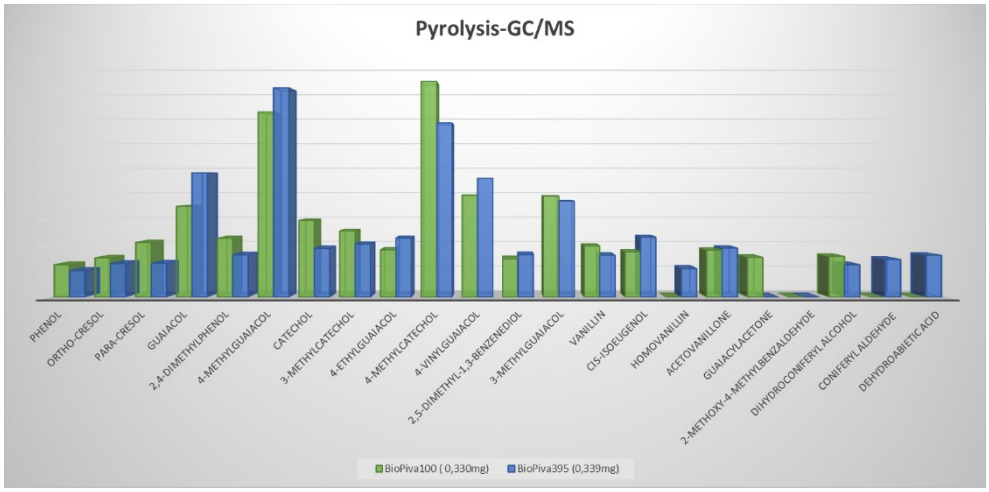

Figure S1.5. Main fragments from pyrolysis-GC/MS of BioPiva100 and BioPiva395. The bars represent the relative area percentages of the single analytes.

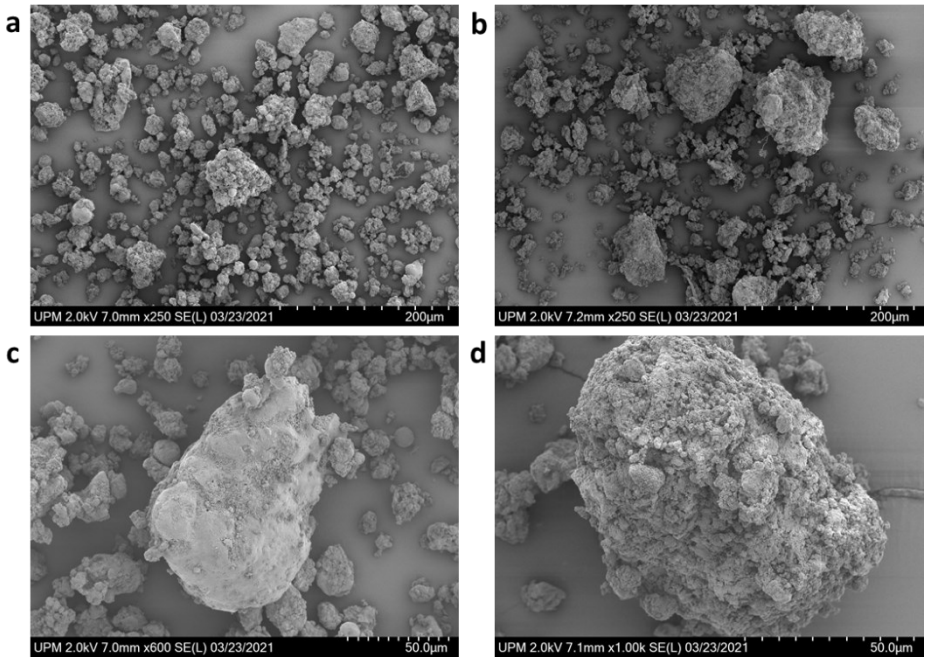

Figure S1.6. SEM images of BioPiva100 (a,c) and BioPiva395 (b,d).

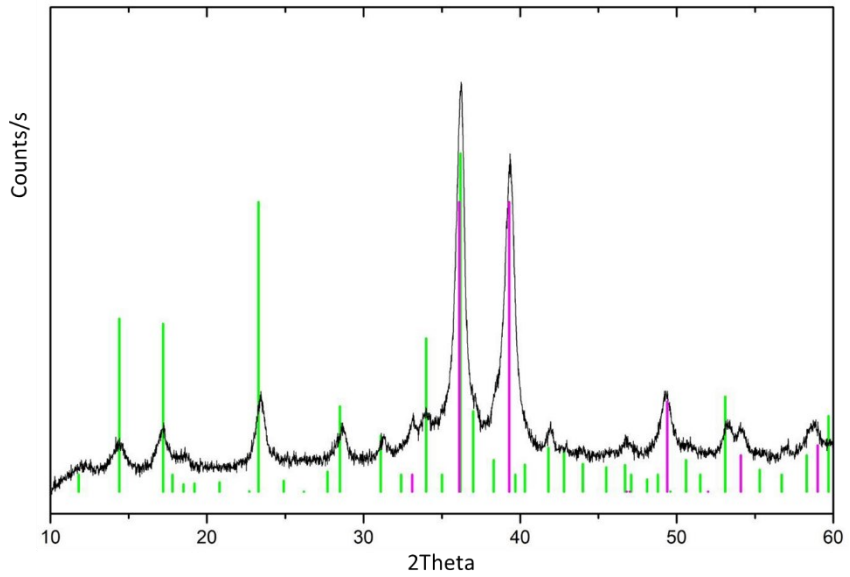

Figure S2.1. Matching between XRPD of CuSO4·5H2O + NaOH (procedure of lignin@brochantite_WET without lignin) and tenorite (CuO) pink peaks, and brochantite $Cu_4(OH)_6(SO_4)$, green peaks.

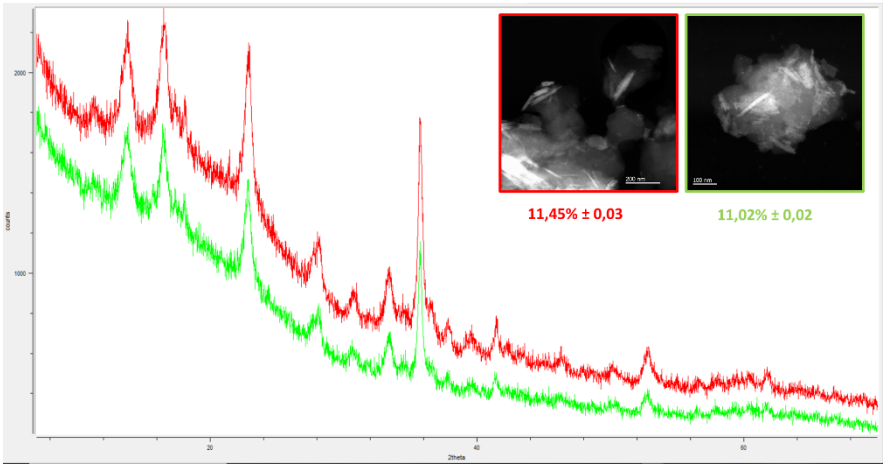

Figure S2.2. Comparison between lignin@brochantite10%_WET materials obtained in 2hours (red) and 24hours (green).

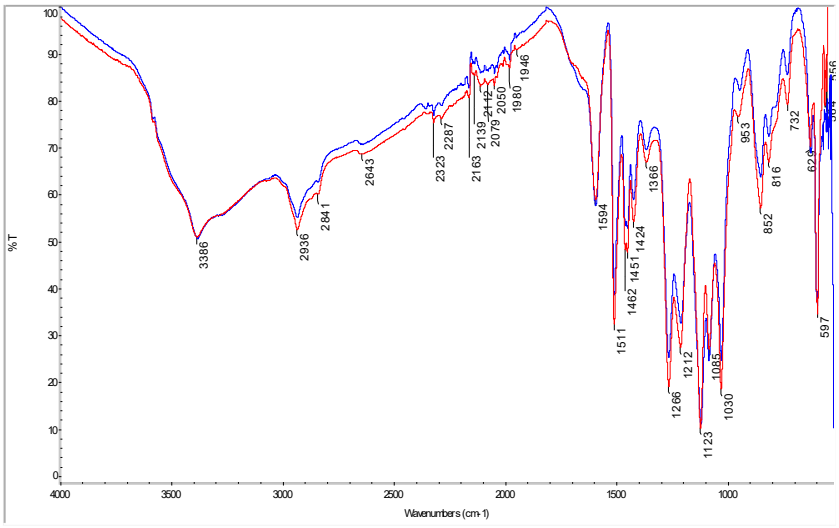

FigureS2.3. IR spectra of lignin@brochantite10%_WET, blue and lignin@brochantite10%_MILL, red

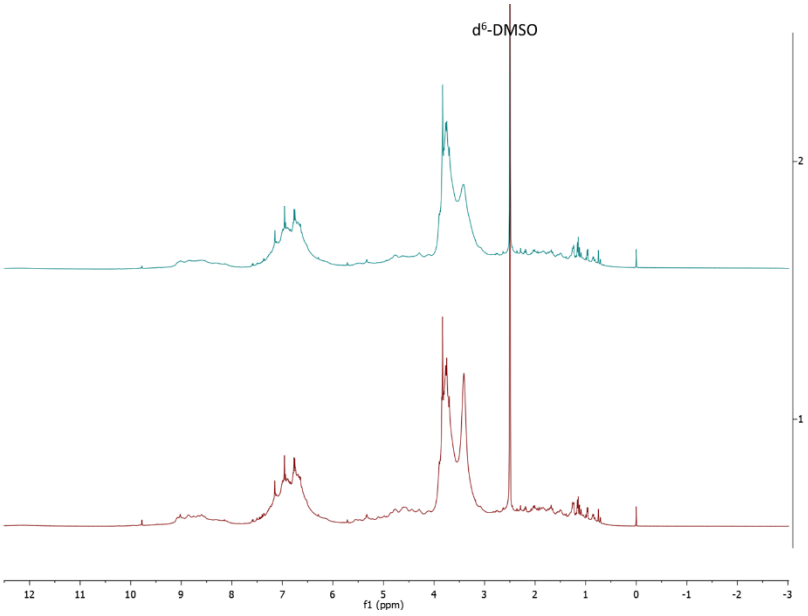

Figure S2.4. ^{1}H-NMR spectra of BioPiva395 (red) and BioPiva395-HCl (green).

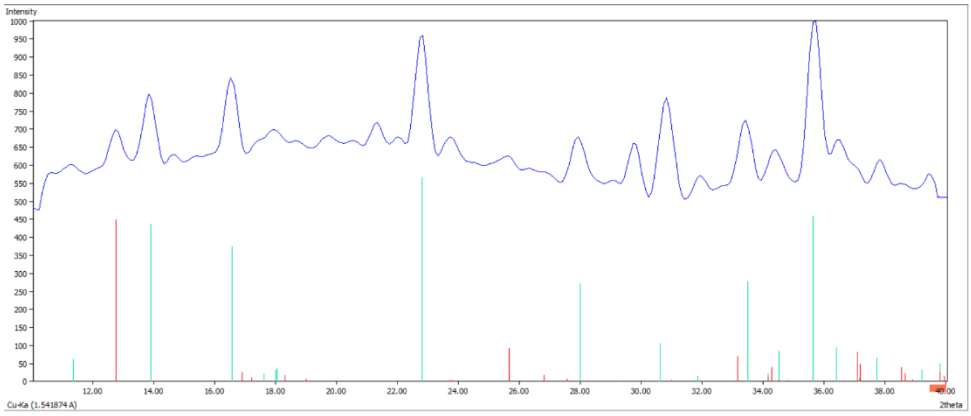

Figure S2.5. XRPD of the material UPM Solargo™ 100@brochantite-posnjakite23%_1, with green lines theoretical peaks of brochantite, red lines, theoretical peaks of posnjakite.

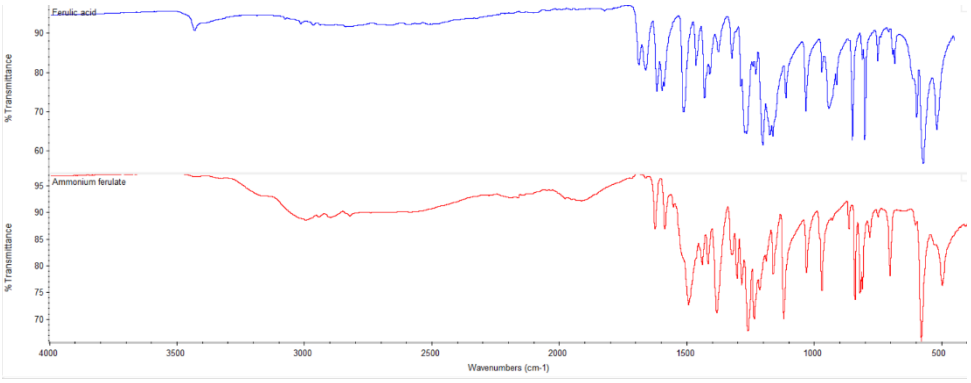

Figure S4.1. IR spectra of ferulic acid (blue) and ammonium ferulate (red).

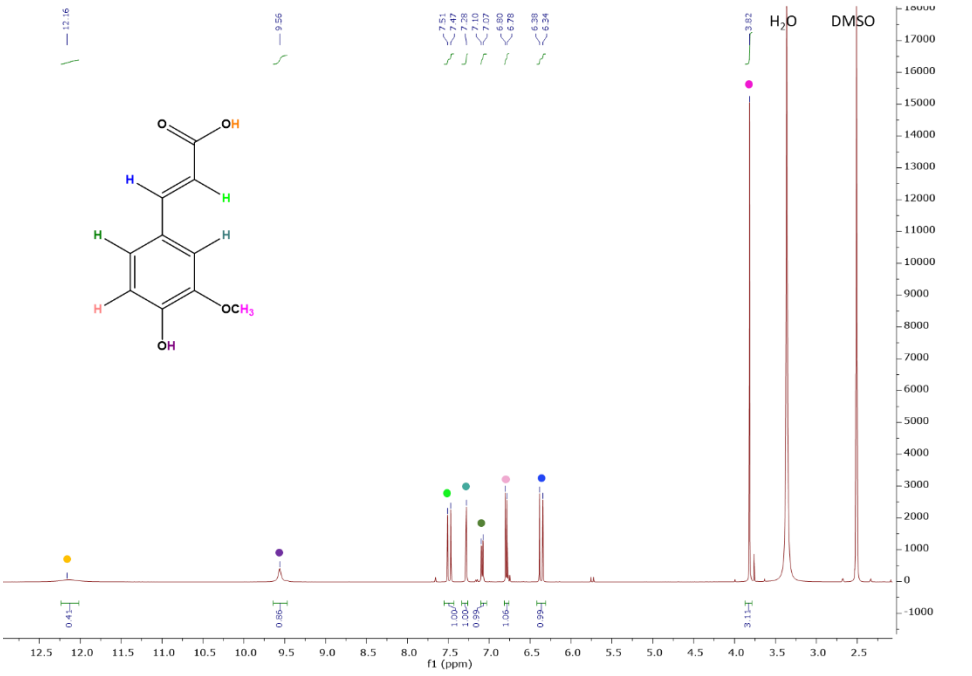

Figure S4.2. ^{1}H-NMR of ferulic acid

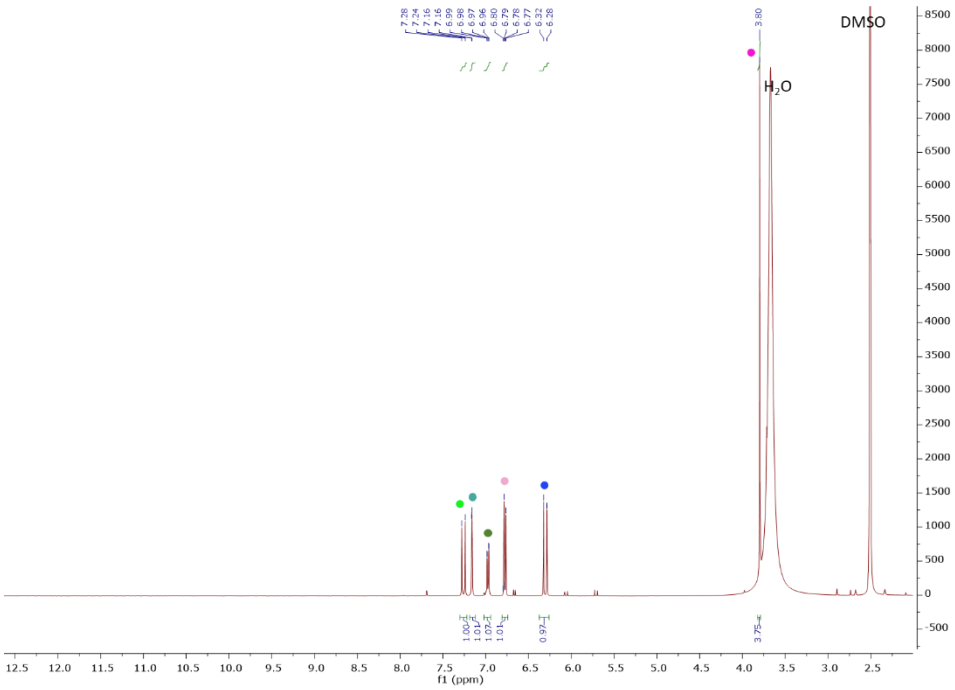

Figure S4.3. ^{1}H-NMR of ammonium ferulate.

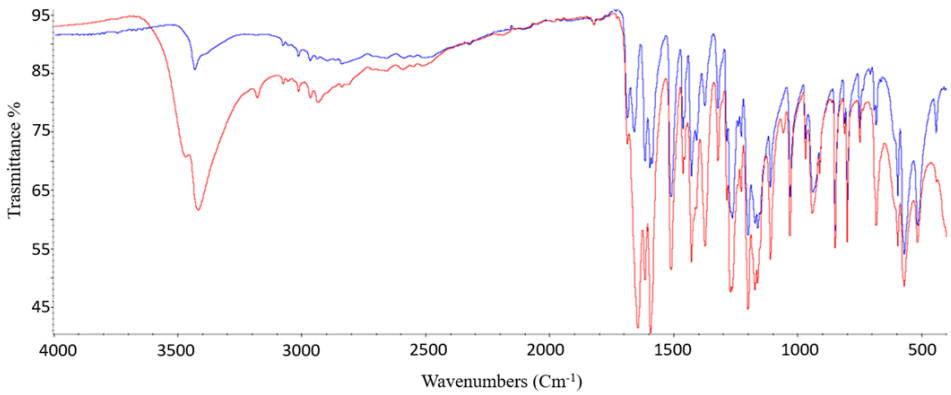

Figure S4.4. IR spectrum of the mechanochemical reaction ferulic acid + cobalt chloride (red) reveals the presence of ferulic acid (blue) as main component.

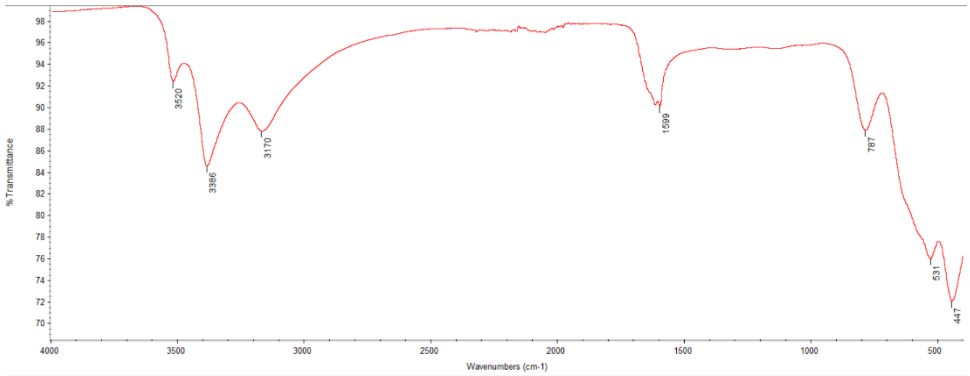

Figure S4.5. IR spectrum of $CoCl_2 \cdot 6H_2O$.

Acknowledgments

The PhD activity was made possible thanks to the collaboration of numerous professional figures. I want to thank Green Innovation (Giuliano Leonardi, Vito Macchia) and UPM-Kymmene Oyj (Suvi Pietarinen, Christian Hubsch) for the support on the research.

Special thanks go to UPM-Kymmene Oyj for hosting me, despite the ongoing Covid-19 pandemic, at North Europe Research Center (UPM-NERC) in Lappeenranta, under the kind supervision of Suvi Pietarinen.

In vivo tests were carried out by Centro Ricerche Agronomiche e Ambientali ResAgraria S.r.l. (Paolo Zazzetta, Antonio Pandolfi and Daniele D'Andrea), while *in vitro* tests by BICT SRL (Simone Stasi). NMR analysis on lignin samples was conducted at Technical Research Centre of Finland Ltd (VTT) by Tommi Virtanen, while TEM/EDS analyses were made possible thanks to Andrea Migliori's work at Consiglio Nazionale delle Ricerche Area Territoriale di Ricerca di Bologna (CNR Bologna). I also thank Chiesi Farmaceutici S.p.A. for using the Bruker D8 Venture diffractometer, Paolo Pio Mazzeo for the structural resolutions and Dominga Rogolino for the valuable scientific advice during these years.

Finally, to my supervisor Paolo Pelagatti, from whom I have learned a lot over the years, goes a special thanks for guiding me step by step in my professional growth.